University of Strathclyde

Department of Naval Architecture, Ocean &

Marine Engineering

Time-Domain Simulation of Seakeeping and Manoeuvring of Ships in Deep and Shallow Water Waves

by

Christos Pollalis

A thesis presented in fulfilment of the requirements for the degree

of Doctor of Philosophy

Glasgow, UK

2020

This thesis is the result of the author's original research. It has been composed by the author and has not been previously submitted for examination which has led to the award of a degree.

Signed: Christos Pollalis *Date: 20/05/2020*

"Life has meaning only in the struggle.
Triumph or defeat is in the hands of the gods.
So let us celebrate the struggle!"

Swahili Warrior Song

Abstract

The present thesis deals with the topic of ship manoeuvring in waves and the effects imposed by the shallow water. In this aspect, ship's manoeuvrability is investigated using a numerical method, which was developed according to a hybrid approach where seakeeping and manoeuvring contributions are blended. In order to ensure that the aforementioned model incorporates correctly seakeeping and calm water manoeuvring approaches, separate validation processes are followed beforehand. In case of nonlinear seakeeping analysis, parametric roll investigation is undertaken as well, as a mean to verify that the developed methodology evaluates properly the fundamental external forces, especially roll damping. In this way, a framework is established which offers the ability to perform holistic hydrodynamic assessment of marine vessels as well.

Validation of the developed computational code is conducted using experimental turning circle trajectories, which refer to deep water conditions. The case studies concern the horizontal motions of the S-175 container ship at long waves and four values of under keel clearance corresponding to medium-deep (UKC=3.0, 2.5, 2.0) and shallow waters (UKC=1.5). In this aspect, the wave forces as well as the manoeuvring-related ones are corrected using relevant methodologies. In particular, a 3D potential flow method is adopted for the evaluation of the former, whilst corrections are applied on the various manoeuvring-related force components defined by the Manoeuvring Modelling Group (Ogawa et al., 1977). Especially in case of the added resistance, near and far-field methods are implemented based on the size of the wavelength with respect to the ship's length.

The empirical corrections which refer to the manoeuvring-related forces and are used in order to incorporate the shallow water effect, concern the hydrodynamic hull forces, the calm water resistance and various hull-rudder-propeller interaction coefficients and are based on regression formulae which are functions of the under keel clearance ratio.

Acknowledgements

First of all, I would like to thank Dr Evangelos Boulougouris who suggested this interesting topic for my research and for making it possible to live a fascinating experience as a PhD student at the University of Strathclyde.

Secondly, I am very grateful of Prof. Osman Turan, Prof. Attila Incecik and all colleagues from the research project SHOPERA at the University of Strathclyde, who showed me how to work as part of a team in order to conduct research of high scientific value.

My special thanks and gratitude go to Mr. Dimitrios Mourkoyannis, researcher at the NTUA, who always insisted that the present study could end successfully, even when it was very hard for me to realize it. The endless moments talking about computer programming and ship hydrodynamics will remain unforgettable to me.

Am I also grateful to Dr Olgun Guven Hizir who offered his unconditional friendship and support during my PhD studies. His assistance concerning complicated hydrodynamic issues was decisive for the progress of my work.

The assistance and continuous support of Ms. Charitini Andriakopoulou concerning many aspects during the hard times of my studies was invaluable.

Many thanks go to my uncle, Mr. Yorghos Gkatzanis who offered his assistance in many practical issues and facilitated my daily life after returning to Greece for the final stage of my study.

Finally, the recent accomplishment, as well as all the previous ones concerning my scientific development as a Naval Architect and Marine Engineer, would have been impossible without the continuous support and encouragement of my parents, Dimitrios and Ioanna, and my bother Elias, to whom I am deeply indebted.

TABLE OF CONTENTS

List of Figures

List of Tables

List of Abbreviations

MMG	Manoeuvring Modelling Group
EEDI	Energy Efficiency Design Index
CFD	Computational Fluid Dynamics
DOF	Degree of Freedom
DSA	Direct Stability Assessment
BVP	Boundary Value Problem
BBC	Body Boundary Condition
FSBC	Free Surface Boundary Condition
IRF	Impulse Response Functions
SGISC	Second Generation Intact Stability Criteria
SWL	Still Water Level
RPM	Revolutions per Minute
AFS	Approximate Forward Speed
UKC	Under Keel Clearance

RSM	Response Surface Method

Nomenclature

Roman Symbols

L	Ship's length between perpendiculars
M	Ship's mass
B	Ship's breadth
T	Ship's draught
S	Ship's wetted surface
KG	Vertical position of the ship's centre of gravity
g	Gravitational acceleration
U	Ship's forward speed
Fn	Froude number
t	Time
dt	Time step
c	Wave celerity
$\vec{V}$	Fluid's velocity vector
x, y, z	Coordinates with respect to the body-fixed reference frame
x_h, y_h, z_h	Coordinates with respect to the hydrodynamic reference frame
x_{hs}, y_{hs}, z_{hs}	Coordinates with respect to the horizontal reference frame
U_{hs}	Ship's surge velocity with respect to the horizontal reference frame
V_{hs}	Ship's sway velocity with respect to the horizontal reference frame
R_{hs}	Ship's roll velocity with respect to the horizontal reference frame
U_n	Ship's surge velocity with respect to the earth-fixed reference frame
V_n	Ship's sway velocity with respect to the earth-fixed reference frame
R_n	Ship's roll velocity with respect to the earth-fixed reference frame
k	Wave number
h	Sea depth
M_{jk}	Mass matrix

A_{jk}	Added masses with respect to the hydrodynamic reference frame
B_{jk}	Damping coefficients with respect to the hydrodynamic reference frame
B_{φ}	Roll damping coefficient
B_e	Equivalent linear roll damping coefficient
C_{jk}	Restoring coefficients with respect to the hydrodynamic reference frame
K_{jk}	Memory functions matrix
$\vec{F}_{I,j}$	j^{th}-mode components of the incident wave forces
$\vec{F}_{D,j}$	j^{th}-mode components of the diffraction forces
f_j^{FK}	j^{th}-mode of Froude-Krylov force
f_j^{HS}	j^{th}-mode of Hydrostatic force
$F_{R,j}$	j^{th}-mode of Radiation force
x_p, z_p	Longitudinal and vertical coordinates of the panel's centre
A_p	Panel area
$\hat{a}$	Phase angle
$\vec{n}$	Unit outward vector
$\vec{r}$	Position vector
W(x,y)	Wave disturbance
$\bar{F}_n$	Second-order force
a_{WL}	Sectional flare angle
m	Angle of elementary wave
$k_j(m)$	Unsteady wave numbers
$H(k_j, m)$	Kochin function
u, v, r	Surge, sway and yaw velocities at body-fixed coordinate system
$\dot{u}, \dot{v}, \dot{r}$	Surge, sway and yaw accelerations at body-fixed coordinate system
X_H, Y_H, K_H, N_H	Surge, sway roll and yaw hull hydrodynamic forces
X_R, Y_R, K_R, N_R	Surge, sway roll and yaw rudder forces
Y_v, N_v	Linear manoeuvring derivatives with respect to the lateral velocity
Y_r, N_r	Linear manoeuvring derivatives with respect to the yaw rate
X_{vv}, X_{vvvv}, Y_{vvv}, N_{vvv}	Nonlinear manoeuvring derivatives with respect to the lateral velocity
X_{rr}, Y_{rrr}, N_{rrr}	Nonlinear manoeuvring derivatives with respect to the yaw rate

X_{vr}, Y_{vvr}, Y_{vrr}, N_{vvr}, N_{vrr}	Cross-coupling manoeuvring derivatives with respect to the lateral velocity and the yaw rate
Y_{δ}	Linear manoeuvring derivative with respect to the rudder angle
X_P	Propeller force
M_x	Surge added mass at zero frequency
M_y	Sway added mass at zero frequency
I_{xx}	Roll moment of inertia at zero frequency
I_{yy}	Pitch moment of inertia at zero frequency
I_{zz}	Yaw moment of inertia at zero frequency
$I_{x'y'}, I_{x'z'}, I_{z'y'}$	Cross-inertial terms at the horizontal body-fixed reference frame
J_{xx}	Roll added inertia at zero frequency
J_{zz}	Yaw added inertia at zero frequency
$M_{x'x'}$	Surge added mass at the horizontal body-fixed reference frame
$M_{y'y'}$	Sway added mass at the horizontal body-fixed reference frame
$I_{x'x'}$	Roll moment of inertia at the horizontal body-fixed reference frame
$I_{z'z'}$	Yaw moment of inertia at the horizontal body-fixed reference frame
$H_{x'}, H_{y'}, H_{z'}$	Components of angular momentum at the horizontal body-fixed reference frame
x_G	Longitudinal position of ship's centre of gravity from midship section
C_{44}	Roll restoring coefficient
B_{44}	Roll damping coefficient
A_R	Rudder area
a_H	Rudder force increase factor
x_H	Longitudinal point of rudder-induced additional lateral force
FN	Normal rudder force
U_R, v_R	Longitudinal and lateral inflow velocity at rudder
f_a	Rudder's gradient of the lift coefficient
a_R	Effective rudder's inflow angle
T_x	Propeller thrust
R	Calm water resistance
t_p	Thrust deduction coefficient

n_p	Propeller revolutions per second
K_T	Open water propeller thrust characteristic
J_p	Propeller advance ratio
D_P	Propeller diameter

Greek Symbols

ζ	Wave elevation
ζ_α	Wave amplitude
ρ	Water density
φ, θ, ψ	Eulerian roll, pitch and yaw angles
ω	Wave frequency
ω_e	Wave frequency of encounter
χ	Incident wave direction
$\check{\zeta}$	Complex wave amplitude
Φ	Total velocity potential
Φ_S	Steady contribution of the velocity potential
Φ_T	Unsteady contribution of the velocity potential
Φ_I	Incident wave potential
Φ_D	Diffracted wave potential
φ_j	Radiation potentials of the j^{th}-mode of motion
ξ_j	Motion amplitude of the j^{th}-mode
$\dot{\xi}_j$	Velocity amplitude of the j^{th}-mode
$\ddot{\xi}_j$	Acceleration amplitude of the j^{th}-mode
λ	Wavelength
τ	Convolution period
Ω	Hanaoka's parameter
δ	Rudder angle

CHAPTER 1

INTRODUCTION

1.1 Preamble

Since the early 1900s, the investigation of a vessel's manoeuvrability at an early design stage has concerned the naval architects, whilst relevant mathematical models were introduced (Lamb, 1932). A review of the achievements in manoeuvring theory the first decades of the previous century can be found in Newman (1979). Additionally, with the huge amount of operating ships nowadays (more than 95000 according to UNCTAD, 2019), hazards related to the possibility of collision or grounding due to poor manoeuvrability, even in open seas, has intensified the interest of naval architects. For this reason, the need for advanced developments in the field of manoeuvring theory has resulted in the formulation of accurate mathematical models, which allow the investigation of a vessel's manoeuvrability in calm water and at different operational and environmental conditions (e.g. presence of extreme wind and current). Nowadays, these models have acquired a wide range of application due to the increase in computational power. Moreover, their combination with experimental techniques has attributed to them a high level of validity, as the physics of the problem are adequately represented.

Although significant progress on ship's manoeuvring prediction in deep and calm water was succeeded by relevant mathematical models, concerns have been raised about the impact of shallow water on her manoeuvring characteristics. Such conditions exist at coastal or harbor areas, where a ship can be found for a short time. However, due to the increased traffic at such areas, the possibility of collision or grounding with adjacent bodies becomes higher. Relevant studies conducted since the early 1990s resulted in various semi-empirical expressions based on regression analysis, where the variation of the added inertias and the manoeuvring derivatives are represented as a function of the under keel clearance.

Things become more complicated when the impact of wave forces during ship manoeuvring has to be taken into consideration as well. In this case, the first and second-order (added resistance, sway and yaw drift forces) wave force contributions shall be incorporated as well, leading to the requirement of integrated mathematical and numerical approaches, which couple seakeeping and manoeuvring in calm water theories.

Accurate modelling of a ship's manoeuvrability in waves, apart from its scientific interest, is useful nowadays from a practical point of view as well. In 2012, in order to enforce the environmental efficiency in ship operation, the EEDI was introduced through the resolution MEPC.214(63). In the following years, concerns were raised, since the most common way to attain satisfactory values of the aforementioned index solely concerned the reduction of the installed vessel power. This tendency will lead to poor manoeuvrability of marine vessels as it directly affected the available power of the propulsion system, combined with weaker action of the steering devices in adverse weather conditions. In this context, the RTD project SHOPERA, funded by the E.U., undertook the responsibility to develop and propose methods and criteria aiming to assess the manoeuvrability of a ship in such condition and propose guidelines for safe marine operation,

Recently, the fifth MASHCON Conference (Ostend, 20-22 May 2019) attempted to investigate the effect of wind, waves and currents on a vessel's manoeuvring characteristics in shallow water. In this respect, the development of a time-domain numerical method capable of assessing a vessel's manoeuvrability in waves and shallow waters was considered necessary. This is addressed in the present thesis with the development of a method, which is capable of conducting time-domain simulations, coupling seakeeping and manoeuvring theories in order to formulate a hybrid method. 3D potential theory was used to calculate the wave force components; the aforementioned are derived from the solution of the linearized Boundary Value Problem which is based on the well-known Green function formulation. Depending on the type of the seakeeping analysis (linear/nonlinear), the values of Froude-Krylov and restoring terms either come from the solution of the Boundary Value Problem, or are calculated at each time increment implementing a direct pressure integration scheme. In order to verify that the developed numerical tool is suitable to conduct nonlinear seakeeping analysis and, consequently, can be used for direct stability assessment, parametric roll investigation concerning a C11-class container ship is performed as well, in a separate section of the present thesis.

Finally, the steady second-order wave forces are obtained from the NTUA's validated software NEWDRIFT v.7 and NEWDRIFT+, which employ the near and the far field approaches, respectively. The selection of each type of analysis was made in accordance with the size of the wavelength with regard to the ship's length (long or short regular waves).

After performing validation studies of every module of the previously mentioned integrated numerical method, studies are conducted concerning the effect that shallow water imposes on ship's manoeuvrability in waves. For this purpose, only small amplitude waves are considered, thus the first-order wave forces result from the solution of the Boundary Value Problem, considering finite sea depth.

In the following chapters, the theoretical background that governs seakeeping and manoeuvring theories, as well as the mathematical expressions that led to the development of the present time-domain numerical tool will be demonstrated, combining existing methodologies, which are critically reviewed. Results of ship's vertical motions and calm water manoeuvring will be presented using full (KVLCC2 tanker) and fine (S-175 and C-11 container ships) hull forms, attempting to identify differences attributed to the geometrical characteristics of such vessels. Results considering manoeuvring in waves simulations, in both deep and shallow waters, are presented for the S-175 container ship.

1.2 Aim and Objectives of the Current Research

The aim of the present PhD study is the **development of an integrated time-domain numerical method, which is capable of assessing a ship's hydrodynamic performance in various environmental and operational conditions, related to manoeuvring in waves in deep and shallow water conditions.** The objectives of the conducted research include the following:

1. Validate the structure of the developed numerical code through the simpler scenario of ship manoeuvring in calm water.
    - The representation of the hydrodynamic forces exerted on the vessel's hull follows a third-order Taylor series expansion.

2. Propeller and rudder actions are incorporated by means of semi-empirical formulae. Provide validated solution of the linear time-domain seakeeping problem, as it will allow the incorporation of the first-order wave forces during ship manoeuvring.
3. Evaluate the nonlinear Froude-Krylov and Restoring forces in case of large amplitude waves,
    - Initially, the numerical evaluation of vertical ship motions is performed at the **hydrodynamic reference frame** which accounts for small pitch angles ($\theta<10^o$).
    - Further enhancement of the time-domain seakeeping analysis concerns the incorporation of roll motion in order to develop a direct stability assessment software.
4. Time-domain manoeuvring simulations in regular waves are conducted by developing a hybrid method, where seakeeping and manoeuvring-related forces are added at a common time step.
5. Empirical investigation of the shallow water effect on a ship's manoeuvrability in regular waves is performed within the framework of the present study.
    - First and steady second-order wave forces are obtained by solving the Boundary Value Problem while assuming a different condition on the seabed as the depth is finite.
    - Empirical corrections are implemented on the deep water values of the manoeuvring derivatives and added inertias, utilizing regression formulae found in the literature.
    - Corrections of the deep water calm water resistance and various hull-rudder-propeller interaction coefficients are employed as well, through the adoption of relevant regression formulae.

1.3 Novelty of the Present Research

The present study led to the development of a time-domain numerical methodology implemented through a novel software, which is capable of simulating a vessel's response in various operational conditions. These include, calm water manoeuvring, linear and nonlinear seakeeping analysis[1], and assessment of a ship's manoeuvrability in regular waves.

[1] Including parametric roll investigation

This requires the adoption of complex mathematical and numerical formulations in order to model the nonlinear force contributions.

Additionally, within the framework of the developed time-domain methodology **several corrections are proposed which concern the shallow water effect, while a ship executes turning circle maneuvers**. The proposed methodology suggests that the following force components should be corrected in a modular way, covering all external force actions experienced by the marine vessel.

- Calculate the oscillatory first-order and steady second-order forces at finite depth using available hydrodynamic software.
- Correct the values of the manoeuvring derivatives according to the considered under keel clearance.
- Correct the values of the vessel's added inertias in accordance to the values of the investigated under keel clearance
- Calculate the increased calm water resistance in shallow water caused by the flow change around the vessel.
- Correct the values of hull-propeller-rudder interaction coefficients which are influenced by the finite sea depth.

1.4 Structure of Present Thesis

After the introductory chapter (Chapter 1), an extensive literature review is presented in Chapter 2. This chapter covers the existing research regarding the investigated phenomena, and it is divided in two major sections, namely manoeuvring in waves and direct stability assessment. The latter, refers to the stability failure mode of parametric roll. In case of ship's manoeuvring in waves, focus is given on the two different concepts that have been used until now in order to succeed the coupling of seakeeping and manoeuvring theories, commenting on their validity and effectiveness. Recent developments, which include the effect of shallow water on a ship's hydrodynamic performance, are also mentioned and critically reviewed.

As a side product of the current study, an effort is made to critically review existing methods concerning parametric instability in waves, highlighting the advantages and the limitations that accompany each simulation technique and the level of the incorporated nonlinearities.

In Chapter 3, an explanatory description of the theoretical background is presented. Initially, the coordinate systems considered in the current analysis are listed, as their proper definition is crucial for the correct formulation of the ship's motion equations, especially when large excitations are taken into consideration. Subsequently, theoretical aspects concerning the solution of the frequency-domain, Boundary Value Problem of a ship interacting with the sea environment are included, as it is considered an important part towards the formulation of an accurate time-domain model. The boundary conditions, which govern the interaction of a rigid body with the sea, are presented in both deep and shallow water conditions.

In the following chapter (Chapter 4), the system of equations in the time-domain is presented, which describe the vessel's motions at each different case (calm water manoeuvring, linear/nonlinear seakeeping, manoeuvring in waves). Additionally, the equations used to calculate the several nonlinear force components are shown as well, whilst a brief presentation of the developed numerical tool is given.

In Chapter 5, a presentation is performed regarding the novel numerical code ELIGMOS. Its main algorithmic procedures are discussed, whilst its integrated seakeeping and manoeuvring module is illustrated by means of two flow charts.

In Chapter 6, validation studies of the adopted methodology are presented. Due to the complexity of the investigated phenomena, it was decided that extensive validation efforts must be carried out covering each module of the unified approach that describes ship's manoeuvring motion in waves. For that reason, the developed numerical tool is used in order to simulate ship's manoeuvring motion in calm water (both deep and shallow) and her seakeeping performance at head seas, comparing the obtained results with available experimental and numerical data found in the literature. Further, validation of the present time-domain seakeeping module is undertaken, in small and large amplitude waves investigating its ability to address the impact of geometrical nonlinearities. Subsequently, results on parametric roll are demonstrated in order to further accredit the developed nonlinear numerical tool.

Finally, the hybrid method developed within the context of the present study in order to predict ship's manoeuvrability in waves is validated using relevant experimental turning circle trajectories.

After the demonstration of the validation studies, the manoeuvring performance of a single ship in shallow seagoing environments is investigated in Chapter 7. In particular, the hybrid model of ship manoeuvring in waves, together with the adopted modifications in case of shallow water, is tested in long waves and at various sea depths for the S-175 container ship.

At this stage, since there are not any available experimental data, only a qualitative investigation is possible, which is succeeded through the comparison of the turning trajectories with those referring to deep water conditions.

In Chapter 8, a detailed discussion of the derived results is conducted, highlighting the main outcome of the present study. Finally, in Chapter 9, conclusions include the achievements of the present study, focusing on the innovation, which will be stated in the next chapter on the basis of the performed literature review. Finally, recommendations for future research are suggested, which will further develop the present methodology.

CHAPTER 2

LITERATURE REVIEW

2.1 Manoeuvring in Waves

2.1.1 Introduction

Ship manoeuvring in waves is a topic that concerns researchers over the last years. Until that time, manoeuvring performance had been investigated in calm water conditions ignoring any force contribution related to waves, although other force components such as wind and current effects were incorporated. Although there are not any relevant criteria established by the IMO, the need to study manoeuvrability of ships in more realistic conditions, forced the introduction of integrated experimental and numerical methods, which incorporated the contribution of low frequency terms and high frequency ones, merging the theories of seakeeping and manoeuvring. The level of the adopted analysis's nonlinearity and the assumptions considered for the representation of the flow's properties (potential or viscous), led to different mathematical models which aim to simulate standard manoeuvring motion in waves

In this chapter, an extended review of the recent research developments in the field of numerical simulations of ship manoeuvring in waves is presented. Each study that is being reviewed is based on a method to describe rigid body dynamics of manoeuvring in a seaway, implementing either a two-time scale method or a hybrid (unified) one, which consist of the two alternatives in order to couple manoeuvring and seakeeping analyses (Tello Ruiz et al., 2012). Other methods, which can be adopted for such an investigation, are the CFD and the experimental ones, which impose significant financial and computational costs and therefore are the minority among the published works, even though they represent physical properties in a more realistic way.

In most of the studies critically reviewed in this chapter, wave induced forces are considered as those having the greatest impact on ship's manoeuvrability in adverse conditions among the viscous forces due to low frequency manoeuvring and any other force resulting from the propeller's and the rudder's action. The aforementioned forces include:

- Diffraction components
- Radiation components
- Froude-Krylov and Restoring components
- Steady second-order wave components (wave drift and added resistance forces)

Depending on the variation of the waterplane area of the ship from a wave trough to a wave crest, Froude-Krylov and Restoring forces may be calculated either linearly or nonlinearly, when the integration of the hydrodynamic and hydrostatic pressures is performed over the instantaneous wetted surface. In case of large roll angles and intense hull flare, nonlinear seakeeping analysis should be implemented, in order to accurately simulate ship's motions, incorporating the effect of geometrical nonlinearities at large wave excitations. In the present thesis, analyses implementing both linear and nonlinear approaches will be discussed, focusing on the considered nonlinearity level. Nonlinear seakeeping codes are also necessary when dynamic stability of a vessel is examined.

According to the ITTC (The manoeuvring committee, 2011), the different methods to study ship manoeuvring in a seaway can be categorized in the following four groups:

i. Experimental methods
ii. Two-time scale methods
iii. Hybrid (unified) methods
iv. CFD methods

Herein, the term "Hybrid" will be used instead of "Unified", following the terminology met in Tello Ruiz et al (2012). Detailed review of the available (ii) and (iii) methods are presented in the following paragraphs as they are considered of greater interest in the context of the present thesis.

2.1.2 Hybrid Method

While using this method, low frequency force components (manoeuvring terms) and high frequency components (wave-induced forces) are mixed up in order to formulate the total external force excitation at each time step.

During the mathematical modelling, attention should be given concerning the proper inclusion of the underlying fluid effects. In all cases, this is succeeded by adopting a modular approach for the calculation of the manoeuvring as well as the seakeeping-related forces.

Hamamoto and Saito (1992) proposed a 6-DOF hybrid mathematical model for the simulation of ship manoeuvring in regular waves, where the external forces consist of low frequency (manoeuvring) and high frequency (seakeeping) terms. Radiation forces in the time domain are calculated through the concept of Impulse Response Functions (Cummins, 1962) of frequency dependent damping coefficients. For the mutual representation of different force components, a new reference system was employed apart from the already known earth fixed and general body axes systems. The so-called Horizontal Body Axes system (Hamamoto and Kim, 1993) enables the calculation of the linear manoeuvring forces, since its XY plane remains on the undisturbed sea level and fixed to the ship's centre of gravity, as well as the addition of first order wave-induced terms after being properly transformed from the general body-fixed reference frame to the horizontal one. Contribution of propulsive and steering forces is suggested according to the MMG modular approach (Yasukawa and Yoshimura, 2015).

Fang et al. (2005) proposed their own 6-DOF model on the basis of Hamamoto and Kim's (1993) work, where nonlinear hydrodynamic manoeuvring forces are blended with the 2D first order wave forces, in order to account for the fundamental fluid effects during turning circle motion in waves. Memory effects were not incorporated according to the concept of retardation functions, whilst hydrodynamic loads were directly evaluated at encounter frequency and imported in the time domain model instead. In that study, results on turning circle with associated ship motions and horizontal velocities were depicted for two containerships. Accordance between numerical and see trial trajectories was better when the initial wave heading was 180 degrees rather than when bow oblique heading was taken as the initial wave direction.

Inclusion of second order drift forces would certainly improve the agreement and allow for more realistic multiple turning circle trajectories.

Sutulo and Soares (2006b) developed a nonlinear hybrid mathematical model applicable to ship manoeuvring in a seagoing environment, based on 2D strip theory, which is appropriate for slender vessels. Calculation of both first and second-order seakeeping forces was conducted by direct integration of the relevant hydrodynamic pressure components, over the ship's wetted surface. Improvement of the actual representation of the problem's physics was attempted by considering the viscous force components as well, apart from the potential ones, in case where experimental results from calm water manoeuvring tests were available. Viscous forces due to low frequency manoeuvring motions have been incorporated, including the effect of instantaneous sinkage and trim by use of semi empirical expressions derived from series of captive model tests. In this work, a different way of considering the memory effects was followed, implementing a state-space representation. This option is less time consuming, as the radiation forces are evaluated in the time domain via ordinary differential equations with constant coefficients. Results on turning circle trajectories in calm and wavy environments show no apparent impact of the drift forces.

Ayaz et al. (2006), aiming to develop their own nonlinear hybrid model for ship manoeuvring in waves, stored the values of added masses and damping coefficients in segments of 10^o, from 0 up to 360 degrees, whilst the selection of the appropriate values was performed through interpolation, depending on the exact wave heading and ship's speed each time. In this way, a more realistic and practical evaluation of radiation forces was succeeded. Manoeuvring related forces were introduced in a modular approach, implementing the Japanese MMG model. Additionally, the proposed method is able to detect failure modes related with dynamic instability phenomena however, results on standard manoeuvers in waves (turning circle, zig-zag test, etc.) are missing.

Sutulo and Soares (2006a) presented a unified 6-DOF manoeuvring model of surface displacement ships in regular waves, which emphasized on the influence of roll angle during curvilinear trajectories. At that time, this issue had been considered as a secondary effect in the previously published works of Bailey et al., 1997 and Ayaz and Vassalos, 2003, or had been treated from the seakeeping safety point of view (Remez, 1985) neglecting the action of viscous manoeuvring forces. Slenderness assumption applied as well, a fact that implied the use of strip theory for the derivation of the seakeeping forces.

The calculation of the Froude-Krylov and restoring force components was performed by considering variable wetted surface, whilst forces due to the diffracted wave were evaluated with respect to a constant wetted surface assumption. Three types of runs were then simulated using the S175 container ship and primary results showed larger maximum roll angle attained in turning motion than in free or constrained straight test, a fact that revealed the augmenting impact of coupled seakeeping and manoeuvring actions. Finally, further studies investigating the impact that an increased forward speed or a reduced metacentric height would have on either the turning trajectory or the roll response, were strongly recommended by the authors.

Fossen (2005) presented a hybrid (unified) model capable of simulating ship's manoeuvring motion in a seaway. In his work, the influence of frequency dependent potential and viscous damping coefficients is represented using a state space formulation (Kristiansen and Egeland, 2003), which consists of the common representation when feedback control systems are incorporated. Linear wave induced forces are incorporated in the model through the use of RAO values, which should have been calculated beforehand by means of frequency-domain analysis. The resulting motion due to the manoeuvring and seakeeping actions is obtained implementing the linear superposition assumption, which allows the summation of the individual motion contributions. In this article, an analytical methodology of matrices' transformations is developed, which facilitates the common representation of manoeuvring and seakeeping equations even in case where nonlinear analysis is considered. However, results that show the verification and validation level of the developed method against experimental data are missing.

More recently, Ghillece and Moctar (2018) presented a 6-DOF hybrid model in order to simulate turning circle in regular waves of the DTC container ship. Wave directions of 0^o, 90^o and 180^o were considered in order to show the influence of mean second order forces, which were the only wave related force components incorporated. For their calculation, two different approaches were implemented. In case of lower forward speed (U=6kn), a double body formulation was adopted whilst, for a greater forward speed of U=12kn a consideration of the nonlinear steady potential was incorporated. Better agreement against experimental and CFD results was pinpointed in the second case, whilst a correction of 9% was applied in the case of lower forward speed. The calculation of the latter was performed by a time domain three dimensional Rankine source code based on previously published works of Söding et al. (2012, 2014) and von Graefe (2014).

Manoeuvring forces were evaluated separately, using the manoeuvring derivatives obtained by PMM tests executed computationally with a RANS technique. Nonlinearity of the model ensured higher accuracy regarding the results, which describe ship's turning trajectory even for higher wave amplitude, which is crucial for a container ship.

2.1.3 Two-time Scale Method

This method accounts for ship manoeuvring simulation in waves as well. This time, seakeeping and manoeuvring equations are treated separately including each time the effect of their counterpart, but are coupled in order to provide the final solution. Herein, 4-DOF manoeuvring equations constitute the low frequency part of the method, where the impact of the seagoing environment is taken into account by considering an extra wave induced force component. On the other hand, the continuously changing forward speed and wave heading introduce the effect of the manoeuvring motion in the rapidly varying 6-DOF seakeeping equations.

Hirano's et al. (1980) study can be considered as a pioneering work in the field of time-domain assessment of a ship's manoeuvrability in waves. More specifically, the wave drift forces were incorporated in the context of a 3-DOF manoeuvring system of equations. All other wave-induced loads were neglected. There were proposed two similar approaches to formulate such a numerical solution. Regarding the first one, (sequential) seakeeping sub-problem is solved after the completion of the manoeuvring part whereas in the other approach (parallel) the seakeeping system of equations is solved several times before manoeuvring evaluates at a single time step. Major drawback of this method was that second-order drift forces corresponded to zero forward speed value, meaning that the effect of forward speed was not taken into consideration.

Skejic and Faltinsen (2008) proposed a two time scale method for the simulation of ship manoeuvring in regular waves based on a coupling between 4-DOF low frequency and 6-DOF rapidly varying sets of equation, which are solved sequentially. The manoeuvring sub-problem (low frequency motion) is formulated using a modular approach for the calculation of the external forces considering the contribution of drift forces as well, whilst the well-known two-dimensional STF approach (Salvesen et al., 1970) accounted for the evaluation of the linear wave induced forces.

In this study, the impact of the full wavelength range on the correct wave drift forces' calculation was considered through the testing of four different methods. More specifically, in case where the wavelength was equal to the ship's length, the theory of Faltinsen et al. (1980) was proposed as the most appropriate, since Salvesen's (1974) has deficits related with full body hull forms whereas, Loukakis and Sclavounos' (1978) method is only valid for the evaluation of the added resistance and the lateral wave drift forces. Concerning the structure of the developed numerical solution, the manoeuvring part evaluates until a predefined increment of the heading angle $\Delta\psi$ is reached, approximately 2 to 3 degrees. At that time, the seakeeping part is activated using the instantaneous forward speed and heading angle resulting from the solution of the manoeuvring sub-problem, as input values.

Another sequential two-time scale method for simulating ship manoeuvring in waves was proposed by Yasukawa and Nakayama (2009). Related to Skejic and Faltinsen's work, a different approach to calculate wave-induced forces was implemented, using a three dimensional quasi-steady panel method in the frequency domain. Additionally, instead of using two different reference frames in order to express manoeuvring and seakeeping sub-problems, as it was performed by Skejic and Faltinsen, the aforementioned horizontal body axes frame was considered, which allowed the introduction of a general integration scheme.

Chroni et al. (2015) published their research work on time domain simulation of S-175 container ship manoeuvring in waves using the two-time scale approach, where the 4-DOF manoeuvring set of equations in calm water was solved considering the effect of the seagoing environment by means of the second-order added resistance and wave drift forces. The values of the second order forces had been pre-calculated and stored for several heading angles and forward speeds, which cover the whole turning, circle. Validation of the model was conducted considering short wave conditions, which is of high interest in the context of the IMO MEPC.212(63) (2012). Additionally, other environmental contributions were incorporated as well, namely wind and current forces. Numerical results on turning circle simulation by use of MATLAB's Simulink show good agreement with the experimental ones however, better convergence may has been attained if first-order wave-induced loads were included as well.

Fournarakis et al. (2016) developed a unified numerical approach for the simulation of a ship's manoeuvrability in regular waves where different computational tools were used in this context.

For instance, the manoeuvring derivatives were evaluated without the need of costly experiments, since this was succeeded by means of CFD simulations whilst, added masses and mean second order forces were pre-calculated by the 3D panel code NEWDRIFT. The calculation of coupled manoeuvring derivatives was performed through virtual CMT tests, using the CFD software STAR-CCM. Subsequently, the aforementioned 4-DOF model (Chroni et al., 2015) was implemented in calm water and regular short wave manoeuvring scenarios of the DTC's container ship (Moctar et al., 2012). Results in both cases show good agreement with the available experimental data.

Seo and Kim (2011) proposed a method to simulate ship's manoeuvrability in regular waves based on a parallel two-time scale approach coupling a 4-DOF manoeuvring model and the 6-DOF time domain numerical code WISH. The latter, implements a linear Rankine panel method, whilst manoeuvring part is formulated in the modular approach proposed by the Japanese MMG. Wave contribution was incorporated through the addition of added resistance and drift forces calculated using a direct pressure integration method. Calm water results on both turning circle and zig-zag simulations show very good agreement with available experimental data for a Series 60 hull, whereas turning circle simulations of the S-175 container ship in waves show better agreement when the initial wave heading is 180^{o} and the wavelength is equal or greater than the ship's length. The latter was expected, since direct pressure integration methods for the calculation of second-order wave forces are suitable in case of long waves.

Zhang et al. (2017) proposed a parallel, two-time scale numerical method, where the total potential is composed incorporating the contributions from the quasi-steady basic potential and the perturbation potential as well. The perturbation potential was further decomposed to a part related with the incident wave potential and a remaining one. The low frequency (manoeuvring) problem associated with the basic flow was treated implementing the aforementioned MMG model adopting a third-order expansion for the evaluation of the viscous forces whilst, the wave induced motions were evaluated by means of a time domain Rankine panel method. The effect of the seakeeping counterpart on the manoeuvring set of equations was introduced by the mean value second-order forces calculated using Joncquez's direct pressure integration method (Joncquez, 2009). Numerical results showed acceptable agreement in case of added resistance and yawing drift moment whereas, underestimated values derived concerning the lateral drift force.

Results in terms of RAO values in straight course for various oblique wave scenarios indicated inaccuracies of the adopted method in case of purely head seas for heave and pitch motions whilst, in case of roll and yaw angular motions poor agreement was observed for a heading angle of -60^{o} probably due to the roll damping and restoring modelling respectively. Turning circle trajectories in a regular seaway, where the wavelength was equal to the ship's length, showed better agreement when the ship was initially positioned against the wave's propagation direction rather than in beam waves, which consists of a more challenging scenario for an accurate estimation of the mean second order wave forces.

Subramanian and Beck (2015) investigated ship's manoeuvrability in waves as well, by means of a two-time scale method. In their work, wave forces were calculated by implementing a body-exact 2D method, aiming to account for the nonlinear effects imposed during the interaction of a moving vessel with large amplitude waves. Results concerning turning trajectories of the S-175 container ship, show remarkable deviations from the experimental ones, although the impact of the drift forces is obvious mainly as the wavelength increases. However, in case of large wave steepness ($H/\lambda=1/35$) the numerically derived turning circles are far from the experimental ones, quantitatively and qualitatively. The authors claim that these discrepancies may be reduced in case where a complete body-exact method is implemented.

2.1.4 Second-order Wave Forces

When a ship sails in a seaway, her calm water might increase from 20% up to 40% due to the presence of waves. In this case, an additional component related to the counteraction of waves is added on the calm water resistance. The accurate calculation of the so-called added resistance during the initial stages of ship design is of great importance, as it is used for the estimation of the ship's power needs, which must ensure safe and efficient navigation. Added resistance is considered as steady force having an opposite action related to the ship's forward speed. Additionally, it is one of the steady second-order force components, because it is proportional to the square of the wave amplitude. The other two, which are primarily involved during the simulation of a ship's manoeuvrability in waves, are the sway drift force and the yaw drift moment. Within this framework, relevant methodologies aiming to calculate these force components are reviewed in this section of the thesis.

Regarding the calculation of the added resistance, two types of methods are available namely the near- field and the far-field approaches. Although someone would expect both near-field and far-field methods produce the same results, in practice this is not valid as each approach is dependent on the accuracy of the solution of the seakeeping problem, which cannot be ensured in all cases.

In general, far-field methods consider the radiated and diffracted wave energy at infinity and use the total rate of momentum change in order to calculate the added resistance whilst, near-field methods implement a direct integration of the second order hydrodynamic pressure on the wetted hull. The first who applied a far-field method to estimate the added resistance was Maruo (1957) whilst, further developments can be found in the works of Maruo (1960, 1963) and Joosen (1966). Iwashita and Ohkusu (1992) used Maruo's (1963) improved approach and included the concept of Kochin functions as well, obtaining very good results. Before that, Salvesen (1974) had developed a method for the calculation of the added resistance based on Gerritsma and Beukelman's (1972) formulation. The asset of Salvesen's method against the latter was that it used more accurate ship motions' values utilizing the superiority of the well-known STF approach (Salvesen et al., 1970). It was thereafter concluded that the accurate estimation of the added resistance is strongly affected by the validity of ship motions' values. Therefore, accurate or even realistic ship motions' data is a prerequisite for the development of robust methods for the calculation of the added resistance. Accurate derivation of ship motions implementing three dimensional hydrodynamic analysis might improve the accuracy of all the aforementioned methods as well.

According to Naito's (2008) review of available methods for the estimation of the added resistance, the approach introduced by Iwashira and Ohkusu, although it provides very good results for all types of ships, still lacks wide implementation due to its complicated structure and high computational cost. The most representative study in the area of near-field methods was populated by Faltinsen et al. (1980), showing good agreement compared against experimental values. This method is based on a direct integration scheme of the second-order hydrodynamic pressure. Its main drawback is the inability to derive accurate results in case of short waves. Answer to this problem was given by the introduction of an asymptotic method, based on a simplified formula that accounts for the dominating effect of the diffraction in case of high wave frequencies.

Liu et al. (2011), implementing Iwashira and Ohkusu's method, published their proposed approach for the calculation of the added resistance using a hybrid Rankine source-Green function formulation integrated within the 3D panel code NEWDRIFT (Liu and Papanikolaou, 2010). Within this study results on added resistance of a submerged spheroid, a floating spheroid and a Wigley hull are compared using several well-established methods for the calculation of the first-order potential, ship's motions and the added resistance. The developed method was proven quite reliable in estimating the added resistance incorporating the outcome of Faltinsen's asymptotic method for high wave frequency ($\lambda/L=0.5$).

Apart from the added resistance, other major components that affect a vessel's trajectory in waves are the sway drift force and yaw drift moment. The effect of these components can be perceived if someone thinks how the generated waves from a throwing stone into a water basin "push" a floating ball towards its sides. Additionally, the same force aligns a singly moored vessel, which was initially exposed in beam waves, with the wave's direction. When a ship manoeuvers in a seagoing environment, the action of steady drift forces has to be incorporated as well, as it may have a significant influence on ship's trajectory depending the vessel's forward speed, the wave's amplitude and the ratio of wavelength to ship's length.

The effects of the drift forces, in contrast to the first-order wave effects, vary with double the wave frequency whilst, their mean value over a period of oscillation is non-zero. Although the drift forces can be better approximated when the second-order potential is known, quasi second-order effects can be calculated by knowing the first-order wave potentials. Thus, similarly to the added resistance calculation, drift forces can be obtained either by means of direct pressure integration (near-field) as indicated by Pinkster and van Oortmerssen (1977), or by implementing a far-field analysis as mentioned before. Papanikolaou and Zaraphonitis (1987) improved the near-field method introduced by Ogilvie (1983) by adding some missing terms in case of arbitrarily selected coordinate systems (off mass centre). Developing the aforementioned innovative formulation, the calculation of drift forces was made possible even for unsymmetrical bodies. In the present study the added resistance in case of short wave seas has been calculated using Liu and Papanikolaou's (2011) far-field method, whilst in other case Papanikolaou and Zaraphonitis' (1987) near-field method is implemented for the calculation of the second-order wave forces.

2.1.5 Derivation of Hydrodynamic Derivatives

The hydrodynamic derivatives (or manoeuvring derivatives) are vital for the calculation of the hydrodynamic hull forces in each method aiming to simulate ship's manoeuvring performance in waves. Herein, a review is performed regarding the available ways in order to be determined. These consist of:

1. Captive model tests
2. System identification techniques
3. Semi-empirical methods
4. Numerical methods

Captive model test are executed in basins with scaled model of a ship, which is forced to move in a specific way. There are four different tests depending on the available infrastructure and scope of the study, namely the Oblique Towing Test (OTT), the Rotating Arm Test (RAT), the Planar Motion Test, which is performed with the use of a planar motion mechanism (PMM) and the Circular Motion Test (CMT). The derivatives are obtained after implementing an analysis of the measured hydrodynamic forces. In the mid-1960s (Chislett and Strom-Tejsen, 1965) first conducted PMM tests of a mariner vessel in order to obtain the hydrodynamic derivatives on the basis of a whole model approach. Subsequently, Norrbin (1970) executed OTT and RAT tests from which the hydrodynamic derivatives were obtained, whilst later Inoue (1981) conducted a series of test on the basis of Kose and Kijima's (1977) recommended procedure. Inoue's tests considered 10 different types of ships in several loading conditions. In this way, The aforementioned test facilitated the development of regression formulae in order to estimate the linear hydrodynamic derivatives, which can be proven quite helpful in cases where model tests are difficult to be performed either due to financial or time limitations. The drawback of these formulae is that they cannot be evaluated for the nonlinear derivatives as there is not a clear connection among ship's form coefficients.

About two decades ago, Simonsen (2004) presented a summary on the procedures which should be followed when conducting captive model tests whereas, many experimental data on hydrodynamic derivatives in deep and shallow water conditions can be found in the studies performed within the framework of relevant conferences and workshops (i.e. SIMMAN, MARSIM etc.) as stated in previous paragraphs.

System identification methods provide a convenient way to estimate the hydrodynamic derivatives from full-scale trails, without facing the disadvantages of captive model test. The most representative works in this field is the study from Abkowitz (1980) and Hwang (1980), who implemented Kalman filter process in order to get the hydrodynamic derivatives of *Esso Osaka's* full-scale trials. Additionally, Yoon and Rhee (2003), implementing *"an estimation before modelling"* technique, performed a study on the aforementioned ship as well.

With the progress in computational power since 1980s, many numerical methods were made possible to be developed. These methods can be summarized in two main categories according to He (2017). The first group includes the methods, which are based on a specific mathematical model and need to simulate certain forced manoeuvring motions in order to obtain the applied hydrodynamic forces and finally, the relevant hydrodynamic derivatives. The most crucial aspect in this type of methods is to incorporate the effect of the fluid's viscosity directly or indirectly as it plays an important role during ship's maneuvers. The methods of this category apply the potential theory and the effect of the viscosity is incorporated indirectly through the consideration of vortices.

Alternatively, CFD methods can be implemented, where the viscosity is incorporated directly, leading to more realistic representation of the flow field. A novel procedure which appeared the last two decades by Hochbaum (2006), Simonsen et al. (2006, 2012) and more recently by Fournarakis et al. (2016) is the use of CFD techniques to perform PMM tests as a way to obtain the hydrodynamic coefficients. The latter is a procedure that it is promoted by benchmarking workshops (i.e. SIMMAN) due to its low financial cost compared with model tests. The methods consisting the second category do not need to perform forced simulations in order to obtain the hydrodynamic derivatives, but implementing CFD techniques, it is possible to represent the flow field around the ship and obtain the hydrodynamic forces in a direct way. Subsequently, the equations of motion can be solved and provide the instantaneous position of the vessel.

Such methods are considered as the most realistic as they can model the complex flow field at the region of the rudder and the propeller and account for the interaction effects between hull-rudder-propeller. The drawbacks of these methods as stated in He (2017) are the high computational resources needed for the simulations and the fact that still some parameters of the CFD method require further investigation (i.e. the turbulence model and accuracy of the numerical solution at large drift angles).

2.1.6 Concluding Remarks

In sections 2.1.2 and 2.1.3 the major studies concerning time-domain methods for simulating ship's manoeuvrability in deep water waves were reviewed. In this aspect, the hybrid and the two-time scale methods consist of the two alternatives in order to couple seakeeping and manoeuvring theories. The importance of having accurate steady second-order wave forces as they drastically affect the derived trajectories was emphasized in all published studies. Subsequently, the review of available methodologies capable of calculating the aforementioned force components revealed that the size of the wavelength plays a significant role for the selection of the most suitable one. More specifically, far-field methods seem to be more appropriate for the calculation of the added resistance in case of short waves (e.g. Chroni et al.), whilst near-field methods should be implemented in case of long waves. Further, a review conducted concerning the available techniques for the determination of the manoeuvring derivatives. The discussion showed that nowadays the development of CFD methods consists of a powerful tool in case where experimental evaluation of the manoeuvring derivatives cannot be performed. Finally, manoeuvring under large amplitude waves requiring the incorporation of nonlinear Froude-Krylov and Restoring forces was performed only in the context of a small number of studies employing the hybrid method.

The need to investigate roll motion during ship manoeuvring in waves was addressed in some of the studies as well, whilst suggestions for future research were made concerning the impact of the vessel's metacentric height and forward speed on the resulting trajectories.

2.2 Calm Water Manoeuvring and Seakeeping Performance in Shallow Water

2.2.1 Manoeuvring in Shallow Water

Ships usually perform manoeuvers inside harbours where the sea depth is restricted however, studies on manoeuvrability and relevant IMO criteria apply in deep water condition, where the sea depth is more than three times the ship's draught and a marine vessel usually does not need to execute manoeuvers. Nevertheless, a straightforward correlation between ship's hydrodynamic response in deep and shallow waters would be invalid as many of the flow's properties change significantly as water depth reduces. For instance, in shallow water, ships sail at lower speed as an excessive increase in resistance is experienced, resulting in different manoeuvring characteristics which make them more "sluggish" (Hooft, 1973). In fact, the latter is true for a considerable range of forward speed values, whilst at high speed the wave resistance can be less than its value in deep water for the same speed value (Havelock, 1963).

In particular, when a ship sails in shallow water, the under keel space reduces in a vertical manner which leads to an increased value of the ratio $\frac{L}{h-T}$, which was introduced by Delefortrie and Vantorre (2007). As the value of the aforementioned ratio increases, which means that for a particular ship with length L the gap between her keel and the seabed becomes smaller, the flow surrounds the vessel more and more, the hydrodynamic reaction forces are increased and the vessel's motion is further restricted. Additionally, according to Fuehrer and Roemisch (1977) a back, or return, flow might appear in shallow or restricted areas (e.g. canals), which acts against ship's forward motion and forces the ship to sail in lower speed with the given installed power. Additionally, the increase of added inertias in shallower sea depths will cause an increase of the time constants related with Nomoto's equation (Nomoto, 1960), which means that the ship will have a delayed response after a rudder's action.

The last two decades more effort has been made in the area of ship manoeuvring in shallow and very shallow waters, where the under keel clearance is below 1.5 and 1.2 respectively (Vantorre, 2001). Moving from deep to medium deep water and then to shallow and very shallow water, the effects of the sea bed on ship's behaviour vary from negligible to highly dominating.

Within the framework of the activities of the 23rd ITTC (The Manoeuvring Committee, 2002), a review of available procedures was performed, which aim to evaluate the manoeuvring behavior of a marine vessel in shallow water and areas limited in width and depth. The problem that hinders the development of a robust approach, apart from its embedded hydrodynamic complexity, is the fact that the available sea trial results are scarce and until recently concerned solely the legendary case of the *Esso Osaka* container ship (Crane, 1979). The methods discussed in the aforementioned review are based on semi-empirical formulae. The first approach provides the values of the linear derivatives, which correspond to shallow water conditions, as a function of the relevant deep water values, implementing conformal mapping (Clarke, 1998). Analytical expressions of the same kind were proposed by Ankudinov et al. (1990) and the Japanese MMG (Hirano et al., 1985, Kijima et al., 1990, Kobayashi, 1995), and cover higher order terms and a broader range of sea depths. Semi-empirical relations of the manoeuvring related added masses and yaw moment of inertia between their shallow and deep water values can be found in Li and Wu's (1990) study.

Maimun et al. (2011) investigated the manoeuvring response of a pusher-barge in deep (h/d=3) and shallow waters (h/d=1.3) using a time domain numerical tool which implements the theoretical model developed by the Japanese MMG. Linear and nonlinear manoeuvring derivatives were obtained by PMM tests whereas semi-empirical values were considered as well using Kijima's empirical formulae (Kijima et al., 1990). Results showed that advance and tactical diameter in shallow water increased by 1.4 and 1.6 times respectively compared with deep water values, when experimental manoeuvring derivatives were used for the calculation of the viscous forces. In case of zig-zag simulations, slightly greater overshoot angles were noticed in shallow water and the motion of the barge becomes more sluggish. Results using empirical values were considered inappropriate at this stage as they could not comply with the relevant IMO procedures and criteria. Their inconsistency is attributed to the fact that they do not provide expressions for the correction of the longitudinal hydrodynamic force in shallow water, which might change significantly at a sea depth of approximately 1.3 times the ship's draught.

Koh et al. (2008) studied the influence that the sea depth has on the manoeuvring performance of a pusher barge as well. Contrary to Maimun's et al. work, their time-domain calculations showed that the turning circle of a pusher was smaller as the water depth decreased for both 20^o and 35^o rudder's angle, concerning mainly the advance values.

In that study, external hydrodynamic, propeller and rudder forces were modelled according to the MMG model, whilst manoeuvring derivatives were obtained from captive model tests for the deep, shallow and very shallow water cases. Additionally, the added inertias were calculated implementing seakeeping analysis where the free surface was modelled as a rigid wall and shallow water effect was taken into consideration. Corrections concerning resistance were not applied as the forward speed of the barge was very low (U=5kn) thus, it was below the sub-critical boundary where corrections are necessary according to Lackenby's (1963) suggestions. Rudder forces increased by an increment of approximately 100% in case of shallow and very shallow waters, which was considered as the major reason for the smaller turning circles.

Amin and Hasegawa (2010) studied ship manoeuvrability in shallow water in time domain as well, introducing expressions for various interaction coefficients between the hull, the rudder and the propeller and added inertias, which derived from regression analysis and incorporate the changes in flow's properties whilst, the shallow water values for the manoeuvring derives were obtained using Kijima's formulae. Contrary to Yasukawa's expressions (Yasukawa, 1998), who observed an increase of the wake factor due to smaller under keel clearance, the newly proposed formulae were considered more suitable for ships with larger block coefficient, and sea depth to ship draught ratio lower than 2. Results investigating *Esso Osaka's* manoeuvring performance in deep (h/d=6.0), shallow (h/d=1.5) and very shallow (h/d=1.2) calm water correlated acceptably with experimental data and depicted more significant effect on characteristic transfer and tactical diameter values as the water became very shallow. Advance seems to be practically unchanged, no matter how deep the water had been.

2.2.2 Vertical Ship Motions in Shallow Water

Most works on seakeeping simulations have been carried out under the assumption of infinite sea depth (deep water). However, as the size of the ships has increased the last decades, there is a high possibility for a marine vessel to sail in shallow waters, especially close to harbor areas or in access channels. In such conditions, ship's vertical motions can be severely affected, imposing hazards that might cause her grounding due to the unfavorable development of squat.

In order to deal with this problem, a few works have been published starting from Kim's (1969) publication, who first studied the effect of water depth on the hydrodynamic forces exerted on fixed and forced oscillating cylinders. For this purpose, he extended the deep water potentials introduced by Grim and Tamura to their shallow water form, exploiting Thorne's method (1953). He concluded that the finite depth has a remarkable impact on the heave, sway and roll hydrodynamic forces, which is expressed with higher wave damping and a varying difference of the added masses (higher or lower) compared with deep water values, for a wide range of frequencies.

Later on, Beck and Tuck (1971) investigated the shallow water effect on vertical motions of a freely oscillating series 60 ship at zero forward speed, implementing a 2D slender body theory, which is valid for long waves, and originally introduced by Tuck (1970) and consisted of a generalized version of Newman and Tuck's (1964) relevant infinite depth theory. Herein, the effect of a conventional mooring system is considered negligible as it plays a major role in horizontal modes of motion. The main objective of this study was to propose expressions for the calculation of the hydrodynamic coefficients and forces in shallow water, in order to facilitate the solution of the linear system of equations in such environmental conditions. Theoretical results, with respect to the ratio of ship length to wavelength, of non-dimensional hydrodynamic coefficients and vertical motions for deep (h/T=2.5) and shallow (h/T=1.5) waters, show small variations. However, it is stated that larger differences are expected if the results are plotted with respect to the wave frequency. The dominancy of the hydrostatic forces compared with the hydrodynamic added mass and damping loads was also highlighted, a fact that enabled the authors to apply a simplified first-order theory for the calculation of vertical motions. At that time, experimental results of ship motions in shallow water were not available thus, only qualitative conclusions could be extracted.

Plotkin (1977) extended the study of vertical ship motions of slender ships in shallow water including the non-zero forward speed case, by means of the so-called *"method of matched asymptotic expansions"* (Tuck, 1970), which is appropriate for wavelengths of the same order as the ship's length. Although it was a step forward considering the calculation of hydrodynamic added mass and damping values in shallow water due to its applicability in non-zero speed cases, the proposed method suffers from the same limitations at high frequencies as Tuck's method.

Contrary to Kim's, Tuck's, Beck and Tuck's 2D methods, Van Oortmerssen (1976) developed a 3D potential method, able to simulate linear ship's motions of a 200000 DWT tanker in shallow water. The selection of a 3D instead of a 2D method is considered more appropriate as it can represent the three-dimensional flow pattern around the ship's hull sufficiently with the reduction of the under keel clearance. Results on hydrodynamic forces showed that as the water depth decreases, added mass and damping terms increase significantly. In this publication, the numerical results were validated using relevant experimental data.

Unsteady RANS solvers have been used in the field of time domain simulations of vertical motions in shallow water as well, offering the possibility to account for the effect of the viscosity, which is considered more significant as the ship's keel approaches the sea's bottom (Beukelman and Gerritsma, 1982). Tezdogan et al. (2016) implemented a CFD analysis in order to investigate the seakeeping performance of a 200000 DWT tanker (Van Oortmerssen, 1976) in deep (h/T=3.0 & 4.365) and very shallow water (h/T=1.2). Comparison of their results was conducted against available 3D potential and experimental ones. At that time, the shortage of the latter caused problems during the process of validation of a numerical method in the field of shallow water seakeeping analysis. That led the Ocean Engineering Committee of the IITC (2014) to suggest the execution of benchmark experiments in order to be used for validation purposes. Results obtained from their developed URANS solution at zero-speed condition, provided quite accurate non-dimensional values (RAO) for heave and pitch motions compared with available experimental data, whilst the 3D potential method generally overestimates ship's motions for a wide range of wave frequencies. Additionally, as the water depth decreased, ship motions tend to be smaller, apart from the case of pitch motion at very low wave frequencies, where an opposite trend is noticed.

Tello Ruiz et al (2015) investigated ship's vertical motions in shallow water as well, in the context of a 6-DOF analysis of ship's manoeuvrability in adverse weather conditions. Experimental data of ship motions and wave forces for a 1/75 scale model of the KVLCC2 tanker, which was systematically tested within the research project SHOPERA, compared against the results of several 2D and 3D hydrodynamic software in both zero and non-zero speed conditions and various wave headings and periods. In general, ship motions and first order wave forces are more accurately predicted when 3D panel methods are employed.

Further, numerical prediction of the first-order yaw moment seems to be the major drawback of the utilized software. The calculation of the mean second-order forces was proven more consistent with the experimental values in case where near, middle and far field methods were adopted (Hydrostar), rather than pressure, moment integration and moment flux on a control surface methods (WAMIT). Finally, it was observed that the maximum amplitude of linear vertical motions occurred at $L_{pp}/\lambda \approx 3$.

The NTUA's 3D panel code NEWDRIFT v.7 includes "not too shallow" water depths within its implemented analysis of first and mean second-order wave forces.

2.2.3 Concluding Remarks

Investigation of shallow water effect on a marine vessel's manoeuvrability in calm water by means of time-domain methods has been primarily achieved by means of corrected values of the manoeuvring derivatives. This process involves the implementation of regression formulae which are functions of the under keel clearance. Among the various efforts, Ankudinov's formulae are distinguished as they consider the values of linear and nonlinear derivatives for a wider range of shallow and very shallow sea depths. Further, since the flow's pattern changes from deep to shallow water, relevant formulae have been published for the correction of other parameters and interaction coefficients.

Concerning the assessment of a ship's seakeeping performance in shallow water, the majority of research works adopt the potential theory (2D or 3D), which has been proven more suitable in case of low wave frequencies (wavelength equal to the vessel's length). Deeper insight on a vessel's seakeeping performance at shallow and very shallow waters was provided by recent CFD methods, which account for the increased viscosity in such cases.

2.3 Direct Stability Assessment

2.3.1 Introduction

Dynamic stability of ships is studied in the context of the Second Generation Intact Stability Criteria (Belenky et al., 2011, Umeda, 2013). These criteria, which are under finalization by the IMO, are based on physical representation of the ship-wave interaction and therefore, can be applied for any type of marine vessel. The studied phenomena include pure loss of stability in astern seas, synchronous roll under dead ship condition, parametric roll, broaching and excessive accelerations. In the context of the present study, emphasis is given on parametric roll of fine form ships through time-domain analysis, as a way to ensure that the developed numerical tool satisfactorily incorporates the nonlinearities associated with the ship-large amplitude wave interaction.

In this section, several works, which have been conducted concerning dynamic stability in waves, will be critically reviewed. Focus is given on the type of the implemented analysis and the coupling among different degrees of freedom (linear or nonlinear), and the considered environmental and operational conditions at the time where each dynamic instability phenomenon identified.

Some of the research works that are mentioned in this chapter, adopt the 2-D strip theory, in order to derive the seakeeping hydrodynamic data (Salvesen et al., 1970), which is appropriate for slender ships. However, some other, are based on 3-D panel theories (e.g. Papanikolaou and Schellin, 1992) for the estimation of the hydrodynamic coefficients (frequency dependant added masses and damping coefficients), which generally provide more accurate results.

2.3.2 Parametric Roll

Hamamoto and Saito (1992) conducted a fundamental research work on 6-DOF time-domain simulations of ships sailing in waves. Coupling between vertical motions (heave-pitch) is taken into consideration. Lateral motions (sway-roll) are also coupled however, coupling between vertical and lateral degrees of freedom was not considered.

Surge motion was considered uncoupled with respect to any other degree of freedom. Radiation forces were incorporated by means of impulse response functions, using frequency dependent damping coefficients. Practical formulae for the calculation of Froude-Krylov and Restoring forces, expressed at the Horizontal Body-Fixed System, were provided. In these expressions, forces are calculated with respect to the actual wetted surface for each 2-D lateral section of the ship and can be used for nonlinear analysis. Apart from the aforementioned appropriateness of this methodology in simulating ship's manoeuvring performance in waves, it is also capable of investigating modes of dynamical instability of ships in waves as it was shown by several following studies.

Hamamoto et al (1991) used the aforementioned practical model as well, for the detection of parametric roll of a container ship. Simulations were carried out for different values of parameters such as the forward speed, the ship's metacentric height and different values of wave height to wavelength ratio. Various values for the relative position of the ship's centre of gravity to a wave crest were also tested, considering waves of approximately the same length as the length of the ship. Parametric roll was detected for encounter frequency less than the natural frequency of roll, 1.07 to 1.38 times. For increasing wave steepness, roll motion became larger leading to capsize ($H/\lambda=0.05$). Same tendency was observed for decreasing values of the ship's metacentric height. Effect of forward speed and heading angle showed that there is not a global response pattern when different speed values were considered. Additionally, small deviations from the pure following condition seem to be more dangerous regarding parametric roll excitation. Implementation of a more sophisticated method than Takahashi's practical formula for the calculation of the roll damping coefficient might have shown more rational roll behaviour.

Ayaz (2003) performed a study on the impact that following and oblique waves have on ship's stability. He investigated roll motion when encounter frequency approaches the value of the wave frequency and surf-riding with resulting broaching when the vessel's velocity is high enough to overtake the waves. Results from numerical simulations using a nonlinear model including wave and environmental forces for surge, sway, heave and roll equations were presented, where lateral plane motions are considered independent of vertical ship motions. Parametric roll and surf-riding/broaching initiation and development criteria were intensively studied for low encounter frequency cases.

Experimental validation of the demonstrated results, as well as extensive investigation of the studied phenomena for more heading angles, consist of the drawbacks of this research. A more extended study on the influence of GM for several wave headings is also essential.

Shin et al. (2004) studied parametric roll in longitudinal seas, both following and head. Explanation of the underline physics of this phenomenon is given by analysing the variation of a ship's waterline from a wave trough to a wave crest. When a ship encounters two crests and two troughs during one natural roll period, roll angle amplification may be initiated, a fact that will lead to parametric excitation if course keeping and sea state stay constant with time. According to their study, head seas parametric roll can happen more easily when it is coupled with heave and pitch motions as these motions are more severe. Apart from the specific condition regarding the encounter frequency of the vessel, nonlinear roll damping plays an important role for the elimination of this phenomenon. In real cases, roll damping rarely decreases below the threshold value where ship could capsize. One degree-of-freedom Mathieu equation is presented in this work for the detection of parametric roll of several container ships implementing nonlinear restoring and damping terms in the context of initial susceptibility check. Importance of restoring characteristics is indicated against roll damping modelling. A verification procedure on parametric roll identification in regular waves was also proposed and tested for nine ships.

Munif and Umeda (2000) studied the effect that low metacentric height values have on the behaviour of a ship under parametric resonance, sailing with moderate forward speed, by implementing a 6-DOF as well as 4-DOF nonlinear mathematical models. For low wave steepness values, 4-DOF numerical simulations compare well with experimental results, whereas for higher wave steepness coupling of heave and pitch has a significant effect on roll angle. Additionally, they claimed that a heading angle between 30 and 45 degrees astern, can be considered as more dangerous regarding parametric resonance than angles between 0 and 15 degrees astern. Further study is needed in order to develop 6 – DOF suitable to simulate ship motions of high speed vessels.

Spanos and Papanikolaou (2006) worked on a 6-DOF nonlinear numerical simulation of parametric roll of a fishing ship in the time-domain and in head seas. They recorded a strong dependence of the vessel's encounter frequency and wave height on parametric roll initiation.

A value of encounter frequency that is double the roll natural frequency was indicated as a fact that may trigger such unstable response. Considering low to high wave amplitudes and low to high forward speed, two types of dynamic instability failure modes were noticed. The first one refers to pure loss of stability at a wave crest, followed by ship's capsizal in steep waves when GM has a low value and the vessel's forward speed is high enough. Concerning the second one, ship's capsizal occurs after the progressive built-up of the roll angle at lower wave amplitude and higher forward speed. Nonlinearities due to the variation of the wetted surface are responsible for a significant coupling between pitch and roll motions which subsequently play an important role for the initiation of parametric roll. Motion induced diffraction and radiation forces were incorporated by the use of a linear, 3-D frequency domain panel code (NEWDRIFT V.6, Papanikolaou, 1989). Experimental validation of their results is still an issue of future research.

Turan et al (2008) presented a study on the impact that some modern modifications, related to propulsion and steering, have on ship's stability. In this context, fixed and azimuthing pods where considered as propulsive and steering mechanisms during ship's course keeping. The analysis performed with a nonlinear 6 – DOF mathematical model, able to conducted analysis for ships having moderate to high forward speed. Auto – parametric rolling behaviour, defined when $\omega_e=2\omega_\varphi$, was detected by implementing the aforementioned nonlinear numerical analysis as a result of the low GM value and reduced roll damping of the ship which had to accommodate in its aft region the heavy pod devices. In the contrary, excellent manoeuvring behaviour was achieved when calm water conditions were considered.

Spyrou (2000) studied parametric roll of ships by implementing a single DOF equation model under bi-chromatic waves' excitation. Limits of the forcing amplitudes which may lead to capsize were provided when adopting linear or nonlinear restoring and damping models.A single Mathieu-type equation for parametric roll investigation is considered quite doubtful because it adopts linear restoring approximation. As it was suggested at that time, although ship designers had theoretical knowledge of the link between parametric instability and nonlinear restoring and damping aspects, still faced the problem of incorporating such knowledge for safer hull forms.

Hashimoto and Umeda (2004) implemented a single-DOF as well, in order to study parametric roll of a container ship in longitudinal and quartering seas.

The wave effect on roll restoring moment was incorporated in a realistic way by direct measurements from captive model tests as Froude-Krylov approximation for roll restoring overestimates the danger of capsizing due to parametric roll in longitudinal seas. Relationship of the measured values of roll restoring moment with Froude number was not confirmed by the calculated results, it was also proved by use of Poincare mapping that parametric roll in longitudinal seas is more possible to happen than in oblique seas. For the sake of a more rigorous validation of the method presented in this work, head seas condition could be a future task.

Bulian and Francescutto (2011) modelled roll dynamics in beam waves under multi-frequency excitation by implementing three different 1-DOF equations. Two of these equations adopt nonlinear expression for the calculation of the roll restoring moment by incorporating the nonlinear GZ(φ) curve once with regards to the absolute roll angle and once for the relative roll angle which is considered as being closer to the actual physics. The third roll equation uses a linear restoring approximation. Nonlinear roll damping was considered in all cases. The difference while a ship sails in beam waves is that roll angle might be unfavourably increased when the wave frequency is approximately equal to the natural roll frequency. Results for a typical bulk carrier show that the adoption of linear roll restoring modelling provide overestimated roll motion leading to capsize.

Almost a decade before the aforementioned publication, Taylan (2000) studied the roll amplitude of four different ships with a single-DOF nonlinear model in regular beam seas. In his work, three different expressions of nonlinear damping and two for roll restoring moment were tested. Duffing's solving technique of differential equations in the frequency domain was used for the derivation of the solution of the nonlinear equations in each case. Results show a significant dependence of roll amplitude on the considered damping model. Discrepancies among the results show that a proper selection of nonlinear damping model as well as a more realistic approximation of roll restoring moment is of vital importance as it concerns the accurate prediction of the maximum roll amplitude. Polynomials of quantic-order for the representation of the GZ-φ curve are thought to be closer to the reality.

Matusiak (2003) investigated parametric roll occurrence for a RoPax vessel using both numerical and experimental techniques.

In the context of the numerical investigation, a "two-stage" 6-DOF nonlinear tool was developed whilst, forcing and response were separated in two parts, namely a linear and a nonlinear part. The conclusions of this research depict that roll amplitude can be related with the square of the amplitude of the wave and a possible increase of the wave's amplitude leads to lower encounter frequencies where parametric roll can be initiated. Same tendency was also observed when initial heel was added to the system of equations. Finally, a roll-yaw coupling relationship was detected during the development of parametric roll.

Nonlinear dynamics associated with parametric roll for the ITTC A2 ship was also studied by Umeda et al (2003) using experimental, geometrical and analytical approaches. Realistic modelling of the restoring moment was considered by means of a 9^{th} order polynomial fitted on the actual GZ-φ curve in still water. Experimental results showed that the Froude-Krylov assumption overestimated the wave effect on ship's stability, providing larger variations of her metacentric height leading to overestimations regarding the dangerous situations where the ship might capsize as well. Numerical results for a wavelength-to-ship length ratio of 1.5 revealed that parametric roll is more possible to happen for a value of the Froude number equal to 0.2 in following seas. Such behaviour vanishes for low wave steepness ratios (< 0.014) whereas for greater values roll angle increase or diminution might occur. Additionally, one of the key findings of the paper discussed in this paragraph is that increasing GM value does not eliminate the possibility of parametric rolling when moving from following to head seas.

Jiang et al. (2014), in their research, presented criteria for the capsizing of vessels due to parametric roll in random beam seas by adopting a single DOF model in roll motion including also the memory effects (Melnikov function). Memory effects play a dominant role regarding the accurate assessment of a ship's motions against parametric roll and possible capsize. A critical value for the significant wave weight was evaluated from this study, which was verified by the numerical simulations.

In October 1998 a C-11class container ship suffered from extreme roll angles when it was found in severe weather conditions, sailing in head seas. The study followed by France et al. (2003) investigated for the first time head and bow-quartering seas parametric roll in regular and short wave irregular seas through numerical and experimental techniques.

Until that time, this failure mode was never considered as a risk for ships therefore, studies were not carried out even during the design stage of a C-11 container ship. The study was performed by implementing low (single-DOF uncoupled Mathieu roll equation) to high level of sophistication numerical tools that revealed that parametric excitation can be initiated when the roll natural period is double the encounter frequency. For the case where linear roll damping was considered, broader range of natural roll to encounter period ratio was recorded where parametric roll was detected, a fact that shows an overestimation of roll response. This demonstrates the significant role that nonlinear roll damping has when conducting parametric roll simulations. For robust conclusions to be made, more ships with flat transom sterns and significant bow flare have to be tested against head-seas parametric roll.

Head – seas parametric roll was also the objective of Neves and Rodriguez's (2006) research work by adopting a derivative mathematical model. Their study involved the investigation of a transom stern fishing vessel against head-seas parametric roll by means of a 3-DOF numerical tool, which incorporates equations for heave, roll and pitch motions. Wave loads consist of Froude-Krylov and diffraction first-order components. Results show that for low GM values and when second-order expressions for the force and moment derivatives are used, roll response is overestimated. With the adoption of third-order formulas, numerical results agree quite satisfactorily with the experimental results. For greater values of GM, no difference between second and third-order model was noticed.

Hamamoto and Munif (1998) presented an analytical mathematical model about ship capsizing due to parametric roll in extreme astern excitations, based on linear strip theory calculations. Instead of the simplified roll restoring moment $M_R=WGM\varphi$, a linearized expression for the roll restoring moment was adopted, when the variation of the ship's metacentric height from a wave trough to a wave crest was incorporated for a 15000GT container ship. Strip theory imposed limitations on the performed analysis such that, it only accounts for small amplitude oscillatory motions of higher frequency, in the context of linear wave theory. Unstable condition with regards to parametric roll development and in terms of wave encounter frequency was given by the following expression.

$$\omega_e = \sqrt{\frac{g}{L}}\left|\sqrt{\frac{2\pi L}{\lambda}} - Fn\frac{2\pi L}{\lambda}\cos\chi\right| \tag{2.1}$$

Results of this study show that for the design and operational values of GM, a heading angle of $\chi=45^{o}$ could lead to dangerous condition regarding parametric roll development, whereas for lower GM value the critical value of the heading angle is $\chi=60^{o}$ in order to satisfy the condition referring to the encounter frequency mentioned before (Eq. 2.1).

In another work by Hamamoto et al (1995), low cycle resonance stable and unstable regions for both a container carrier and a purse seiner were defined by use of a single DOF roll equation. Roll restoring action was estimated by a newly proposed method which provided linearized approximation of the variation of the metacentric height. Parametrical studies conducted for different encounter periods and wave heights. Studies have shown that in case of the container ship, unstable region which may lead to the ship's capsizal appears for ratios of encounter period to natural roll period $T_e/T=0.25$, 0.50, 0.75 and 1.0. The aforementioned values coincide with the ones proposed from the solution of a Mathieu – type equation. Additionally, the unstable region was increased when higher values of wave steepness were considered. In case of purse seiner, unstable region was indicated only for the case where wavelength was equal to the ship's length. For both ships, stable region was increased for ratios of wavelength to ship length greater than 1.0.

The 26th ITTC Report of the Specialist Committee on Stability in Waves (2011), presented the state-of -the art on numerical and physical investigation of parametric roll until that time. Emphasis was given on the accurate incorporation of roll damping in the developed numerical tools. For that reason, new methods that could analyse, in a better way, experimental results from roll decay tests together with numerical methods which predict roll damping should combine for a more realistic evaluation of roll damping. In order to validate and accredit numerical methods that simulate ship's dynamic stability governed by large amplitude motions, predicted hydrodynamic forces have to be compared against experimental results such those published by Fullerton et al. (2008). Such comparison between experimental and numerical time histories of the hydrodynamic forces and moments provided also by Belknap and Telste (2008) as well as by Grochowalski and Jankowski, (2009) ensures naval architects that the physics of ship dynamics is properly modelled.

In case of head-seas parametric roll, vertical motions become more severe as it was mentioned previously. For that reason, it is of vital importance that they are accurately predicted. In this context, a recent study by Riesner et al (2016) attempted to present a 3D boundary element nonlinear method capable of simulating vertical motions with satisfactory agreement. Impulse response functions calculated for both added masses and damping coefficients. Results of the adopted model in 6-DOF showed that even when linear Froude-Krylov and restoring forces were incorporated into the model, discrepancies still existed compared against linear frequency domain and CFD studies. For zero forward speed it was suggested that convolution integrals of the damping coefficients should be used, although for the case of non-zero forward speed both impulse response approximations show their own advantages and disadvantages. Further, nonlinear incorporation of Froude – Krylov and restoring forces and moments introduce a shift on the results presented in their research work.

At this point, it should be noted that valuable benchmark data regarding the numerical investigation of parametric rolling in regular, group and irregular waves were provided through the international study delivered in 2009 within research project SAFEDOR (Spanos and Papanikolaou, 2009). The study referred to the ITTC A1 hull form, whereas 13 were the total participants. The study concluded that further work was needed at that time since the validity of the numerical codes was proved low. Additionally, better predictions were observed for codes that adopted 3D hydrodynamic theory.

Recently, in IMO's report of the 6th session of the SDC (2018) on the finalization of the SGISC, guidelines were published concerning the recommended procedures which must be followed in order to perform a direct stability assessment of a ship. The aforementioned report, determine the requirements that a time-domain numerical tool must fulfill in order to be judged suitable for the investigation of each stability failure mode. Specifically, in case of parametric roll, it is recommended that the developed software must be able to perform at least a 3-DOF (heave-roll-pitch) nonlinear analysis. Concerning the other degrees of freedom a static equilibrium assumption can be considered. Additionally, instructions are given regarding the proper incorporation of significant force elements (i.e. roll damping) and the modelling of the environmental and operational conditions where each failure mode is expected to occur. Further, instructions on how to verify and validate software aiming to perform DSA are included in this report.

The aforementioned guidelines had been taken into consideration during the development of the numerical tool ELIGMOS, which was further used for the Direct Stability Assessment against head-seas parametric roll of a C-11 class container ship against parametric roll.

Broaching-to is another stability failure mode, which is characterized by an unintentional and violent yaw motion, despite maximum opposite rudder's deflection, when a rapidly moving ship overtakes following waves. In such heading angle, where encounter frequency tends to be zero, hydrodynamic forces consist mainly of lift components and together with high forward speed (Fn>0.3) may lead to unfavourable surf-riding and finally broaching-to conditions. Usually, broaching is accompanied by a significant heel angle, which may cause the ship's capsizal in extreme environmental conditions. Together with, pure loss of stability, dead ship condition and excessive accelerations, they constitute the framework of the Second Generation Intact Stability Criteria. However, due to the time constraints of the present study, made their investigation impossible.

2.3.3 Concluding Remarks

Review of research works dealing with the investigation of parametric roll in the time-domain revealed the complexity that accompanies the process of its identification. In order to perform DSA of a ship against parametric roll, the inclusion of (at least) heave and pitch degrees of freedom is considered necessary as the severity of the aforementioned motions decisively affects the development of this stability failure mode. Thus, valid nonlinear time-domain modeling of a ship's vertical motions is a prerequisite. Parametric roll may occur in pure following or head waves, whilst the performed review showed that stern oblique waves consist of the most dangerous operational condition. Finally, ships with large deviations of their waterplane area far from the still water level (e.g. container ships) are more prone to suffer from parametric roll. Therefore, DSA with validated numerical codes consists of a powerful tool during their design stage.

2.4 Summary-Research Gap

Starting this chapter, an extensive review of published studies in the field of ship manoeuvring waves was presented. The two available methods in order to perform such an analysis are the two-time scale and the hybrid one. The difference between the aforementioned approaches is that in the former, seakeeping and manoeuvring modules are solved independently, whilst an interaction between them is established at a predefined slow varying heading angle or forward speed increment. Concerning the hybrid method, the equations of ship manoeuvring motion in waves are solved simultaneously, accounting for both seakeeping and manoeuvring force components. In two-time scale methods, mean second-order forces are considered the only contribution from the waves, as they seem to have a major impact on the ship's manoeuvring trajectory. Additionally, almost all studies referred to regular seaway and deep water conditions. For that reason, the flow's changing hydrodynamic properties in shallow water were discussed solely in the context of manoeuvring in calm water and seakeeping analyses. From the existing research, it was indicated that hydrodynamic loads increase with the reduction of the under keel clearance as an increasing portion of the flow passes around the ship and not beneath it, making her more sluggish.

Therefore, it is concluded that **there is a knowledge gap in the field of time-domain simulation of ship manoeuvring in shallow water seaways**, where a ship might face close to harbor areas or access channels. The hazards that arise from such environmental conditions would have a negative impact on the collision avoidance capabilities of a marine vessel, making her collision or grounding a possible scenario.

As a way to ensure that a nonlinear method can be implemented for the investigation of ship's manoeuvrability in adverse weather conditions, its ability to perform direct ability assessment is considered necessary. In the present thesis, this is done through the identification of parametric roll, which consists of one of the dynamic stability failure modes investigated within the framework of the SGISC. An accumulative table where someone can find and compare the available numerical methods, which are able to conduct manoeuvring simulations in waves, is given below.

Table 2.1: Taxonomy of existing time domain methods
for ship manoeuvring simulation in waves

Available Numerical Methods used for the Investigation of Ship's Manoeuvring Performance in Waves	**Seakeeping Modelling**	**Number of Considered Degrees of Freedom**	**Wave Modelling**
Hybrid Method	2D/3D	3DOF/4DOF/6DOF	Excitations & Sea Depth
Bailey et al. (1997)	NA	6DOF	Small & Deep
Hamamoto and Saito (1992)	NA	6DOF	Large & Deep
Fang et al. (2005)	2D	6DOF	Large & Deep
Sutulo and Soares (2006)	2D	6DOF	Large & Deep
Ayaz et al. (2006)	2D	6DOF	Large & Deep
Fossen (2005)	2D	6DOF	Large & Deep
Ghillece and el Moctar (2018)	3D	6DOF	Small & Deep
Present	**3D**	**4DOF**	**Large & Shallow**
Two-Time Scale Method			
Hirano (1980)	2D	3DOF	Small & Deep
Skejic and Faltinsen (2008)	2D	6DOF	Small & Deep
Yasukawa and Nakayama (2009)	3D	6DOF	Large & Deep
Chroni et al. (2015)	3D	4DOF	Small & Deep
Fournarakis et al. (2016)	3D	4DOF	Small & Deep
Seo and Kim (2011)	3D	6DOF	Small & Deep
Zhang and Zou (2015)	3D	6DOF	Small & Deep
Subramanian and Beck (2015)	2D	6DOF	Large & Deep
He (2017)	2.5D	4DOF	Small & Deep

In Table 2.1 the existing methods developed in the context of time domain ship manoeuvring simulations in waves are presented. Their main characteristics are described in columns 2, 3 and 4. In each study, the aforementioned characteristics refer to the method adopted to calculate the seakeeping-related forces (i.e. added mass, damping and, when applied, the first-order wave forces), the motions that are included in the adopted analysis and the way the environmental conditions were modelled. The latter, concern the size of the waves (small or large amplitude waves), which impose the implementation of either linear or nonlinear seakeeping analysis. In the present thesis, the crucial element in order to classify each method to the linear or the nonlinear ones, in terms of the implemented methodology used to incorporate the first-order wave forces, is whether the formulation of the equations of motion is given with respect to the horizontal axes system. Additionally, nonlinearity can be captured when body-exact seakeeping methods are implemented, as those proposed by Subramanian and Beck (2015).

The aforementioned alternatives allow the incorporation of nonlinearities associated with the wave force calculation at large amplitude waves. As it is indicated in the last column, the studies depicted in Table 2.1 were conducted under the assumption of infinite sea depth, which is a fact that verifies our inceptive allegation stated previously in this section, that the present research, which studies ship's manoeuvrability in shallow water, is innovative.

CHAPTER 3

THEORETICAL BACKGROUND

3.1 Introduction

The extensive review presented in the previous chapter revealed the available methods which can be used in the field of direct stability assessment and in time domain simulation of a ship manoeuvring in a seaway. Additional studies attempting to model the effect of shallow water on the flow's characteristics in case of calm water manoeuvers and straight course keeping in waves were also discussed. The latter, were investigated in the context of potential flow theory whilst manoeuvring related lift and drag forces, were calculated using experimentally or empirically evaluated derivatives.

In Chapter 3, the theoretical background used for the formulation of adopted methodology will be demonstrated, starting from the description of the wave-rigid body interaction problem in deep and shallow waters adopting frequency domain analysis. The approach implemented in the present study in order to express all the external forces and moments due to the presence of waves in the time- domain will be demonstrated as well, emphasizing on the derivation of the Impulse Response Functions of the frequency dependent damping coefficients. Numerical results used for validation purposes of the time-domain seakeeping analysis will be depicted in Chapter 6.

Apart from the seakeeping analysis, focus will be given on the formulation of the nonlinear equations that govern the manoeuvring motion of a ship in calm water. Usually, this problem is studied on the horizontal plane (surge-sway-yaw) however, for ships with high metacentric height, the inclusion of roll equation is required as it significantly affects vessel's manoeuvrability. In the present thesis both 3-DOF and 4-DOF nonlinear manoeuvring models have been developed, which are validated against experimental results or available sea trials in following chapter.

At the begging of the present chapter, a detailed presentation of the coordinate systems used in the framework of the present thesis will be given. The considered reference frames consist of the **earth-fixed (n-frame)**, the **hydrodynamic or seakeeping (h-frame)** and the **horizontal body-fixed (b-frame)** used for seakeeping, manoeuvring and manoeuvring in a seaway analyses.

3.2 Coordinate Systems

- **Earth-Fixed Reference Frame, OXYZ (n-frame):** This reference system remains fixed at a certain point on the mean free surface. At the end of each time step, all translational and rotational displacements are expressed with respect to the earth fixed reference frame. Within the present analysis, Z-axis points upwards and X-axis points towards the direction of the forward speed.
- **Hydrodynamic or Seakeeping Reference Frame, $O_hX_hY_hZ_h$ (h-frame):** Hydrodynamic reference frame is an inertial coordinate system as well, which is used in time domain seakeeping simulations. The orientation of the h-frame with respect to the earth-fixed coordinate system is fixed however, h-frame moves with the ship's average speed lying at the equilibrium position of the undisturbed sea surface. Usually, the origin of the h-frame is placed on the longitudinal position of the vessel's centre of gravity and on the calm water leverl, in order to simplify the equations of vertical motions. Transformation of the body coordinates to the h-frame is done through the non-orthogonal matrix $T_h(\theta)$, where θ is the eulerian pitch angle which defines the instantaneous angular position of the ship with respect to the h-frame since yaw and roll angles in case of seakeeping analysis are zero.

$$T_\theta = \begin{bmatrix} \cos\theta & 0 & \sin\theta \\ 0 & 1 & 0 \\ -\sin\theta & 0 & \cos\theta \end{bmatrix} \tag{3.1}$$

$$\begin{bmatrix} x_h \\ y_h \\ z_h \end{bmatrix} = T_\theta \begin{bmatrix} x \\ y \\ z \end{bmatrix} \tag{3.2}$$

Added mass and moment of inertia can be considered constant in time since pitch angle is less than 8-10 degrees even when large excitations take place (Fonesca and Soares, 1998).

When the numerical method is used for the simulation of large amplitude motions, or when roll oscillations occur, hydrodynamic reference frame is not valid anymore therefore, the hydrodynamic body-fixed reference frame has to be used in order to construct the system of motions' equations.

- **Horizontal Body-Fixed Reference Frame, $O_{hs}X_{hs}Y_{hs}Z_{hs}$ (hs-frame):** As mentioned in Chapter II, Horizontal Body-Fixed Reference Frame was first introduced by Hamamoto and Kim (1993). This system allows the mutual representation of nonlinear seakeeping and manoeuvring terms thus, it is suggested in the context of time domain simulation of ship's manoeuvrability in a seaway. Additionally, in absence of waves, this reference system can be used for calm water manoeuvring simulations whilst, in case of zero rudder deflection seakeeping simulations can be conducted investigating dynamic failure modes such as parametric roll. The matrix, which is used in order to rotate the body's coordinates from a general body-fixed reference system to the horizontal body-fixed reference frame, can be shown below.

$$T = \begin{bmatrix} \cos\theta & \sin\theta\sin\varphi & \sin\theta\cos\varphi \\ 0 & \cos\varphi & -\sin\varphi \\ -\sin\theta & \cos\theta\sin\varphi & \cos\theta\cos\varphi \end{bmatrix} \tag{3.3}$$

$$\begin{bmatrix} x_{hs} \\ y_{hs} \\ z_{hs} \end{bmatrix} = T \begin{bmatrix} x \\ y \\ z \end{bmatrix} \tag{3.4}$$

Subsequently, the equation of the elevation of the free surface with respect to the horizontal body-fixed reference frame at each time increment is depicted.

$$\zeta = x_{hs}\theta + a\cos k(x + x_{hs}\cos\psi - y_{hs}\sin\psi - ct) \tag{3.5}$$

In the former Equations (3.3)-(3.5) x_{hs}, y_{hs}, z_{hs} are the coordinates of the body's surface at the horizontal body-fixed reference frame while, φ, θ, ψ denote the eulerian roll, pitch and yaw angles respectively. Further, a and c are the wave's amplitude and celerity respectively whilst, k is the wave number.

As it was mentioned before, the final motions and position of the ship is given in the earth-fixed (n-frame) reference system. This is succeeded by applying the following transformations of the velocities.

$$U_n = \cos\psi \cdot U_{hs} - (\sin\psi \cdot \cos\varphi)V_{hs} \tag{3.6}$$

$$V_n = \sin\psi \cdot U_{hs} + (\cos\psi \cdot \cos\varphi)V_{hs} \tag{3.7}$$

$$R_n = \cos\varphi \cdot R_{hs} \tag{3.8}$$

In the relationships 3.6-3.8 subscript "n" refers to the velocities in the earth-fixed reference frame whilst, subscript "hs" refers to the velocities in the horizontal body-fixed reference system. Schematic representation of the aforementioned reference frames can be seen below.

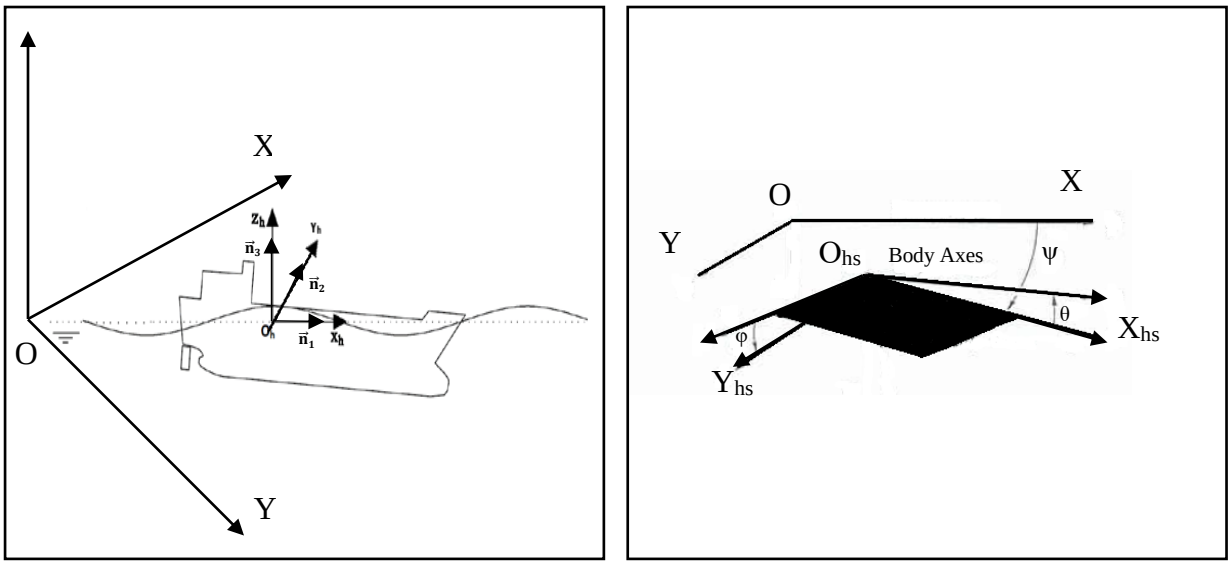

Figure 3.1: Coordinate systems

3.3 Seakeeping Theory

In the present sub-chapter of the thesis, the formulation of the frequency-domain, wave-rigid body interaction BVP will be presented, as the current time-domain solution (both linear and nonlinear) depends on the aforementioned frequency-domain analysis. At the beginning (Chapter 3.3.1), the formulation of the nonlinear BVP will be given, providing the adopted linearization procedure using the properties of the potential theory that will finally result to the decomposition of the velocity potential. Frequency-domain analysis of linear ship motions is performed using the numerical software PRECAL (Van't Veer, 2009) and NEWDRIFT (Papanikolaou, 1985), (Papanikolaou and Zaraphonitis, 1987). The latter, was further developed by Liu et al. (2011) and Liu et al. (2015), in order to offer the possibility to calculate the ship's added resistance implementing a more appropriate method in case of short waves.

3.3.1 Formulation of the Frequency Domain Boundary Value Problem

As stated in Newman (2017), the motion of every viscous fluid is governed by the Navier-Stokes and continuity ($\nabla \cdot \vec{V} = 0$) equations, assuming it has constant density and follows a Newtonian stress-strain expression. However, due to difficulties in solving the aforementioned coupled nonlinear system of partial differential equations, certain simplifications must be implemented.

The first one involves the neglect of the fluid's viscous attributes by considering the creation of a thin boundary layer. In this case, a fluid's volume can be thought practically as **inviscid or ideal**. The aforementioned simplification has a decisive impact on Navier-Stokes equations, whose solution becomes more feasible for various types of physical problems employing the inviscid flow property.

The second assumption that further simplifies the equations that govern the fluid's motion is that the latter remains **irrotational** for every closed contour of a moving body in the fluid (equivalently someone can say that the flow's vorticity is zero, namely $\nabla \times \vec{V} = 0$). This property results from Kelvin's theorem of the conservation of circulation, which is a direct outcome after considering no shear stresses imposed by the fluid that could change the rotation rate of its particles.

A significant outcome that is derived when assuming a flow as irrotational is that its velocity field can be represented by means of the gradient of a scalar function, namely the velocity potential Φ based on the three spatial coordinates x, y, z and the time t.

According to Ogilvie and Tuck (1969) the total velocity potential Φ can be decomposed into a steady and an unsteady component, namely Φ_S and Φ_T. Such a decomposition is valid under the assumption of low forward speed and small amplitude incident waves, resulting in proportionally small ship motions.

$$\Phi(x,y,z;t) = [-Ux + \Phi_S(x,y,z)] + \Phi_T(x,y,z)e^{-i\omega_e t} \tag{3.9}$$

In Equation (3.9), ω_e is the frequency of encounter, which is calculated using the following relationship

$$\omega_e = \left|\omega - \omega^2 \frac{U}{g}\cos\chi\right| \tag{3.10}$$

where, ω is the wave frequency, U is ship's forward speed, χ is the heading angle with respect to the wave's direction and g is the gravitational acceleration. Additionally, i stands for the imaginary unit namely, $i = \sqrt{-1}$.

Wave potential relationships for a wave propagating in the positive x direction in case of shallow and deep waters are given in Equations (3.11) and (3.12) (Bertram, 2000).

$$\Phi = \mathrm{Re}\{-ic\check{\zeta}e^{-kz}e^{i(\omega t - kx)}\}, \text{ infinite depth} \tag{3.11}$$

$$\Phi = \mathrm{Re}\left\{\frac{-ic\check{\zeta}}{\sinh(kh)}\cosh(k(z-h))e^{i(\omega t - kx)}\right\}, \text{ finite depth} \tag{3.12}$$

In the previous equations, $\check{\zeta}$ is the complex wave amplitude, Re denotes the real part of a number and h is the depth of the sea. Equation (3.11) should be used for a sea depth larger than 0.5 times the wavelength.

The unsteady potential Φ_T can be further decomposed into the incident, the diffracted and the radiation potentials. Radiation potentials result from a unit amplitude oscillation in the j^{th} mode (i.e. surge, sway, heave, roll, pitch, yaw).

$$\Phi_T(x,y,z) = \Phi_I + \Phi_D + \sum_{j=1}^{6} \xi_j \varphi_j \quad (3.13)$$

In Equation (3.13) Φ_I denotes the potential due to the incident wave, Φ_D the diffracted wave potential and φ_j the radiation potentials at j^{th} degree of freedom. The expression of the incident wave potential for infinite sea depth and as a function of the sea depth is depicted in Equations (3.14) and (3.15).

$$\Phi_I = -ig\frac{\zeta_\alpha}{\omega} e^{ikz(x\cos\chi + y\sin\chi)} \quad (3.14)$$

$$\Phi_I = -ig\frac{\zeta_\alpha}{\omega}\frac{\cosh k(z+h)}{\cosh(kh)} e^{ik(x\cos\chi + y\sin\chi)} \quad (3.15)$$

In the latter, ζ_α is the wave amplitude whilst, the wave frequency ω is calculated by means of the linear dispersion relationship

$$\omega^2 = gk\tanh(kh) \quad (3.16)$$

External hydrodynamic forces can be calculated after finding the hydrodynamic pressure implementing the well-known Bernoulli's equation.

$$P = -\rho\left(\frac{\partial \Phi}{\partial t} + \frac{1}{2}|\nabla\Phi|^2 + gz\right) \quad (3.17)$$

In order to solve Equation (3.17) it is clear that the functions of the wave potentials must be obtained in advance. These functions must satisfy three conditions, namely the Laplace equation in the fluid domain, the linearized boundary condition on the free surface (FSBC) and the linearized body boundary condition (BBC). According to Salvesen (1970), linearization is valid when assuming slender ship geometry, which provides small values of the steady potential (Φ_S) and its derivatives. Moreover, small values of the unsteady potential (Φ_T) and its derivatives are considered as well, since the vessel's motions are small.

- Laplace equation in the fluid domain:

$$\nabla^2\Phi = 0 \quad (3.18)$$

- Linearized Free Surface Boundary Condition (FSBC):

  On the undisturbed water surface (z=0) the diffracted and radiation wave potentials have to satisfy the following conditions:

$$\left[\left(i\omega + U\frac{\partial}{\partial x}\right)^2 + g\frac{\partial}{\partial z}\right]\Phi_I = 0 \tag{3.19}$$

$$\left[\left(i\omega + U\frac{\partial}{\partial x}\right)^2 + g\frac{\partial}{\partial z}\right]\Phi_D = 0 \tag{3.20}$$

$$\left[\left(i\omega + U\frac{\partial}{\partial x}\right)^2 + g\frac{\partial}{\partial z}\right]\varphi_j = 0 \tag{3.21}$$

- Linearized boundary condition on ship's surface S (BBC):

  On the mean position of the hull, the boundary conditions with respect to incident, diffracted and radiation potentials are the following

$$\vec{n}\cdot\nabla\Phi_D = -\vec{n}\cdot\nabla\Phi_I \tag{3.22}$$

$$\vec{n}\cdot\nabla\varphi_j = -i\omega\cdot n_j + U\cdot m_j \tag{3.23}$$

  In Equations (3.22)-(3.23), $\vec{n}$ is the surface's normal unit vector pointing outwards. In NEWDRIFT, simplification of the BBC (3.23) is attained by decomposing the radiation potentials in a speed independent and a speed dependent part (Papanikolaou and Schellin, 1992). In particular,

$$\varphi_j = \varphi_j^o - \frac{U}{i\omega}\varphi_j^U \tag{3.24}$$

  which results to the following expressions.

$$\begin{cases}\vec{n}\cdot\nabla\varphi_j^o = -i\omega\cdot n_j \\ \vec{n}\cdot\nabla\varphi_j^U = -i\omega\cdot m_j\end{cases} \tag{3.25}$$

In case where $\varphi_j^U = 0$ (for j=1, 2, 3, 4), $m_5=n_3$ and $m_6=-n_2$ (Neumann-Kelvin Simplification) the final expressions of the radiation potentials in terms of the speed-independent components can be evaluated:

$$\begin{cases} \varphi_j = \varphi_j^o, \text{for } i = 1,2,3,4 \\ \varphi_5 = \varphi_5^o - \frac{U}{i\omega}\varphi_3^o \\ \varphi_6 = \varphi_6^o - \frac{U}{i\omega}\varphi_2^o \end{cases} \quad (3.26)$$

In general, the m-terms that appear in Equation (3.23) are difficult to evaluate, since the following equations have to be solved:

$$(m_1, m_2, m_3) = -(\vec{n}\cdot\nabla)\nabla(\Phi_S - x) \quad (3.27)$$

$$(m_4, m_5, m_6) = -(\vec{n}\cdot\nabla)[\vec{r}\times\nabla(\Phi_S - x)] \quad (3.28)$$

Equations (3.27-3.28) include terms that have to be differentiated twice therefore, it is hard to evaluate numerically. Both NEWDRIFT and PRECAL neglect the influence of the steady component Φ_S occurring by the ship's forward motion, adopting a slender body assumption and a uniform (Neumann-Kelvin) base flow. Alternatively, PRECAL is able to implement a, so-called, Double-Body flow model as well, that leads to more realistic representation of the steady wave potential.

In case where the uniform flow modelling is chosen (default option in PRECAL), the steady component includes only the term –Ux, whereas in case where the Double-Body flow modelling is selected, Φ_S satisfies the following conditions on the free surface (3.29) and the impermeability condition on the vessel's body (3.30).

$$\frac{\partial}{\partial n}\Phi_S = 0 \qquad \text{on z=0} \quad (3.29)$$

$$\frac{\partial}{\partial n}(-Ux - \Phi_S) = 0 \qquad \text{on the mean body surface} \quad (3.30)$$

Double-Body method is accurate in case of low forward speeds whilst, for faster ships the calculation of the steady perturbation potential in advance is a prerequisite. Comparison of calculated RAO values using the uniform and the Double-Body methods against experimental ones for the S-175 container ship sailing at Fn=0.25, proved the aforementioned allegation (Hizir, 2015).

- Radiation condition at infinity:

  - *Radiation (j=1, 2,...,6) and diffraction (j=7) potentials Φ_j:* According to Newman (2017; Ch. 6, Section 6.15), the Sommerfeld's radiation condition must be satisfied that allows only outgoing waves at infinity (see also Papanikolaou, 1985). More specifically, for large $r = \sqrt{x^2 + y^2}$

    $$\Phi_j = O(r^{-\frac{1}{2}} e^{-ikr}) \tag{3.31}$$

    where the constants of the asymptotic-order symbol O may depend on the remaining coordinates but not on r.

  - *Steady potential Φ_S:* According to Wehausen and Laitone (1960), the energy flux associated with the disturbance of the steadily moving body is directed downstream towards infinity ($x \rightarrow -\infty$) and thus there are no upstream waves. In more detail for the deep water case, according to Baar and Price (1988) Φ_S generates a wave disturbance W(x,y) behaving for large r as below:

    $$W \sim \begin{cases} O(r^{-1}) \\ O(r^{-\frac{1}{3}}) \\ O(r^{-\frac{1}{2}}) \end{cases} \quad \text{if} \begin{cases} x < 2\sqrt{2}y \\ x \approx 2\sqrt{2}y \\ x > 2\sqrt{2}y \end{cases} \quad \text{as } r \rightarrow \infty \tag{3.32}$$

- Bottom condition:

  - *Finite depth case:* The normal derivative of the unsteady potential Φ_T vanishes on the bottom boundary.

  - *Deep water case:* The unsteady potential Φ_T vanishes exponentially with z as z goes to infinity.

Following the aforementioned analysis and after obtaining the velocity potential adopting a Green's function representation, the solution of the linear Boundary Value Problem can be performed through Equation (3.17) in order to get the hydrodynamic pressure P on the body's surface.

$$P = -\rho\left\{[-i\omega_e\Phi_T + U\nabla(\Phi_S - x)\cdot\nabla\Phi_T]e^{-i\omega_e t} + \frac{1}{2}\left(\nabla\Phi_T e^{-i\omega_e t}\right)^2 + \right.$$
$$\left. + \frac{1}{2}U^2[\nabla(\Phi_S - x)]^2 + gz\right\} \quad (3.33)$$

The last term in Equation (3.33) represents the hydrostatic pressure contribution coming from the action of the buoyancy. Additionally, the squared term that includes the steady component Φ_S corresponds to the wave resistance, while the terms multiplied by the exponential function refer to the perturbed force resulting from the unsteady wave potential.

Simplification of the above equation is succeeded after neglecting the higher order terms and the terms resulting from the multiplication of steady and unsteady potentials. The simplified relationship of the time-varying hydrodynamic pressure is depicted in Equation (3.34)

$$P = -\rho\left(-i\omega_e - U\frac{\partial}{\partial x}\right)\Phi_T e^{-i\omega_e t} \quad (3.34)$$

Finally, by integrating the hydrodynamic pressure on the body's surface for every degree of freedom j, the frequency dependent forces and moments can be obtained, namely,

$$F_j = \iint_S Pn_j dS = \rho\iint_S \left(i\omega_e + U\frac{\partial}{\partial x}\right)\Phi_T n_j dS \quad (3.35)$$

where, n_j are the components of the unit normal vector.

More specifically, the hydrodynamic forces caused by the incident, the diffracted and the radiation potentials are calculated in the frequency domain by placing the relevant component of the unsteady potential in Equation (3.35).

Further, the hydrodynamic coefficients, consisting by the added masses and the damping coefficients, are taken as the real and the imaginary part of the frequency dependent radiation forces respectively.

$$F_{I,j} = \rho \iint_S \left(i\omega_e + U\frac{\partial}{\partial x}\right) \Phi_I n_j dS \tag{3.36}$$

$$F_{D,j} = \rho \iint_S \left(i\omega_e + U\frac{\partial}{\partial x}\right) \Phi_D n_j dS \tag{3.37}$$

$$F_{R,j} = \rho \iint_S \left(i\omega_e + U\frac{\partial}{\partial x}\right) \varphi_k n_j dS = \omega_e^2 A_{jk} + i\omega_e B_{jk} \tag{3.38}$$

Having the hydrodynamic forces and coefficients calculated, the formulation of the frequency domain system of equations can be established as shown in Equation (3.39). Forces and motions are expressed in terms of the magnitude of the complex number.

$$\left\{-\omega_e^2\left[M_{jk} + A_{jk}(\omega_e)\right] - i\omega_e B_{jk}(\omega_e) + C_{jk}\right\}\left|\vec{\xi}_j\right| = \left|\vec{F}_{I,j}(\omega_e)\right| + \left|\vec{F}_{D,j}(\omega_e)\right| \tag{3.39}$$

In Equation (3.39) M_{jk} is the matrix of masses and moments of inertias for pitch and heave motions whilst, A_{jk} is the matrix of frequency dependent added masses and added moment of inertias and B_{jk} is the matrix of frequency dependent damping coefficients. Additionally, C_{jk} is the matrix of the linear restoring coefficients and $\left|\vec{\xi}_j\right|$ is the vector of motions' amplitudes.

Finally, the RHS includes the summation of the amplitudes of the frequency dependent wave excitation forces for each DOF considered in the context of the seakeeping problem. The aforementioned hydrodynamic forces and coefficients have been calculated with respect to the hydrodynamic (or seakeeping) reference frame. The adoption of frequency domain analysis for the solution of the linear boundary value problem of a ship moving in a seaway is valid when small and sinusoidal excitations are assumed. Therefore, in case of large amplitude waves a time domain solution of the problem must be employed, taking into account the exact Froude-Krylov and hydrostatic forces exerted on ship's hull. Such an implementation will be presented in Chapter 4 demonstrating the methodologies used in order to evaluate the external force contributions in a modular basis. An important element for an accurate time domain solution of the linear and the nonlinear seakeeping problems, is to ensure the smoothness of the memory functions. The latter results by implementing an inverse Fourier transformation of the frequency dependent damping coefficients. For this reason, it is of high importance to use smooth damping curves where all irregular values, which appear close to resonant frequencies, will be eliminated.

At irregular frequencies the boundary value problem either can not be solved, or the solution of the exterior Neumann problem is not unique. In order to overcome the aforementioned problem a numerical "lid" has to be placed considering panels at the free surface level, which enclose the body's interior free surface. In PRECAL, the so-called *Lid Panel Method* (Lee and Sclavounos, 1989) is adopted to alleviate the irregular frequencies, using a zero-speed Green's function. Recently, a similar approach was introduced to NTUA's in-house code NEWDRIFT (Dafermos et al., 2019) as a way to remove the irregular frequencies.

Another aspect, which deserves consideration regarding the solution of the aforementioned boundary value problem using frequency domain analysis, is the procedure followed in case where the forward speed is not zero. In general, this a highly demanding task as it is quite difficult to find a suitable Green's function satisfying the exact FSBC depicted in Equations (3.19), (3.20) and (3.21) due to the rapidly oscillating derivatives which appear and induce numerical instabilities. In PRECAL, it is possible to solve the exact forward speed case considering the exact FSBC via the Green's function proposed by Wehausen and Laitone (1960) however, this is a time consuming task and also numerical instabilities might occur as aforementioned. Instead of the exact forward speed case, PRECAL and NEWDRIFT are able to apply an approximate method where the term $\frac{\partial}{\partial x}U$ can be neglected in (3.19), (3.20) and (3.21) for slender ships, or when the vessel's forward speed is low (or both), resulting in the following expressions:

$$-\omega_e^2\Phi_I + g\frac{\partial}{\partial z}\Phi_I = 0 \tag{3.40}$$

$$-\omega_e^2\Phi_D + g\frac{\partial}{\partial z}\Phi_D = 0 \tag{3.41}$$

$$-\omega_e^2\varphi_j + g\frac{\partial}{\partial z}\varphi_j = 0 \tag{3.42}$$

The above expressions are widely known as "zero-speed FSBC" or "approximate forward speed solution" and are commonly incorporated in many 2D and 3D seakeeping codes as they provide easier and more stable results. In this case, the contribution of the forward speed on the solution of the boundary value problem is taken into consideration through correction terms during the calculation of the hydrodynamic pressure using Equation (3.33).

Comparison of heave motions in terms of RAO values against experimental evidence using exact and approximate forward speed cases, show better agreement when the former was used however, the computational cost and the instability of damping coefficients are considered as significant drawbacks of the method (Hizir, 2015).

To conclude with, in the context of the present study the accurate solution of the linear boundary value problem of a ship interacting with regular waves is a prerequisite as the hydrodynamic outcome will be used for the formulation of the time domain methodology even in the nonlinear case. For this reason, the uniform base flow will be implemented in seakeeping calculations as it was proven faster and more accurate compared with the Double-Body method, and an approximate forward speed realization of the FSBC will be adopted. The aforementioned modelling provides a balanced combination between computational cost and numerical accuracy. In case of shallow water conditions, seakeeping problem is solved using NEWDRIFT, implementing a rigid wall condition on the seabed.

3.4 Manoeuvring Theory

In contrast to the formulation of the seakeeping problem described in the former sections (3.3.1-3.3.2), manoeuvring in calm water requires a different conception in order to describe the underlying physics. In manoeuvring, ship motions are being investigated on the horizontal *XY* plane (surge-sway-yaw), whilst through standard IMO tests conclusions can be drawn regarding a vessel's manoeuvrability. For this purpose, various models have been developed starting from the first, classical approach published by Lamb (1932) which ignored viscous and free-surface effects at that time. As it will be demonstrated in the following sections of this chapter, the mathematical models, which are being used for the simulation of ship manoeuvres, are based on the differential equations of motion considering irrotational flow and ideal fluid characteristics, whilst viscous, free-surface and lifting-surface effects are incorporated through semi-empirical corrections.

3.4.1 General Remarks

Among the aforementioned nonlinear effects, lifting-surface contribution plays a significant role on the formulation of a theoretical manoeuvring problem, since the effective angle of attack of the hull against the incoming flow (drift angle) is relatively large. In case where the drift angle is small, ship's motion can be described by adopting an inviscid and irrotational flow model including the effect of a trailing shed vortex from the stern, which has a significant impact on the development of the sway and yaw lift force and moment. The latter, were initially evaluated within the context of slender body theory (Newman, 1979).

Free-surface effects although they play a significant role while investigating other problems related to hydrodynamics of ships (i.e. the estimation of the wave resistance and the seakeeping performance of a ship), they have a minor impact on calm water manoeuvring. Hu (1961) and Chapman (1975) suggested that for low and moderate Froude numbers the influence of free-surface effects on manoeuvring can be disregarded.

Viscosity has to be accounted as well, when the hydrodynamic performance of a ship is investigated. Concerning the straight motion, viscosity leads to the formation of a boundary layer, where the fluid's velocity changes substantially. The aforementioned phenomenon has a direct impact on ship's resistance in forward motion, whilst in case of ship manoeuvring, separation of the flow may occur on the vessel's side of low pressure. Consequently, flow separation produces a cross-flow drag proportional to the square of the lateral velocity, which increases the side forces on the ship's hull. Separation which takes place at the region of the ship's stern is another complicated phenomenon, which affects both ship's resistance, the onset flow to the propeller and rudder (wake) and the interaction between the rudder and the propeller.

Manoeuvring performance of a ship, accounting for the phenomena mentioned above, can be evaluated at her initial design stage by means of the following methods (ITTC, 2005):

1. Free-running model tests
2. Numerical models implementing various mathematical models
3. Estimations based on regression formulae from data found in database
4. CFD based simulations

Free-running models, although they can be considered as the most direct and reliable way in order to estimate the manoeuvring performance of a marine vessel, they are costly and errors are introduced due to scale effects. Additionally, conducting free-running tests at the design stage of the ship is rare for merchant ships due to the cost it is needed in order to build the model thus, it is usually avoided. Experimental setup and relevant results for deep and shallow water manoeuvring have been presented in several conferences and workshops (i.e. SIMMAN, MARSIM etc.) providing useful benchmark case studies, contributing to the establishment of robust mathematical models.

Another method to evaluate a ship's manoeuvring performance, which does not require numerical simulation, is by using regression analysis on data collected from a large number of experiments. By this mean, the calculation of the manoeuvring characteristics of a marine vessel can be performed by knowing solely the main particulars of the studied vessel (Haraguchi, 2000). The major drawback of this method is that it is approximative and unique features of the studied hull cannot be captured. The necessary data in order to perform a regression analysis of this kind are even less in case of new types of hull forms.

Within the framework of the present study, numerical simulations were conducted adopting the well-known MMG model (Mathematical Modelling Group is part of the Japanese Towing Tank) initially introduced by Ogawa et al. (1977), Hamamoto (1977) and Kasai and Yushitsu (1977). The aforementioned model accounts for the external hydrodynamic, propeller and rudder forces in a modular basis focusing on the interconnected physics of each module. This approach is different from the simulation-based Abkowitz (1964) model, which considers the ship as a whole. In both MMG and Abkowitz models, the generalized hydrodynamic forces in calm water are expressed as a Taylor expansion with the use of the perturbation analysis. In order to formulate the aforementioned expansion, several coefficients, known as the manoeuvring derivatives, must be known in advance either by use of captive model tests, or by semi-empirical and CFD analyses. Therefore, the process of calculating the hydrodynamic forces on the ship's hull requires experimental, analytical and numerical contributions. In the context of the present simulations, experimentally derived manoeuvring derivatives for KVLCC2 and S-175 container ship have been used.

A mathematical analysis of this process is given below (Abkowitz, 1964). The developed methodology is based on the assumptions that the motion of the ship is relatively slow and the hydrodynamic generalized forces depend on the instantaneous values of the ship's velocities and accelerations. The latter implies that there are not "memory effects" which have to be taken into consideration.

3.4.2 Hull Hydrodynamic Forces

The hydrodynamic forces in surge, sway and yaw, namely *X*, *Y*, *N* can be expressed as functions of the state-space variables as shown below:

$$X = f_1(u, v, r, \dot{u}, \dot{v}, \dot{r}) \tag{3.43}$$

$$Y = f_2(u, v, r, \dot{u}, \dot{v}, \dot{r}) \tag{3.44}$$

$$N = f_3(u, v, r, \dot{u}, \dot{v}, \dot{r}) \tag{3.45}$$

In Equations (3.43)-(3.45) u, v, r denote the vessel's velocities and $\dot{u}, \dot{v}, \dot{r}$ her accelerations at the body-fixed reference frame. Subsequently, according to Abkowitz (1964), the functions f_1, f_2, f_3 can be expressed by means of a Taylor expansion near the point x_o as it is depicted in (3.46):

$$f(x) = f(x_o) + \frac{\delta x}{1!}\frac{df(x)}{dx}\Big|_{x=x_0} + \frac{\delta x^2}{2!}\frac{d^2 f(x)}{dx^2}\Big|_{x=x_0} + \cdots \tag{3.46}$$

The Taylor expansion of Equation (3.46) can be implemented in case of more than one variables as in Equations (3.42)-(3.44). In such case, for the linear hydrodynamic forces we have:

$$X = f_1(u_o, v_o, r_o, \dot{u}_o, \dot{v}_o, \dot{r}_o) + \delta u\frac{\partial X}{\partial u} + \cdots + \delta\dot{r}\frac{\partial X}{\partial \dot{r}} \tag{3.47}$$

$$Y = f_2(u_o, v_o, r_o, \dot{u}_o, \dot{v}_o, \dot{r}_o) + \delta u\frac{\partial Y}{\partial u} + \cdots + \delta\dot{r}\frac{\partial Y}{\partial \dot{r}} \tag{3.48}$$

$$N = f_3(u_o, v_o, r_o, \dot{u}_o, \dot{v}_o, \dot{r}_o) + \delta u\frac{\partial N}{\partial u} + \cdots + \delta\dot{r}\frac{\partial N}{\partial \dot{r}} \tag{3.49}$$

If we consider that surge motion is uncoupled with respect to the other two (sway, yaw), many terms in Equation (3.46) can be omitted leading to the following expression:

$$X = f_1(u_o, \dot{u}_o) + \frac{\partial X}{\partial u}(u - u_o) + \frac{\partial X}{\partial \dot{u}}(\dot{u} - \dot{u}_o) \tag{3.50}$$

The symbols $X_u = \frac{\partial X}{\partial u}$ and $X_{\dot{u}} = \frac{\partial X}{\partial \dot{u}}$ can replace the partial derivatives in Equation (3.49). Similarly, for Equations (3.47) and (3.48) we get:

$Y_v = \frac{\partial Y}{\partial v}$, $Y_r = \frac{\partial Y}{\partial r}$, $Y_{\dot{r}} = \frac{\partial Y}{\partial \dot{r}}$, $N_v = \frac{\partial N}{\partial v}$ etc.

All the aforementioned coefficients will be considered constant in manoeuvring calculations. As a simplified example where only the linear terms are considered, the equations of the hydrodynamic forces excerted on the ship's hull can be derived.

$$Y = Y_{\dot{v}}\dot{v} + Y_{\dot{r}}\dot{r} + Y_v v + Y_r r \tag{3.51}$$

$$N = N_{\dot{r}}\dot{r} + N_{\dot{v}}\dot{v} + N_v v + N_r r \tag{3.52}$$

The coefficients taking part in Equations (3.51) and (3.52) will be called *hydrodynamic (or manoeuvring) derivatives* from now on. Generally, they are calculated in a non-dimensional form to facilitate their use either in model scale or in full scale ships. The Taylor expansions showed in Equations (3.47)-(3.49) is rather unusual to include only the first-order partial derivative. According to the potential theory and due to the fact that the interactions between viscous and inertia properties of the fluid are loose, solely the acceleration terms must be linear. Simplifications of the equations of motion may further occur due to the symmetries arising (i.e. $X_{\dot{v}} = 0$ and $X_{\dot{r}} = 0$).

3.5 Summary

In Chapter 3, the main elements of seakeeping and manoeuvring in calm water theories were presented. Starting from the seakeeping theory, the fundamentals of potential theory were presented, which lead to the derivation of the linear wave forces. The analysis adopts the concept of the transient Green's function in order to solve the three dimensional Boundary Value Problem. Subsequently, the available methods for the calculation of the drift forces are given, which consist of near field and far field approaches.

The need for special treatment in case of short wave seas is emphasized, as it is of high importance nowadays for environmentally efficient and safe navigation in rough seas. In following paragraphs, the fundamentals of the manoeuvring theory were presented highlighting the impact of the viscous and lift forces in ship's trajectory. Two model-based approaches, which are able to simulate ship's manoeuvring motion in the time domain can be found in the literature, namely the whole (Abkowitz) and the MMG models. The latter, implements a modular approach for the calculation of the hydrodynamic-propeller-rudder forces allowing for the incorporation of new scientific developments in one module without affecting the rest. Interaction effects between different modules, which appear due to the wake field at the vicinity of the ship's stern, are taking into account.

In light of the aforementioned theoretical background, numerical models are developed within the context of the present study, which simulate ship's manoeuvring motion in calm water and in adverse weather conditions. The considered models exploit the results of the frequency domain analysis however, they incorporate nonlinear contributions resulting from the instantaneously changing wetted surface. In Chapter 4, an exhaustive description of the developed method is given discussing the different force components in a modular basis.

CHAPTER 4

DEVELOPED METHODOLOGY

4.1 Introduction

In the previous chapter, a detailed discussion of the theoretical background concerning seakeeping and manoeuvring theories was presented. Concerning the seakeeping theory, focus was given on the linear Boundary Value Problem governing the wave-ship interaction, providing the solution based on the potential theory. Using the results of this process, someone is able to perform linear time domain analysis, using the results of Froude-Krylov, Diffraction, Radiation and Restoring forces obtained by implementing frequency domain analysis. In the context of the linear seakeeping theory, the wetted surface is considered constant thus, it is incapable of incorporating the effects of a ship's geometrical nonlinearities which take part for larger wave excitations mostly in case of fine hull forms. For this reason, a level of nonlinearity is accounted in the adopted methodology, which offers more realistic modelling of the ship's response in rough seas. The latter, was accomplished by considering nonlinear Froude-Krylov and Restoring forces, which are considered as the major sources of nonlinearity. In case of the present time domain analysis, the calculation of the aforementioned forces is performed through the direct integration of the hydrodynamic and hydrostatic pressures over the vessel's instantaneous wetted surface.

The study of the linear and the nonlinear seakeeping performance of a vessel in terms of her vertical motions is performed using the inertial Hydrodynamic Reference Frame ($OX_hY_hZ_h$) shown in Chapter 3, since the rotation about the ship's transverse axis (pitch motion) remains small even for large wave amplitudes (<10 degrees). It is also stated in Fonseca and Soares (1998) that *"the forces and moments may be represented on the inertial reference system and the equations of motion solved directly"*. However, in order to perform a direct ship's stability assessment, ship's roll motion has to be taken into consideration as well. Roll angle can take excessive values in case of dynamic instability (parametric roll or pure loss of stability) and consequently, the ship's inertia cannot be considered constant anymore.

In this case, the system of motions' equations must be formulated utilizing the Horizontal Body-Fixed Reference Frame ($OX_{hs}Y_{hs}Z_{hs}$) which can be used for nonlinear seakeeping simulations as well, when there is not deflection of the rudder.

Before the presentation of the hybrid model, which describes the manoeuvring performance of a marine vessel in waves, the equations governing ship's manoeuvring in calm water will be presented as well. The adopted modelling is based on the modular MMG model where the external forces are calculated at each time step. The total value of the generalized forces results from the summation of the hydrodynamic forces and the forces due to the rudder's and the propeller's actions. Apart from the description of the horizontal motions (surge-sway-yaw), a 4-DOF model is formulated as well, incorporating the effect of heel during turning, which was discussed in the previous chapter. At the end of this chapter, the hybrid seakeeping and manoeuvring model is presented and the proposed inclusion of the shallow water effect, which is the novelty of the present research, is finally discussed.

The developed methodology has been implemented through the newly developed software in the present research, called ELIGMOS. The latter is a time domain simulation tool, written in C++ programming environment. As it will be shown in the following chapters, ELIGMOS is capable of performing linear and nonlinear seakeeping and manoeuvring simulations whilst, its main novelty is that it can be used for manoeuvring simulations in adverse sea conditions by adopting a "hybrid" approach (see Chapter 2).

4.2 Time Domain Seakeeping Modelling

4.2.1 General Remarks

In previous paragraphs, it was highlighted that frequency domain analysis can describe ship's motions satisfactorily when the wave excitations are small compared with the vessel's dimensions. However, in case of large amplitude excitations the time domain approach must be implemented. Firstly, the time domain formulation concerning the vessel's vertical motions (heave and pitch) will be presented based on Cummin's (1962) linear system of equations, who introduced the IRF approach for the calculation of the radiation forces.

$$\left[M_{jk} + A_{jk}(\infty)\right]\ddot{\xi}_k(t) + B_{jk}(\infty)\dot{\xi}_k(t) + \int_0^t K_{jk}(t-\tau)\dot{\xi}_k(\tau)d\tau + C_{jk}\xi_k = \\ = F_j^I(t) + F_j^D(t),\ j = 3,5 \tag{4.1}$$

In Equation (4.1), subscripts j, k take the values 3 and 5 since the vertical motions are considered uncoupled from any other DOF whilst, matrices M_{jk}, $A_{jk}(\infty)$, $B_{jk}(\infty)$, K_{jk} and C_{jk} are expressed at the Hydrodynamic Reference Frame. The aforementioned matrices refer to the ship's masses and inertias, infinite frequency added masses and inertias, infinite frequency damping coefficients, memory functions for the considered motions and constant restoring forces respectively. At the RHS of (4.1) the summation of the incident and diffracted wave excitation forces in the time domain are depicted. In order to express these force components in the time domain, using their pre-calculated frequency domain magnitude and phase angle, the following transformation must be implemented for both incident and diffracted wave forces.

$$F^I(t), F^D(t) = \zeta_\alpha \Re(F^{real} + iF^{imag})e^{i\omega_e t} \tag{4.2}$$

where, the frequency dependent real (in-phase) and imaginary (out-of-phase) parts of the force components can be evaluated through Equations (4.3) and (4.4).

$$F^{real} = \left|\vec{F}\right|\cos\hat{a} \tag{4.3}$$

$$F^{imag} = \left|\vec{F}\right|\sin\hat{a} \tag{4.4}$$

In the equations shown above, $\left|\vec{F}\right|$ is the magnitude of the frequency-dependent wave excitation force and $\hat{a}$ is the phase angle, which are obtained after the implementation of frequency domain analysis. To ensure that a linear time-domain seakeeping analysis is performed correctly, the results of the vertical motions in terms of non-dimensional transfer functions must be equal (or having small discrepancies) with their relevant frequency domain values for both zero and non-zero forward speed (validation studies are depicted in Chapter 6). Herein, results are shown concerning the nondimensional heave and pitch amplitudes at several wave frequencies after implementing the developed linear time-domain seakeeping methodology for the KVLCC2 tanker, at both zero and non-zero forward speed values (Figure 4.1 and 4.2).

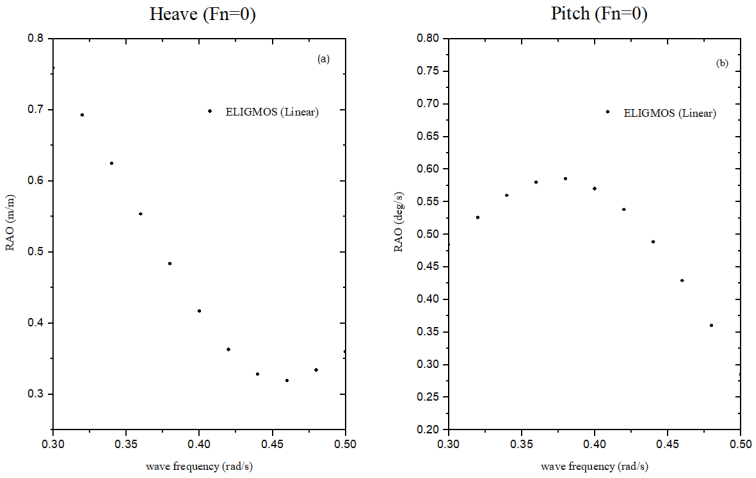

Figure 4.1: Linear heave (a) and pitch (b) RAO values for KVLCC2 at zero forward speed (head waves)

Heave and pitch non-dimensional amplitudes derived in case of non-zero forward speed value (Fn=0.142) can be seen below.

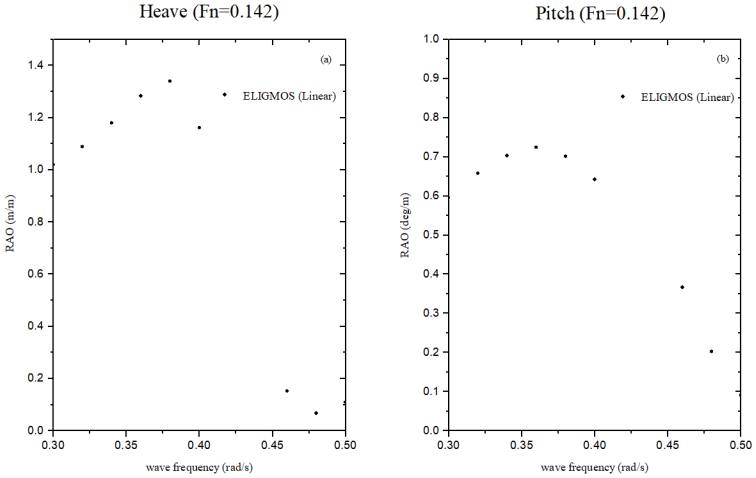

Figure 4.2: Linear heave (a) and pitch (b) RAO values for KVLCC2 at non-zero forward speed (head waves, Fn=0.142)

For larger wave amplitude, the matrix of the linear restoring coefficients can no longer be used. Additionally, the general description for the calculation of the Froude-Krylov forces has to be replaced by a direct pressure integration scheme. In the present analysis, nonlinearity of the radiation and diffraction forces is not considered.

In order to conduct a Level 2 nonlinear time-domain seakeeping analysis (nonlinear Froude-Krylov and Restoring forces), the instantaneous alteration of the vessel's wetted surface must be taken into account.

These two updates of the methodology formulate the first (and more important) level of nonlinearity. The way that the radiation and diffraction forces are embedded in a time domain seakeeping approach can increase the level of its nonlinearity leading to more realistic representation of a ship's vertical motions.

However, the excessive demands in time and computational power are usually the major inhibitory factors. In the following paragraphs, the way of incorporating the nonlinearities associated with Froude-Krylov and Restoring forces will be explained. In an effort to show that ELIGMOS is able to incorporate the nonlinear force components, successful identification of parametric roll investigation of a C11-class container ship will be demonstrated in the following chapter. In all cases radiation and diffraction forces are evaluated with respect to the mean sea level. Since the interaction of a ship is progressing rapidly, the inclusion of memory effects is taken into consideration as well. The process in order to evaluate the memory functions from frequency dependent damping coefficients will be discussed in detail. Additionally, as part of the seakeeping analysis, which has a significant impact on a ship's manoeuvring performance as well, an analytical presentation of the methods used to calculate the second order wave forces will be presented.

4.2.2 Nonlinear Froude-Krylov and Restoring Forces

Froude-Krylov and Restoring force components are the dominant ones compared with the radiation and diffraction contributions in the context of a seakeeping analysis in deep water, while their importance becomes more significant as the wavelength over the ship's length ratio (λ/L_{pp}) increases (Hizir, 2015). For a nonlinear seakeeping analysis, Froude-Krylov forces have to be integrated up to the instantaneous wetted surface. However, their calculation above the still water level cannot be performed using the linear incident wave potential therefore, certain approximations must be adopted in this case.

According to these approximations the pressure above the mean wetted surface can be considered as hydrostatic or a stretching correction might be applied up to the actual water level.

Additionally, the Froude-Krylov pressure above the mean sea level can be evaluated adopting the same (unmodified) formula, which is used for the calculation of the pressure below this level. Singh and Sen (2007) mentioned another approximation method which is based on the utilization of Fourier series (Rienecker and Fenton, 1981). The approximation method that adopts a hydrostatic expression of the Froude-Krylov pressure above the still water is implemented within the framework of the present modelling. An explanatory graph of the pressure distribution can be seen below.

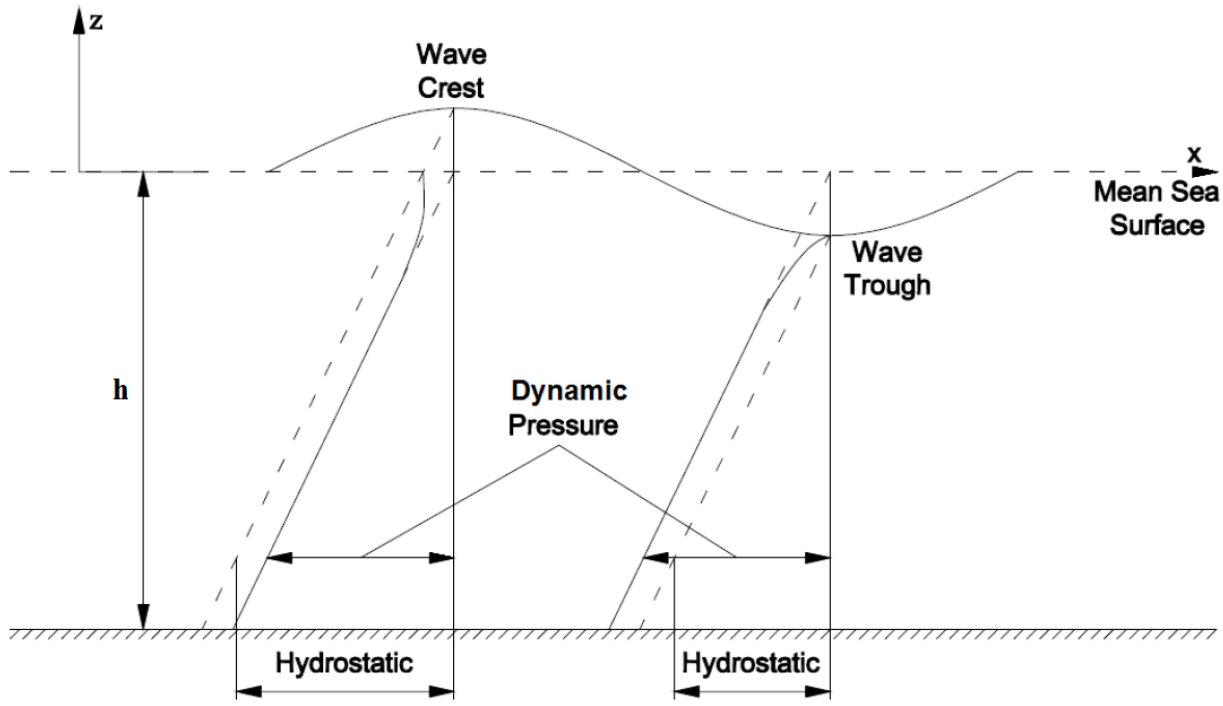

Figure 4.3: Distribution of the dynamic wave pressure (Hizir, 2015)

According to the aforementioned formulation, the Froude-Krylov and hydrostatic generalized forces over a wetted panel of the ship's hull are obtained using the following expressions.

For the Froude-Krylov forces we have:

$$f_3^{FK} = \Re\begin{cases} \rho g A_p(\zeta_\alpha - z_p)\cdot n_3 e^{ikx_p}, & 0 \le z_p \le \zeta_\alpha \\ e^{ikx_p}\cdot \rho g A_p \zeta_\alpha e^{kz_p}\cdot n_3 e^{ikx_p}, & z_p \le -\zeta_\alpha \end{cases} \tag{4.5}$$

$$f_5^{FK} = \Re\begin{cases} \rho g A_p(\zeta_\alpha - z_p)\cdot (z_p n_1 - x_p n_3) e^{ikx_p}, & 0 \le z_p \le \zeta_\alpha \\ \rho g A_p \zeta_\alpha e^{kz_p}\cdot (z_p n_1 - x_p n_3) e^{ikx_p}, & z_p \le -\zeta_\alpha \end{cases} \tag{4.6}$$

For the hydrostatic forces we have:

$$f_3^{HS} = \begin{cases} 0, & 0 \le z_p \le \zeta_\alpha \\ \rho g A_p z_p \cdot n_3, & z_p \le -\zeta_\alpha \end{cases} \quad (4.7)$$

$$f_5^{FK} = \begin{cases} 0, & 0 \le z_p \le \zeta_\alpha \\ \rho g A_p z_p \cdot (z_p n_1 - x_p n_3), & z_p \le -\zeta_\alpha \end{cases} \quad (4.8)$$

In Equations (4.5)-(4.8) A_p, z_p and x_p are the area, the longitudinal position and the vertical position of the centre of each panel respectively, whereas k is the wave number. The total Froude-Krylov and hydrostatic forces at each time step for the whole vessel can be obtained after the summation of all the elemental components. Specifically,

$$F_{FK+HS,j} = \sum_{i=1}^{N} (f_j^{FK} + f_j^{HS}),\ j=3, 5 \quad (4.9)$$

In Equation (4.9), N is the total number of panels which are located below the wave profile at each time increment and consequently, are considered wet.

4.2.3 Radiation Forces

Radiation forces result from the radiation potential and can be calculated in the frequency domain implementing the following expression.

$$F_{R,j}(\omega_e) = -\rho \iint_S \left\{ i\omega_e + U \frac{\partial}{\partial x} \right\} \varphi_{R,k} n_j dS = \sum_j \sum_k \left(\omega_e^2 A_{jk} + i\omega_e B_{jk} \right),\ (j,k) = 1, 2, \dots, 6 \quad (4.10)$$

Cummins (1962) proposed a time domain representation of the radiation forces by means of Impulse Response Functions (IRF), which can be seen in Equation (4.11).

$$F_{R,jk}(t) = A_{jk}(\infty)\ddot{\xi}_k(t) + B_{jk}(\infty)\dot{\xi}_k(t) + \int_0^\infty K_{jk}(t-\tau)\xi_k(\tau)d\tau, (j,k) = 1, 2, \dots, 6 \quad (4.11)$$

For seakeeping simulations indices j, k take the values 3, 5 which refer to heave and pitch DOF respectively.

The frequency dependent "memory functions" or "Impulse Response Functions" are indicated in Equation (4.11) with the term K_{jk}. Further, $A_{jk}(\infty)$ and $B_{jk}(\infty)$ stand for the added masses and damping coefficients at infinite frequency respectively. The added masses depend only on the underwater geometry of the ship, whilst the damping coefficients depend on the underwater geometry and on the ship's forward velocity. The adoption of the convolution integral in Equation (4.11) declares that the radiation forces exerted on a ship's hull are partially dependent on the previous motion history. This transient component of the radiation forces resulting from the oscillation of the free surface and the time history of the vessel's motions at each time step is called "memory effect". For a full-scale ship, a period of 30 seconds is sufficient as the considered period of convolution (Hizir, 2015). Memory functions after that time can be assumed equal to zero.

The calculation of the frequency dependent memory functions is conducted by integrating the damping coefficients derived from the solution of the linear BVP in a range of encounter frequencies, adopting an inverse Discrete Fourier Transformation (DFT). The calculation of the IRF is performed implementing the Simpson's integration rule over 1001 equally spaced interpolated values (Hizir, 2015) derived from the pre-calculated data obtained from PRECAL (Van't Veer, 2009). In order to be consistent with the theory, the integration of the damping coefficients must be conducted from zero frequency up to its infinite value, where the damping values vanish. However, PRECAL faces problems to calculate the damping coefficients in large encounter frequencies as the latter is restricted by a factor of the characteristic panel length as shown in Equation (4.12) (Van't Veer, 2009).

$$\omega_{e,max} \cong \frac{3.5}{\sqrt{\text{characteristic panel length}}} \tag{4.12}$$

The problem arising from the aforementioned relationship is that in order to compute the damping coefficients at large encounter frequencies a very fine mesh is required. Consequently, the memory demands will augment exponentially with the panel shortening and this would lead to impractical needs of computational resources. The calculation of the memory function in forward speed case is performed according to the Equation (4.13).

$$K_{jk} = \frac{2}{\pi}\int_0^{\infty}\left[B_{jk}(\omega_e) - B_{jk}(\infty)\right]\cos(\omega_e\tau)d\omega_e \tag{4.13}$$

A correction of the frequency dependent damping coefficients by subtracting their infinite value is necessary in this case, in order to get zero damping at infinite frequency. The integral in Equation (4.13) for a full-scale ship can be easily computed by implementing the well-known Simpson's rule over 1001 interpolated points. The most practical way to account for the memory effects during time-domain seakeeping simulations in order to reduce the computational cost, is to import the pre-calculated matrix of the IRF values for the considered convolution period, which will be multiplied with the matrix of the velocities' history to derive the convolution integral. Examples of the calculation of the diagonal and cross-coupling memory functions of the KVLCC2 tanker and of a C-11 class container ship at non-zero forward speed are illustrated below.

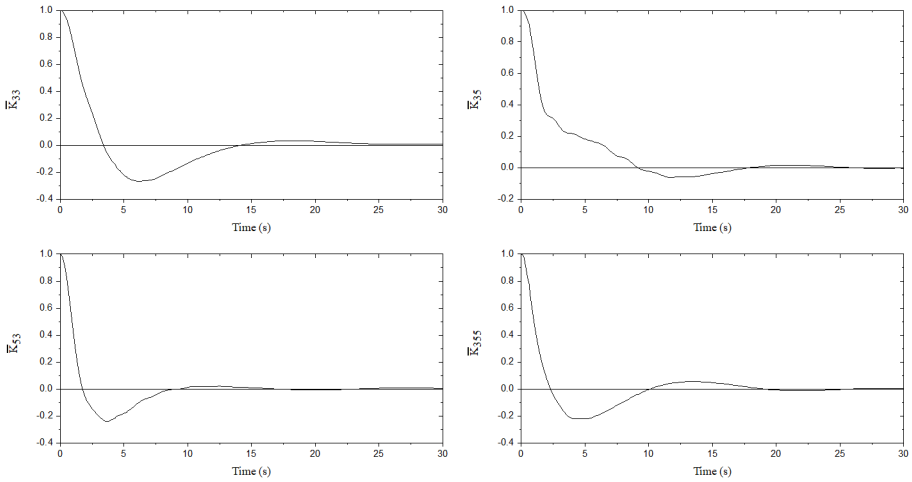

Figure 4.4: Normalized Kernel functions of KVLCC2 at Fn=0.142

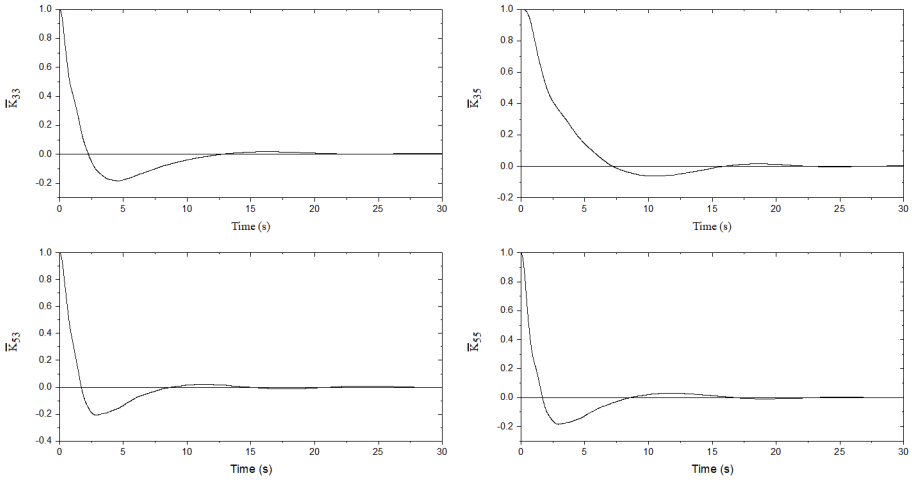

Figure 4.5: Normalized Kernel functions of a C-11 class container ship at Fn=0.1624

Ogilvie (1964) provided a relationship which can be used in order to derive the frequency dependent added mass and damping coefficients when their infinite values and the time domain memory functions are known. The latter calculations can be performed using Equations (4.14) and (4.15).

$$B_{jk}(\omega_e) = B_{jk}(\infty) + \int_0^\infty K_{jk}(\tau)\cos(\omega_e\tau)\,d\tau \qquad (4.14)$$

j, k= 1,…, 6

$$A_{jk}(\omega_e) = A_{jk}(\infty) - \frac{1}{\omega_e}\int_0^\infty K_{jk}(\tau)\sin(\omega_e\tau)\,d\tau \qquad (4.15)$$

4.2.4 Roll Damping

Roll motion is the most significant response that should be investigated in terms of ship stability and requires special care during its modelling. Among the various moments acting on the ship's hull (restoring, damping, actual and added inertial contributions, wave excitation etc.) roll damping moment has the greatest impact due to the dominant viscous effects that take part during ship's oscillation about her longitudinal axis and should be predicted adopting methods of high accuracy, which satisfactorily represent the underlying physics of the problem. Subsequently, verified and validated time domain tools may be employed for the early dynamic stability assessment of a marine vessel and for the investigation of a ship's heel angle during turning. The importance of developing accurate methods for the calculation of the roll damping moment was pointed out since 1981 as part of the Seakeeping Committee's report of the 16th ITTC (1981).

Nowadays, many available methods exist which aim to calculate roll damping moment based on linear and nonlinear algebraic expressions or resulting from either forced-roll or fixed-roll experiments. A nonlinear formulation of the roll damping moment B_φ can be written as a series of $\dot{\varphi}$ and $|\dot{\varphi}|$ (Himeno, 1981).

$$B_\varphi(\dot{\varphi}) = B_1\dot{\varphi} + B_2\dot{\varphi}\,|\dot{\varphi}| + B_3\dot{\varphi}^3 + \cdots \qquad (4.16)$$

Coefficients B_1, B_2, B_3, etc. depend on the roll amplitude φ_A and on the wave frequency ω when a periodic roll oscillation is established.

The determination of the aforementioned coefficients is hard to be achieved in the context of nonlinear roll damping calculation therefore, the adoption of an equivalent linear coefficient B_ε is suggested. In this case, the roll damping moment is represented by the following expression.

$$B_\varphi(\dot{\varphi}) = B_e\dot{\varphi} \tag{4.17}$$

For a simple sinusoidal motion, the equivalent linear damping coefficient can be obtained by the following formula.

$$B_e = B_1 + \frac{8}{3\pi}\omega\varphi_A + \frac{3}{4}\omega^2\varphi_A^2 B_3 \tag{4.18}$$

In general, B_1, B_2 and B_3 are considered independent of the roll amplitude however, B_2 which mainly incorporates the effect of the bilge keels, depends on the roll amplitude. The aforementioned coefficients can be obtained from regression analysis exploiting experimental data. Performing such an analysis, Takaki and Tasai (1973) generated a table of non-dimensional damping coefficients for four representative hull forms namely, a container ship, a tanker, an ore carrier and a general cargo ship. Coefficients from this table are used in the present study in order to directly assess the stability of a C-11 class container ship against parametric roll.

Apart from the simple method described above, approaches that are more sophisticated can be employed in order to calculate the damping coefficient such as the component analysis. According to this method, the various underlying flow phenomena have to be taken into consideration namely, the hull's skin friction, the eddies shedding from the hull etc. In such case the roll damping coefficient is given by the following expression.

$$B_e = B_F + B_E + B_W + B_L + B_{BK} \tag{4.19}$$

In the latter, B_F stands for the skin-friction forces acting on the ship's hull whilst, B_E is a the so-called eddy making term that is similar to the nonlinear product $B_2\dot{\varphi}|\dot{\varphi}|$. Additionally, B_W refers to the damping caused by the radiated free surface waves and B_L is the linear part of the lifting effect that the moving ship creates. Finally, B_{BK} is the damping due to pressure alterations caused by the ship's bilge keels.

Although this method accounts for the physics that govern roll motion, it is not applied within the present study as parametric roll investigation is conducted only in order to verify the ability of ELIGMOS to identify parametric roll.

For the modelling of roll motion, the hydrodynamic reference frame can no longer be used as for high heel angles that might appear in the event of dynamic instability ship's inertia change. For that reason, the equations of ship motions must be expressed at the horizontal reference frame with the assistance of a body-fixed coordinate system. This will be discussed in following paragraphs, as a special case of the hybrid (coupled) seakeeping and manoeuvring mathematical formulation.

4.2.5 Diffraction Forces

Diffraction forces can be calculated at each time step using the Equation (4.2) which utilizes the solution of the linear BVP separating the complex force amplitude into a real and an imaginary part as depicted in Equations (4.3) and (4.4). The aforementioned way to incorporate the effect of diffraction forces is commonly used in Level 1 (linear) and Level 2 seakeeping simulations (Froude-Krylov nonlinear) which are employed in the present research study. It was mentioned in previous chapters that higher levels of nonlinearity can be adopted in order to evaluate a ship's time domain seakeeping performance. Specifically, in level 3 computations (Body Nonlinear Methods) the diffraction (and radiation) potential is solved instantaneously over the exact wetted surface. As a way to reduce the computational cost that is caused from the continuous re-panelization at each positon, pre-calculated values of the diffraction (and radiation) forces for different ship's positions are stored and interpolation techniques are used subsequently in order to account for the exact diffraction (and radiation) forces.

Additionally, level 4 methods (Body-Exact) are more sophisticated compared with the level 3 methods and they incorporate the highest level of nonlinearities adopting the Eulerian approach. In level 4 methods the immersed hull surface must be re-mapped instantaneously leading to large computational cost as the perturbation potential must be evaluated at each time increment. Review of the existing level 3 and level 4 methods will not be conducted in the present thesis as they are considered out of the scope of a hybrid method, which simulates a ship's manoeuvring motion in waves.

4.2.6 Second-Order Steady Wave Forces

Accurate modelling of ship's second order wave forces is of great importance both in the case of straight course keeping and in the case of manoeuvring in a seaway as they affect the selection process of a proper engine and propulsion system. These should be able to provide the necessary power requirements for a safe and environmentally sustainable journey. Additionally, due to the increase in ships' length the recent years, the ratio of wavelength to ship length, which is of practical interest is 0.5 (Liu et al., 2015). The aforementioned value corresponds to a characteristic wave period of 6 seconds which is commonly met in coastal and pelagic seas, whereas for larger ships (> 250m), which operate in open seas, the typical wave period is 9 seconds thus, the short wave approximation is verified as well.

In this context, Faltinsen (1980) proposed a formula for the practical calculation of the second-order force for vertical sided speeds within the limitations of potential flow theory.

$$\bar{F}_n \approx \frac{1}{2}\rho g \zeta_\alpha^2 \left\{ \sin^2(w + \chi) + \frac{2\omega U}{g}[1 - \cos\theta \cos(w + \chi)] \right\} \tag{4.20}$$

After the evaluation of $\bar{F}_n$, the mean second order forces and yaw moment can be calculated by implementing the following formulae.

$$\bar{F}_i = \int_L \bar{F}_n n_i dl \tag{4.21}$$

The integral in Equation (4.21) is calculated over the non-shadow region of the ship's hull and

$$n_1 = \sin\theta \tag{4.22}$$

$$n_2 = \cos\theta \tag{4.23}$$

$$n_3 = x\cos\theta - y\sin\theta \tag{4.24}$$

In Equation (4.20), ω is the circular wave frequency, ψ is the direction of wave propagation and θ is defined as the inclination angle of a line segment. Additionally, U is the vessel's forward speed. It was mentioned before that Faltinsen's formula is valid only for full hull forms (i.e. tankers and bulk carriers) therefore, a correction should be applied in order to account for the flare at sections near the ship's bow.

Papanikolaou and Zaraphonitis (1987) implementing a near field approach, proposed a corrected formula for the estimation of the second order wave force for an arbitrary selection of the position of the coordinate system's origin , where they introduced the coefficient α_{WL} which represents the sectional flare angle (0 stands for wall-sided geometry) above the Still Water Level (SWL).

The aforementioned formula at zero speed is depicted in Equation (4.25).

$$\bar{F}_n \approx -\frac{1}{2}\rho g \int_L {\zeta_r^{(1)}}^2 \sec\alpha_{WL} dl + \frac{1}{2}\rho \iint_S \left|\nabla\Phi^{(1)}\right|^2 dS \tag{4.25}$$

In Equation (4.25), $\zeta_r^{(1)}$ is the first order relative wave height along the vessel's waterline and $\Phi^{(1)}$ is the first order total wave potential.

Liu et al., (2015) exploiting the latter equation, proposed an updated form of Faltinsen's original formula for short waves which can be seen below.

$$\bar{F}_n \approx \frac{1}{2}\rho g \zeta_\alpha^2 \sec\alpha_{WL} \left\{\sin^2(w+\chi) + \frac{2\omega U}{g}[1 - \cos\theta\cos(w+\chi)]\right\} \tag{4.26}$$

Further, since Faltinsen's original formula was initially proposed for head seas, it did not incorporate the effect that oblique to beam seas have on the flow around ship's stern. Especially for modern design concepts, where a significant flare is noticed at the end sections, having a very small local draught. The effect of local draft is embedded in the formula proposed by Liu et al., (2015) by means of the modified coefficient α_d.

$$\alpha_d = \frac{\pi^2 I_1^2(k_e d)}{\pi^2 I_1^2(k_e d) + K_1^2(k_e d)} \tag{4.27}$$

The updated expression, which is used to calculate the mean second order force including the effect of local draught, is shown below.

$$\bar{F}_n \approx \frac{1}{2}\rho g \zeta_\alpha^2 \alpha_d \sec\alpha_{WL} \left\{\sin^2(w+\chi) + \frac{2\omega U}{g}[1 - \cos\theta\cos(w+\chi)]\right\} \tag{4.28}$$

The latter equation is further corrected regarding the ship's hull form. For full forms having a typical block coefficient equal to 0.87, Liu et al., (2015) recommend that the final expression of the second order wave forces should be multiplied by the value

$$(\frac{0.87}{C_B})^{\cos\psi(1+n\sqrt{Fn})} \tag{4.29}$$

The final practical formula proposed by Liu et al., (2015) within the framework of a near field method, can be seen in Equation (4.30).

$$\bar{F}_n \approx \frac{1}{2}\rho g\zeta_\alpha^2\alpha_d \sec\alpha_{WL}(\frac{0.87}{C_B})^{\cos\psi(1+n\sqrt{Fn})}\left\{\sin^2(w+\chi)+\frac{2\omega U}{g}[1-\cos w\cos(w+\chi)]\right\} \tag{4.30}$$

Results found in Liu et al., (2015) on added resistance for the S-175 container ship based on the aforementioned methodology, showed that underestimated values are obtained whilst, the deviation from the more exact far field results increased when moving from head to beam seas. For this reason, it is concluded that an exact far field method (Liu et al., 2011) is capable of more accurately calculating the mean second order wave forces.

According to Maruo's (1963) far field method, the Kochin function $H(k_j,\theta)$, which describes the elementary waves, is employed for the calculation of the added resistance.

$$H(k_j,\theta) = \iint_S(\Phi\frac{\partial}{\partial n} - \frac{\partial\Phi}{\partial n}G_j(m)dS \tag{4.31}$$

whilst, $$G_j(\theta) = \exp\left[(k_j(m)z + ik_j(m)(x\cos m + y\sin m)\right] \tag{4.32}$$

In Equation (4.32) $k_j(m)$, j=1, 2 are the unsteady wave numbers derived from the following expression.

$$k_j(m) = \begin{cases} \frac{K_0}{2}\frac{1-2\Omega\cos m+\sqrt{1-4\Omega\cos m}}{\cos^2 m}, & \text{for } j=1 \\ \frac{K_0}{2}\frac{1-2\Omega\cos m-\sqrt{1-4\Omega\cos m}}{\cos^2 m}, & \text{for } j=2 \end{cases} \tag{4.33}$$

In the latter equation, θ stands for the angle of the elementary waves generated by the ship, whilst $\Omega = {\omega_e U}/{g}$ is Hanaoka's parameter. Finally, $K_0 = {g}/{U^2}$ is the steady wave number.

Adopting the aforementioned analysis, the added resistance in terms of the far field approach can be calculated using the following formula.

$$R_{AW} = \frac{\rho k^2}{8\pi}\int_0^{2\pi}|H(m)|^2\,(cosm - cos\chi)^2 \tag{4.34}$$

whilst, $$H(\theta) = \iint_S \exp\left[(k_j(m)z + ik_j(m)(xcosm + ysinm)\right] \left[\Phi k(n_3 + icosmn_1 + isinmn_2) - \frac{\partial\Phi}{\partial n}\right] dS \tag{4.35}$$

The results of the second order wave forces implementing the aforementioned near and far field methods are illustrated below for the S-175 container ship at unit amplitude short wave seas (λ/L_{pp})=0.5 and various heading angles and forward speed values. The following values have been calculated with the use of NEWDRIFT (implements a near field which is applicable only at zero or low speeds) and NEWDRIFT+ (implements a far field method) hydrodynamic software. The latter has been used only for the calculation of the added resistance at short waves (λ/L=0.5).

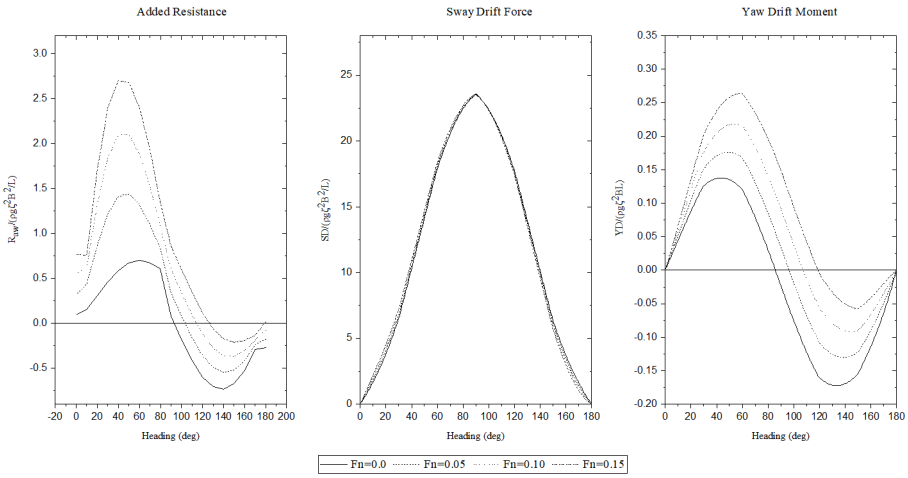

Figure 4.6: Nondimensional added resistance, sway drift force and yaw drift moment for S-175 at heading angles [0, 180°] and Fn=0.0, 0.05, 0.10 and 0.15 (λ/L=0.5)

Results from both methods have been used in the present simulations. Especially, in case of shallow water manoeuvring in a seagoing environment, the near field formulation is employed as it is capable of incorporating this effect. The adopted numerical scheme that facilitated the proper use of the aforementioned force components will be presented in following paragraphs.

4.3 Time Domain Manoeuvring Modelling

4.3.1 General Remarks

The calm water manoeuvring performance of a marine vessel at her early design stage can be investigated by means of theoretical, experimental and numerical approaches. In the present study, ship's manoeuvrability is studied by means of modular and whole ship time domain simulations exploiting experimental and theoretical methods for the determination of the hydrodynamic derivatives.

Usual 3-DOF nonlinear mathematical formulation of a ship's manoeuvring motion taking place on the horizontal plane will be provided whereas, 4-DOF approaches will be presented as well. The latter, offers the possibility to investigate a ship's heeling response during circular turning motion. Necessary modifications found in the literature in case of ship's manoeuvring in shallow water will be discussed as well.

Manoeuvring modelling in calm water is considered as an elemental module within the process of developing a hybrid method for the investigation of a ship's manoeuvrability in regular waves thus, its analytical presentation and validation effort is chosen. External forces will be presented in parts (hull, rudder, and propeller components) as their individual performance can be judged separately.

4.3.2 Equations of Calm Water Manoeuvring Motion

Sano and Yasukawa (2008) presented the following nonlinear mathematical model based on the MMG approach, which is adopted in the context of the present research. The equations of motion are described at a body-fixed coordinate system, which can be thought as a special case of the horizontal reference frame resulting by the absence of waves and having its origin at the ship's centre of gravity. The instantaneous position of the vessel is obtained after implementing the velocities' transformations depicted in Equations (3.6)-(3.8).

$$(M + M_x)\dot{U}_{hs} - (M + M_y)V_{hs}R_{hs} = X \quad (4.36)$$

$$(M + M_x)U_{hs}R_{hs} + (M + M_y)\dot{V}_{hs} = Y \quad (4.37)$$

$$(I_Z + J_{zz})\dot{R}_{hs} = N \quad (4.38)$$

In Equations (4.36)-(4.38) M_x, M_y, and J_{zz} are the surge and sway added masses and yaw added moment of inertia at zero frequency respectively. Additionally, M and I_z are the ship's mass and moment of inertia about her vertical axis whilst, U_{hs}, V_{hs} and R_{hs} are velocities at surge, sway and yaw directions respectively. For slow manoeuvring motion in calm water, these values refer to the zeroth frequency of encounter. The right hand sides correspond to the external forces in surge, sway and yaw degrees of freedom. The external forces consist of hydrodynamic, rudder and propeller components.

$$X = X_H + X_P + X_R \quad (4.39)$$

$$Y = Y_H + Y_R \quad (4.40)$$

$$N = N_H + N_R - (Y_H + Y_R)x_G \quad (4.41)$$

Subscripts H, P, R stand for hydrodynamic, propeller and rudder forces respectively and their calculation process will be explained in detail in following chapters. Calm water resistance is considered as a part of the hydrodynamic forces X_H exerted on ship's hull.

In case where heel effect is also considered during the analysis of a ship's manoeuvrability, a fourth equation, modelling her roll motion, has to be incorporated as well. Usually, medium to high speed vessels with high position of the vertical position of their centre of gravity, such as container ships and passenger ships, tend to develop intense roll angle which affect their manoeuvring performance.

$$(I_{xx} + J_{xx})\dot{P}_{hs} = K \quad (4.42)$$

In the aforementioned equation, K denotes the external roll moment, which can be evaluated by the summation of the following hull hydrodynamic and rudder components.

$$K = K_H + K_R - z_H Y_H \quad (4.43)$$

In Equation (4.43) K_H is the hydrodynamic roll moment acting on the ship's hull, K_R is the roll moment generated by the rudder $z_H Y_H$ is the roll moment resulting from the action of the lateral hydrodynamic force at a vertical position z_H on the vessel's hull. Detailed calculation methods for all the aforementioned force components at each degree of freedom can be found in the following paragraphs of this chapter and in Appendix A.

4.3.3 Hull Hydrodynamic Forces

These forces include first-order lift components and second-order (or higher) elements which represent the impact of cross-flow and separation viscous effects. Hydrodynamic (hull) forces consist of the most critical part in the process of developing a manoeuvring model. On the basis of the analysis presented in Chapter 3, hydrodynamic reaction forces on the ship's hull are calculated by means of Taylor expansion, using the hydrodynamic derivatives, which can be obtained by theoretical, experimental, semi-empirical and numerical (CFD) methods. In the present study, the hydrodynamic forces are modelled using a fourth-order formulation, as the one proposed by the Japanese MMG whilst, the necessary hydrodynamic derivatives are obtained from physical Captive Model Tests, performed at Hiroshima University. For the investigation of ship's manoeuvring performance in shallow water, corrections of the hydrodynamic derivatives based on the under keel clearance and the vessel's principal particulars have been applied, based on Ankudinov et al. (1990) semi-empirical formulae. The analytical expressions for the calculation of the hydrodynamic forces in surge, sway, yaw and roll can be seen below.

$$X'_H = -R'_0 + X'_{vv}v'^2 + (X'_{vr} + M' + A_{22\rightarrow 0}{}')v'r' + X'_{rr}r'^2 + X'_{vvvv}v'^4 \quad (4.44)$$

$$Y'_H = Y'_v v' + (Y'_r - M' - A_{11\rightarrow 0}{}')r' + Y'_{vvv}v'^3 + Y'_{vvr}v'^2 r' + Y'_{vrr}v'r'^2 + Y'_{rrr}r'^3 \quad (4.45)$$

$$N'_H = N'_v v' + N'_r r' + N'_{vvv}v'^3 + N'_{vvr}v'^2 r' + N'_{vrr}v'r'^2 + N'_{rrr}r'^3 \quad (4.45)$$

Superscript " $'$ " refers to the non-dimensional values of the forces, hydrodynamic derivatives and velocities. Using non-dimensional values of the hydrodynamic derivatives is a helpful procedure as they can be used in the same manner for either full scale or model scale ships.

Calm water resistance R_0 is considered as part of the hydrodynamic force acting on the ship's hull opposite to her forward motion. Calm water resistance usually is calculated from model tests for various forward speed values. Subsequently, regression analysis can be implemented in order to formulate a second-order function of the following form. In the present study, parameters a_1, a_0 have been obtained from published data.

$$R_0' = a_1 u'^2 + a_0 u' \tag{4.46}$$

The hydrodynamic roll moment on the ship's hull based on Yasukawa and Sano's publication can be derived from the following expression.

$$K_H = -C_{44}\varphi - B_{44}\dot{\varphi} \tag{4.47}$$

where, B_{44} is the roll damping coefficient and can be either determined experimentally or approximated by use of specific expressions included in Appendix A. Additionally, C_{44} is the linear roll restoring coefficient, which depends on the vessel's metacentric height as depicted in Appendix A. Finally, the heel effect on yaw hydrodynamic moment can be incorporated by introducing two additional coupling terms in (4.45) namely, the $N'_{\varphi}\varphi$ and $N'_{r\varphi}r'|\varphi|$.

4.3.4 Rudder Forces

Rudder forces play a significant role during ship's manoeuvring in calm water whilst, sufficient steering action must be ensured in adverse weather conditions as well. Hydrodynamic lift and drag forces generated by the rudder's action are calculated in a separate module employing the directives provided by the Japanese MMG. According to the proposed modelling, the rudder is treated as a wing, which is placed at an effective angle against the incoming flow exploiting the increased velocity behind the ship's propeller. Additionally, rudder forces are strongly affected by the interactions among the vessel's hull and propeller. In light of the aforementioned background, the suggested methodology is presented, used for the calculation of rudder's forces in surge, sway and yaw DOF.

$$X_R = -(1 - t_R)FN\sin\delta \quad (4.48)$$

$$Y_R = -(1 + a_H)FN\cos\delta \quad (4.49)$$

$$N_R = -(x_R + a_H x_H)FN\cos\delta \quad (4.50)$$

In Equations (4.48)-(4.50) FN is the rudder's normal force whilst, t_R expresses both a reduction factor of the steering resistance and an increase of the propeller's thrust due to steering action. Further, α_H is a factor, which reveals the increase of the lateral force induced by steering, against the normal force FN and x_R is the longitudinal location along the ship, where the aforementioned lateral force is acting. The rudder's normal force can be evaluated implementing the following expression.

$$FN = \frac{1}{2}\rho A_R U_R^2 f_a \sin a_R \quad (4.51)$$

In the latter equation, A_R is the rudder's area and α_R is the inflow rudder's angle which can be approximated by the expression

$$\alpha_R \approx \delta - \frac{v_R}{U_R} \quad (4.52)$$

In Equation (4.52) δ is the rudder's angle whilst, v_R, u_R are the lateral a longitudinal rudder's inflow velocities respectively. Additionally, f_a is the rudder's gradient of the lift coefficient which is a function of the rudder's aspect ratio. Finally, flow-straightening mechanisms, resulting from the presence of the hull and the propeller position in front of the rudder reduce the actual inflow angle from its geometrical value by a factor γ_R which is, normally, smaller than 1.

In 4-DOF manoeuvring models, the rolling moments due to the rudder's action is given by the following equation.

$$K_R = -z_R Y_R \quad (4.53)$$

In the latter equation, z_R is the point where the lateral rudder force is acting and is positioned at about 70% of the rudder's height.

4.3.5 Propeller Force

According to Yasukawa and Yoshimura (2015), propeller's thrust X_P is calculated at each time increment by use of the following formula.

$$X_P = (1 - t_P)T_x \tag{4.54}$$

$$T_x = \rho n_P^2 D_P^4 K_T(J_P) \tag{4.55}$$

In the aforementioned equations, t_P is the thrust deduction coefficient, which depends on the instantaneous propeller's load. However, in sale of simplicity, t_P is kept constant throughout the ship's manoeuvring motion. Additionally, D_P is the propeller's diameter and n_P are the revolutions of the propeller (per second) which are kept unchanged as a constant rpm strategy is adopted in the present study. The open water propeller's characteristic value K_T is expressed by means of a second-order polynomial of the advance ration J_P namely,

$$K_T(J_P) = k_2 J_P^2 + k_1 J_P + k_0 \tag{4.56}$$

The advance ratio J_P can be evaluated by the following expression.

$$J_P = \frac{u(1-w_P)}{n_P D_P} \tag{4.57}$$

The wake fraction w_P has to be determined instantaneously during the manoeuvring trajectory. For this purpose, the simplest formula depicted below is adopted, where only the drift angle at the propeller's position needs to be known.

$$\frac{w_P}{w_{P0}} = \exp(C_1 \beta_P^2) \tag{4.58}$$

$$\text{where, } \beta_P = \beta - x'_P r' \tag{4.59}$$

In the Equation (4.59), β is the drift angle at the amidships and x'_P, r' are the non-dimensional propeller's positon along the ship's length and yaw rate.

4.4 Hybrid Seakeeping and Manoeuvring Mathematical Formulation

4.4.1 General Remarks

In order to model ship's manoeuvring motion in regular waves, the aforementioned approaches, namely seakeeping and manoeuvring in calm water, have to be coupled. In the present research work, this is done by incorporating the wave forces in the system of manoeuvring equations simultaneously at any time *t*.

In case where small wave amplitudes are considered, all wave forces are incorporated with the implementation of a multidimensional interpolation technique, which will be discussed during the presentation of the implemented numerical scheme. The interpolation is performed over pre-calculated values of the wave forces (first-order Froude-Krylov and Diffraction forces and second-order mean wave forces) and is based on the vessel's instantaneous forward speed and heading angle. Alternatively, in cases where the ship's manoeuvring performance is conducted in large amplitude waves, the equations of motion are expressed at the horizontal body-fixed reference frame in order to account for the nonlinearities in the calculation of Froude-Krylov forces and the alteration of the vessel's inertial matrix, occurring at large rotational displacements.

4.4.2 Hybrid Seakeeping and Manoeuvring Model

Two different approaches are suggested in order to simulate a ship's manoeuvring motion in regular waves,. The first one refers to the use of linear seakeeping theory coupled with the nonlinear manoeuvring force contributions, when the wave excitations are considered of small amplitude. Alternatively, a coupled formulation has to be employed, which incorporates the nonlinearities associated with the modelling of the seakeeping forces (Froude-Krylov and Restoring contributions) in large amplitude waves. In the former scenario, seakeeping and manoeuvring force components can be expressed at the hydrodynamic (seakeeping elements) and body-fixed (manoeuvring elements) reference frames as it is considered that they coincide during slow evolving manoeuvring motion in seas of small waves.

In case where ship's manoeuvring performance is investigated in the presence of large amplitude waves, the system of horizontal motion equations is formulated on the basis of Hamamoto and Kim's (1993) and Fang's (2005) model. In this respect, the general form of Newton's second law of dynamics provides the equations of motion of a ship exposed in various external disturbances, which expressed at the earth-fixed reference frame using the following equations.

$$M\dot{\vec{V}}_G + \omega \times \dot{V}_G = \vec{F} \tag{4.60}$$

$$\dot{\vec{H}}_G + \omega \times \vec{H}_G = \vec{M} \tag{4.61}$$

In the previous expressions, $M\vec{V}_G$ is the vector of the linear momentum and $\vec{H}_G$ the vector of the angular momentum about the ship's centre of the gravity. Finally, $\vec{F}$ and $\vec{M}$ are the vectors of external forces and moments. However, transformation of Equations (4.60) and (4.61) is needed in order to express the equations of motion at the horizontal body-fixed reference frame which is used within the framework of the present simulations of ship manoeuvring in regular waves. The transformed equations are the following.

$$M\left(\dot{\vec{V}}_G + \vec{k}\dot{\psi} \times \vec{V}_G\right) = -\iint_S p\vec{n}dS + \vec{F} \tag{4.62}$$

$$\dot{\vec{H}}_G + \vec{k}\dot{\psi} \times \vec{H}_G = -\iint_S p(r \times \vec{n})dS + \vec{M} \tag{4.63}$$

In the Equations (4.62) and (4.63) $\vec{V}_G = \vec{i}U_{hs} + \vec{j}V_{hs} + \vec{k}W_{hs}$ and $\vec{H}_G = \vec{i}H_{x'} + \vec{j}H_{y'} + \vec{k}H_{z'}$ where, U_{hs}, V_{hs}, W_{hs} are the linear surge, sway and heave velocities and $H_{x'}$, $H_{y'}$ and $H_{z'}$ are the components of the angular momentum about the horizontal body-fixed reference frame which are defined by the following expression.

$$\begin{bmatrix} H_{x'} \\ H_{y'} \\ H_{z'} \end{bmatrix} = \begin{bmatrix} I_{x'x'} & -I_{x'y'} & -I_{x'z'} \\ -I_{y'x'} & I_{y'y'} & -I_{y'z'} \\ -I_{z'x'} & -I_{z'y'} & I_{z'z'} \end{bmatrix} \begin{bmatrix} \dot{\Phi}_{hs} \\ \dot{\Theta}_{hs} \\ \dot{\Psi}_{hs} \end{bmatrix} \tag{4.64}$$

In the aforementioned equation, moments and cross-inertial terms are expressed at the horizontal body-fixed reference frame applying transformations that will be shown later in this section.

Using expressions (4.62)-(4.64), the equations of surge, sway, yaw and roll at the horizontal body-fixed reference frame are the following.

Surge equation: $$M\left(\dot{U}_{hs} - V_{hs}\dot{\Psi}_{hs}\right) = X' + T_x(1-t) - R \tag{4.65}$$

Sway equation: $$M\left(\dot{V}_{hs} - U_{hs}\dot{\Psi}_{hs}\right) = Y' \tag{4.66}$$

Roll equation: $$\dot{H}_{x'} - H_{y'}\dot{\Psi}_{hs} = K' \tag{4.67}$$

Yaw equation: $$\dot{H}_{z'} = N' \tag{4.68}$$

In Equations (4.65)-(4.68) the RHS refer to the external forces at each DOF with respect to the horizontal body-fixed reference frame. Since vertical motions are not considered in the aforementioned system of equations, the following transformations apply to the added masses and added moments of inertias.

$$\begin{cases} M_{x'} = M_x \\ M_{y'} = M_y\cos^2\varphi + M_z\sin^2\varphi \\ I_{x'x'} = I_{xx} \\ I_{z'z'} = I_{zz}\cos^2\varphi + I_{yy}\sin^2\varphi \end{cases} \tag{4.69}$$

Stressed values refer to the horizontal body-fixed reference frame, whereas no-stressed values refer to the general body axes system. Finally, φ is the Eulerian roll angle of rotation. These values has been decided to refer to zero frequency.

Other researchers (i.e. Fang, 2005) claim that the frequency dependency of the hydrodynamic coefficients must be incorporated in the mathematical model. In the context of the present thesis, it is judged that since the vessel's accelerations are generally small, apart from the time period shortly after the rudder's deflection where transient phenomena take part, selection of a proper modelling for the incorporation of the added inertias may consist of an open issue.

After the presentation of the mathematical equations that describe ship's vertical motions and ship's manoeuvring motion in calm water and in regular waves, a detailed presentation of the structure of the developed time domain numerical tool ELIGMOS will be provided in the following chapter.

4.5 Summary

In Chapter 4 a detailed presentation of the adopted time domain mathematical analysis, which describes ship's motion in either calm water or in regular waves, is presented. Specifically, four different sailing conditions are considered namely, linear and nonlinear seakeeping simulations, nonlinear manoeuvring simulation in calm water and ship's manoeuvring simulation in waves.

For each modelling, the general equations of motion were presented with respect to the suitable reference frame. Additionally, all force components that appear in any case, are discussed and relevant mathematical expressions used for their calculation are depicted.

Subsequently, two flow charts of the developed hybrid numerical tool ELIGMOS are presented. The first one (Figure 5.1) applies in simulations of ship manoeuvring response in regular small waves, where the wave forces are incorporated implementing a multidimensional interpolation technique as their values depend on both the instantaneous forward speed and the heading angle. The second one (Figure 5.2) schematically illustrates the structure of the numerical method when large wave excitations are considered. In such condition, the adoption of linear seakeeping properties is not valid anymore thus, transformations are needed in order to account for the effect of extreme angular motions (mainly in roll direction).

In order to validate the aforementioned mathematical methodology, results concerning ship's nonlinear seakeeping performance (including results on direct stability assessment against parametric rolling of ships), nonlinear manoeuvring response in calm water and results on hybrid seakeeping and manoeuvring performance will be presented in Chapter V. The aforementioned validation process is selected, as an elemental approach during the validation of a numerical method that simulates ship's manoeuvring ability in regular waves *"provides insight into a simulation's ability to capture the overall physics of the ship motions in waves problem"* as stated in Reed and Zuzick (2015).

CHAPTER 5

IMPLEMENTATION OF THE DEVELOPED METHODOLOGY

5.1 Introduction

After demonstrating the analysis of the implemented time-domain methodology in the previous chapter, it is considered necessary to present the structure of the numerical code that was developed in order to investigate a vessel's hydrodynamic performance. The time-domain code ELIGMOS is capable of performing nonlinear calm water manoeuvring simulations in both deep and shallow waters, linear and nonlinear time-domain seakeeping analysis and simulation of a ship's manoeuvring performance in regular waves. ELIGMOS is written in C++ programming language, which is supported by a vast amount of libraries and offers a convenient usage of the properties of object-oriented programming.

In general, the algorithmic structure of every module of ELIGMOS is the same and can be represented by the numerical solution of a system of motion equations over time, formulated in matrix form. The latter, as well as the various input data needed for each analysis, will be presented in detail in the following sections of this chapter. Moreover, in order to make the structure of ELIGMOS more understandable, especially at its integrated version where seakeeping and manoeuvring approaches are coupled, two flow charts describing the code's operation are included as well. These refer to two different realizations, which depend on the height of the considered waves.

5.2 Basic formulation of ELIGMOS

The equations of ship motion regarding calm water manoeuvring (4.36-4.38), seakeeping (4.1) and manoeuvring simulations in waves (4.65-4.68) are solved numerically, formulating in each case the matrix of masses and added inertias $[M_{ij}]$ and the column vector of external forces $[F_j]$ as shown in (5.1). The unknown accelerations at each DOF are included in the column vector $[\ddot{X}_j]$.

$$[M_{ij}] \cdot [\ddot{X}_j] = [F_j] \qquad i,j=1...4 \tag{5.1}$$

If the selection of the general body-fixed reference frame is necessary for the desirable simulation, the transformation matrices (3.1) or (3.3) have to be implemented in order to express ship motions in either the hydrodynamic reference frame or the horizontal body-fixed one.

The solution of (5.1) provides the second-order time derivatives in the following form.

$$[\ddot{X}_j] = [M_{ij}]^{-1}[F_j] \qquad i,j=1...4 \tag{5.2}$$

In ELIGMOS, the numerical process that derives the solution of the system of equations depicted in (5.2) is succeeded by using the well-known technique of decomposing matrix M_{ij} into a Lower and an Upper triangular matrix (LU Decomposition). Having the accelerations ($\ddot{X}_j$) and the velocities (V_j) at each DOF at time *t*, the values of ship motions and velocities at time *t+dt* can be derived by solving the following first-order differential equations depicted in Equation (5.3).

$$\begin{aligned} \frac{d}{dt}X_{j(t+dt)} &= V_{j(t)} \\ \frac{d}{dt}\dot{X}_{j(t+dt)} &= [M_{ij}]^{-1}[F_j]_{(t)} \end{aligned} \tag{5.3}$$

The resulting first-order differential equations can be solved by any scheme that is suitable for time integration. For this purpose, ELIGMOS implements the well-known Runge-Kutta 4th-order scheme, due to its accuracy and stable performance (Jasionowski, 2001), despite the increased computational time it needs compared to other numerical schemes (e.g. Euler, Runge-Kutta 2nd-order etc.). For manoeuvring simulations and linear seakeeping analysis the adopted time step is equal to 0.1 s, offering quite accurate and fast solutions (7 seconds of CPU time correspond to 150 seconds of a real scenario).

At this point, it is important to mention that ELIGMOS implements Hess and Smith's method (1962) in order to calculate the necessary geometrical characteristics of each panel that are needed for the evaluation of the nonlinear Froude-Krylov and Restoring forces, through a direct pressure integration scheme. By using this method, the main properties of each panel can be determined, namely its area, the coordinates of its center point and the components of its unit normal vector.

The aforementioned characteristics are evaluated at the hydrodynamic reference frame by applying the necessary transformations. Subsequently, for each panel, it is examined whether it is above or below the wave's profile and finally, the calculation of the instantaneous forces can be evaluated. In order to improve the computational efficiency of ELIGMOS, the vectorized evaluation of the previously mentioned wetted panel characteristics (Hizir, 2015) shall be implemented in the future, as the time needed for a nonlinear simulation consists of the major drawback of the code.

The following flow charts that describe the way ELIGMOS operates can be seen straight after. In the context of small amplitude wave excitations, the flow chart representing the adopted methodology has the following form.

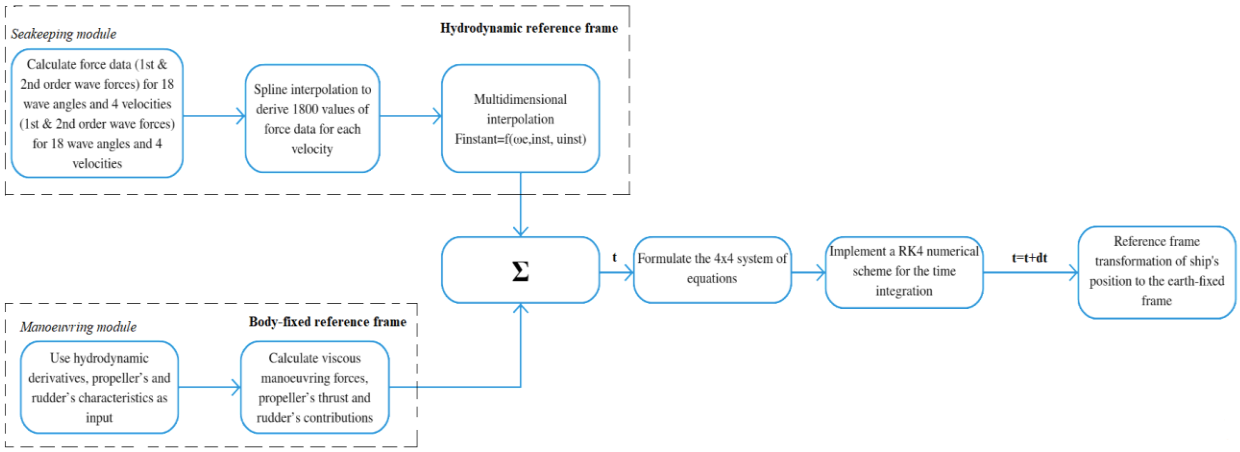

Figure 5.1: Flow chart of the developed numerical method (small wave excitations)

The multidimensional interpolation concerning the first and second order wave forces is performed with regard to the instantaneous heading angle and the value of the longitudinal component of the vessel's forward speed, consisting of a Response Surface Method (RSM). The process to succeed this is the following:

1. Pre-calculate the first and second order forces from 0^o to 180^o in segments of $10^{o,}$ exploiting the equality of the forces between 0^o-180^o and 180^o-360^o due to the vessel's port-starboard symmetry. Additionally, the values of the aforementioned forces were calculated for four different forward speed values, in order to account for the speed alteration during manoeuvring. The calculations are performed using NEWDRIFT v.7 and NEWDRIFT+ hydrodynamic software.

2. Having the forces calculated in 19 heading angles (0^o, 10^o, 20^o, …, 180^o) for each forward speed, 1800 spline points are generated, as a way to express the alteration of the forces for every 0.1^o of heading angle.

   This gives us a more realistic representation of how forces change in relation to the wave's relative direction. When the aforementioned process is finalized, these values are imported in ELIGMOS and the numerical interpolation scheme can be implemented.

3. During the interpolation scheme, a repetitive loop is executed, which provides the values of the first and second order forces for the considered forward speeds, at the instantaneous heading angle namely, $R_{aw,1}(u_1, \chi)$, $R_{aw,2}(u_2, \chi)$, $R_{aw,3}(u_3, \chi)$ and $R_{aw,4}(u_4, \chi)$.

Here, R_{aw} is used as an example and stands for the value of the added resistance at four different forward speeds (u_1, u_2, u_3, and u_4) and at the instantaneous heading angle. Having these values determined [$R_{aw,1}(\chi)$, $R_{aw,2}(\chi)$, $R_{aw,3}(\chi)$, $R_{aw41}(\chi)$], the Newton's interpolation rule (Dahlquist and Björck, 2003) can be implemented which provides, in a practical way, the value of the added resistance at the instantaneous value of the longitudinal component of the ship's forward speed. The performed calculations are illustrated below.

$$\mu_1 = \frac{R_{aw,2} - R_{aw,1}}{u_2 - u_1} \tag{5.4}$$

$$\mu_2 = \frac{R_{aw,3} - 2 \cdot R_{aw,2} + R_{aw,1}}{(u_2 - u_1)(u_3 - u_1)} \tag{5.5}$$

$$\mu_3 = \frac{R_{aw,4} - 3 \cdot R_{aw,3} + 3 \cdot R_{aw,2} - R_{aw,1}}{(u_2 - u_1)(u_3 - u_1)(u_4 - u_1)} \tag{5.6}$$

Consequently, the resulting value of the force with respect to the instantaneous speed and heading angle is calculated using the following expression.

$$R_{aw}(u, \chi) = R_{aw,1} + (u - u_1)\mu_1 + (u - u_1)(u - u_2)\mu_2 + (u - u_1)(u - u_2)(u - u_3)\mu_3 \tag{5.7}$$

The presented numerical scheme is implemented for the instantaneous evaluation of every first and second-order force component. The practicality of the method is attributed to the fact that the performed calculations are quite simple and the simulation time is kept low.

In case where large wave excitations are considered, the numerical method shown in Figure 5.1 is not valid anymore. This time, transformations of the vessel's inertia matrix and of the incident wave forces must apply. As a result, the updated flow chart can be seen below.

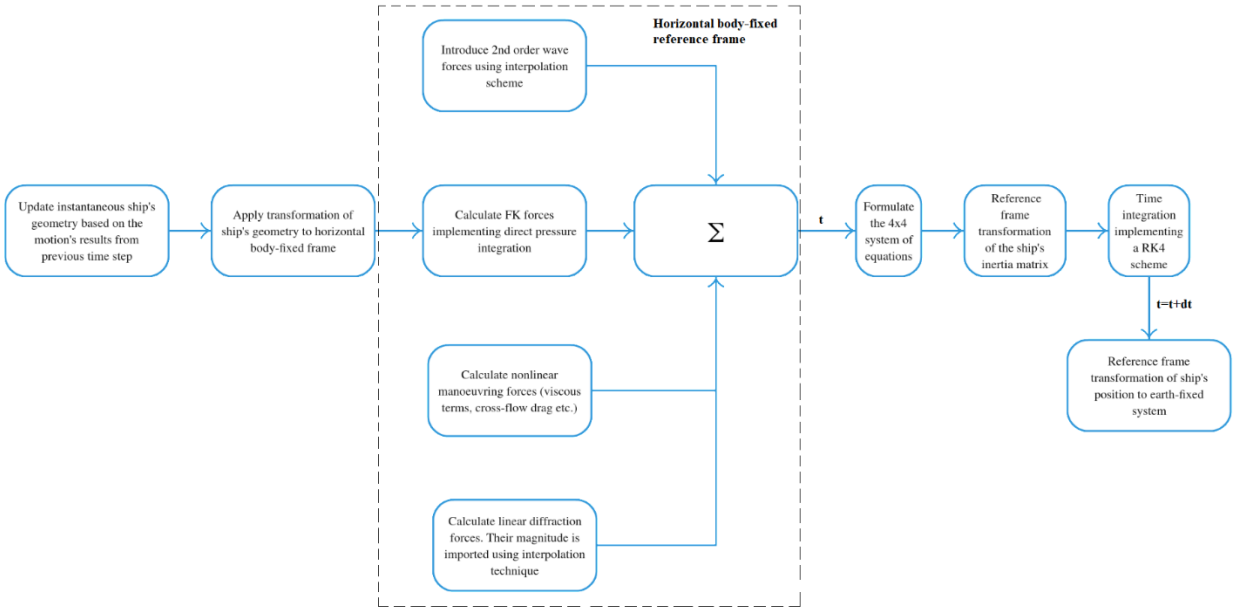

Figure 5.2: Flow chart of the developed nonlinear numerical method (large amplitude waves)

5.3 Summary

In this chapter, a brief presentation of the developed software ELIGMOS was conducted. Although ELIGMOS offers the possibility to simulate a vessel's performance in several operational and environmental conditions with acceptable accuracy exploiting practical approaches, there is still much room for improvement especially as it concerns its computational efficiency. At this stage, for a real nonlinear seakeeping analysis of 6 minutes are required about 40 minutes of CPU time for an i5 processor at 3.50 GHz. This amount of time is considered one of the code's main drawbacks, which needs improvement in the future.

CHAPTER 6

VALIDATION STUDIES

6.1 Introduction

In Chapter 4, the adopted methodology for the time domain simulation of ship manoeuvring motion in regular waves was presented. The equations in surge, sway, yaw and roll were formulated, providing expressions for all external force components in a modular basis. In this context, two distinct cases were considered: a) manoeuvring in small amplitude regular waves and b) manoeuvring in large amplitude waves. In case (a), pre-calculated linear wave forces are incorporated through multidimensional interpolation based on the instantaneous value of the ship's forward speed and her relative angle with the incoming waves. Alternatively, in case (b), linear wave forces are not valid anymore as the wave excitations are of large amplitude and, at first stage, geometrical nonlinearities of the ship's hull must be taken into consideration. In this case, the significant Froude-Krylov and Restoring (when applicable) forces and the force components originating from the low frequency manoeuvring motion must be calculated with respect to the horizontal reference frame. Necessary transformations of the ship's geometry, the wave forces and the ship's inertia matrix are described in detail.

Before the presentation of the hybrid system of equations, analytical discussion on the fundamental approaches (seakeeping and manoeuvring in calm water) was performed. This was done by showing the equations of motion in each case, based on linear and nonlinear analyses. Especially, in nonlinear seakeeping analysis, it was underlined that apart from pure vertical motion simulations, investigating parametric roll would offer additional accreditation to the developed numerical tool, as it consists of a highly nonlinear phenomenon attracting the interest of naval architects as an effort to establish the performance-based SGISC.

Based on the aforementioned, it is easily understood that a newly developed numerical tool dealing with the highly demanding task of accurately simulating ship's manoeuvring performance in a seaway, has to be rigorously validated.

This process will be presented in this chapter, providing evidence, which proves that the developed software ELIGMOS is able to conduct hydrodynamic analysis related with ship's manoeuvring in calm water, linear and nonlinear seakeeping performance, parametric roll investigation and manoeuvring in regular waves.

6.2 Manoeuvring in Calm Water

6.2.1 Simulations in Deep Water

The presentation of validation studies starts from the case of ship manoeuvring in calm water. The performed manoeuvers consist of standard turning circle and zig-zag tests as those prescribed in ITTC Recommended Procedures for Manoeuvring Trials (2002) in both deep and shallow waters, according to the system of Equations (4.36)-(4.38) and (4.42). Simulation results are expressed by use of the earth-fixed coordinates and are compared against experimental and numerical trajectories found in the literature. Validation of this module is performed using full scale KVLCC2 and 1:50 model scale S-175 container ship as case studies. In Figure 6.1 turning circle trajectories, which were derived implementing the present method, are plotted together with experimental ones concerning the L7-model found in Yasukawa and Yoshimura (2015).

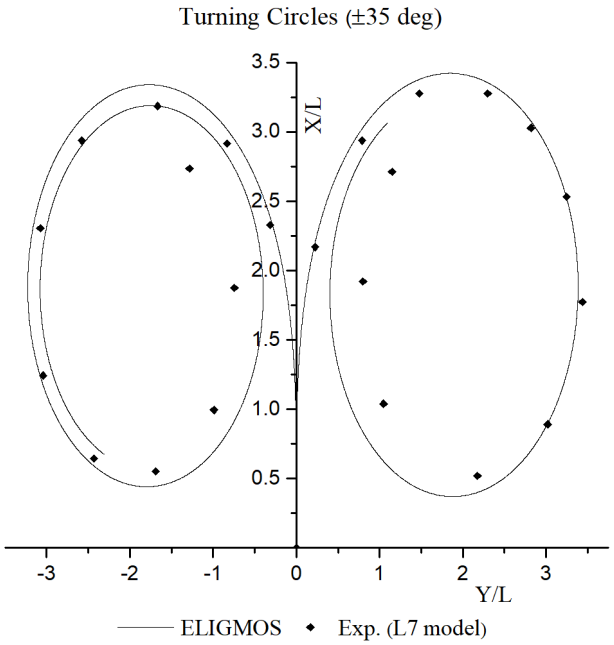

Figure 6.1: Comparison of turning circle trajectories for KVLCC2 (δ=±35°)

The asymmetry observed between the previously depicted turning circles results from the different magnitude of the flow straightening coefficient (γ_R) for port and starboard turning motion of a single-screw ship. The so-called flow straightening phenomenon occurs due to the development of hull and propeller slip stream and results in smaller actual inflow angle to the rudder (Fujii and Tuda, 1961).

In the following tables, various characteristic manoeuvring values concerning ±35^o turning circle and 10/10 and 20/20 zig-zag maneuvers of KVLCC2 are summarized, demonstrating the level of accuracy of the present calculations. The values have been obtained from other numerical and experimental methods conducted within the framework of SIMMAN 2008. The former include experimental and time-domain simulation methods based on hydrodynamic values calculated by use of empirical, PMM/CMT or RANS techniques.

Table 6.1: Comparison of KVLCC2 characteristic manoeuvring values (rudder at +35^o)

Values	Units	MARIN (exp.)	MARINTEK	MOERI	FORCE	Hiroshima University	HSVA NEPIII	ELIGMOS
Speed	kn	**15.5**	15.5	15.5	15.5	15.5	15.5	**15.5**
Rudder angle	deg	**35**	35	35	35	35	35	**35**
Advance (AD)	m	**954.0**	998.3	926.1	1230.0	1056.9	1002.8	**1089.5**
Transfer (TR)	m	**405.0**	423.1	381.7	642.0	473.1	407.4	**515.5**
Tactical Diameter (TD)	m	**988.0**	1058.1	898.1	1510.0	1093.7	944.4	**1083.4**
T_{90}	s	**165.0**	170.5	163.0	232.0	188.5	172.0	**196.8**
T_{180}	s	**345.0**	344.5	333.6	500.0	374.0	336.0	**380.2**
T_{360}	s	**758.0**	766.1	715.9	1136.0	774.5	723.0	**831.4**

Table 6.2: Comparison of KVLCC2 characteristic manoeuvring values (rudder at -35^o)

Values	Units	MARIN (exp.)	MARINTEK	MOERI	FORCE	Hiroshima University	HSVA NEPIII	ELIGMOS
Speed	kn	**15.5**	15.5	15.5	15.5	15.5	15.5	**15.5**
Rudder angle	deg	**-35**	-35	-35	-35	-35	-35	**-35**
Advance (AD)	m	**984.0**	1004.5	849.4	1310.0	1042.7	1002.9	**1063.3**
Transfer (TR)	m	**440.0**	428.5	336.3	770.0	465.6	426.2	**493.4**
Tactical Diameter (TD)	m	**1067.0**	1068.5	811.2	1780.0	1078.5	899.8	**1031.5**
T_{90}	s	**177.0**	172.0	150.8	230.0	185.0	175.0	**191.9**
T_{180}	s	**372.0**	347.5	315.3	460.0	366.0	350.0	**369.8**
T_{360}	s	**804.0**	NA	676.3	978.0	756.0	756.0	**810.7**

In Tables 6.1 and 6.2, **MARIN** refers to results obtained by free sailing experiments, whilst MARINTEK's results come from modular simulations where the hydrodynamic forces were calculated implementing virtual CMT tests. Additionally, **MOERI** and **FORCE** conducted numerical simulations, where PMM generated hydrodynamic derivatives were employed. In the latter, the calculation of the hydrodynamic forces was performed with data provided by INSEAN. Finally, simulations by **Hiroshima University** and **HSVA (NEPIII)** are based on CMT tests and RANS-generated PMM data respectively.

Comparison, which shows the agreement of the present method against experimental trajectories in case of 10/10 and 20/20 zig-zag tests, is depicted in Figures 6.2 and 6.3. Note that X-axis refers to nondimensional time ($t' = t\frac{U}{L}$). Additionally, the level of accuracy of the adopted methodology is assessed in terms of execute times and first and second overshoot angles. The results of the present simulations are compared against the results of the methods included in Tables 5.1 and 5.2 and are depicted in the following tables.

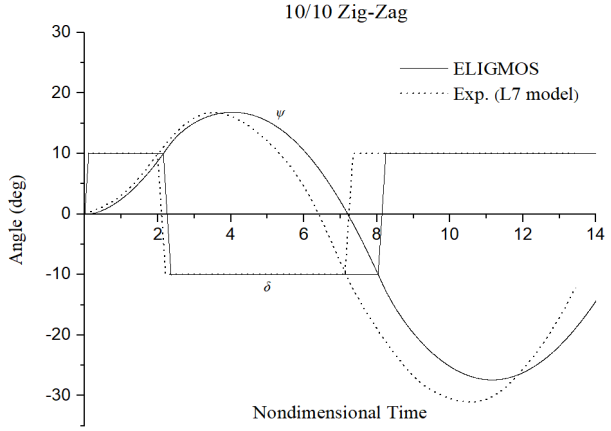

Figure 6.2: Comparison of 10/10 zig-zag trajectories for KVLCC2

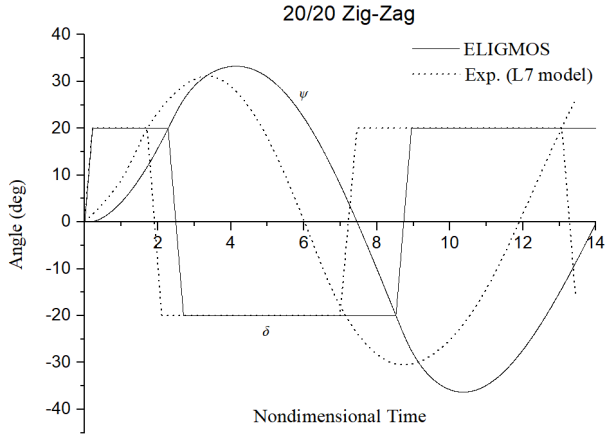

Figure 6.3: Comparison of 20/20 zig-zag trajectories for KVLCC2

Table 6.3: Comparison of KVLCC2 10/10 zig-zag manoeuvring characteristic values

Values	Units	MARIN (exp.)	MARINTEK	MOERI	FORCE	Hiroshima University	HSVA NEPIII	ELIGMOS
Speed	kn	**15.5**	15.5	15.5	15.5	15.5	15.5	**15.5**
2nd execute	s	**77.0**	68.6	64.0	74.0	70.5	68.0	**86,5**
3rd execute	s	**283.0**	259.0	316.8	276.0	268.5	263.0	**323,3**
1st overshoot	deg	**7.9**	6.6	9.1	5.8	5.1	7.4	**6,5**
2nd overshoot	deg	**21.6**	10.3	7.8	10.2	7.3	18.8	**17,4**

Table 6.4: Comparison of KVLCC2 20/20 zig-zag manoeuvring characteristic values

Values	Units	MARIN (exp.)	MARINTEK	MOERI	FORCE	Hiroshima University	HSVA NEPIII	ELIGMOS
Speed	kn	**15.5**	15.5	15.5	15.5	15.5	15.5	**15.5**
2nd execute	s	**68.0**	73.6	68.5	84.0	78.5	74.0	**91.8**
3rd execute	s	**283.0**	270.0	290.9	310.0	276.0	288.0	**343.0**
1st overshoot	deg	**13.3**	10.0	12.6	12.6	8.6	14.0	**13.3**
2nd overshoot	deg	**14.6**	10.8	11..0	11.0	11.2	20.2	**16.3**

At the beginning of this chapter it was mentioned that apart from KVLCC2, the manoeuvring performance of S-175 container ship is investigated as well. In case of the latter, it is considered that the validity of the presented method can be better justified when both input and experimental values refer to the 1:50 scaled model. In Figure 6.4, simulations of the port and starboard turning trajectories in calm water are depicted, where the agreement against the experimental ones is excellent. Comparison of the longitudinal speed and yaw rate versus measured values shows that our model is capable of accurately calculating the velocities in each DOF during turning as well.

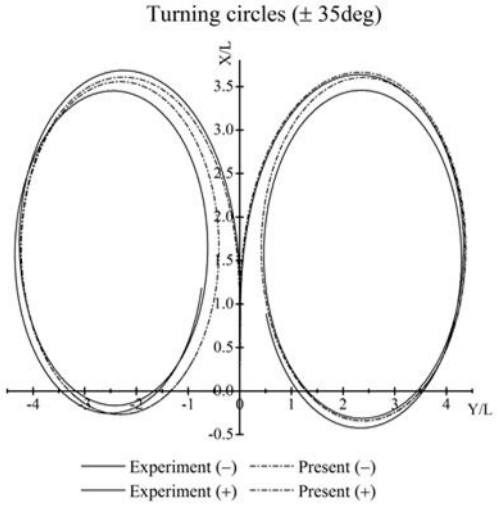

Figure 6.4: Comparison of turning circle trajectories for S-175 (δ=±35°)

When the metacentric height of the ship is low, sway-yaw-roll coupling becomes stronger as it is stated in Son and Nomoto (1982) and a 4-DOF system of equations must be employed instead. Further, in this case the minimization of yaw damping and the increase of the wetted surface result to an increased sway force and consequently in reduced turning trajectory of the ship. Numerical results showing the roll response of the vessel during turning motion with $\delta=15^{o}$ in three conditions characterized by different GM value, are depicted in Figure 6.5.

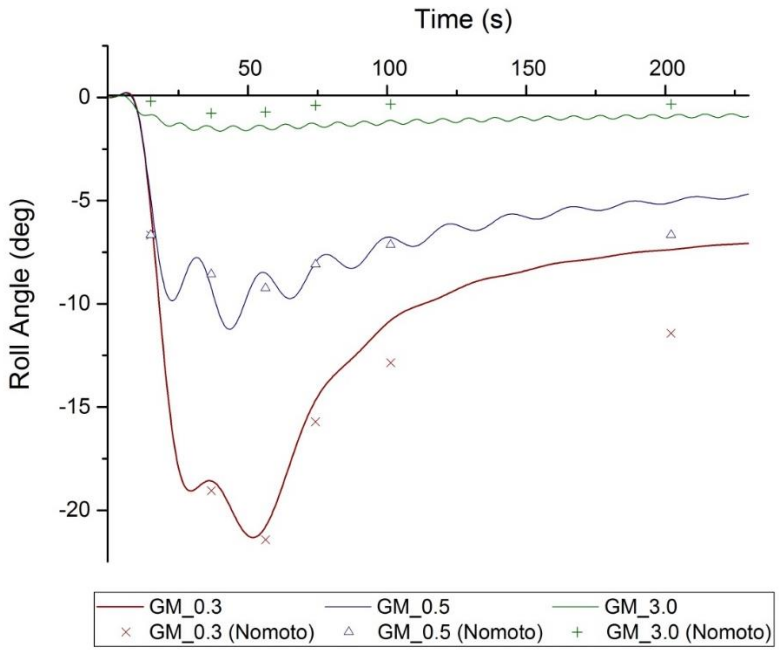

Figure 6.5: Heel angle of S-175 during turning for different GM values ($\delta=15^{o}$)

6.2.2 Simulations in Shallow Water

The impact of shallow water in calm water manoeuvring is primarily expressed by the change of hydrodynamic forces exerted on ship's hull through a revaluation of the manoeuvring derivatives using regression formulae. As it was mentioned in Chapter 2, these formulae are functions of the under keel clearance. Except for the changes in hydrodynamic forces (longitudinal, lateral and yaw moment), due to the different flow characteristics around the vessel, differences in hydrodynamic interactions among hull-rudder-propeller must be taken into consideration as well. The relevant formulae that were adopted in order to perform the aforementioned corrections can be found in Appendix A.

Herein, the regression formulae proposed by Amin and Hasegawa (2010) have been employed, which are considered improved related with Yasukawa's (1998) suggested formula for the change of wake fraction at zero drift angle (w_{po}) in shallow water, as they refer to more sea depths and to ships with larger block coefficients. Additionally, formulae demonstrating the change of the thrust deduction coefficient (t_P) and the propeller's race amplification (κ) and flow straightening (γ_R) coefficients with the under keel clearance are provided as well.

Analytical expressions of the aforementioned empirical functions implemented in the present study are included in Appendix B. In order to validate the proposed method, numerical simulations in calm water conditions are performed for the KVLCC2 tanker, considering shallow (h/T=1.5) and very shallow (h/T=1.2) sea depths at low forward speed (7 knots). Experimental and numerical data used for comparison were extracted from He's et al., (2016) publication. These include turning trajectories up to the point where heading angle equals 40^o (Figures 6.6 and 6.7). At this point, mean values of characteristic parameters for the aforementioned UKC are accumulated in Table 6.5. Comparative trajectories of 20/5 zig-zag tests are depicted in Figures 6.8 and 6.9 as well.

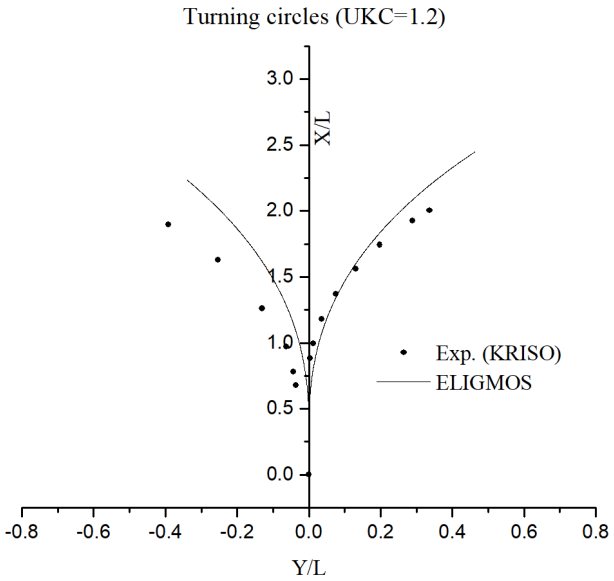

Figure 6.6: Turning circle trajectories up to 40^o heading angle for UKC=1.2 (δ=±35^o)

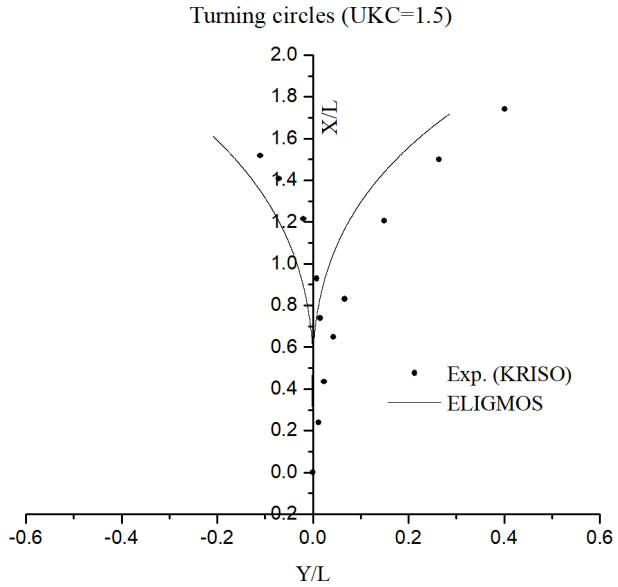

Figure 6.7: Turning circle trajectories up to 40º heading angle for UKC=1.5 (δ=±35º)

Table 6.5: Mean values of characteristic parameters of initial turning trajectories

h/T	1.2		1.5	
	Exp.	ELIGMOS	Exp.	ELIGMOS
$\bar{X}$	2.0L	**2.45L**	1.69L	**1.75L**
$\bar{Y}$	0.39L	**0.51L**	0.29L	**0.295L**
Mean duration/-s	184	**215.5**	157	**140.2**

From Figure 6.6 and 6.7 and table 6.5 it can be realized that the presented method produces satisfactorily accurate results in case of shallow water (h/T=1.5), whereas underestimated manoeuvrability is noticed when the sea depth is very shallow (h/T=1.2). The latter shows a reduced validity of the proposed methodology in very shallow water, which is probably occurred due to the inability of the adopted empirical formulae to express the updated values of the interaction coefficients at very low sea depth. As mentioned before, 20/5 zig-zag performance of KVLCC2 in shallow and very shallow waters is depicted in Figures 6.8 and 6.9. The performed simulations show good agreement with the experimental data in terms of the first and second overshoot angles for both shallow and very shallow water conditions.

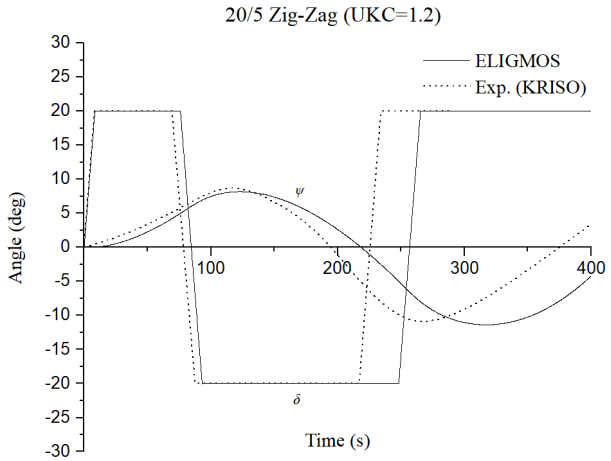

Figure 6.8: 20/5 heading and rudder angle time histories at UKC=1.2

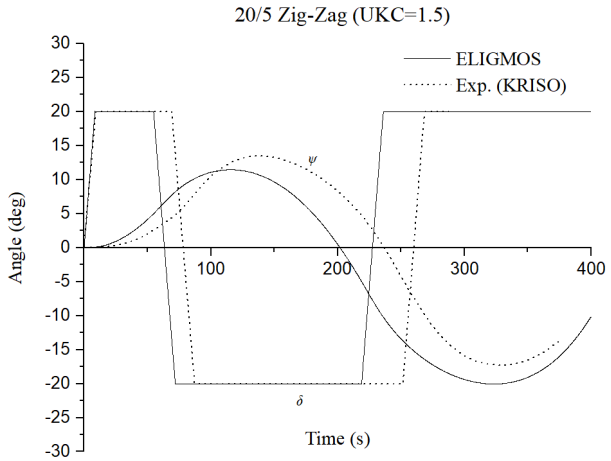

Figure 6.9: 20/5 heading and rudder angle time histories at UKC=1.5

To conclude with, the prediction of ship's manoeuvrability in calm water by means of the developed numerical tool ELIGMOS within the framework of the present study, is considered successful for both deep and shallow water conditions especially concerning the predicted turning trajectories. Discrepancies are more district at calm water zig-zag tests for both deep and shallow water cases. Further investigation is needed in case of very shallow water, implementing more accurate methods for the calculation of manoeuvring derivatives and calm water resistance at UKC values lower than 1.5. Finally, the effect of shallow and very shallow sea depths on hydrodynamic rudder-induced forces should be investigated as well in future studies.

6.3 Seakeeping Simulations

In this section, the level of accuracy of the developed numerical method concerning the ship's seakeeping performance is demonstrated through extensive comparison with published results from validated software and experimental data. Validation process starts from the values of the memory functions, which is a crucial element in order to derive accurate radiation forces and vertical ship motions. Subsequently, results of heave and pitch motions for a full (KVLCC2) and a fine (C11-class container ship) hull forms in various wave steepnesses will be provided, implementing a Level 2 nonlinear seakeeping analysis. In this way, the influence of the geometrical nonlinearities on the time histories of vertical ship motions will be addressed. The aforementioned analysis is performed for the zero and the non-zero forward speed cases.

As part of the seakeeping analysis, results on parametric roll investigation will be presented as well, as an additional evidence of the ability of ELIGMOS to perform nonlinear hydrodynamic analysis and to manipulate the complicated mathematical theory of ship kinematics, needed for the representation of such an extreme phenomenon.

6.3.1 Linear Vertical Motion Analysis

This stage within the validation process is necessary in order to ensure that the basic formulation of the equations of motion is correct and the different hydrodynamic force components are calculated accurately. This will provide a solid background for the more demanding task of nonlinear vertical motion evaluation and parametric roll investigation in large waves, which will be presented in following sections. Before showing validation results of ship motions, comparison of normalized ($\overline{K}_{ij} = \frac{K_{ij}}{K_{ij,max}}$) memory functions in head seas will be demonstrated using the results of the validated time-domain software LARes (Hizir, 2015) as reference values. As already mentioned in previous chapter, the accurate calculation of memory functions is very important in order to obtain accurate radiation forces, thus a separate validation process is considered necessary.

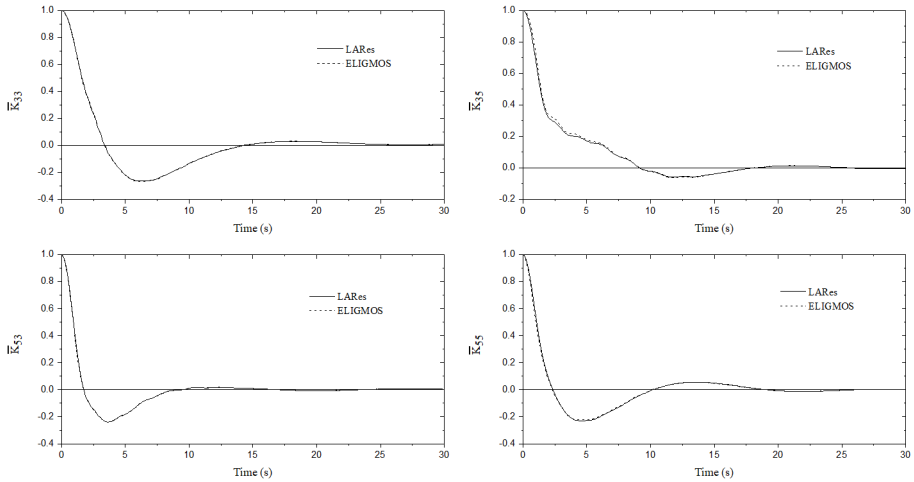

Figure 6.10: Normalized memory functions in heave, pitch and cross-coupling terms of KVLCC2 (Fn=0.142, χ=180^o)

Figure 6.10 shows that ELIGMOS calculates the memory functions associated with ship's vertical motions with sufficient accuracy for a time period of 30 seconds. Small discrepancies at t=0 are considered of low importance since they do not affect motions' amplitudes as it will be shown later on. In linear seakeeping analysis, memory functions are pre-calculated from 0 to 30s for every 0.1 seconds and they are multiplied with the actual and velocities' history in order to evaluate the convolution integrals. Ship's vertical motions are depicted in Figures 6.11 and 6.12 for the KVLCC2 at zero and non-zero forward speeds in head seas, in terms of nondimensional Response Amplitude Operators.

It can be easily understood that the results implementing frequency-domain analysis, using the validated software PRECAL, coincide with those derived by ELIGMOS which adopts the hydrodynamic data provided by the aforementioned software. Small discrepancies are observed at the region of maximum pitch motion, when Fn=0.

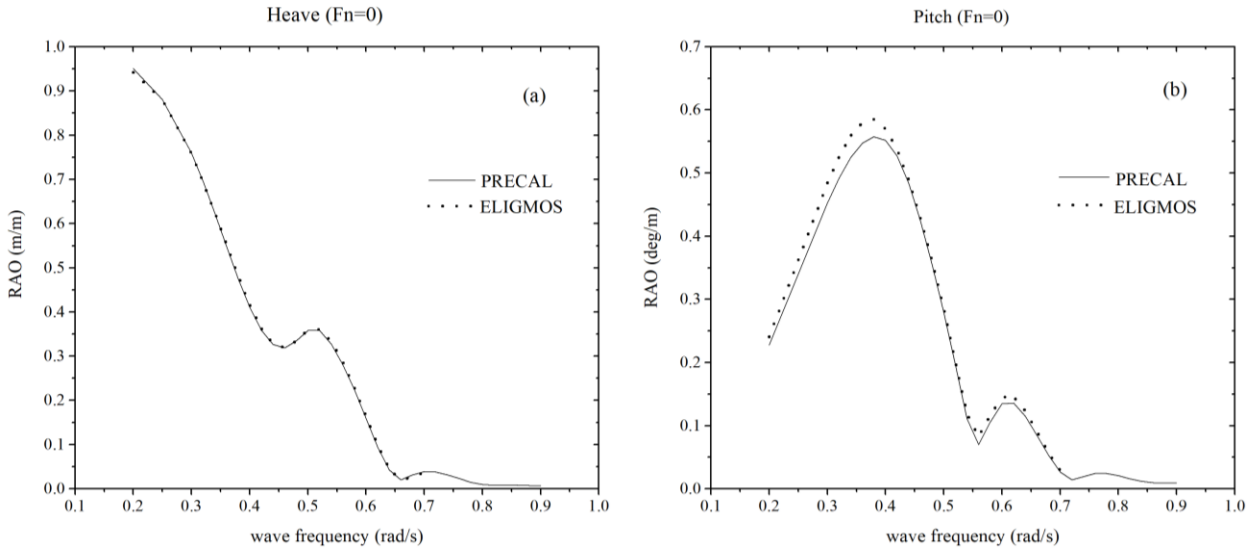

Figure 6.11: Comparison of heave (a) and pitch (b) linear RAO values for KVLCC2 at Fn=0

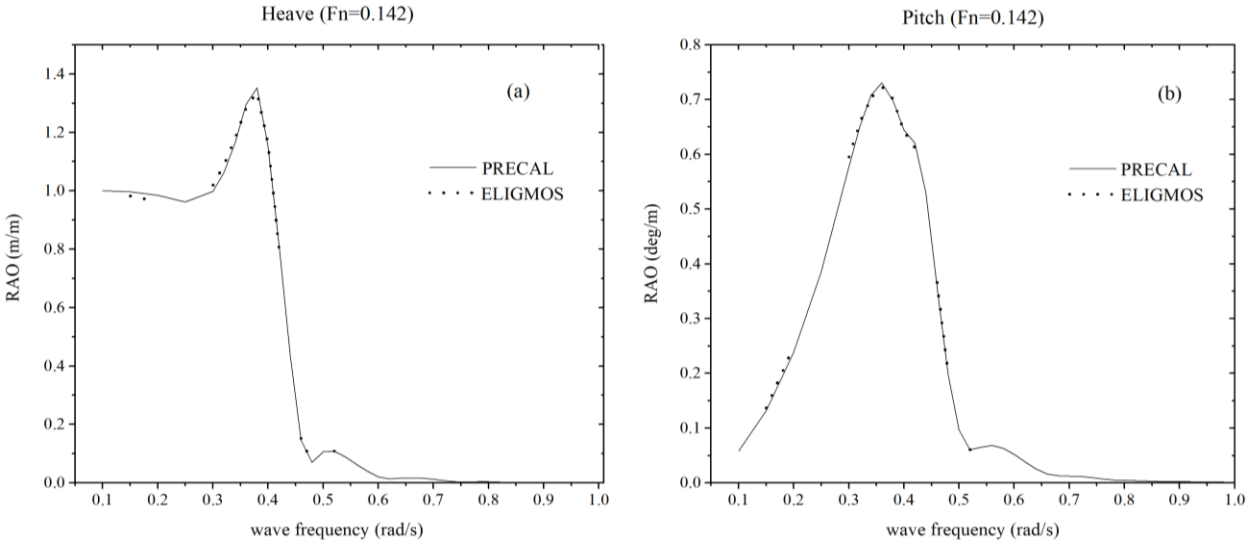

Figure 6.12: Comparison of heave (a) and pitch (b) liner RAO values for KVLCC2 at Fn=0.142

Theoretically, such differences should not exist, as the aforementioned types of analyses (frequency-domain and time-domain) are related by a Fourier transformation and should match in pure linear seakeeping analysis (Hizir, 2015).

However, slightly different amplitudes can be explained because in the present calculations of memory functions, the upper limit of the integration of the damping coefficients was taken equal with the maximum frequency imposed by the frequency-domain analysis and not with the infinite frequency, which is suggested theoretically.

Additionally, discrepancies can be caused due to the fact that only the past 30 seconds of the memory functions take part during the calculation of the convolution integrals, neglecting the contribution of previous memory effects. A similar trend, as this discussed for the KVLCC2, is observed in case of the C11-class container ship. In Figures 6.13 and 6.14 we see that when the forward speed is zero, there are still small discrepancies in the vicinity of the maximum pitch amplitude, whereas at Fn=0.10 frequency-domain and time-domain results coincide.

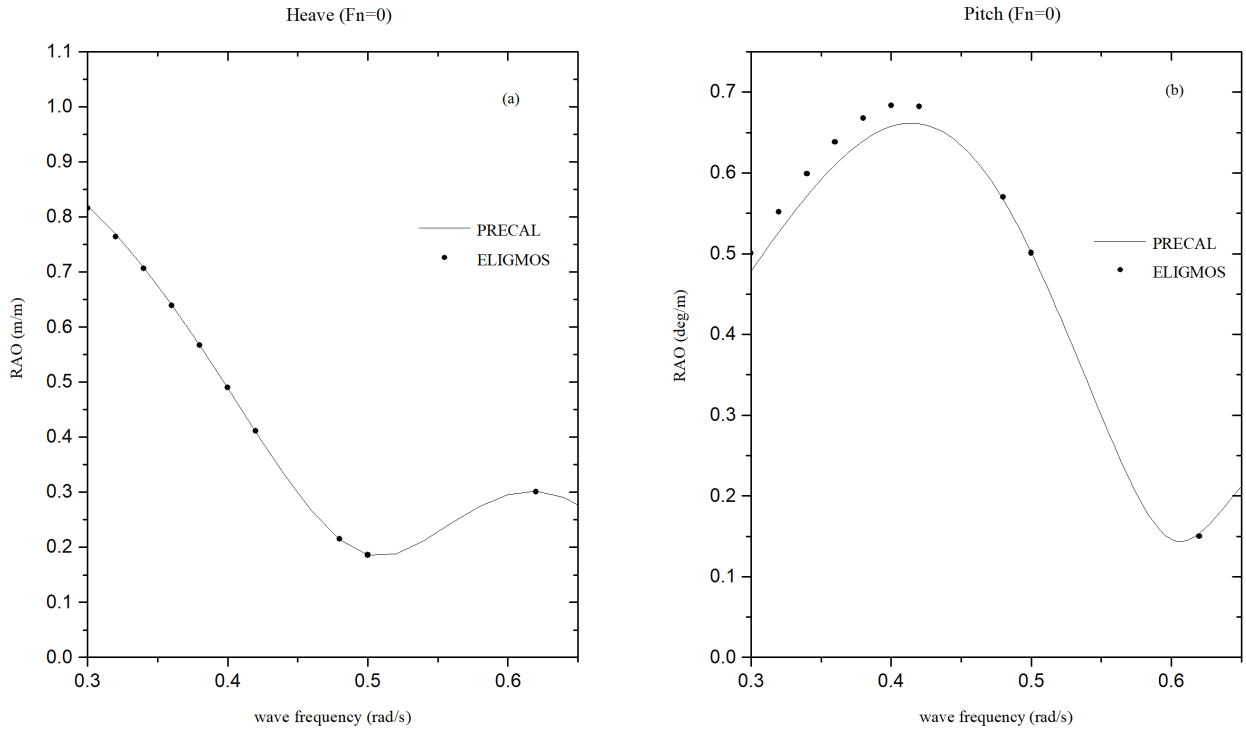

Figure 6.13: Comparison of heave (a) and pitch (b) linear RAO values for C11 container ship at Fn=0

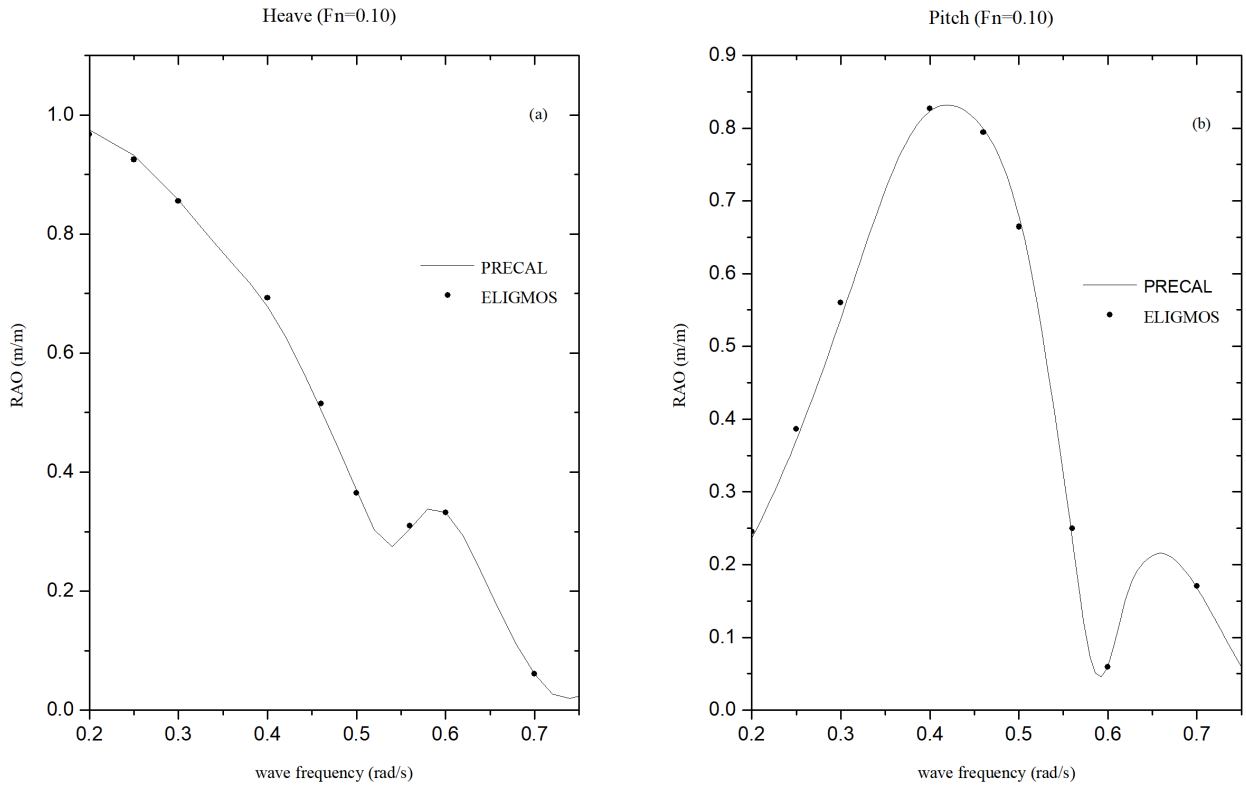

Figure 6.14: Comparison of heave (a) and pitch (b) liner RAO values for C11 container ship at Fn=0.10

With the presented analysis, it was shown that the developed linear time-domain seakeeping method provides accurate results concerning ship's vertical motions. Time histories of the various force components could not be compared, as there were no available data, either experimental or obtained from other validated software.

6.3.2 Nonlinear Vertical Motion Analysis

Herein, the numerical results of nonlinear heave and pitch motions are presented and validated, implementing the F-K (Level 2) nonlinear analysis. In this way, it can be tested the accuracy of the calculated Froude-Krylov and Restoring forces obtained by implementing a direct pressure integration scheme on the vessel's instantaneous wetted surface. Results in small, regular head waves, derived from the developed numerical tool ELIGMOS, are compared against published experimental and numerical results implementing CFD method, found in Riesner et al. (2016) and Hizir et al. (2019) respectively.

Especially at such environmental conditions, linear and nonlinear results must be identical (or almost identical), as the wetted surface can be considered equal with the mean wetted surface used in linear calculations. The latter consists of the first stage of a V&V process of nonlinear seakeeping codes as described in ITTC Recommended Procedures and Guidelines (2011). Nonlinear simulations are performed for the KVLCC2 tanker for the simpler zero speed condition and for the more complicated non-zero (Fn=0.142) forward speed case. Comparison of linear and nonlinear motion amplitudes in small, head seas is performed for a C11-class container ship as well, aiming to identify the way that the geometrical nonlinearities of such fine hull forms affect the vessel's response in heave and pitch.

The vertical motion amplitudes of KVLCC2 in head seas are depicted in Figures 6.15 and 6.16 in terms of nondimensional RAO values. In case of nonlinear analysis, the aforementioned values correspond to the amplitudes of the first harmonic frequency, derived by applying a Fourier transformation of the relevant time histories. Firstly, comparison is performed at zero forward speed case using linear frequency-domain results and the previously shown (Chapter 4) linear results derived using the developed code ELIGMOS.

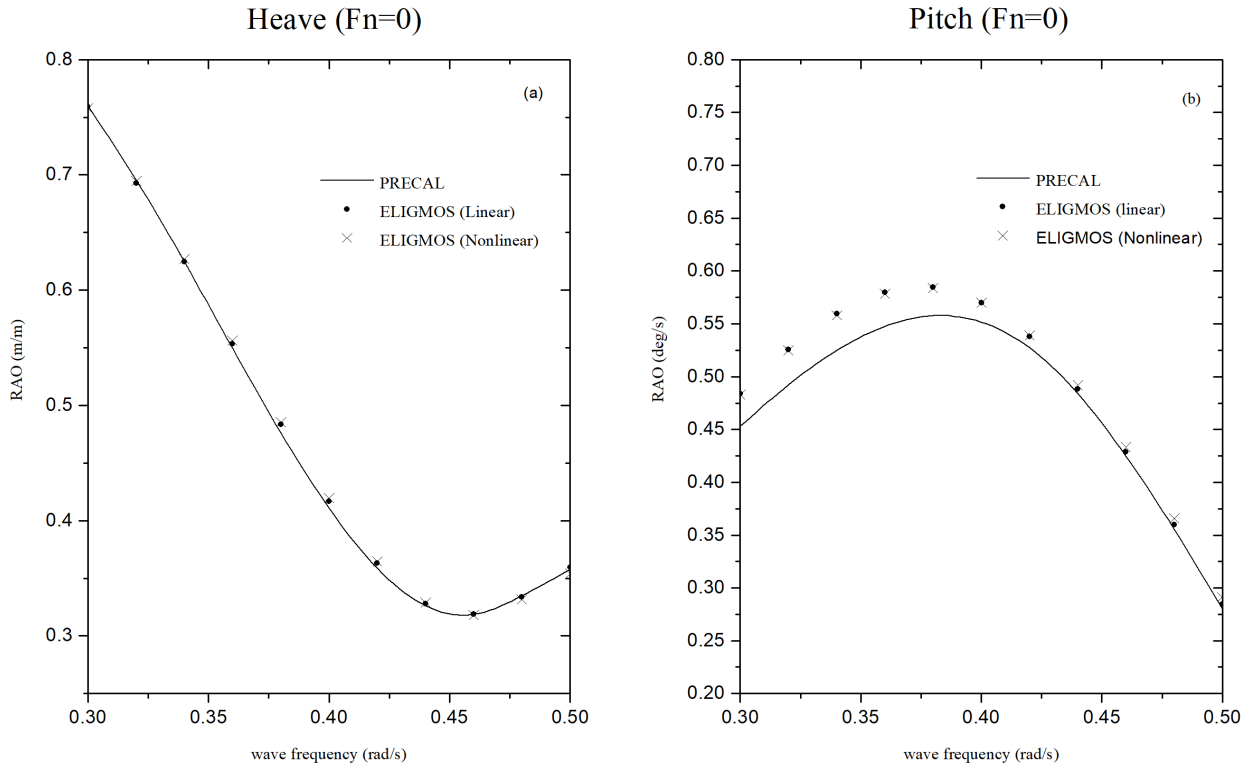

Figure 6.15: Comparison of nonlinear heave (a) and pitch (b) RAO values with linear time-domain and frequency-domain results for KVLCC2 (Fn=0.0)

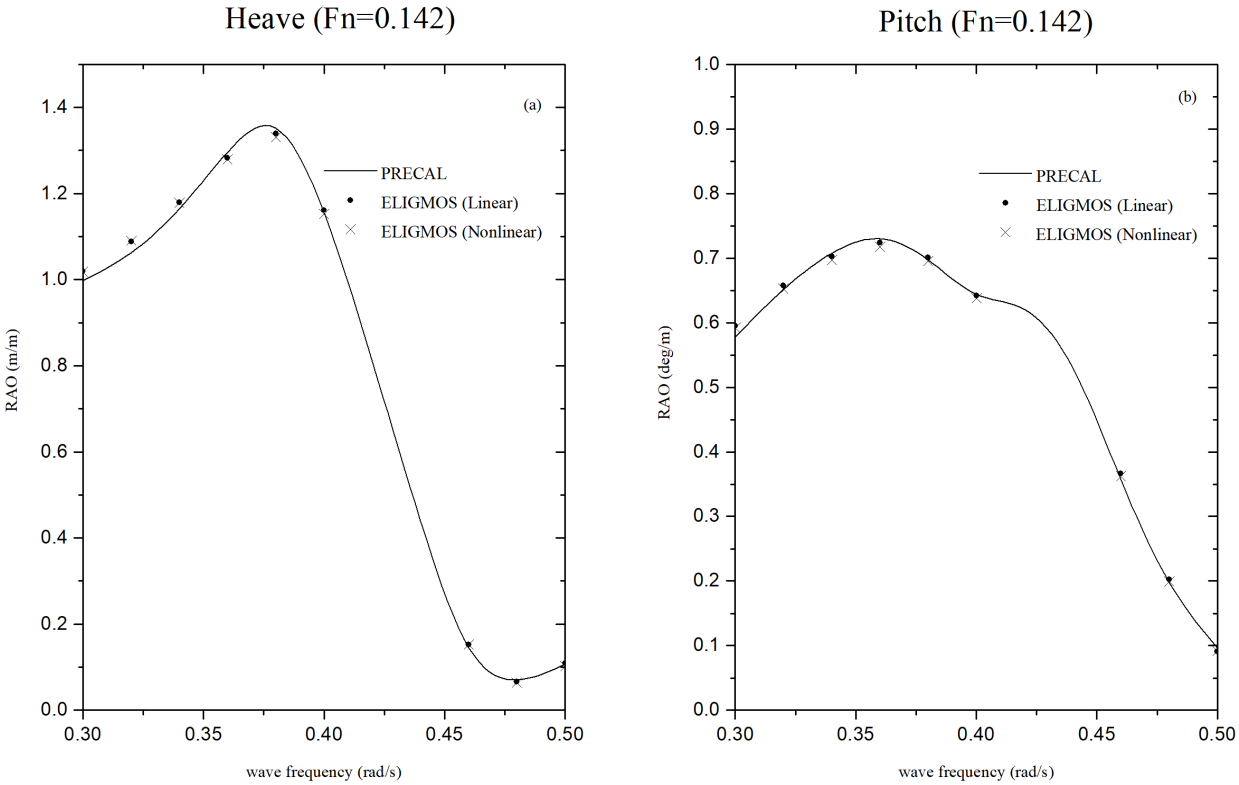

Figure 6.16: Comparison of the nonlinear heave (a) and pitch (b) RAO values with linear time-domain and frequency-domain results for KVLCC2 (Fn=0.142)

In the figures shown above, nonlinear RAO values at small wave amplitude have an excellent agreement with those derived implementing either a linear time-domain or a frequency domain analysis, which shows the validity of the developed numerical model. In all cases, frequency domain data were obtained from the hydrodynamic software PRECAL Similar values of motion amplitudes were expected, because the KVLCC2 tanker has a so-called "wall-sided" geometry, which means that the waterplane area is almost constant around the mean sea level and the Froude-Krylov and Restoring forces can be considered linear. Additionally, in the following figures it is depicted that linearity of ship motions for the KVLCC2 is maintained even for large amplitude waves (ζ_α=4m) for the zero and the non-zero speed case.

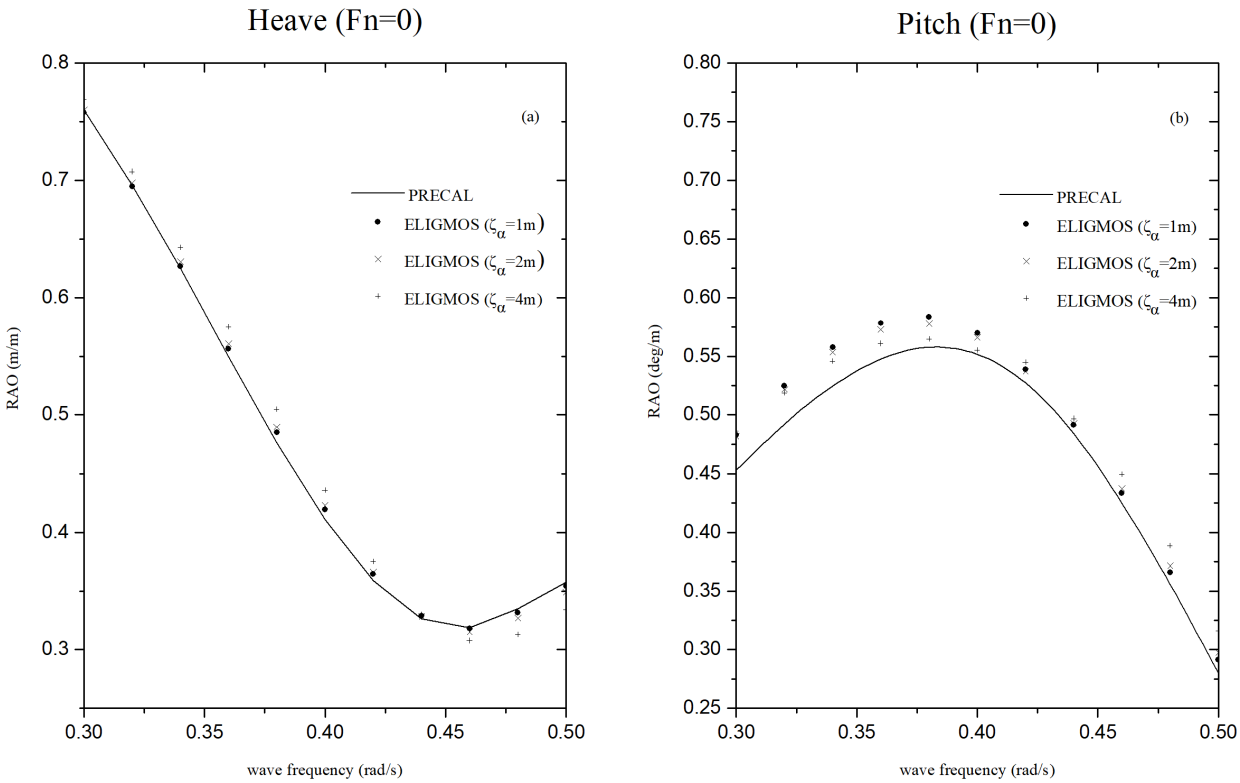

Figure 6.17: Nonlinear heave (a) and pitch (b) RAO values for KVLCC2 at several wave amplitudes (Fn=0.0)

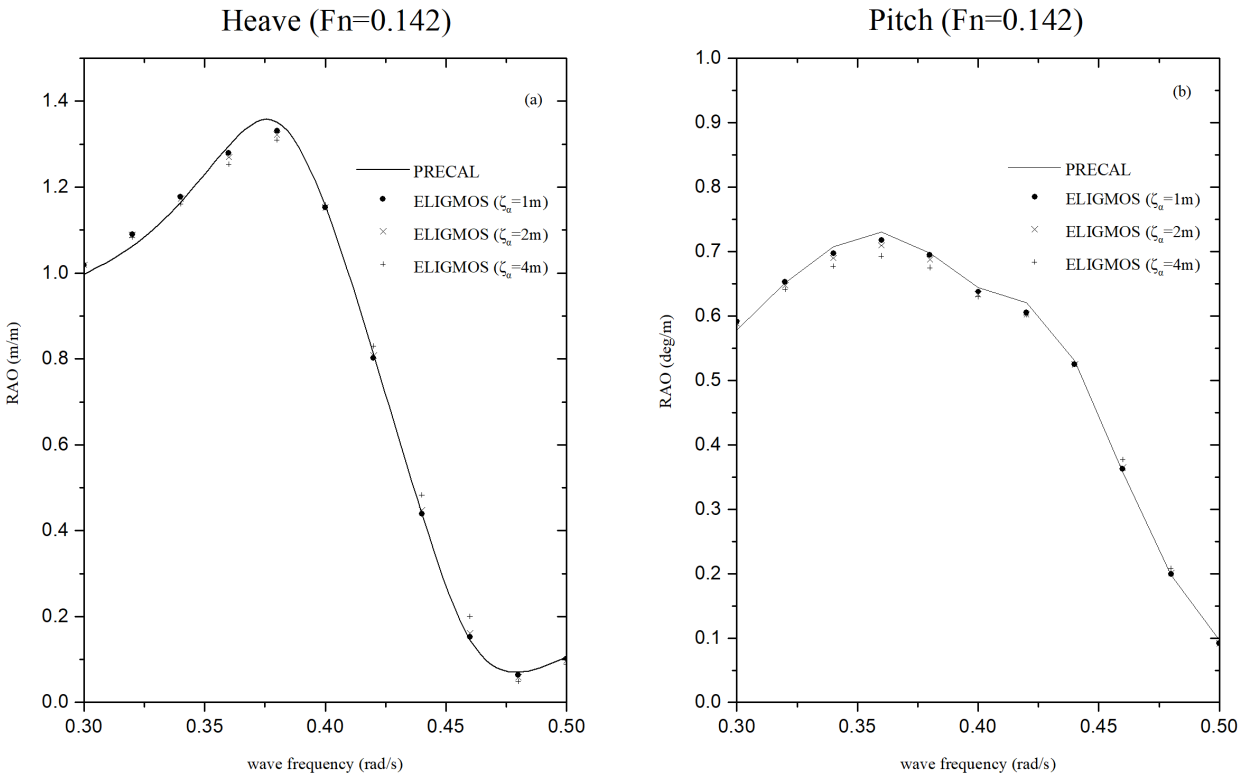

Figure 6.18: Nonlinear heave (a) and pitch (b) RAO values for KVLCC2 at several wave amplitudes (Fn=0.142)

Apart from the comparison with linear methods, it is interesting to investigate the level of agreement of the present, nonlinear RAO values with other nonlinear methods, such as the CFD. The latter, is presented in Figures 6.19 and 6.20, where the RAO values at Fn=0.142 are obtained for several wave steepnesses at short wave (λ/L=0.5) and long wave (λ/L=1.2) head seas and compared against published CFD data (Hizir et al., 2019). It can be noticed that results obtained with the present method indicate a better agreement at short wave seas, where the motions are minimized and consequently nonlinear effects do not have a major impact as the wetted surface approaches its mean value. On the contrary, larger discrepancies between the present calculations and the CFD ones are observed concerning heave motion amplitudes in case of long wave seas. The latter can be attributed to the selection of the AFS boundary condition during the solution of the BVP.

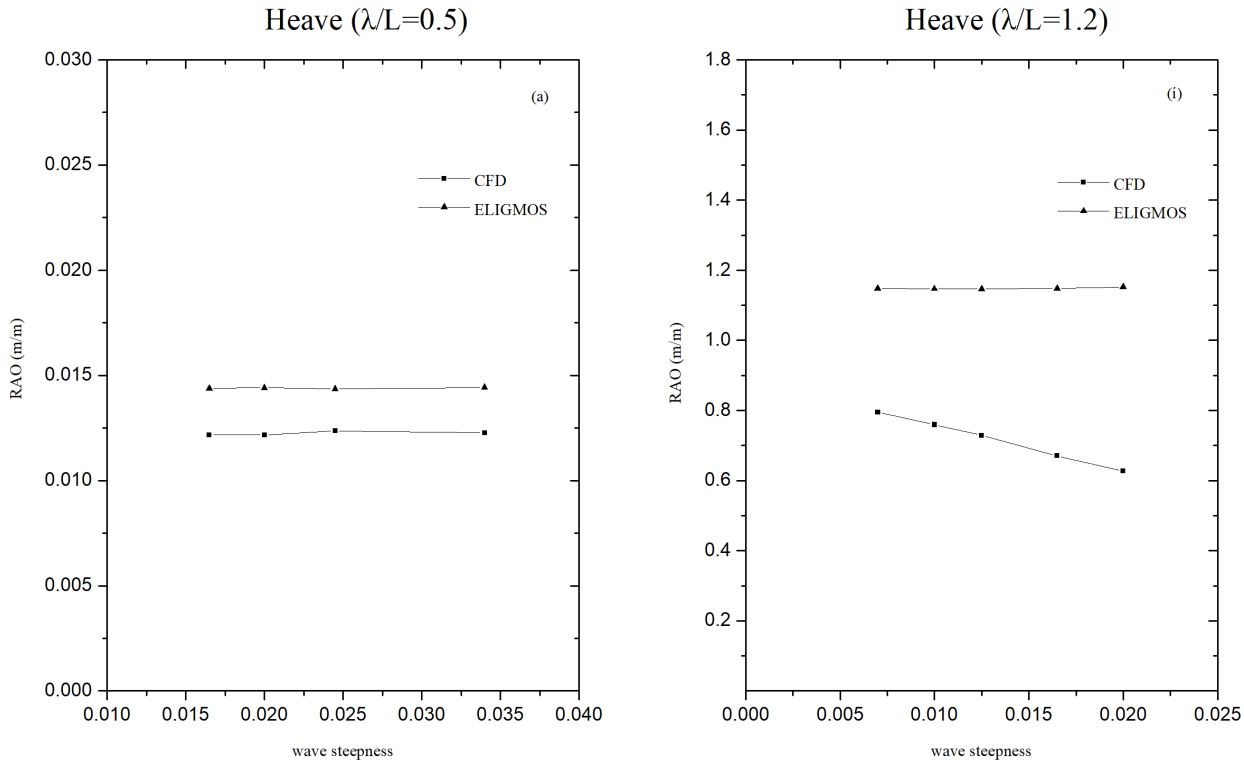

Figure 6.19: Heave nondimensional RAO values of KVLCC2 at different wave steepnesses for short (a) and long (b) waves (Fn=0.142)

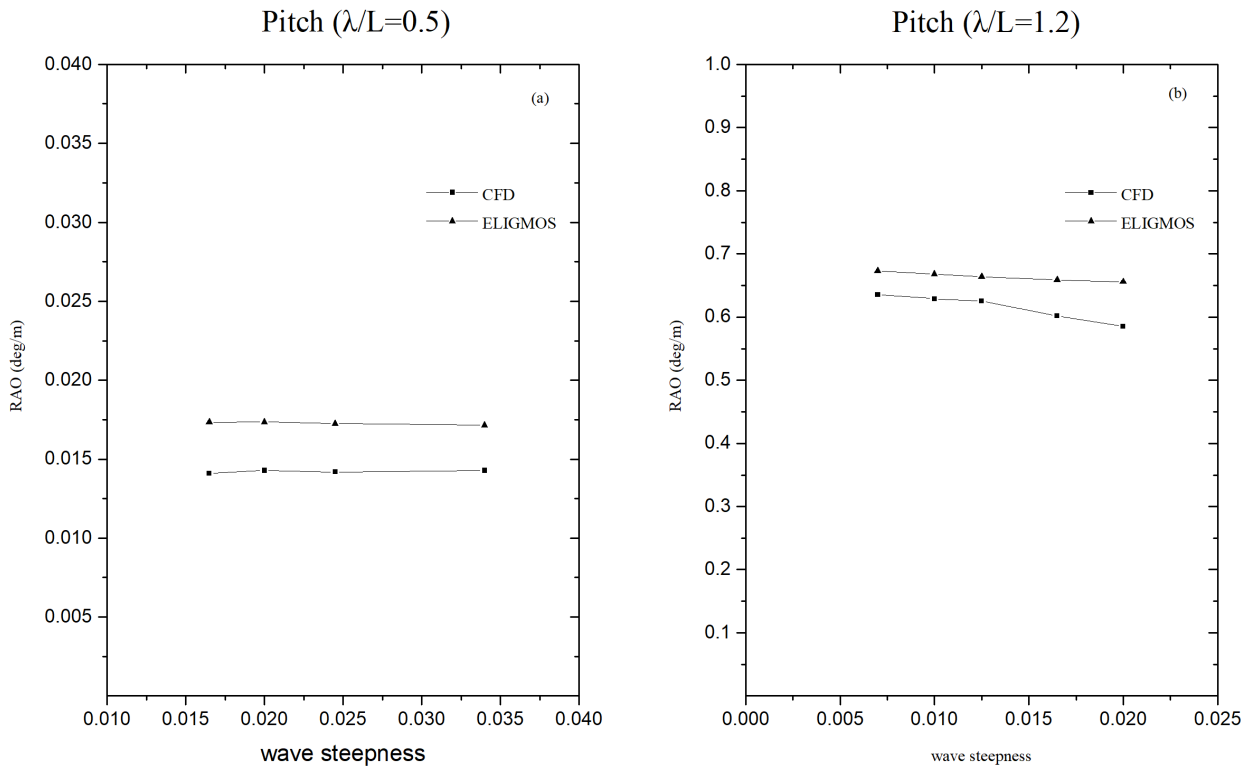

Figure 6.20: Pitch nondimensional RAO values of KVLCC2 at different wave steepnesses for short and long wave seas (Fn=0.142)

Comparison of the present results with available experimental data found in Riesner et al. (2016) is shown in Figure 6.21, where better agreement is observed concerning pitch motion, whereas in heave motion present results are significantly overestimated and closer to the frequency-domain ones. This, can be attributed to errors incorporated by the frequency-domain solution concerning the values of the added masses and the frequency-dependent damping coefficients. Additionally, further validation effort has to be conducted in the future by comparing the results obtained by use of ELIGMOS with other experimental data, as questions arise about the validity of those referring to heave motion, as they do not converge to 1 as the wave frequency goes to 0.

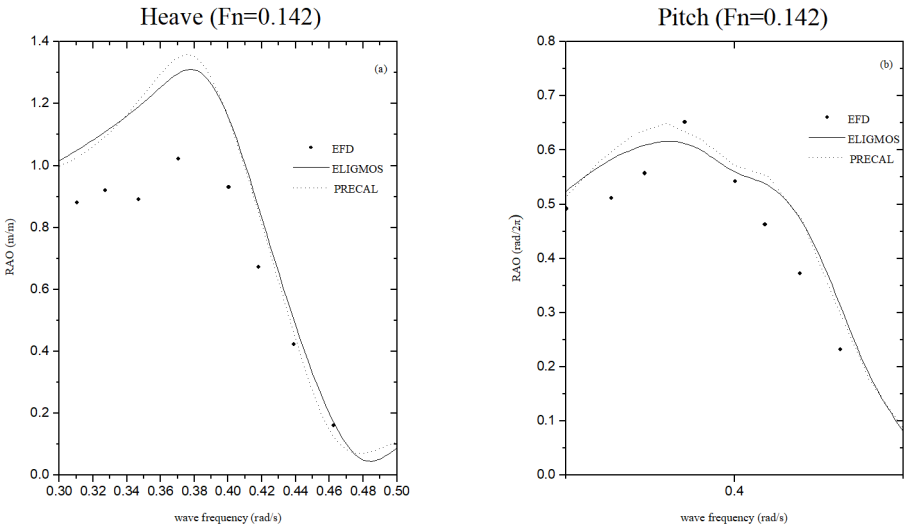

Figure 6.21: Comparison of heave (a) and pitch (b) nondimensional RAO values with experimental and frequency-domain results (Fn=0.142)

Apart from the adoption of the AFS method, which introduces errors in the present analysis, the discrepancies indicated in Figures 6.21. may have been caused due to the following factors as well:

- Use of the hydrodynamic reference frame and need to incorporate more degrees of freedom
- Adopted level of nonlinearity during force calculations

The present nonlinear seakeeping analysis was performed by considering only the vertical ship motions, ignoring their coupling with other DOF, especially surge and roll motion. As it is stated in Hizir (2015), the accelerations and, subsequently, ship's velocities and motions derived at each time step would be different if more DOF took part in such an analysis. In this case, the hydrodynamic reference frame used in the present study, would not be valid anymore, thus the system of motion equations should be expressed according to a body-fixed coordinate system which would allow the calculation of large amplitude motions. Additionally, a more sophisticated level of nonlinearity during the calculation of the hydrodynamic forces, which enables the calculation of radiation and diffraction forces over the instantaneous wetted surface, would have provided more accurate results, although the computational cost would have increased.

In order to demonstrate the capability of the present methodology to capture the geometrical nonlinearities, simulations performed for a C11-class container ship, which has a distinct flare. The water plane area of such ships changes drastically from its mean value when the wave excitations are large.

The latter, induces nonlinearities concerning the Froude-Krylov and Restoring forces, which leads to nonlinear seakeeping performance. This is depicted in Figure 6.22, where heave and pitch time histories are plotted for various wave amplitudes.

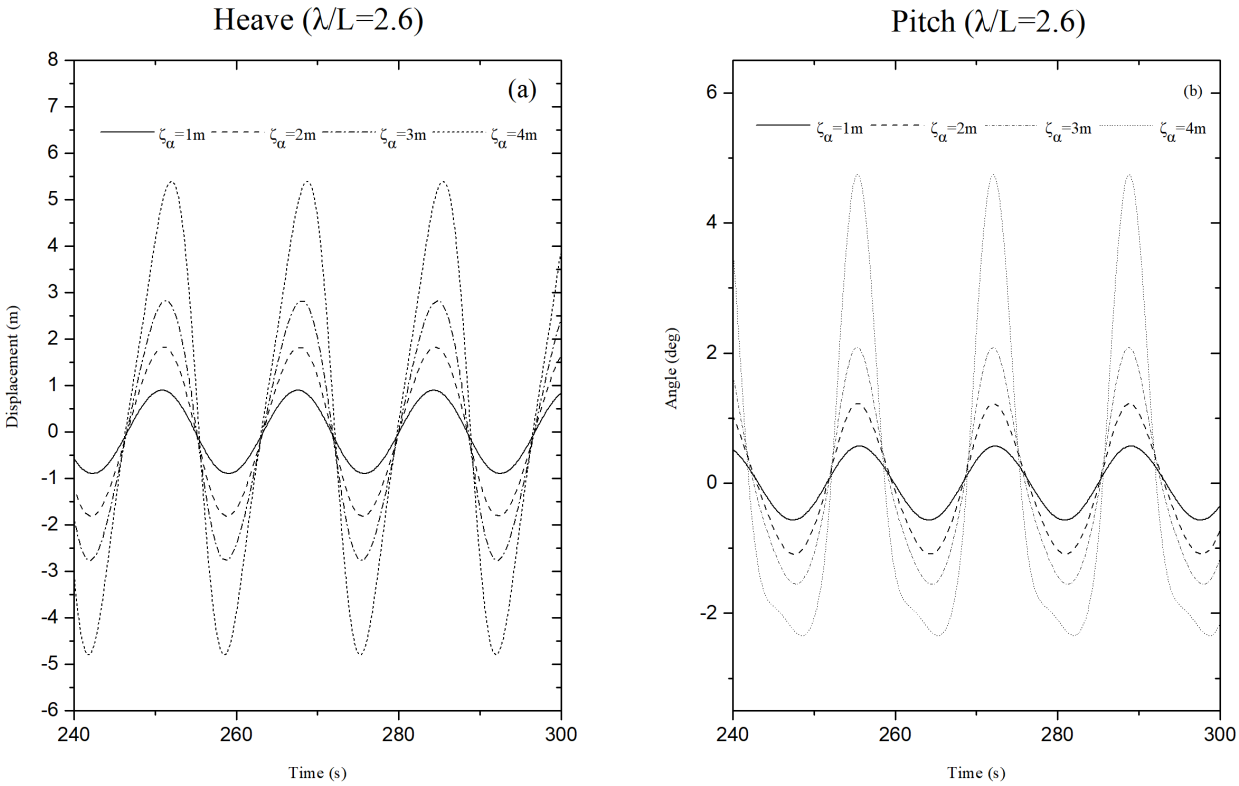

Figure 6.22: Time histories of heave (a) and pitch (b) motions at different wave amplitudes for C11 (Fn=0.1624)

From Figures 6.22, it is easily understood that as the wave amplitude increases, the vertical motions become nonlinear. Especially, when the wave amplitude is equal to 4 meters, ship motions show a highly nonlinear trend, especially concerning pitch angle. Nonlinearities regarding heave response are not significant and remains an open issue for future study. Finally, the effect of increasing wave steepness on nondimensional heave and pitch motions is illustrated in the following figure.

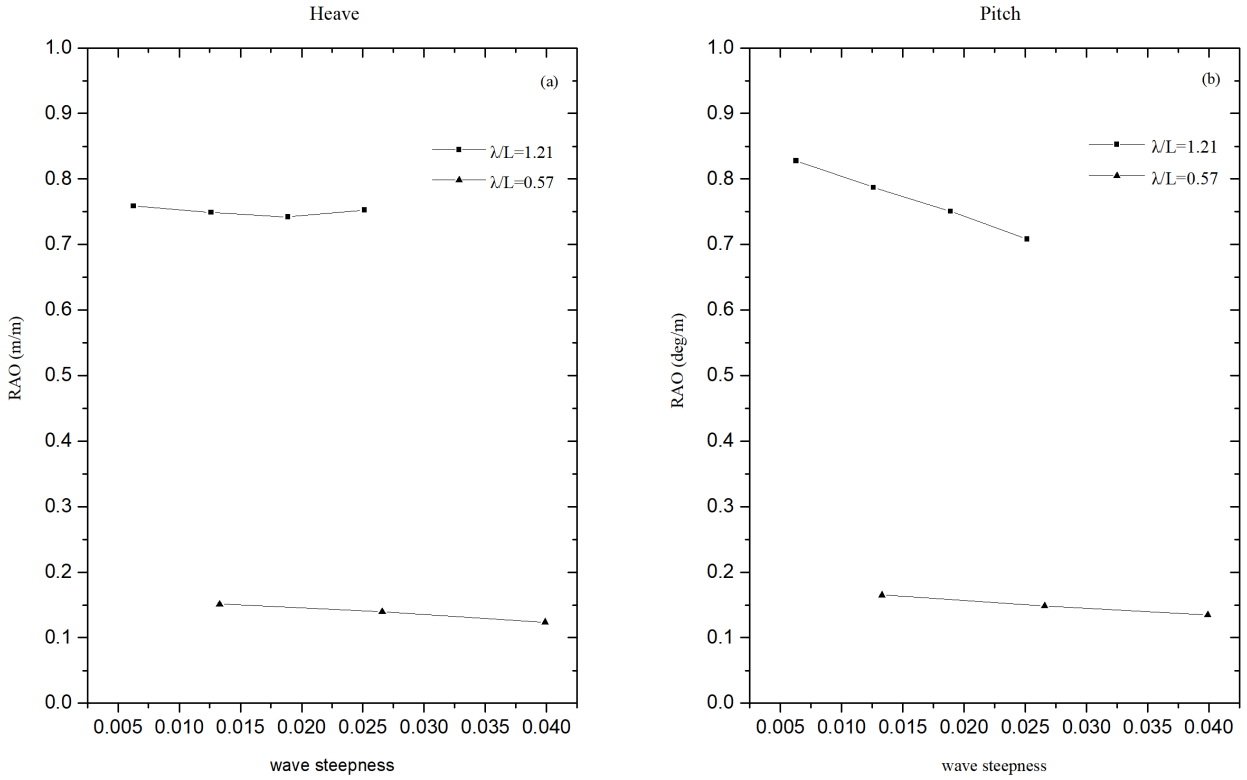

Figure 6.23: Heave (a) and pitch (b) nondimensional RAO values at different wave steepnesses for C11 at short and long wave seas (Fn=0.162)

From Figure 6.23 it is understood that the C11-class container ship has nonlinear heave and pitch responses as wave steepness increases, because the slope of the curves is not constant.

To sum up with, although comparison of the time histories of the hydrodynamic forces is missing due to the unavailability of relevant data, the seakeeping analysis performed within the context of the present study attains an acceptable level of validation however, comparison with other experimental data is considered necessary. Use of other potential theory panel codes (e.g. NEWDRIFT) would offer the possibility to identify discrepancies between time-domain solutions originated from the adoption of different values of the hydrodynamic coefficients. The evidence that prove the level of validity of the developed method are the following:

1. Linear time-domain RAO values coincide with the frequency-domain ones for a large amount of wave frequencies, whilst small discrepancies are noticed in case of pitch motion at zero forward speed and in the area of its maximum value for the investigated vessels.

2. Nonlinear calculations performed by calculating Froude-Krylov and Restoring forces over the instantaneous wetted surface by adopting a direct pressure integration scheme (Level 2 of nonlinearity). For small waves, RAO values are almost equal with the linearly derived ones, observing larger deviations for the C11-class container ship. This was expected, because for a full form vessel (KVLCC2) the waterplane area does not change significantly and the wetted surface does not deviate drastically in case of small wave excitations, whereas for the fine hull form (container ship) even in small waves the differences from the linear amplitudes are more obvious due to the geometrical nonlinearities. When experimental data were available, it was shown that the present method predicted well the amplitude of pitch motion for various wave frequencies, whilst for heave motion further validation effort is needed exploiting additional experimental values.
3. The previous characteristic becomes more evident when the wave steepness increases. As it was depicted, in case of the KVLCC2, a linear trend of the vertical motions is maintained in both long wave and short wave head seas, whilst for the C11-class container ship nonlinear seakeeping response has been identified.

The aforementioned conclusions prove that the developed methodology satisfactorily models the seakeeping performance of a marine vessel in regular waves. This is an important step towards the development of a nonlinear mathematical methodology, which can be used for the investigation of nonlinear dynamic failure modes, such as parametric roll. The latter, is investigated in the following section using the C11-class container ship, whose rolling behavior has been thoroughly studied in the past.

6.3.3 Parametric Roll Investigation

Parametric roll occurs from the periodic change of ship's stability, when a certain frequency is encountered (must be twice the natural roll frequency approximately). The crucial variable, which plays the major role for the development of this phenomenon, is *the waterplane area*.

For ships having a distinct flare (e.g. C11-class container ship), the waterplane area increases significantly when they are found on a wave trough, whereas a drastic decrease of the waterplane area is experienced when a wave crest is amidships.

The aforementioned variations of the waterplane area has a direct impact on ship's stability, as the waterplane area participates in the calculation of the vessel's *GZ-φ* curve.

According to the aforementioned theoretical elements, when such a ship with increased stability is found on a wave trough and experiences a gust of wind, larger restoring action will be created leading to high roll rate. Subsequently, when the ship is placed on a wave crest, her reduced stability will result to a violent roll motion to the opposite side. Going to the next wave trough this mechanism will lead to the amplification of roll motion, resulting to the development of parametric roll at certain encounter frequency (Belenky et al., 2011).

Conditions like those mentioned above, led to the development of extreme roll response (parametric roll) of a C11-class container ship in 1998, while sailing in head seas. In order to verify the ability of the developed methodology to capture parametric roll, the aforementioned case study is investigated herein. Nonlinear simulations in 3-DOF (heave-roll-pitch) using the horizontal body-fixed system with zero rudder angle, performed for several forward speeds, encounter frequencies and wave heights in order to identify whether the current methodology is able to capture parametric roll at the environmental conditions prescribed by the physics of this phenomenon. In order to accurately simulate the initial conditions, a starting value of 5^o is set for the roll angle when the ship's centre of gravity is positioned at the wave's down-slope. Due to numerical problems related with the generation of the ship's mesh, in the present simulations the vessel's draft is taken equal to 14 meters, different from the 12.34 meters which was considered in the context of the simulations provided by France et al (2003). Small discrepancies exist for the values of the ship's metacentric height as well as for the longitudinal moment of inertia and added moment of inertia, which result to slightly different values of the natural roll frequency and subsequently the frequency of encounter where parametric roll occurs.

Roll damping in the present study is modelled adopting the concept of the equivalent linear coefficient B_φ exploiting Tasai and Takaki's experimental data. Frequency-domain roll amplitude against wave frequency are plotted in Figure 6.24.

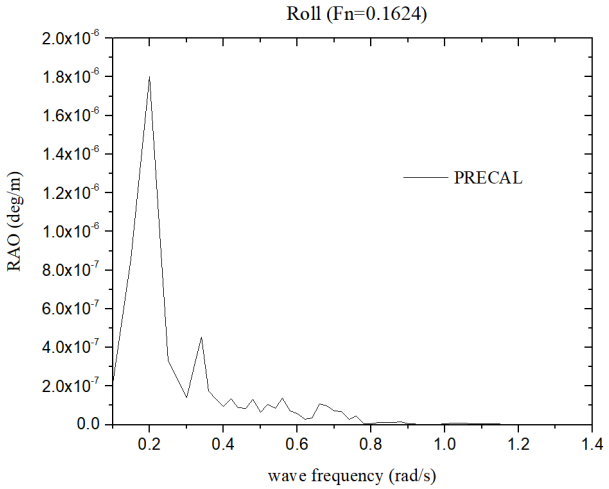

Figure 6.24: Nondimensional roll amplitude against wave frequency implementing frequency-domain analysis (Fn=0.1624)

In the figure shown above, it is deduced that the wave frequency where parametric roll may be possibly identified is either 0.20 rad/s or around 0.35 rad/s. However, using the following equation for the estimation of the natural roll period found in Papanikolaou (2014), the region of intense parametric roll can be justified. Specifically,

$$T_n = \frac{2\pi i_\varphi}{\sqrt{g \cdot GM}} \tag{6.1}$$

In Equation (6.1), T_n is the natural roll period, i_φ stands for the roll radius of gyration together with the added moment of inertia and GM is the metacentric height of the ship. A mean value of 0.38B is suggested in Papanikolaou (2014) for the estimation of i_φ. The latter, depends on the ship type and loading condition. Additionally, the considered GM value is 1.999 meters. Using the aforementioned data, the value of the natural roll period is 21.571 seconds resulting to a natural frequency of 0.29 rad/s. This means that parametric roll is expected to initiate close to an encounter frequency of $\omega_e = 2 \cdot \omega_n = 0.58\,\mathrm{rad/sec}$. Therefore, several time-domain simulations, concerning the history of roll motion, are demonstrated below starting from a wave frequency of 0.34 rad/s.

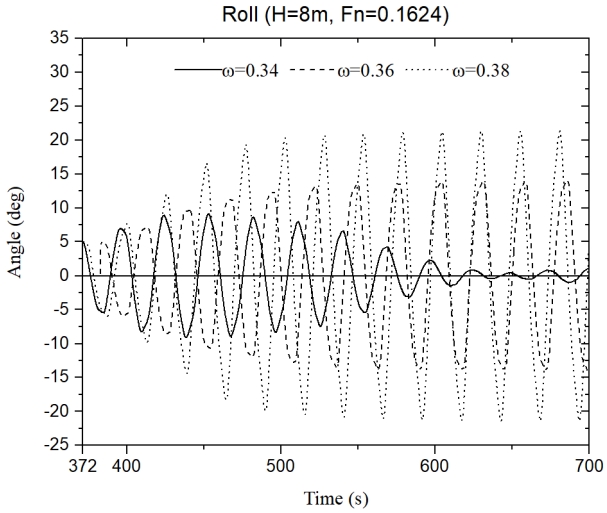

Figure 6.25: Time histories of roll motion at various wave frequencies for C11

From the figure shown above, it can be understood that parametric roll initially occurs when the wave frequency is 0.36 rad/s, which corresponds to an encounter frequency of 0.47 rad/s. having an amplitude of 14.55^{o} at the first harmonic frequency. Maximum roll amplitude of 21.4^{o} is found when the wave frequency is 0.38 rad/s. Additionally, simulations showed that smaller parametric roll excitation exists for wave frequencies up to 0.44 rad/s, corresponding to an encounter frequency of 0.60 rad/s. From the aforementioned analysis, it is confirmed that the present method is able to identify parametric roll within a range of encounter frequencies that are close to the theoretically estimated encounter frequency where this phenomenon is expected to occur.

Time histories of heave, roll and pitch motion at ω=0.38 rad/s are presented in the following figure proving that the roll encounter period is almost double the encounter period of heave and pitch motions.

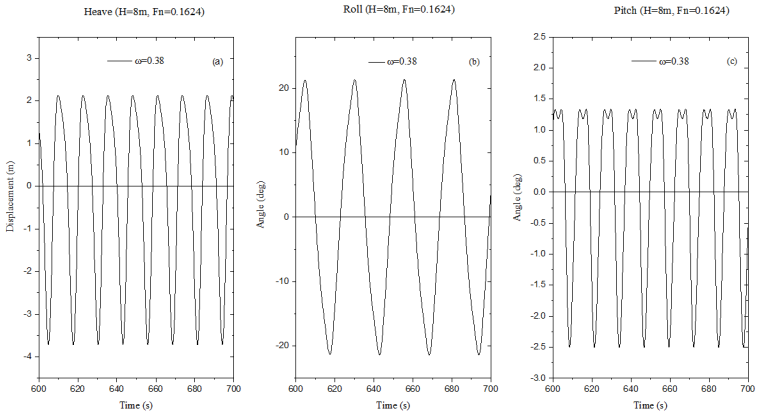

Figure 6.26: Time histories of heave (a), roll (b) and pitch (c) motions at ω=0.38 for C11 (H=8m, Fn=0.1624)

Subsequently, in Table 6.6 the development of parametric roll in each case is indicated filling the corresponding cells with red color.

Table 6.6: Development of parametric roll for the tested environmental conditions

H (m) / ω (rad/s)	2	4	6	8
0.30	**X**	**X**	**X**	**X**
0.34	**X**	**X**	**X**	**X**
0.38	**X**			
0.42	**X**			
0.44	**X**	**X**	**X**	
0.46	**X**	**X**	**X**	**X**

With the aforementioned discussion and presented results, it is considered that the verification process of the developed numerical code, which is defined by the accurate representation of the theoretical aspects of parametric roll, is successful. Validation of the proposed methodology is not conducted herein, as it is considered out of the scope of the present study. Besides, due to the implementation of a simplified method for the calculation of the roll damping, a comparison of the numerical results with experimental ones would be brushless. **It was emphasized several times in previous chapters that the investigation of dynamic stability failure modes, such as parametric roll, would be utilized as a way to verify the ability of the developed numerical tool to perform direct stability assessment, which incorporates a higher level of nonlinearity.**

6.4 Manoeuvring in Waves

The validation studies presented in the previous sections of this chapter were performed in order to ascertain that the elemental modules (calm water manoeuvring, linear/nonlinear seakeeping), of the integrated time domain analysis which are required in order to simulate ship's manoeuvring motion in waves, are well defined and the sources of conceptual and numerical errors are limited. In the present section, extensive validation studies considering ship's manoeuvrability in waves are demonstrated, implementing the developed methodology.

Comparison with experimental turning circle trajectories (rudder at ±35) is conducted for λ/L_{pp}=0.5, λ/L_{pp}=0.7 and λ/L_{pp}=1.0, for a 1:50 scaled model of the S-175 container ship.

The aforementioned data were provided by Prof Yasukawa. In the studied cases, initially beam and head waves are considered. Additionally, time histories of the longitudinal speed and yaw rate are compared, since relevant experimental data are also provided. The vessel's initial velocities and position with respect to the earth-fixed reference frame were adjusted according to the experimental initial set up. Small deviations are noticed from the value of 0.879 m/s (Fn=0.15), which are attributed to the fact that a speed loss was occurred due to the added resistance encountered by the model when sailing in waves. Results of the turning trajectories are illustrated below. Especially in case of port side turning circle at λ/L_{pp}=0.5, the influence of the first-order wave forces on the accuracy of the developed method is demonstrated.

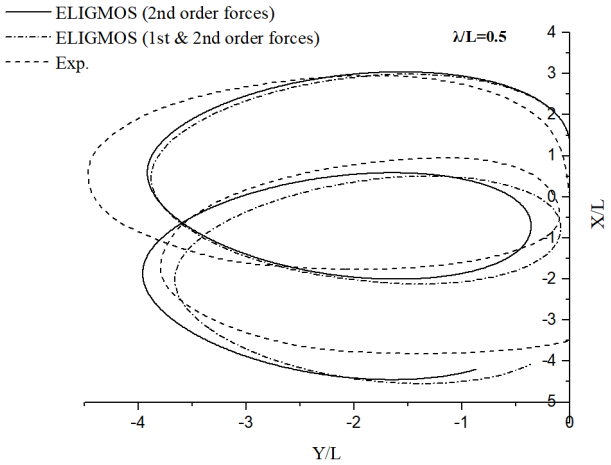

Figure 6.27: Comparison of port side turning circle in head waves with available experimental results (λ/L=0.5)

From Figure 6.27, it can be understood that the incorporation of the first-order forces (Froude-Krylov and Diffraction forces) apart from the second-order forces, improves the agreement of the present simulations with the experimental ones, especially concerning the Y- coordinated of the vessel's trajectory and after the first 180^o of yaw angle. Additionally, results derived with the use of ELIGMOS show better accuracy than Yasukawa and Nakayama's (2009), probably due to the adopted methodology which was implemented for the calculation of the second order wave forces, as the linear RAO values for λ/L_{pp}=0.5 presented in the aforementioned publication were calculated with acceptable accuracy.

Comparison of results for λ/L_{pp}=0.5, 0.7 and 1.0 at ±35^o of rudder angle in head waves is shown below, together with the comparison of the time history of surge and yaw velocities.

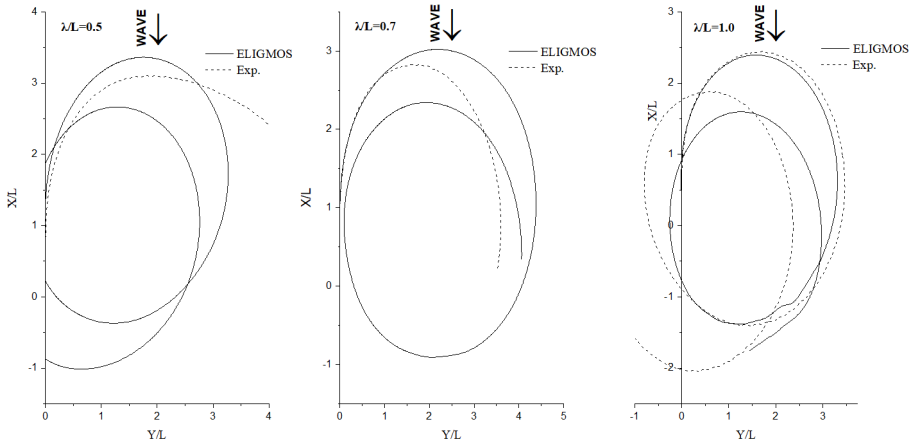

Figure 6.28: Comparison of starboard side turning circles in head waves with available experimental results

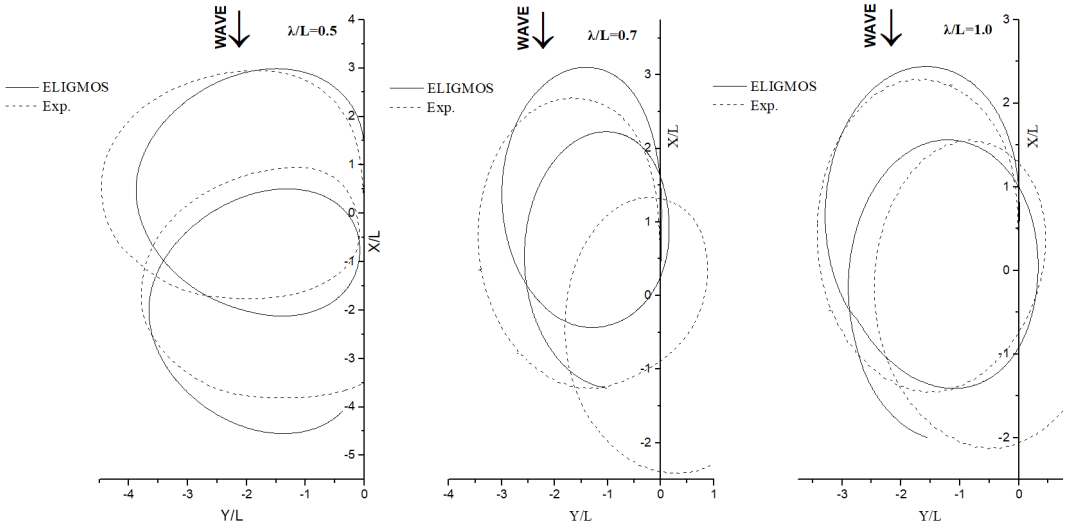

Figure 6.29: Comparison of port side turning circles in head waves with available experimental results

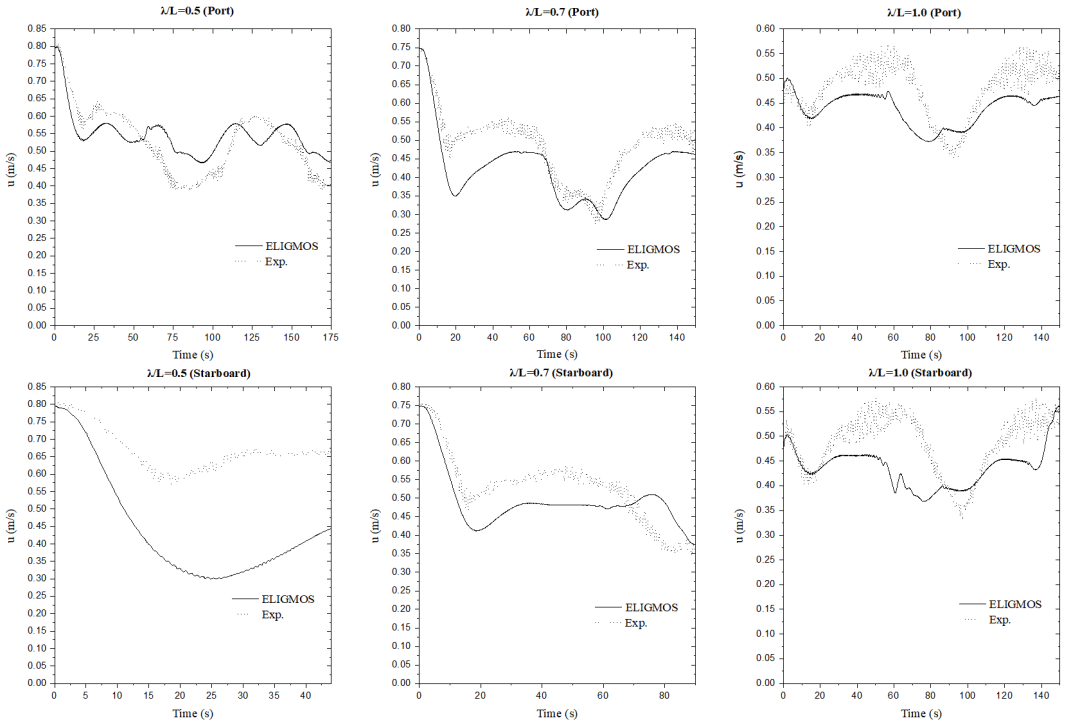

Figure 6.30: Comparison of longitudinal velocity during turning motion in head waves with available experimental results

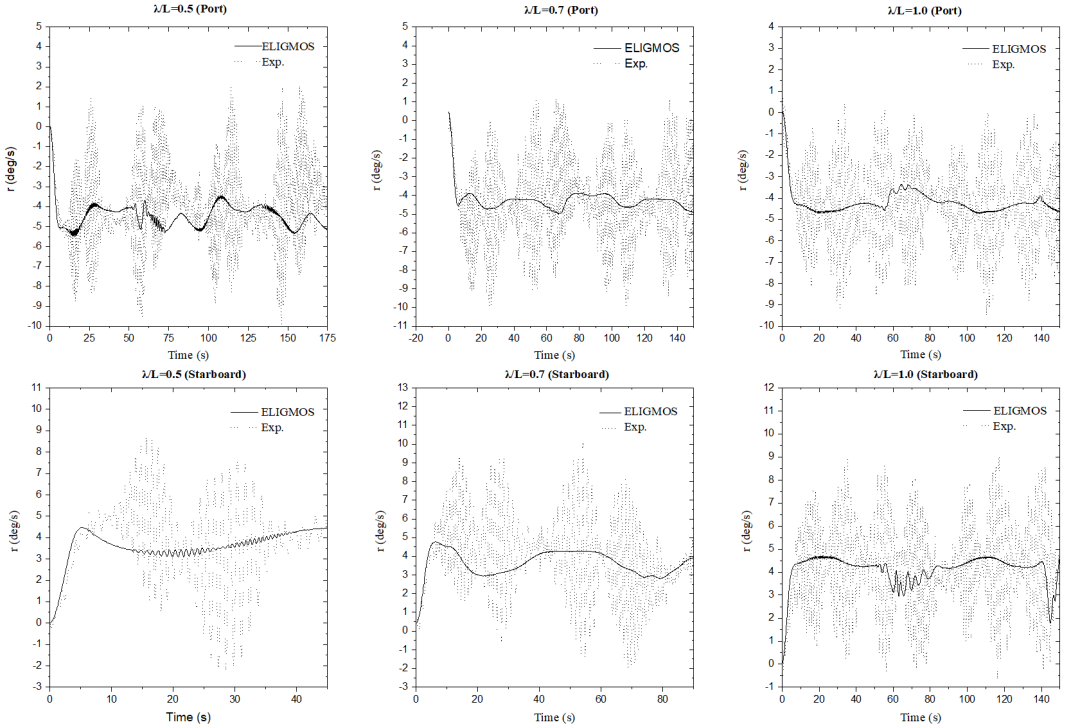

Figure 6.31: Comparison of yaw rate during turning motion in head waves with available experimental results

Turning trajectories with the same rudder angle (±35°) in beam waves are depicted below. In these cases, comparison of surge and yaw velocities is performed as well.

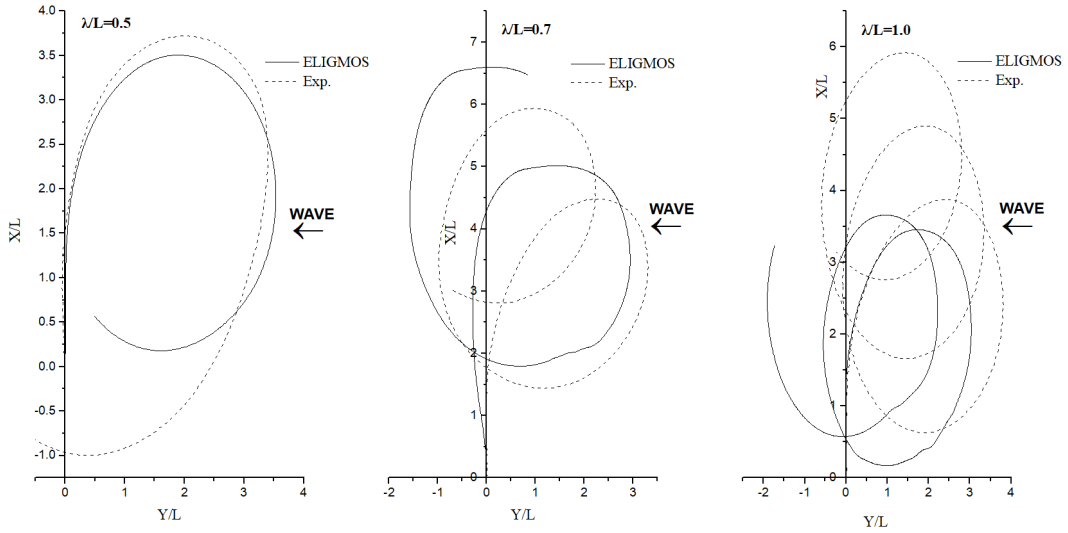

Figure 6.32: Comparison of starboard side turning circles in beam waves with available experimental results

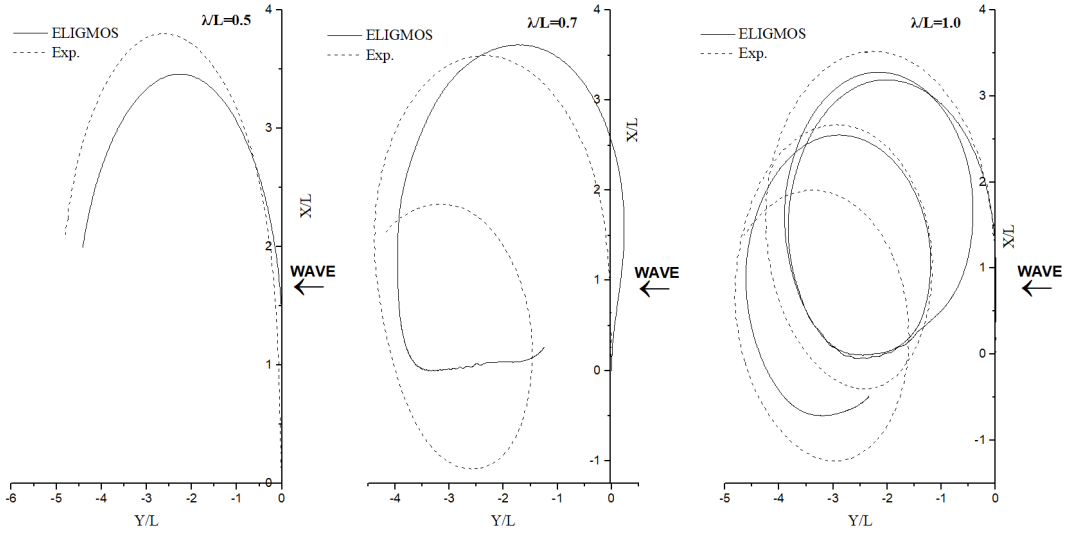

Figure 6.33: Comparison of port side turning circles in beam waves with available experimental results

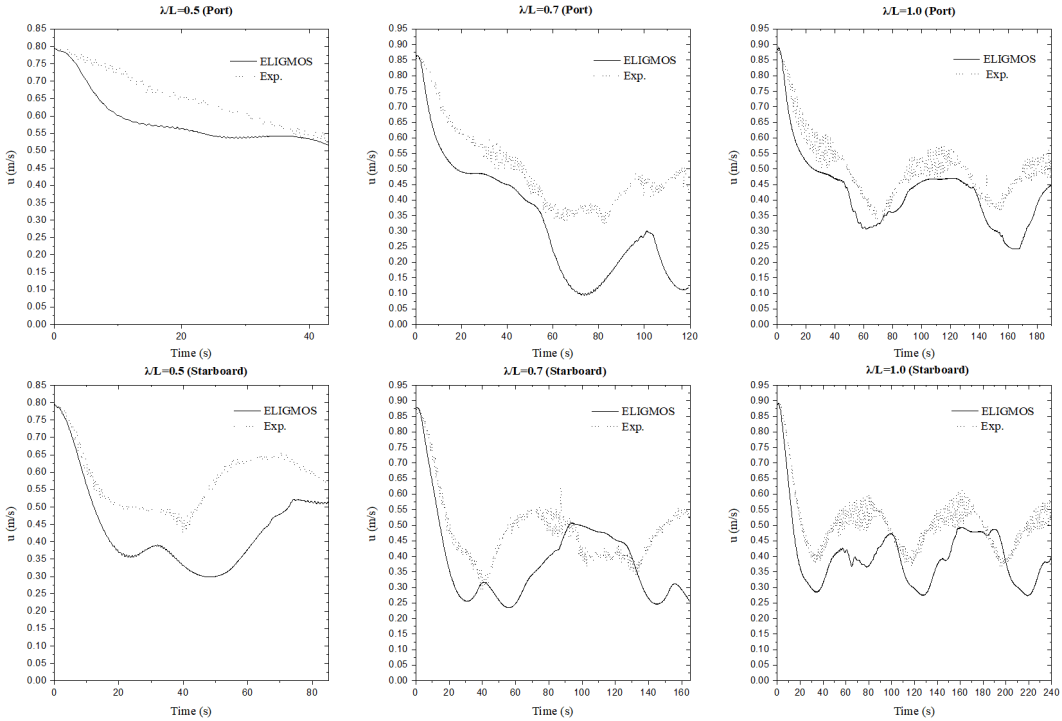

Figure 6.34: Comparison of longitudinal velocity during turning motion in beam waves with available experimental results

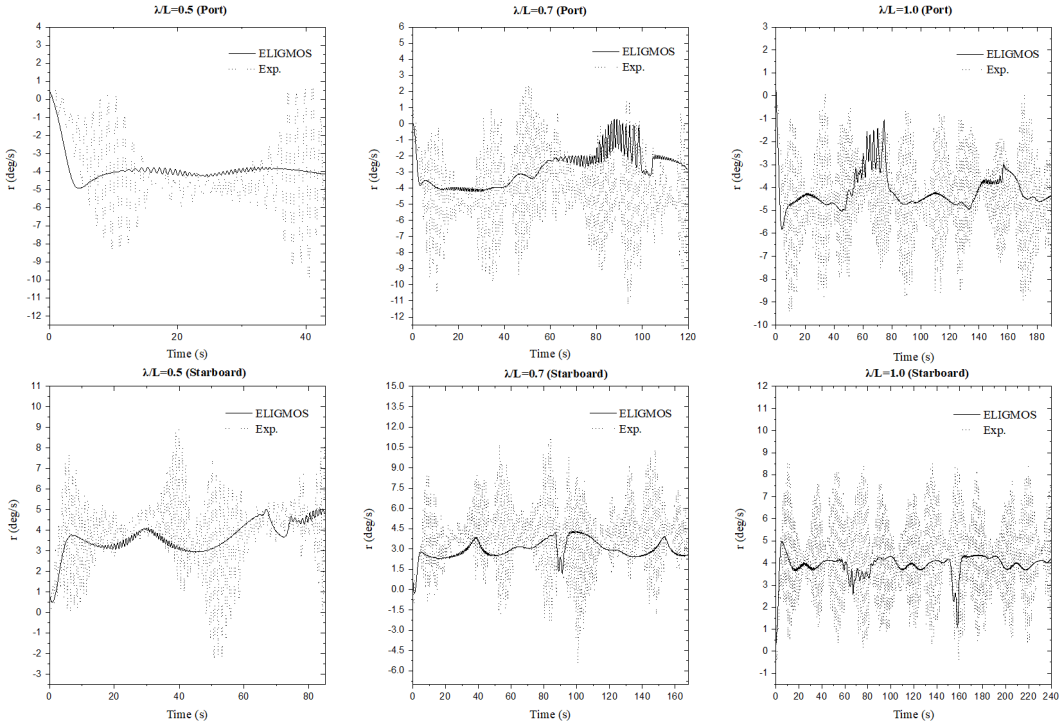

Figure 6.35: Comparison of yaw rate during turning motion in beam waves with available experimental results

Detailed presentation of the second-order forces that were used in the context of the previously depicted simulations and consist of the major wave impact during turning motion can be seen in Appendix C of the present thesis. Additionally, in all cases, comparison in terms of the main manoeuvring characteristics (Advance, Transfer and Tactical Diameter) is depicted in Tables 6.7, 6.8, 6.9 and 6.10.

Table 6.7: Turning circle characteristics in head seas (rudder angle at +35^o)

	AD	TR	DT
	Exp / **ELIGMOS**	Exp / **ELIGMOS**	Exp / **ELIGMOS**
λ/L_{pp}=0.5	3.099 / **3.308**	2.005 / **1.362**	NA / **3.237**
λ/L_{pp}=0.7	2.813 / **3.022**	1.458 / **2.186**	3.574 / **4.385**
λ/L_{pp}=1.0	2.407 / **2.394**	1.389 / **1.566**	3.444 / **3.309**

Table 6.8: Turning circle characteristics in head seas (rudder angle at -35^o)

	AD	TR	DT
	Exp / **ELIGMOS**	Exp / **ELIGMOS**	Exp / **ELIGMOS**
λ/L_{pp}=0.5	2.977 / **3.009**	-1.945 / **-1.471**	-4.44 / **-3.99**
λ/L_{pp}=0.7	2.679 / **3.102**	-1.504 / **-1.417**	-3.417 / **-3.001**
λ/L_{pp}=1.0	2.265 / **2.440**	-1.403 / **-1.563**	-3.390 / **-3.288**

Table 6.9: Turning circle characteristics in beam seas (rudder angle at +35^o)

	AD	TR	DT
	Exp / **ELIGMOS**	Exp / **ELIGMOS**	Exp / **ELIGMOS**
λ/L_{pp}=0.5	3.68 / **3.35**	1.66 / **1.43**	3.40 / **3.35**
λ/L_{pp}=0.7	4.43 / **5.02**	1.87 / **1.38**	3.29 / **2.94**
λ/L_{pp}=1.0	3.83 / **3.45**	1.98 / **1.79**	3.77 / **3.03**

Table 6.10: Turning circle characteristics in beam seas (rudder angle at -35^o)

	AD	TR	DT
	Exp / **ELIGMOS**	Exp / **ELIGMOS**	Exp / **ELIGMOS**
λ/L_{pp}=0.5	3.77 / **3.46**	-2.26 / **-2.06**	-4.79 / **-4.54**
λ/L_{pp}=0.7	3.47 / **3.61**	-2.02 / **-1.52**	-4.32 / **-3.95**
λ/L_{pp}=1.0	3.48 / **3.19**	-1.87 / **-1.98**	-4.19 / **-3.83**

However, Ueno (2003) claimed that comparison of the turning trajectories in waves should adopt the concepts of drifting distance and drifting angle as shown below.

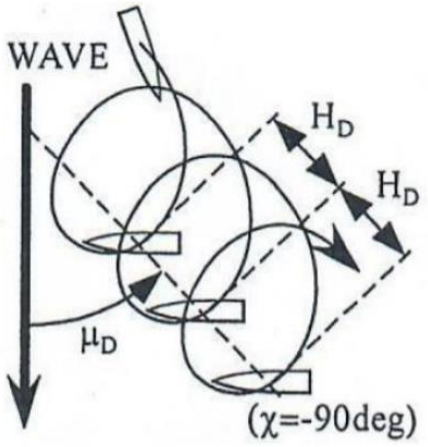

Figure 6.36: Drifting distance and drifting angle (Ueno et al., 2003)

Additionally, Kim (2018) added that the first 90^o of turning motion should not be used for comparison of the turning trajectories in waves as there has not been succeeded a steady state. Depending on the availability of experimental data, the comparison of drifting distances at 270^o and 630^o in head waves is depicted in the following figure for port turning circle.

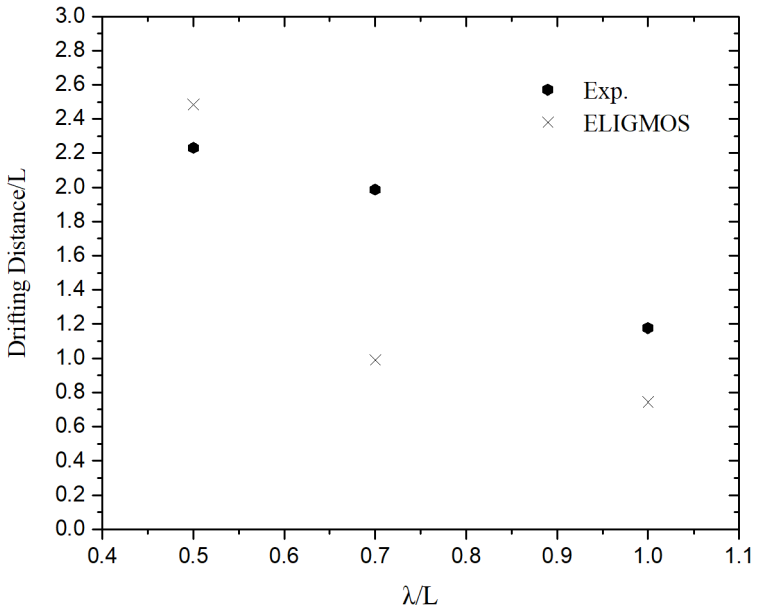

Figure 6.37: Comparison of drifting distance for S-175 at port side manoeuvring in regular head waves

6.5 Summary

In the present chapter, extensive validation studies were conducted employing the newly developed code ELIGMOS. The main scope of the aforementioned code is to simulate the manoeuvring behavior of a ship in a seagoing environment, implementing a hybrid approach. As long as the wave amplitude is small (ζ_α=1m), the manoeuvring and seakeeping contributions can be expressed by use of a body-fixed reference frame, which coincides with the slowly turning hydrodynamic coordinate system.

Manoeuvring related forces, together with the first and second-order wave forces are calculated in a modular basis, which allows targeted improvements that do not affect other parts of the code. Hydrodynamic forces exerted on the vessel's hull have been calculated adopting a third-order nonlinear model, utilizing experimental values of the manoeuvring derivatives, whilst the MMG proposed procedures for the calculation of propeller's and rudder's actions have been considered as well. Mena second-order wave forces have been incorporated by means of a multidimensional interpolation scheme, which facilitates the introduction of their instantaneous value based on the exact longitudinal speed and heading angle.

Especially in case of the added resistance, near and far field methodologies, embedded in the codes NEWDRIFT v.7 and NEWDRIFT+ respectively, have been implemented in order to accurately calculate the aforementioned force in long and short wave seas. The integrated methodology was validated exploiting turning circle results of the well-documented S-175 container ship.

In case of shallow water simulations in calm water, modifications have been considered considering the inertial forces, the hydrodynamic hull forces including wave resistance and the hull-rudder-propeller interaction coefficients. The aforementioned modifications were made according to the under keel clearance, implementing relevant regression formulae found in the literature. The developed methodology was validated at shallow (h/T=1.5) and very shallow waters (h/T=1.2) using relevant data of KVLCC2 and S-175 marine vessels.

Results related with nonlinear seakeeping and parametric roll investigation can be considered as a step forward towards the development of a fully nonlinear numerical modelling of the hydrodynamic response of a ship in rough seas.

At this stage, validation is not considered completed however, the fact that the code captures such complex dynamic phenomena proves that a satisfactory level of verification has been attained.

In the following chapter, the developed numerical tool will be used for manoeuvring simulations in waves in case were the sea has finite depth. This will be succeeded through the incorporation of the pre-calculated first and second-order forces, obtained after solving the linear BVP at finite depth using NEWDRIFT v.7.

CHAPTER 7

MANOEUVRING IN SHALLOW AND LONG WAVE REGULAR SEAS

7.1 Introduction

In Chapter 6, it was presented an effort to validate the developed numerical tool against calm water manoeuvring, seakeeping performance employing linear and nonlinear analyses, parametric roll and manoeuvring in waves. The validation followed a step-by-step process starting from the simpler modules and moving towards the more complicated time-domain simulation of ship manoeuvring in waves.

Having attained a satisfactory agreement of numerical results with the experimental ones in case of ship manoeuvring in waves, the last part of the present research considers the effect of restricted sea depth on ship's manoeuvrability in a seagoing environment. Manoeuvring related forces are corrected according taking into account the under keel clearance, exploiting the expressions discussed in the previous chapter and shown analytically in Appendix A. Concerning the first and second-order wave forces, they are incorporated through the adoption of the potential theory from the solution of the three-dimensional BVP. In this case, the potential is expressed as a function of the sea depth, which is considered finite.

In the following simulations, the manoeuvring performance of S-175 is investigated in the range of sea depths which are considered shallow, from the value of h/T=3.0 down to h/T=1.5 is step of 0.5. Since the validation of the present methodology at very shallow, calm water (h/T=1.2) is not considered successful, it is thought as rational to exclude this case from the present investigation.

Regarding the results presented in the previous chapter, it is judged that quantitative comparison in terms of the main characteristics of the turning trajectories can be performed when the wave's direction with respect to the initial course of the ship is 90 degrees, the wavelength to ship length ratio is equal to 1 for both starboard and port turning circles. In all other cases, a preliminary qualitative comparison is possible, which will demonstrate the effect of shallow water on a ship's turning trajectory in waves.

Due to unavailability of data regarding the second-order forces calculated at shallow water short wave seas (λ/L_{pp}=0.5) with the use of the previously discussed far-field method, numerical simulations at this condition are not carried out. The manoeuvrability of S-175 at an additional wavelength to ship length ratio (λ/L_{pp}=1.2) is examined as well, since the near-field method is considered more suitable in case of long wave seas.

7.2 Case Studies

In this section, the results of time-domain simulations of S-175 manoeuvring in waves at shallow water seas are presented. The corrections that have been implemented in order to incorporate the effect of the finite depth are the following.

1. Calculation of the second-order wave forces at finite depth using NEWDRIFT v.7.
2. Calculation of the first-order hydrodynamic loads at finite depth using NEWDRIFT v.7.
3. The manoeuvring-related forces have been re-evaluated through the adoption of Ankudinov's regression formulae for the calculation of the manoeuvring derivatives at finite depth.
4. Calculation of the added masses at finite depth using Li and Wu's (1990) regression formulae.
5. Calculation of certain hull-rudder-propeller interaction coefficients at finite depth using Amin and Hasegawa (2010).
6. The finite sea depth affects calm water resistance as well, which is expressed in the current simulations implementing the regression formula proposed by Furukawa et al. (2016).

Time-domain simulations at λ/L_{pp}=1.0 and λ/L_{pp}=1.2 have been conducted taking into consideration the aforementioned modifications, for UKC=3, 2.5, 2 and 1.5. The results are compared with the turning trajectories at deep water condition in order to demonstrate in each case the shallow water effect more distinctly.

- **λ/L$_{pp}$=1.0**

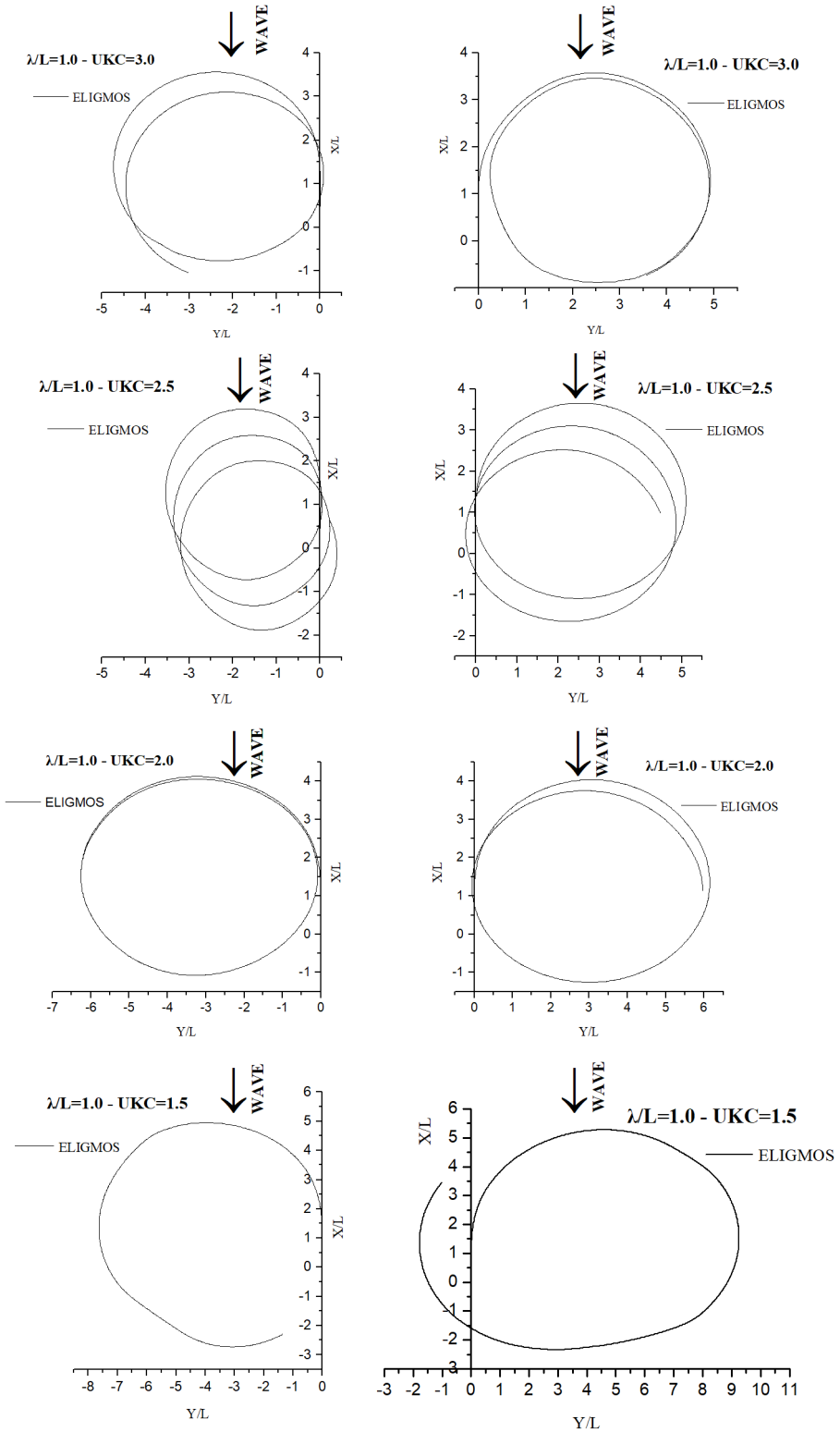

Figure 7.1: Port and starboard turning circles of S-175 in head waves (λ/L=1.0 - UKC=3.0, 2.5, 2.0, 1.5)

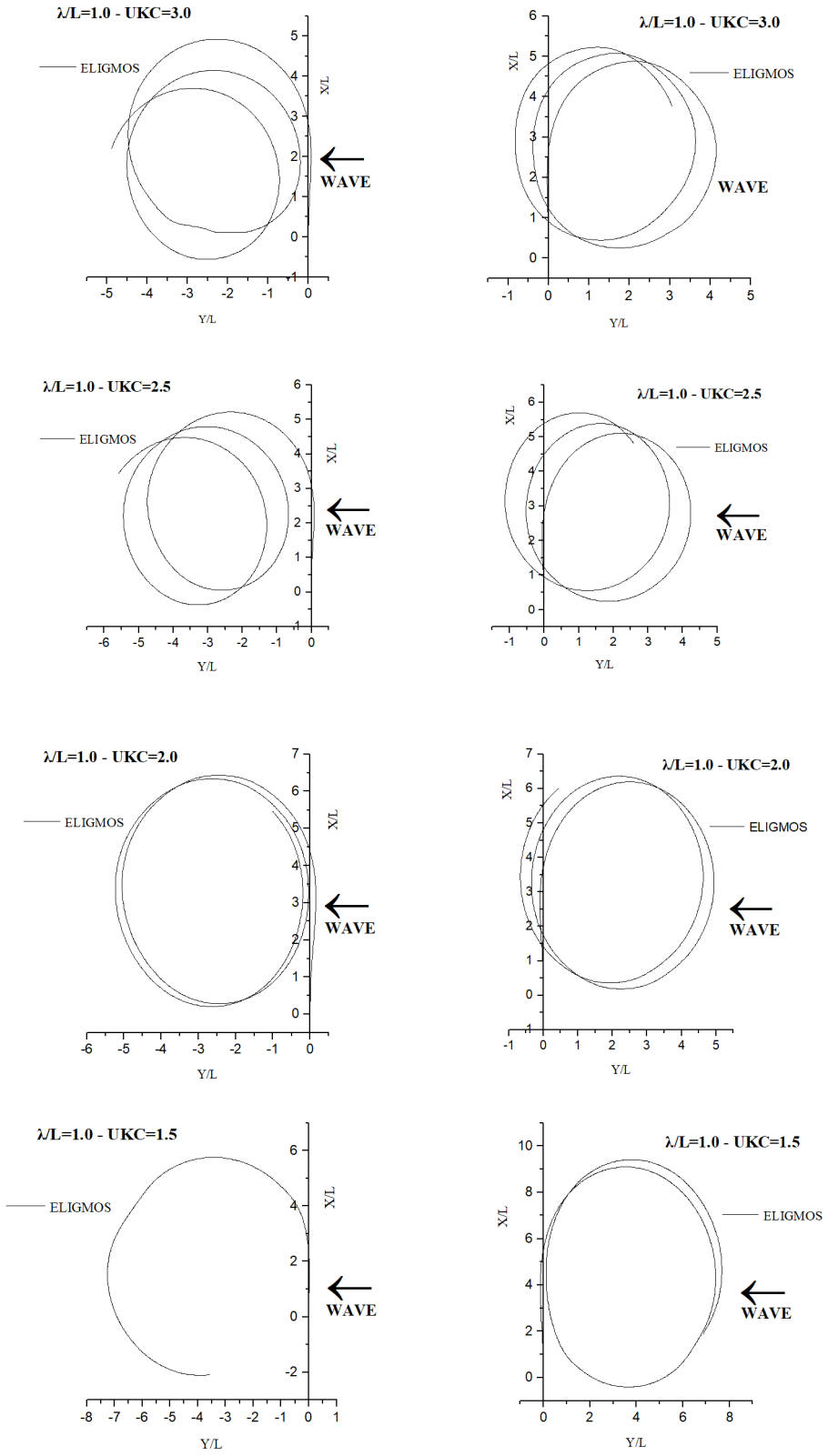

Figure 7.2: Port and starboard turning circles of S-175 in beam waves (λ/L=1.0 - UKC=3.0, 2.5, 2.0, 1.5)

- **λ/L_{pp}=1.2**

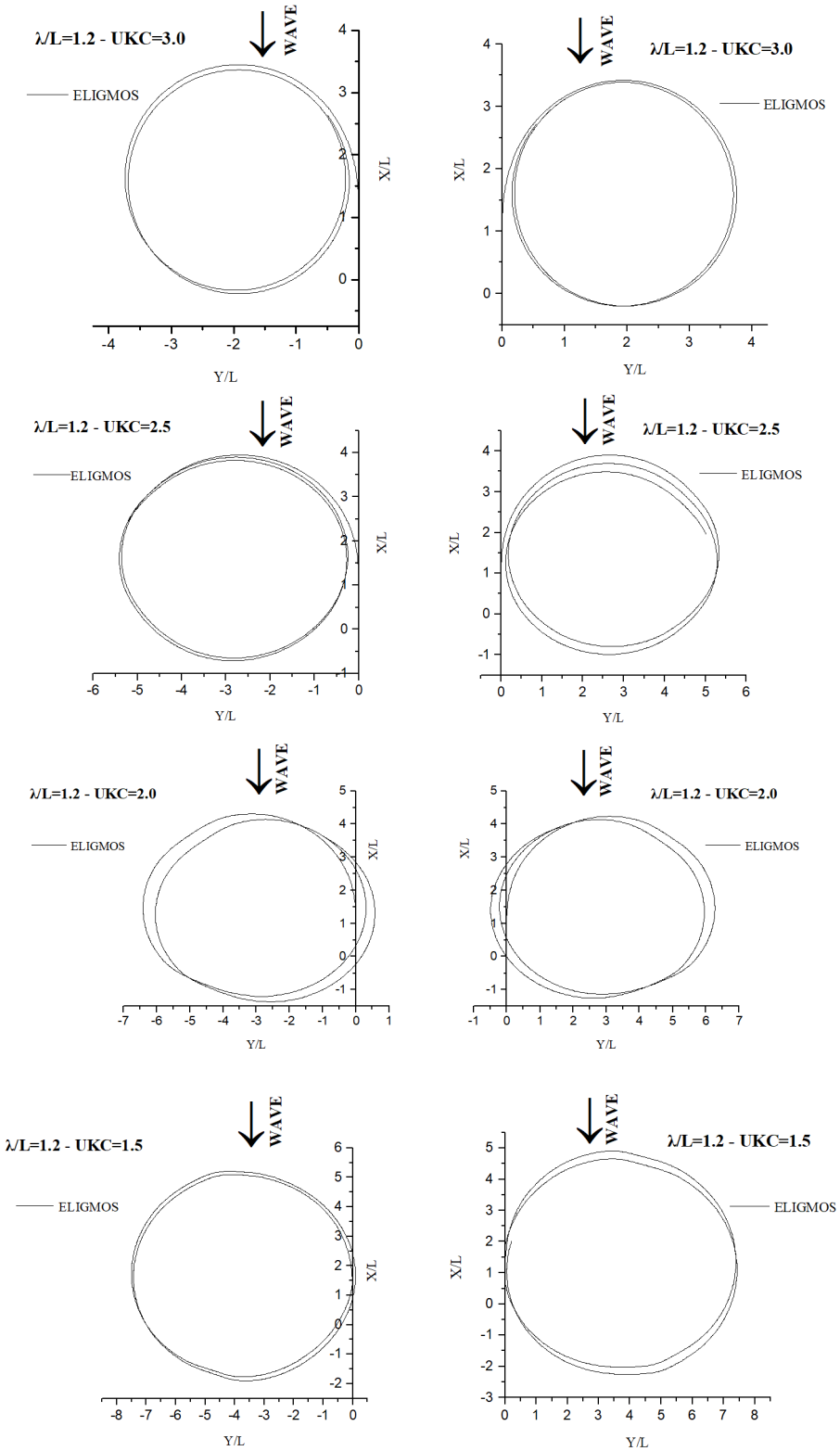

Figure 7.3: Port and starboard turning circles of S-175 in head waves (λ/L=1.2 - UKC=3.0, 2.5, 2.0, 1.5)

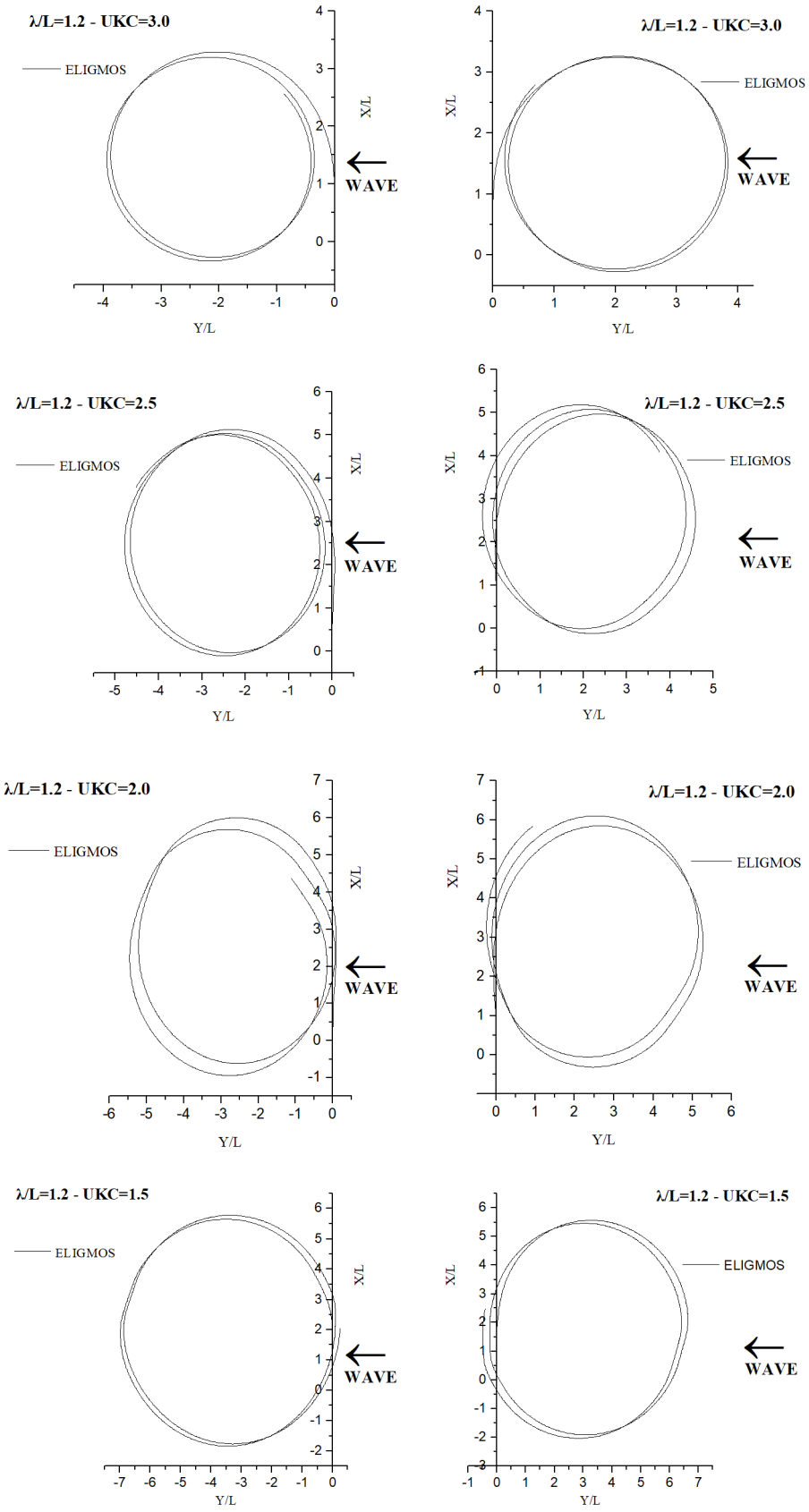

Figure 7.4: Port and starboard turning circles of S-175 in beam waves (λ/L=1.2 - UKC=3.0, 2.5, 2.0, 1.5)

7.3 Summary

In the present chapter, a further development of the methodology that is capable of simulating the manoeuvring performance of a marine vessel in waves was shown, emphasizing on the shallow water effect. For this purpose, several interventions were incorporated, aiming to express the impact of the updated flow pattern experienced by the ship, due to the restricted sea depth, on the various external force contributions. One the one hand, the latter refer to the wave forces resulting from the solution of the BVP at finite sea depth implementing the potential theory. On the other hand, the restricted sea depth provokes changes on the manoeuvring-related forces, which are expressed by regression formulae that are functions of the UKC.

The aforementioned methodology was tested for the S-175 container ship at long wave seas, where it was possible to perform calculations with regards to the second-order wave forces. Although experimental data were not found in order to perform validation studies of the proposed methodology, several qualitative remarks will be discussed in the following chapter, exploiting the present preliminary study. The major findings concern the impact of drift forces and the radius of the performed turning circles as the UKC is diminished.

CHAPTER 8

DISCUSSION

8.1 Introduction

In the present thesis, a methodology was presented that can be used in order to simulate the manoeuvring behavior of a ship in regular waves and shallow waters through the novel numerical tool ELIGMOS. The aforementioned methodology, which was discussed in detail in Chapter 4, couples seakeeping and manoeuvring theories implementing a 3-DOF hybrid formulation, where the low and high frequency external force components are summarized at each time step. In this way, it is possible to incorporate the effect of the manoeuvring-related hydrodynamic lift and drag forces, as well as the contribution of the first and second-order (drift) wave forces. The latter are imported through a multidimensional interpolation scheme, using the longitudinal speed and the exact heading angle as control parameters.

After demonstrating an extensive validation study of the aforementioned methodology in Chapter 5, several modifications are proposed concerning the shallow water effect in various force components. Subsequently, time-domain simulations were presented in Chapter 6, showing the impact of finite sea depth on the turning ability of S-175 at long wave seas. The qualitative findings will be discussed in the following section.

Although in all cases, simulation of ship manoeuvring in waves has been discussed assuming small wave excitations, an effort was made to extend the adopted methodology so that a certain level of nonlinearity can be attained, which would facilitate the investigation of large amplitude motions during manoeuvring in waves. In this sense, apart from the linear time-domain solution of the seakeeping problem, a nonlinear one is developed adopting the Froude-Krylov nonlinearity level. A further enhancement of the latter, including roll equation of motion, led to the development of a 3-DOF time-domain numerical tool which can be used for the investigation of parametric roll in the context of Second Generation Intact Stability Criteria.

Finally, as it was considered a necessary step before moving to the integrated model, calm water nonlinear manoeuvring simulations have been shown as well, mostly as a way to verify the correctness of the applied numerical scheme.

8.2 Key Findings

Starting from the simplest case of a ship manoeuvring in calm and deep water, results depicted in Tables 6.1 and 6.2 showed acceptable agreement with the free sailing results provided by MARIN, with regards to the turning circle manoeuvring of KVLCC2 at Fn=0.142. As it concerns 10/10 and 20/20 zig-zag tests, the agreement in terms of first and second overshoot angles is much better than the second and third execute times, which are higher than any other prediction based on numerical studies. The latter can be attributed to the simple equation that used for representing the wave resistance and the inertial loads expressed via the added masses. Additionally, the accuracy of the manoeuvring derivatives used for the calculation of the hydrodynamic hull forces are a question in this kind of simulations. In case of S-175, where the simulations executed according to the detailed experimental setup, high accuracy was succeeded as illustrated in Figure 6.4. Preliminary simulations considering the sway-roll-yaw coupling were also performed, illustrating the impact of the metacentric height on the heeling response.

When calm water manoeuvring was examined in shallow water for the KVLCC2, an acceptable agreement with the experimental trajectories was found. both for the case of turning circle and for the 20/5 zig-zag manoeuvre as shown in Table 6.5 and in Figures 6.7 and 6.9. On the contrary, the results concerning turning circle manoeuvring of KVLCC2 in very shallow water derived by using ELIGMOS were proved overestimated compared with available experimental data, as depicted in Table 6.5 and in Figures 6.6 and 6.8. The significant differences are attributed to the formula used in order to account for the impact of the sea depth on the calm water resistance. Besides, Furukawa et al. (2016), who introduced the relevant formula, suggest that experimentally determined value of the calm water resistance is preferred due to its significance during the calculation of the longitudinal forces. According to the aforementioned, it is considered that the developed numerical tool has attained a satisfactory level of validation that is needed for time-domain simulations of ship manoeuvring in calm water, needing further improvements concerning the shallow water case.

Special care must be given during the collection or calculation of input data (i.e. manoeuvring derivatives, hull-rudder-propeller-interaction coefficients, open-water propeller characteristics) as they strongly affect the external forces and the vessel's trajectory.

Concerning the time-domain seakeeping analysis conducted within the framework of the present research, several remarks can be made. Initially, the validity of the developed numerical tool was tested in the context of linear analysis, using the force data derived by the solution of the BVP with the 3D panel code PRECAL. This was considered a prerequisite in order to ensure that the developed numerical scheme implemented accurately the convolution integrals. Primary element of the aforementioned convolution integral is the memory functions of the linearly calculated damping coefficients, which were validated independently exploiting relevant data of an existing software (Figure 6.10). Results of nondimensional RAO values presented in Figures 6.11 and 6.12 denote satisfactory agreement against the frequency-domain data.

Having validated ELGIMOS in linear seakeeping analysis, a further development was succeeded which would allow the analysis of a vessel's seakeeping performance in rough seas, incorporating a level of nonlinearity in the calculations. In this context, it was decided that Froude-Krylov and Restoring forces should be instantaneously calculated over the hull's surface, implementing a direct pressure integration scheme. The latter offered the possibility to account for the geometrical nonlinearities of ships with distinct flare, whose waterplane area significantly differs far away from the mean sea level. A preliminary validation of such nonlinear time-domain seakeeping methods can be performed considering small wave amplitudes. In such conditions, the differences in vessel's response compared with her linear results must negligible. The latter was demonstrated in detail in Pollalis et al. (2019). Further, the proposed nonlinear seakeeping analysis was proved capable of detecting the differences between full and fine hull forms as wave steepness increases. The latter can be seen in Figures 6.19-6.20 and 6.23. In these figures, the amplitude of nonlinear heave and pitch motions is taken equal to the amplitude of motion at the first harmonic frequency, which was obtained after implementing Fourier analysis. Validation of time-domain results with experimental data remains an issue of future investigation as the only available showed distinct differences, especially for heave motion (Pollalis et al., 2019). This is mainly attributed to the fact that the software, which was used for solving the BVP ignores the presence of the steady flow potential, while adopts a uniform base flow when the ship moves with a steady forward speed.

In order to capture interesting intact stability phenomena such as parametric rolling, the nonlinear seakeeping model was extended and the roll motion was included in the system of equations. In this way, it was made possible to perform direct stability assessment of a C-11 class container ship and detect parametric roll. At this stage of code development, a simplified equation for the calculation of the roll damping moment was adopted, which is based on the equivalent linear damping coefficient approach. The developed methodology succeeded to detect when the parametric roll was initiated, namely at encounter frequency approximately twice the value of the natural roll frequency as shown in Table 6.6. Enhancing the roll damping moment model, is expected to improve roll prediction. In this context, the Ikeda's method would be a suitable alternative. Due to time limitations, this could not happen within the framework of the present study.

The largest and more significant part of the present research, which consists the scope of the present study, concerns the investigation of a ship's manoeuvrability in waves, giving emphasis on the shallow water effect. Concerning the simulations in deep water, where experimental data were available for validation purposes of the numerical tool ELIGMOS, the comparison was acceptable in terms of the Advance, Transfer and Tactical Diameter in case of beam seas as shown in Tables 6.9 and 6.10. In most cases, after the first 180^o of turning motion, the trajectories varied significantly. This is attributed to the larger speed loss predicted by ELIGMOS due to the higher incorporated values of added resistance, especially in cases where $\lambda/L_{pp}=0.7$ and $\lambda/L_{pp}=1.0$. Additionally, a reason for the discrepancies mentioned before could be the fact that the yaw drift moment calculated with the near field method for the aforementioned environmental conditions is relatively much higher than the one calculated by means of the far field method in case where $\lambda/L_{pp}=0.5$.

In head seas, comparison of the time-domain results obtained with ELIGMOS against the relevant experimental data showed better agreement, also for the long wave sea cases, although there are still distinct discrepancies after the first 180^o or turning motion. Comparison in terms of Advance, Transfer and Tactical Diameter was illustrated in Tables 6.7 and 6.8.

The improvement of the numerical results in relation to the beam sea cases was also witnessed in Figure 6.35. which depicted the time histories of the forward speed and yaw velocity.

At this point, it must be noted that experimental data might vary among different laboratories (e.g. experimental trajectories in He's thesis differ from the adopted) thus, the validation of the developed code is considered an open topic, which needs further investigation.

After the discussion of the results concerning ship manoeuvring in waves, several modifications were proposed in Chapter 7 in order to incorporate the effect of shallow water. Although the investigated operational condition is not likely to happen in real life (ships usually sail in slow steaming condition in shallow water), some interesting remarks can be made. First of all, it was decided to assess ship's manoeuvrability in long wave seas (λ/L_{pp}=1.0, 1.2) as the available hydrodynamic software, which was used in order to calculate the second-order wave loads at finite depth, implements the near field method. Additionally, it was decided to study ship's manoeuvrability as the UKC reduces from 3 to 1.5 as a way to detect any accompanied qualitative changes. In case of λ/L_{pp}=1.0 it is realized that the vessel's trajectory enlarges as the water becomes shallower, whilst the impact of the sway drift force weakens. The latter can be attributed to the fact that the more the UKC reduces, the more the flow surrounds the ship making her lateral drifting more difficult. When the wavelength increases (λ/L_{pp}=1.2) no significant variations were noticed compared to the previous case study, apart from the case where UKC=1.5 where much larger trajectory was derived for the smaller wavelength. Additionally, in the larger wavelength case, looser impact of the sway drift force was pinpointed. Further, more manoeuvrability-related difficulties have been identified concerning the larger wavelength case.

Since the calm water resistance increased with the reduction of the UKC, adjustments of the propeller's revolutions were implemented in order to succeed equivalent thrust. In this aspect, for UKC values 2.5, 2.0 and 1.5 the relevant revolutions per second were 10.07, 10.11 and 10.32 respectively. In case of UKC=3.0 there was no need for any alteration of the propeller's revolutions.

8.3 Summary

In the previous section, a discussion of the key findings of the present study was performed. The discussion in the same way with the structure of the thesis, from the simpler module of calm water manoeuvring, up to the more complicated manoeuvring in shallow seagoing environment.

Regarding calm water manoeuvring, simulation results showed that ELIGMOS has the correct numerical structure and can be further developed in order to simulate more complicated ship behavior. Shallow water results depicted that the adopted methodology needs improvements when the sea depth is very low.

Additionally, linear seakeeping analysis by use of ELIGMOS was proven successful, a thing that verified the proper calculation of the radiation forces, employing the concept of memory functions of pre-calculated damping coefficients derived by use of potential theory . Further development of the seakeeping module through the adoption of Level 2 nonlinearities and primitive investigation of parametric roll, revealed that the novel numerical tool could be used in the context of direct stability assessment of ships against dynamic failure modes of stability in waves.

Finally, the validation studies conducted in the context of ship manoeuvring in waves showed promising results, although further effort is suggested. Simulations based on several modifications suggested for calculating seakeeping and manoeuvring-related forces in long wave and shallow seas, contributed in drawing preliminary qualitative conclusions about ship’s manoeuvrability in such case.

CHAPTER 9

CONCLUSIONS AND RECOMMENDATIONS FOR FUTURE RESEARCH

9.1 Conclusions

As stated in Chapter 1, the aim of the present research is to develop a time-domain methodology capable of holistically assessing the hydrodynamic performance of a ship in various environmental and operational conditions. This was made possible through the successful simulation of a ship's manoeuvring motion in calm water, the valid linear and nonlinear seakeeping analysis, the detection of head seas parametric roll and the effort to integrate seakeeping and manoeuvring approaches as a way to simulate a vessel's manoeuvring performance in regular waves. The latter, was further enhanced in order to assess a ship's manoeuvrability in waves, giving emphasis on the shallow water effect. The aforementioned time-domain analyses conducted using the novel numerical code ELIGMOS, which was developed within the framework of the present study and it is written in C++ programming language. The novelty of the present study consists of the following major points:

- A modular hybrid methodology was developed, able to couple seakeeping and manoeuvring theories. An innovative multidimensional interpolating scheme was incorporated, allowing the practical incorporation of the pre-calculated seakeeping forces based on the instantaneous forward speed and heading angle. Herein, first and second-order wave forces were obtained from the solution of the linearized BVP, by means of the 3D potential theory code NEWDRIFT. Manoeuvring-related external forces were incorporated according to the MMG model, whereas experimental values of the manoeuvring derivatives were employed.
- The aforementioned methodology was further developed in order to account for the shallow water effect. Concerning the wave forces, the solution of the BVP was adopted with an updated boundary condition on the sea bed, which allowed the calculation of the wave forces at finite depth.

Additionally, hydrodynamic forces exerted on the vessel's hull were revaluated adopting updated values of the manoeuvring derivatives using Ankudinov's regression formulae. Further, the impact of the shallow water on the calm water resistance, added inertias and hull-rudder-propeller interaction coefficients was expressed through relevant formulae found in the literature.

- The study of the manoeuvrability of S-175 in a shallow seagoing environment, employing the aforementioned methodology, led to the following preliminary qualitative conclusions:
    1. As the sea depth reduces, sway drift forces do not play an important role during the vessel's motion.
    2. In general, the aforementioned tendency is more obvious as the wavelength increases.
    3. For larger wavelength ($\lambda/L=1.2$), difficulties related with the vessel's manoeuvrability might arise.

9.2 Recommendations for Future Research

Although the developed methodology is able to assess a ship's hydrodynamic performance in various conditions, including turning circle manoeuvres in shallow and wavy seas, there are still a lot that could be done in order to improve it. Specifically,

- Validation studies concerning ship manoeuvring in shallow seagoing environment are needed in order to assess the accuracy of the proposed methodology.
- Validation of the second-order wave forces is crucial, especially in case of finite sea depth calculations.
- Improved calculation of the manoeuvring derivatives at finite sea depth.
- Enhancement of the developed methodology incorporating more equations of motion would be advantageous for its accuracy. As a first step, it is proposed to account for the heeling effect during turning motion in waves. For the specific case studied in the context of the present research, the metacentric height of the S-175 container ship was relatively large, so roll-coupling induced by the manoeuvring motion was not significant.

- The successful development of a methodology able to model a ship's nonlinear seakeeping performance in large waves should be integrated with manoeuvring approach in order to account for the effect of rough seas during manoeuvring. The optimization of ELIGMOS in terms of computational efficiency is a prerequisite towards the accomplishment of the aforementioned task.
- In order to be consistent with real ship operations, the methodology needs to be extended to manoeuvring simulations in irregular seas in the future.
- The effect of the finite sea depth on the rudder-induced forces should be represented in future developments of the presented methodology.

References

Abkowitz, M. A. (1964). *Lectures on ship hydrodynamics – Steering and maneuverability.* Lyngsby, Denmark: Hydro-og Aerodynamisk Laboratorium.

Abkowitz, M. A. (1980). Measurement of hydrodynamic characteristics from ship maneuvering trials by system identification. *Transactions of The Society of Naval Architects and Marine Engineers, 88,* 283-318.

Amin, O., & Hasegawa, K. (2010). Generalised Mathematical Model for Ship Manoeuvrability Considering Shallow Water Effect. *Conference Proc. of Japan Society of Naval Architects and Ocean Engineers.*

Ankudinov, V. K., Miller, E. R., Jakobsen, B. K., & Daggett, L. L. (1990). Maneuvering performance of tug/barge assemblies in restricted waterways. *Proceedings of MARSIM & ICMS 90,* (pp. 515-525). Tokyo, Japan.

Ayaz, Z. (2003). *Manoeuvring Behaviour of Ships in Extreme Astern Seas. PhD Thesis.* Glasgow, U.K.

Ayaz, Z., & Vassalos , D. (2003). Towards an Improved Mathematical Model for Ship Manoeuvring in Astern Seas. *Proceedings of MARSIM '03,* (pp. RC-14-1-RC-14-10). Kanazawa, Japan.

Ayaz, Z., Vassalos, D., & Spyrou, K. J. (2006). Manoeuvring behaviour of ships in extreme astern seas. *Ocean Engineering, 33,* 2381-2434.

Baar, J. J. M., & Price, W. G. (1988). Developments in the Calculation of the Wavemaking Resistance of Ships. *Proceedings of the Royal Society of London. Series A, Mathematical and Physical Physical Sciences, 416*(1850), 115-147.

Bailey, P. A., Price, W. G., & Temarel, P. (1997). A Unified Mathematic Model Describing the Manoeuvring of a Ship Travelling in a Seaway. *Trans. RINA, 140,* 131-149.

Beck, R. F., & Tuck, E. O. (1971). Heave and Pitch of Ships in Shallow Water. *4th Australasian Conference on Hydraulics and Fluid Mechancs,* (pp. 272-279). Melbourne.

Belenky, V., Bassler, C. C., & Spyrou, K. J. (2011). *Development of Second Generation Intact Stability Criteria.* West Bathesda, USA: Naval Surface Warfare Center, Hydromechanics Department Report.

Belknap, W., & Telste, J. (2008). Identification of Leading Order Nonlinearities from Numerical Forced Motion Experiment Results. *Proceedings of the 27th Symposium on Naval Hydrodynamics.* Seoul, Korea.

Bertram, V. (2000). *Practical Ship Hydrodynamics.* Butterworth-Heinemann.

Beukelman, W., & Gerritsma, J. (1982). The distribution of hydrodynamic mass and damping of an oscillating ship form in shallow water. *International Shipbuilding Progress, 29*(339), 297-315.

Bulian, G., & Francescutto, A. (2011). Effect of roll modelling in beam waves under multi-frequency excitation. *Ocean Engineering, 38,* 1448–1463.

Chapman, R. B. (1975). Numerical solution for hydrodynamic forces on a surface-piercing plate oscillating in yaw and sway. *1st International Conference on Numerical Ship Hydrodynamics,* (pp. 333-350).

Chislett, M. S., & Storm-Tejsen, J. (1965). *Planar motion mechanism tests and full scale steering maneuvering predictions for a mariner class vessel. Report No. Hy A6.* Lyngby, Denmark: Hydro and Aerodynamics Laboratory.

Chroni, D., Liu, S., Plessas, T., & Papanikolaou, A. (2015). Simulation of the maneuvering behaviour of ships under the influence of environmental forces. *Towards Green Marine Technology and Transport* (pp. 111-119). Pula, Croatia: Taylor and Francis Group, London.

Clarke, D. (1998). The effect of shallow water on manoeuvring derivatives using conformal mapping. *Control Engineering Practice, 6*, 629-634.

Crane, C. L. (1979). Maneuvering Trials of a 278000-DWT Tanker in Shallow and Deep Waters. *Transactions of the Society of Naval Architects and Marine Engineers, 87*, 251-283.

Cummins, W. E. (1962). The impulse response function and ship motions. *Ship Technology Research, 9*, 101-109.

Dafermos, G. K., Zaraphonitis, G. N., & Papanikolaou, A. D. (2019). On an extended boundary method for the removal of irregular frequencies in 3D pulsating source panel methods. *International Maritime Association of the Mediterranean*, (pp. 53-59). Varna, Bulgaria.

Dahlquist, G., & Björck, Å. (2003). *Numerical Methods.* Dover Books on Mathematics.

Delefortrie, G., & Vantorre, M. (2007). Modeling the Maneuvering Behavior of Container Carriers in Shallow Water. *Journal of Ship Research, 51*(4), 287-296.

Faltinsen, O. M., Minsaas, K., Liapis, N., & Skjørdal, S. O. (1980). Prediction of resistance and propulsion of a ship in a seaway. *13th Symposium of Naval Hydrodynamics*, (pp. 505-529). Tokyo, Japan.

Fang, M. C., Luo, J. H., & Lee, M. L. (2005). A Nonlinear Mathematical Model for Ship Turning Circle Simulation in Waves. *Journal of Ship Research, 49*(2), 69-79.

Fonseca, N., & Soares, C. G. (1998). Time-domain analysis of large-amplitude vertical ship motions and wave Loads. *Journal of Ship Research, 42*(2), 139-153.

Fossen, T. I. (2005). A Nonlinear Unified State-Space Model for Ship Maneuvering and Control in a Seaway. *International Journal of Bifurcation and Chaos, 15*(9), 2717-2746.

Fossen, T. I. (2011). *Hanbook of Marine Craft Hydrodynamics and Motion Control.* John Wiley and Sons, Ltd.

Fournarakis N., Chroni, D., Plessas, T., Liu, S., & Papanikolaou, A. (2016). Estimation of the maneuvering characteristics of the DTC containership using URANS based simulations. *3rd International Conference on Marine Technology and Engineering* (pp. 259-268). Lisbon, Portugal: Taylor and Francis Group, London.

France, W. N., Levadou, M., Treakle, T. W., Paulling, J. R., Michel, R. K., & Moore, C. (2003). An Investigation of Head-Sea Parametric Rolling and Its Influence on Container Lashing Systems. *Marine Technology, 40*(1), 1-19.

Fuehrer, & Roemisch. (1977). *XXIV International Maritime Congress.* Leningrad, USSR.

Fujii, H., & Tuda, T. (1961). Experimental research on rudder performance (2). *Journal of the Society of Naval Architects in Japan*, 31-42.

Fullerton, A. M., Fu, T. C., & Reed, A. M. (2008). The Moments on a Tumblehome Hull Form Undergoing Forced Roll. *Proceedings of the 27th Symposium on Naval Hydrodynamics.* Seoul, Korea.

Gerritsma, J., & Beukelman, W. (1972). Analysis of the resistance increase in waves of a fast cargoship. *International Shipbuilding Progress, 19*(217).

Ghillece, G., & Moctar, O. (2018). A numerical method for manoeuvring simulation in regular waves. *Ocean Engineering, 170*, 434-444.

Grochowalski, S., & Jankowski, J. (2009). Validation methodology for simulation software of ship behaviour in extreme seas. *Proceedings of the 10th International Conference on Stability of Ships and Ocean Vehicles.* St. Petersburg, Russia.

Hamamoto , M., & Kim, Y. (1993). A New Coordinate System and the Equations Describing Manoeuvring Motion of a Ship in Waves. *Journal of Naval Architects of Japan, 173*.

Hamamoto, M. (1977). MMG Report II: The Theoretical Background of the Mathematical Model of Ship Maneuverability. *The Bulletin of The Society of Naval Architects of Japan, 577*, 322-329.

Hamamoto, M., & Munif, A. (1998). A Mathematical Model to Describe Ship Motions Leading to Capsize in Severe Astern Waves. *Journal of the Society of Naval Architects of Japan, 184*, 111-118.

Hamamoto, M., & Saito, K. (1992). Time-domain analysis of ship motions in following waves. *11th Australasian Fluid Mechanics Conference*, (pp. 355-358). Hobart, Australia.

Hamamoto, M., Kim, Y., & Uwatoko, K. (1991). Study on Ship Motions andCapsizing in Following Seas. *Journal of the Society of Naval Architects of Japan, 170*, 173-182.

Hamamoto, M., Umeda, N., Matsuda, A., & Sera, W. (1995). Analyses on Low Cycle Resonance of Ship in Astern Seas. *Journal of the Society of Naval Architects of Japan, 177*, 197-206.

Haraguchi, T. (2000). Simple estimating method on ship manoeuvrability by means of manoeuvring performance database. *MARSIM*, (pp. 289-299). Orlando, USA.

Hashimoto, H., & Umeda, N. (2004). Nonlinear analysis of parametric rolling in longitudinal and quartering seas with realistic modeling of roll-restoring moment. *Journal of Marine Science and Technology, 9*, 117-126.

Havelock, T. H. (1963). *Collected papers.* Washington, U.S.: Government Printing Office.

He, S. (2017). *Numerical Prediction of Ship Manoeuvring in Regular Waves by a 2.5D Approach. PhD Thesis.* Glasgow, Uk.K: University of Strathclyde.

He, S., Yuan, Z., Incecik, A., Turan, O., & Boulougouris, E. (2016). Manoeuvring prediction based on CFD generated derivatives. *Journal of Hydrodynamics, 28*(2), 284-292.

Hess, F. (1977). Rudder effectiveness and course-keeping stability in shallow waters: a theoretical model. *International Shipbuilding Progress, 24*, 206-221.

Hess, J. L., & Smith, A. O. (1962). *Calculation of non-lifting potential flow about arbitrarty three-dimensional bodies.*

Himeno, Y. (1981). *Prediction of Ship Roll Damping - State of the Art.* The University of Michigan.

Hirano, M., Takaishi, Y., & Saruta, T. (1980). Ship turning trajectory in regular waves. *Transactions of the West-Japan Society of Naval Architects, 60*, 17-31.

Hirano, M., Takashina, J., Moriya, S., & Nakamura, Y. (1985). An experimental study on maneuvering hydrodynamic forces in shallow water. *Transcriptions oif West-Japan Society of Naval Architects, 69*, 101-110.

Hizir, O. G. (2015). *Three Dimensional Time Domain Simulation of Ship Motions and Loads in Large Amplitude Head Waves. PhD Thesis.* Glasgow, U.K.: University of Strathclyde.

Hizir, O. G., Kim, M., Turan, O., Day, A., Incecik, A., & Yongwon, L. (2019). Numerical studies on non-linearity of added resistance and ship motions of KVLCC2 in short and long waves. *International Journal of Naval Architecture and Ocean Engineering, 11*, 143-153.

Hochbaum, A. C. (2006). Virtual PMM tests for manoeuvring prediction. *26th Symposium on Naval Hydrodynamics.* Rome, Italy.

Hooft, J. (1973). Manoeuvring Large Ships in Shallow Water-I. *Journal of Navigation, 26*(2), 189-201.
Hu, P. (1961). *Forward speed effect on lateral stability derivatives of a ship.* Stevens Institute of Technology, Davidson Laboratory.
Hwang, W. Y. (1980). *Application of system identification to ship maneuvering.* USA: Massachusetts Institute of Technology.
IMO. (2012). *Guidelines on the method of calculation of the attained energy efficient design index (EEDI) for new ships, resolution MEPC. 212(63).*
IMO. (2018). *Report of the 6th session of the Sub-Committee on Ship Design and Construction.*
Inoue, S. (1981). Hydrodynamic derivatives on ship manoeuvring. *International Shipbuilding Progress, 28*(321), 112-125.
ITTC. (1981). *The Seakeeping Committee.* Leningrad, USSR.
ITTC. (2002). *The Manoeuvring Committee.* Venice, Italy.
ITTC. (2011). *The Manoeuvring Committee, Technical Report.* Rio de Janeiro, Brazil.
ITTC. (2011). *The Specialist Committee on Stability in Waves.* Rio de Janeiro, Brazil.
ITTC. (2011). *Verification and Validation of Linear and Weakly Nonlinear Seakeeping Computer Codes.*
ITTC. (2014). *The Ocean Engineering Committee.* Copenhagen, Denmark.
Iwashita, H., & Ohkusu, M. (1992). The Green function method for ship motions at forward speed. *Ship Technology Research, 39*(2), 3-21.
Jasionowski, A. (2001). *An Integrated Approach to Damage Ship Survivability Assessment. PhD Thesis.* Glasgow, U.K.: University of Strathclyde.
Jiang, C., Troesch, A. W., & Shaw, S. W. (2014). Capsize criteria for ship models with memory-dependent hydrodynamics and random excitation. *Philosophical Transactions of The Royal Society, 358*, 1761-1791.
Joncquez, S. A. (2009). *Second-order forces and moments acting on ships in waves. PhD Thesis.* DTU.
Joosen, W. P. (1966). Added resistance of ships in waves. *Proceedings of the 6th Symposium on Naval Hydrodynamics.* Washington, D.C.
Kasai, H., & Yumuro, A. (1977). MMG report III: The forces on the Rudder and their Interactions with Hull and Propeller. *The Bulletin of the Society of Naval Architects of Japan, 578*, 358-372.
Kijima, K., Nakiri, Y., Tsutsui, Y., & Matsunaga, M. (1990). Prediction method of ship manoeuvrability in deep and shallow waters. *Proceedings of MARSIM & ICSM 90*, (pp. 311-318). Tokyo, Japan.
Kim, C. H. (1969). Hydrodynamic forces and moments for heaving, swaying and rolling cylinders on water of finite depth. *Journal of Ship Research, 13*(7), 137-154.
Kim, Y. G., Lee, G. J., Nam, B. W., Seo, M. K., Kim, D. J., Yeo, D. J., & Yun, K. (2018). Simplified maneuvering simulation of a ship in waves. *Proceedings of the Asian Conference on Maritime System and Safety Research*, (pp. 29-36).
Koh, K. K., Yasukawa, H., & Hirata, N. (2008). Shallow water Effect on Turning Motion of a Pusher-Barge System. *The 4th Asia-Pacific Workshop on Marine Hydrodynamics.* Taipei.
Kose, K., & Kijima, K. (1997). MMG report IV: The Methods of the Captive Model Test and the Test Installations. *The Bulletin of The Society of Naval Architects of Japan, 579*, 404-413.

Kristiansen, E., & Egeland, O. (2003). Frequency-Dependent Added Mass in Models for Controller Design for Wave Motion Damping. *IFAC Conference on Maneuvering and Control of Marine Systems (MCMC '03).* Girona, Spain.

Lackenby, H. (1963). The Effect of Shallow Water on Ship Speed. *Shipbuilder, 70*(672).

Lamb, H. (1932). Chapter VI. In *Hydrodynamics.* Cambridge University Press.

Lee, C. H., & Sclavounos, P. D. (1989). Removing the irregular frequencies from integral equations in wave-body interactions. *Journal of Fluid Mechanics, 207*, 393-418.

Li, M., & Wu, X. (1990). Simulation calculation and comprehensive assessment on ship maneuverabilities in wind, wave, current and shallow water. *Proceedings of MARSIM and ICSM 90*, (pp. 403-411, 459-465). Tokyo, Japan.

Liu, S., & Papanikolaou, A. (2010). Time-domain hybrid method for simulating large amplitude motionsofships advancing in waves. *Proceedings of theITTC Workshop on Seakeeping.* Seoul, Korea.

Liu, S., Papanikolaou, A., & Zaraphonitis, G. (2011). Prediction ofaddedresistanceofshipsinwaves. *Ocean Engineering, 38*, 641–650.

Liu, S., Papanikolaou, A., & Zaraphonitis, G. (2015). Practical Approach to the Added Resistance of a Ship in Short Waves. *25th International Ocean and Polar Engineering Conference, ISOPE2015*, (pp. 11-18). Kona, Hawaii, USA.

Loukakis, T. A., & Sclavounos, P. D. (1978). Some extensions of the classical approach to strip theory of ship motions. *Journal of Ship Research, 22*, 1-19.

Maimun, A., Priyanto, A., Muhammad, A. H., Scully, C. C., & Awal, Z. I. (2011). Manoeuvring prediction of pusher barge in deep and shallow water. *Ocean Engineering, 38*, 1291-1299.

Maruo, H. (1957). The excess resistance of a ship in rough seas. *International Shipbuilding Progress, 4*(35).

Maruo, H. (1960). The drift of a body floating on waves. *Journa lof Ship Research, 4*(3), 1-10.

Maruo, H. (1963). Resistance in waves. *60thanniversarySeries.TheSocietyofNaval Architects ofJapan, 8*, 67-102.

Matusiak, J. (2003). On the effects of wave amplitude, damping and initial conditions on the parametric roll resonance. *8th International Conferfence on the Stability of Ships and Ocean Vehicles, STAB2003*, (pp. 341-347). Madrid, Spain.

Moctar , O., Shigunov, V., & Zorn, T. (2012). Duisburg Test Case: Post Panamax Container Ship for Benchmarking. *Ship Technology Research, 59*(3), 50-64.

Munif, A., & Umeda, N. (2000). Modeling Extreme Roll Motions and Capsizing of a Moderate-Speed Ship in Astern Waves. *Journal of The Society of Naval Architects of Japan, 187*.

Naito, S. (2008). Propulsive performance of ships in actual seas. *Proceedings of 7th Osaka Colloquium on Seakeeping and Stability.* Osaka, Japan.

Neves, M. A., & Rodriguez, C. A. (2006). On unstable ship motions resulting from strong non-linear coupling. *Ocean Engineering, 33*, 1853–1883.

Newman, J. N. (1966). Some hydrodynamic aspects of ship maneuverability. *6th Symposium on Naval Hydrodynamics*, (pp. 203-237). Washington D.C.

Newman, J. N. (1979). *Theoretical Methods in Ship Maneuvering.* Massachusetts: Massachusetts Institute of Technology.

Newman, J. N. (2017). *Marine Hydrodynamics, 40th Anniversary Edition.* Cambridge, MA: The MIT Press.

Newman, J. N., & Tuck, E. O. (1964). Current Progress in the Slender Body Theory for Ship Motions. *5th Symposium on Naval Hydrodynamics.* Bergen.

Nomoto, K. (1960). Analysis of Kempf's standard maneuver test and proposed steering quality indices. *First Symposium on Ship Maneuverability.* Washington.

Norrbin, N. H. (1970). Theory and observations on the use of a mathematical model for ship manoeuvring in deep and confined waters. *8th Symposium on Naval Hydrodynamics.*

Ogawa, A., Koyama, T., & Kijima, K. (1977). MMG report I: On the mathematical model of Ship Manoeuvring. *The Bulletin of The Society of Naval Architects of Japan, 575*, 22-28.

Ogilvie, T. (1964). Recent Progress Toward the Understanding and Prediction of Ship Motions. *5th Symposium on Naval Hydrodynamics.* Bergen, Norway.

Ogilvie, T. F. (1983). Second-Order Hydrodynamic Effects on Ocean Platforms. *International Workshop on Ship and Platform Motion*, (pp. 205-265). Berkeley.

Ogilvie, T. F., & Tuck, E. O. (1969). *A rational strip theory for ship motions - part 1.* Dept. NA&ME, University of Michigan.

Papanikolaou, A. (1985). On Integral-Equation Methods for the Evaluation of Motions and Loads of Arbitrary Bodies in Waves. *Journ. Ingenieur-Archiv, 55*, 17-29.

Papanikolaou, A. (2014). *Ship Design. Methodologies of Preliminary Design.* Springer.

Papanikolaou, A., & Schellin, T. E. (1992). A Three-Dimensional Panel Method for Motions and Loads of Ships with Forward Speed. *Ship Technology Research, 39*, 147-156.

Papanikolaou, A., & Zaraphonitis, G. (1987). On an Improved Method for the Evaluation of Second Order Motions and Loads on 3D Floating Bodies in Waves. *Schiffstechnik, 34*, 170-211.

Pinkster, J. A., & van Oortmerssen, G. (1977). Computation of the first and second order wave forces on oscillating bodies in regular waves. *2nd International Conference on Numerical Ship Hydrodynamics*, (pp. 136-159). Berkeley.

Plotkin, A. (1977). Heave and pitch motions in shallow water including the effect of forward speed. *Journal of Fluid Mechanics, 80*(3), 433-441.

Reed, A. M., & Zuzick, A. V. (2015). Direct Assessment Will Require Accreditation - What This Means. *Proceedings of the 12th International Conference on the Stability of Ships and Ocean Vehicles, STAB2015*, (pp. 51-78). Glasgow, U.K.

Remez, V. (1985). Dynamics of Curvilinear Motion of a Ship in Regular Seas. *5th National Congress on Theoretical and Applied Mechanics and 14th Scientific and Methodological Seminar on Ship Hydrodynamics*, (pp. 2-1-2-7). Varna, Bulgaria.

Rienecker, M. M., & Fenton, J. D. (1981). A Fourier approximation method for steady water waves. *Journal of Fluid Mechanics, 104*, 119-137.

Riesner, M., von Graefe, A., Shigunov, V., & Moctar, O. (2016). Prediction of non-linear ship responses in waves considering forward speed effects. *Ship Technology Research, 63*(3), 1-11.

Salvesen, N. (1974). Second-order steady state forces and moments on surface ships in oblique regular waves. *Proceedings of the international symposium on dynamics of marine vehicles and structures in waves*, (pp. 212-227). London, U.K.

Salvesen, N., Tuck, E. O., & Faltinsen, O. M. (1970). Ship motions and sea loads. *Tansactions of the Society of Naval Architects and Marine Engineers, 78*, 250-287.

Sano, M., & Yasukawa, H. (2008). Maneuvering Motions of KVLCC1 and KVLCC2 using MMG model. *SIMMAN, Part E*, (pp. 51-55).

Seo, M. G., & Kim, Y. (2011). Numerical analysis on ship maneuvering coupled with ship motion in waves. *Ocean Engineering, 38*, 1934-1945.

Shin, Y. S., Belenky, V. I., Paulling, J. R., Weems, K. M., & Lin, V. M. (2004). Criteria for Parametric Roll of Large Containerships in Longitudinal Seas. *Transactions of the Society of Naval Architects and Marine Engineers, 112*, 14-47.

Simonsen, C. D. (2004). *PMM model test with DDG51 including uncertainty assessment.* Lyngby, Denmark: FORCE Technology.

Simonsen, C. D., Otzen, J. F., Klint, C., Larsen , N. L., & Stern, F. (2012). Maneuvering predictions in the early design phase using CFD generated PMM data. *29th Symposium on Naval Hydrodynamics*, (pp. 26-31). Gothenburg, Sweden.

Simonsen, C. D., Stern, F., & Agdrup, K. (2006). CFD with PMM test validation for manoeuvring VLCC2 tanker in deep and shallow water. *MARSIM.* Terschelling, The Netherlands.

Singh, S. P., & Sen, D. (2007). A comparative linear and nonlinear ship motion study using 3-D time domain methods. *Ocean Engineering, 34*(13), 1863-1881.

Skejic, R., & Faltinsen, O. M. (2008). A unified seakeeping and maneuvering analysis of ship in regular waves. *Journal of Marine Science and Technology, 13*, 371-394.

Söding, H., von Graefe, A., Moctar, O., & Shigunov, V. (2012). Rankine source method for seakeeping predictions. *International Conference on Offshore Mechanics and Arctic Engineering.* Rio de Janeiro, Brazil.

Son, K. H., & Nomoto, K. (1982). On the Coupled Motion of Steering and Rolling of a High-speed Container Ship. *Journal of the Society of Naval Architects of Japan, 150*, 73-83.

Spanos, D., & Papanikolaou, A. (2006). Numerical Simulation of a Fishing vessel in Parametric Roll in Head Seas. *Proceedings of the 8th International Ship Stability Workshop.* Instabul, Turkey.

Spyrou, K. J. (2000). Designing against parametric instability in following seas. *Ocean Engineering, 27*(6), 625-653.

Spyrou, K. J. (2002). NM403 Ship Manoeuvrability, Lecture Notes. Glasgow, U.K.: University of Strathclyde.

Subramanian, R., & Beck, R. F. (2015). A time-domain strip theory approach to maneuvering in a seaway. *Ocean Engineering, 104*, 107-118.

Sutulo, S., & Soares, C. G. (2006a). Numerical Study of Ship Rolling in Turning Manoeuvres. *Proceedings of STAB 2006.*

Sutulo, S., & Soares, C. G. (2006b). A Unified Nonlinear Mathematical Model for Simulating Ship Manoeuvring and Seakeeping in Regular Waves. *International Conference on Marine Simulation and Ship Maneuverability MARSIM.* Terschelling, The Netherlands.

Takaki, M., & Tasai, F. (1973). On the Hydrodynamic Derivative Coefficientsof the Equations for Lateral Motion of Ships. *Transactions of the West-Japan Society of Naval Architects (In Japanese), 46*.

Taylan, M. (2000). The effect of nonlinear damping and restoring in ship rolling. *Ocean Engineering, 27,* 921–932.

Tello Ruiz, M., Candries, M., Vantorre, M., Delefortrie, G., Peters, D., & Mostaert, F. (2012). *Ship Manoeuvring in Waves: A literature review.* Antwerp, Belgium: Flanders Hydraulics Research & Ghent University.

Tello Ruiz, M., De Caluwé, S., Van Zwijnsvoorde, T., Delefortrie, G., & Vantorre, M. (2015). Wave effects in 6DOF on a ship in shallow water. *International Conference on Ship Manoeuvrability and Maritime Simulation, MARSIM2015.* Newcastle Upon Tyne, U.K.

Tesdogan, T., Incecik, A., & Turan, O. (2016). Full-scale unsteady RANS simulations of vertical ship motions in shallow water. *Ocean Engineering, 123*.

Thorne, B. C. (1953). Multipole Expansions in the Theory of Surface Waves. *Cambridge Philosophical Society, 49*, 707-716.

Tuck, E. O. (1970). Ship motions in shallow water. *Journal of Ship Research, 14*.

Turan, O., Ayaz, Z., Aksu, S., Kanar, J., & Bednarek, A. (2008). Parametric rolling behaviour of azimuthing propulsion-driven ships. *Ocean Engineering, 35*, 1339– 1356.

Ueno, M., Nimura, T., & Miyazaki, H. (2003). An experimental study on manoeuvring motion of a ship in waves. *Proceedings of the International Conference on Marine Simulation and Ship Maneuverability (MARSIM'03).*

Umeda, N. (2013). Current Status of Second Generation Intact Stability Criteria. Development and Some Recent Efforts. *Proceedings of the 13th International Ship Stability Workshop.* Brest.

Umeda, N., Hashimoto, H., Vassalos, D., Urano, S., & Okou, K. (2003). Nonlinear dynamics on parametric roll resonance with realistic numerical modelling. *8th International Conference on Stability of Ships and Ocean Vehicles, STAB2003*, (pp. 281-290). Madrid, Spain.

UNCTAD. (2019). *Review of Maritime Transport 2019.* UNITED NATIONS.

van Oortmerssen, G. (1976). *The Motions of a Moored Ship in Waves. PhD Thesis.* Wageningen, The Netherlands.

Van't Veer, A. P. (2009). *PRECAL v6.5 Theory Manual.*

Vantorre, M. (2001). Manoeuvring coefficients for a container carrier in shallow water: an evaluation of semi-empirical formulae. *Mini Symposium on Prediction of Ship Manoeuvring Performance*, (pp. 71-81). Tokyo, Japan.

Wehausen, J. V., & Laitone, C. V. (1960). *Surface Waves.* Berlin: Springer Verlag.

Yasukawa, H. (1998). Computation of effective rudder forces of a ship in shallow water. *Symposium of forces acting on a manoeuvring vessel*, (pp. 125-133). Val de Reuil.

Yasukawa, H., & Nakayama, Y. (2009). 6-DOF motion simulations of a turning ship in regular waves. *International Conference on Marine Simulation and Ship Maneuverability MARSIM*. Panama City, Panama.

Yasukawa, H., & Yoshimura, Y. (2015). Introduction of MMG standard model for ship maneuvering predictions. *Journal of Marine Science and Technology*, *20*(1), 37-52.

Yoon, R. W., & Rhee, K. P. (2003). Identification of hydrodynamic coefficients in ship maneuvering equations of motion. *Ocean Engineering, 30*(18), 2379-2404.

Zhang, W., Zou, Z., & De-Heng, D. (2017). A study on prediction of ship maneuvering in regular waves. *Ocean Engineering, 137*, 367-381.

APPENDIX A: BASIC MATHEMATICAL EQUATIONS

A1. 3-DOF AND 4-DOF MANOEUVRING MODELS

In the present section, the mathematical equations used at each module of the performed simulations are presented. Focus will be given on 3-DOF and 4-DOF manoeuvring equations and the external hydrodynamic and restoring forces in each case. Additionally, the regression formulae adopted in the present study in order to incorporate the shallow water effects regarding the manoeuvring derivatives and the hull-rudder-propeller interaction coefficients are provided as well.

According to Sano and Yasukawa (2008), the equations which describe the motion of a marine vessel on the horizontal plane with regards to a body-fixed coordinate system at the ship's midship section, are the following.

$$(M + A_{11\to 0})\dot{u} - (M + A_{22\to 0})vr - Mx_G r^2 = X \tag{A-1}$$

$$(M + A_{11\to 0})ur + (M + A_{22\to 0})v + M\dot{x_G}r = Y \tag{A-2}$$

$$(I_{zz} + A_{66\to 0})\dot{r} + Mx_G(\dot{v} + ur) = N \tag{A-3}$$

The external forces at the right hand side of the aforementioned equations consist of hydrodynamic forces exerted on the ship's hull and contributions from the propeller and the rudder. In the present simulations, third order, nonlinear polynomials were adopted concerning the calculation of the hull's hydrodynamic forces, as those proposed by Sano and Yasukawa (2008).

$$X_H = X_{\beta\beta}\beta^2 + X_{\beta r}\beta r + X_{rr}r^2 \tag{A-4}$$

$$Y_H = Y_\beta \beta + Y_r r + Y_{\beta\beta\beta}\beta^3 + Y_{\beta\beta r}\beta^2 r + Y_{\beta rr}\beta r^2 + Y_{rrr}r^3 \tag{A-5}$$

$$N_H = N_\beta \beta + N_r r + N_{\beta\beta\beta}\beta^3 + N_{\beta\beta r}\beta^2 r + N_{\beta rr}\beta r^2 + N_{rrr}r^3 \tag{A-6}$$

In case where the roll effect is incorporated in the system of equations, Son and Nomoto's (1982) proposed formulation was adopted. According to this, roll equation takes the following form.

$$(I_{xx} + A_{44\to 0})\ddot{\varphi} - A_{22\to 0} l_y \dot{v} - A_{11\to 0} l_x ur = K_H - C_{44}\varphi - B_{44}\dot{\varphi} \quad \text{(A-7)}$$

In Son and Nomoto's (1982) publication, the hydrodynamic force K_H is evaluated adopting the following expression. Sway-yaw-roll coupling is succeeded as well through the adoption of the nonlinear manoeuvring derivatives.

$$K_H = K_u u + K_r r + K_\varphi \varphi + K_{vvv} v^3 + K_{rrr} r^3 + K_{vvr} v^2 r + K_{vrr} v r^2 + \\ + K_{vv\varphi} v^2 \varphi + K_{v\varphi\varphi} v \varphi^2 + K_{rr\varphi} r^2 \varphi + K_{r\varphi\varphi} r \varphi^2 \quad \text{(A-8)}$$

In Equation (A-7), C_{44} stands for the linear roll restoring coefficient, which can be calculated using the following expression.

$$C_{44} = W \cdot GM\varphi \quad \text{(A-9)}$$

where, W, GM are the vessel's weight and metacentric height respectively. Concerning the roll damping coefficient B_{44}, an expression was found in Fukui et al., (2016) for its approximate calculation.

$$B_{44} = \frac{2a}{\pi}\sqrt{W \cdot GM(I_{xx} + A_{44\to 0})} \quad \text{(A-10)}$$

where, a is the linear term of the equation of the roll extinction curve.

The hydrodynamic derivatives shown in Equations (A-4)-(A-6) and (A-8), most of the times are given in a nondimensional form in order to be suitable in case of model scale or full scale simulations. Ship's calm water resistance is usually approximated by means of a second order polynomial, derived from regression analysis of theoretical or experimental methods. The expressions used in order to take the nondimensional values of forces and moments can be seen below.

$$X', Y' = \frac{X,Y}{0.5\rho L T U^2} \quad \text{(A-11)}$$

$$N' = \frac{N}{0.5\rho L^2 T U^2} \quad \text{(A-12)}$$

In Son and Nomoto's proposed model, nondimensional values of forces and moments is slightly different and can be seen below.

$$X', Y' = \frac{X,Y}{0.5\rho L^2 U^2} \tag{A-13}$$

$$K', N' = \frac{N}{0.5\rho L^3 U^2} \tag{A-14}$$

In general, when a ship's manoeuvrability is investigated by use of a time-domain numerical tool like the one developed in the context of the present research, limitations may arise related to the availability of the manoeuvring derivatives. In this case, various terms from those incorporated in the calculation of the hydrodynamic forces might be omitted and the accuracy of the simulations would probably get worse. For example, Yasukawa and Sano (2008) investigated the manoeuvrability of KCS including heel effect, taking only the actions of roll damping and restoring moments as external force contributions.

A2. SHALLOW WATER CORRECTIONS

In this section a detailed presentation of the expressions used to express the alteration of the added inertias, the manoeuvring derivatives, the calm water resistance and other interaction coefficients in shallow water is performed. The aforementioned expressions are functions of the under keel clearance and the vessel's principal particulars and are based on regression analysis.

The added inertias are corrected according to Li and Wu's (1990) formulae which are depicted below.

$$\frac{A_{11\to 0}}{A_{11\to 0\infty}} = 1 + \frac{3.77+1.14\frac{B}{T}-0.233\frac{L_{pp}}{T}-3.43C_b}{\left(\frac{h}{T}-1\right)^{1.30}} \tag{A-15}$$

$$\frac{A_{22\to 0}}{A_{22\to 0\infty}} = 1 + \frac{0.413+0.032\frac{B}{T}+0.0129(\frac{B}{T})^2}{\left(\frac{h}{T}-1\right)^{0.82}} \tag{A-16}$$

$$\frac{A_{66\to 0}}{A_{66\to 0\infty}} = 1 + \frac{0.413+0.0192\frac{B}{T}+0.00554(\frac{B}{T})^2}{\left(\frac{h}{T}-1\right)^{0.82}} \tag{A-17}$$

Subscript "∞" denotes that the value refers to infinite water depth. Linear and nonlinear manoeuvring derivatives have been corrected according to the formulae proposed by Ankudinov et al., (1990). The aforementioned formulae are suitable for a wider range of sea depths. The linear terms referring to sway and yaw forces are the following.

$$\frac{Y'_{\dot{v}}}{Y'_{\dot{v}\infty}} = gv \qquad \frac{Y'_{\dot{r}}}{Y'_{\dot{r}\infty}} = gv \qquad \frac{N'_{\dot{v}}}{N'_{\dot{v}\infty}} = gv$$

$$\frac{N'_{\dot{r}}}{N'_{\dot{r}\infty}} = gnr \qquad \frac{Y'_{v}}{Y'_{v\infty}} = fyv \qquad \frac{Y'_{r}}{Y'_{r\infty}} = fyr$$

$$\frac{N'_{v}}{N'_{v\infty}} = fnv \qquad \frac{N'_{r}}{N'_{r\infty}} = fnr \tag{A-18}$$

The nonlinear and coupled terms referring to sway and yaw forces are depicted below.

$$\frac{Y'_{v|v|}}{Y'_{v|v|\infty}} = \frac{9}{4}fnv - \frac{5}{4} \qquad \frac{Y'_{r|r|}}{Y'_{r|r|\infty}} = fnr \qquad \frac{Y'_{vrr}}{Y'_{vrr\infty}} = fyv$$

$$\frac{Y'_{r|v|}}{Y'_{r|v|\infty}} = fyv \qquad \frac{N'_{vrr}}{N'_{vrr\infty}} = gnr \qquad \frac{N'_{v|v|}}{N'_{v|v|\infty}} = \frac{9}{4}fnv - \frac{5}{4}$$

$$\frac{N'_{r|r|}}{N'_{r|r|\infty}} = gv \qquad \frac{N'_{r|v|}}{N'_{r|v|\infty}} = gnr \tag{A-19}$$

The terms appearing at the right hand side of (A-18) and (A-19) can be calculated implementing the following formulae.

$$fyv = \frac{3}{2}fnv - \frac{1}{2} \qquad fnv = K_0 + K_1\frac{B_1}{T} + K_2\left(\frac{B_1}{T}\right)^2$$

$$fyr = K_0 + \frac{2}{5}K_1\frac{B_1}{T} + \frac{24}{105}K_2\left(\frac{B_1}{T}\right)^2 \qquad fnr = K_0 + \frac{1}{2}K_1\frac{B_1}{T} + \frac{1}{3}K_2\left(\frac{B_1}{T}\right)^2$$

$$gv = K_0 + \frac{2}{3}K_1\frac{B_1}{T} + \frac{8}{15}K_2\left(\frac{B_1}{T}\right)^2 \qquad gnr = K_0 + \frac{8}{15}K_1\frac{B_1}{T} + \frac{40}{105}K_2\left(\frac{B_1}{T}\right)^2 \tag{A-20}$$

The calculation of K_0, K_1, K_2, and B_1 can be performed according to the expressions shown below, which are functions of the under keel clearance.

$$K_0 = 1 + \frac{0.0775}{\left(\frac{h}{T}-1\right)^2} - \frac{0.0110}{\left(\frac{h}{T}-1\right)^3} + \frac{0.000068}{\left(\frac{h}{T}-1\right)^5} \qquad K_1 = -\frac{0.0643}{\frac{h}{T}-1} + \frac{0.0742}{\left(\frac{h}{T}-1\right)^2} - \frac{0.0113}{\left(\frac{h}{T}-1\right)^3} + \frac{0.0000767}{\left(\frac{h}{T}-1\right)^5}$$

$$K_2 = \begin{cases} \frac{0,0342}{\frac{h}{T}-1}, \text{when } \frac{B}{T} > 4 \\ \frac{0,137}{\frac{h}{T}-1}\frac{T}{B}, \text{in any other case} \end{cases} \qquad B_1 = C_B B\left(1 + \frac{B}{L}\right)^2$$

(A-21)

Apart from the corrections of the manoeuvring coefficients, the calm water resistance changes in shallow water due to the different flow pattern around a vessel's hull. In this aspect, In this context, the expression proposed by Furukawa et al., (2016) was adopted in the present study. As it can be seen below, the nondimensional coefficient X'_0 is a function of the inverse value of the under keel clearance.

$$\frac{X'_0}{X'_{0\infty}} = 0.38 + \left(\frac{T}{h}\right)^2 + 1 \tag{A-22}$$

In the aforementioned study, other corrections related to various longitudinal derivatives are proposed, which were not considered in the present study.

Finally, thrust deduction coefficient t_p, wake fraction coefficient at straight course w_{p0}, propeller's race amplification coefficient κ and flow straightening coefficient γ_R have been calculated in shallow water using Amin and Hasegawa's (2010) regression formulae, which are depicted below.

$$\frac{(1-t_p)}{(1-t_p)_\infty} = 1 + \left(29.495 - 14.089\frac{C_B L_{pp}}{B} + 1.6486\left(\frac{C_B L_{pp}}{B}\right)^2\right) \cdot \cdot \left(0.004 - 0.035\frac{T}{h} - 0.104\left(\frac{T}{h}\right)^2\right) \tag{A-23}$$

$$\frac{\kappa}{\kappa_\infty} = 1 + \left(1220.41 - 396.037\frac{L_{pp}}{B} + 31.676\left(\frac{L_{pp}}{B}\right)^2\right)\left(\frac{T}{h}\right)^{3.56}, \text{ if } \frac{T}{h} \le -0.204\frac{L_{pp}}{B} + 1.930$$

else,

$$\frac{\kappa}{\kappa_\infty} = 1 + \left(212.225 - 30.003C_B\frac{L_{pp}}{T} + 1.017\left(C_B\frac{L_{pp}}{T}\right)^2\right)\left(-0.139 + 1.002\frac{T}{h} - 0.757\left(\frac{T}{h}\right)^2\right)$$

(A-24)

$$\frac{\gamma_R}{\gamma_{R_\infty}} = 1 + \left(-135.247 - 2432.95 C_B \frac{B}{L_{pp}} - 10137.7 \left(C_B \frac{B}{L_{pp}}\right)^2\right)\left(\frac{T}{h}\right)^{4.81}, \text{ if } \frac{T}{h} \leq -0.33\frac{T}{B} + 0.58$$

else,

$$\frac{\gamma_R}{\gamma_{R_\infty}} = 1 + \left(-10.258 + 178.287 C_B \frac{B}{L_{pp}} - 686.249 \left(C_B \frac{B}{L_{pp}}\right)^2\right) \cdot \cdot \left(-3.854 + 13.665\frac{T}{h} - 10.468\left(\frac{T}{h}\right)^2\right) \quad \text{(A-25)}$$

The Equations (A-15)-(A-25) have been implemented in the context of the present research order to express the changes on hydrodynamic, propeller and rudder forces due to the modified flow characteristics in shallow water.

APPENDIX B: SHIP DATA

B1. KVLCC2 Tanker

In this section, the main data of KVLCC2 derived by implementing frequency-domain analysis are demonstrated. These comprise of her 3D geometry in quadrilateral panels (3090 representing her half body) up to the draft of 20.8 meters, her principal particulars and data referring to her frequency dependent added mass and damping coefficients. The values of her infinite added masses and infinite damping coefficients are shown as well.

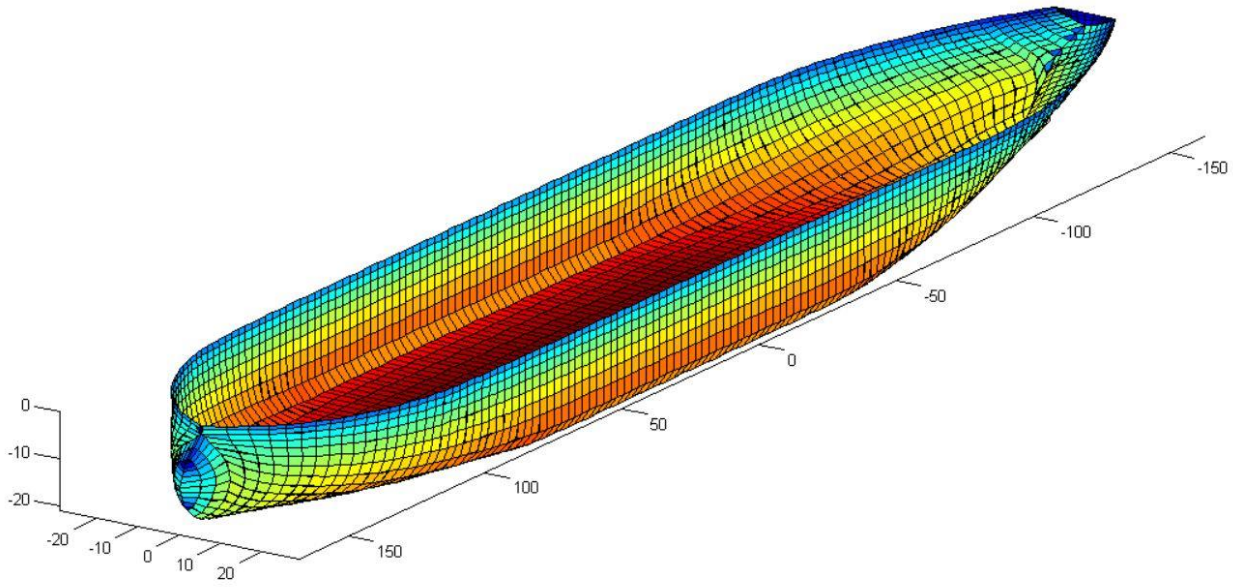

Figure B.1: 3D panel geometry of KVLCC2

The principal particulars of KVLCC2 at full scale are depicted in the following table.

Table B.1: Principal particulars of KVLCC2

Ship	KVLCC2
L_{pp} (m)	320.0
B (m)	58.0
T (m)	20.8
Δ (tons)	318826.23
C_B	0.8098

The frequency dependent added mass and damping curves at Fn=0 and Fn=0142 for heave, pitch and cross-coupling terms are shown in Figures B.2, B.3, B.4 and B.5, whilst their infinite values are given in Tables B.2 and B.3.

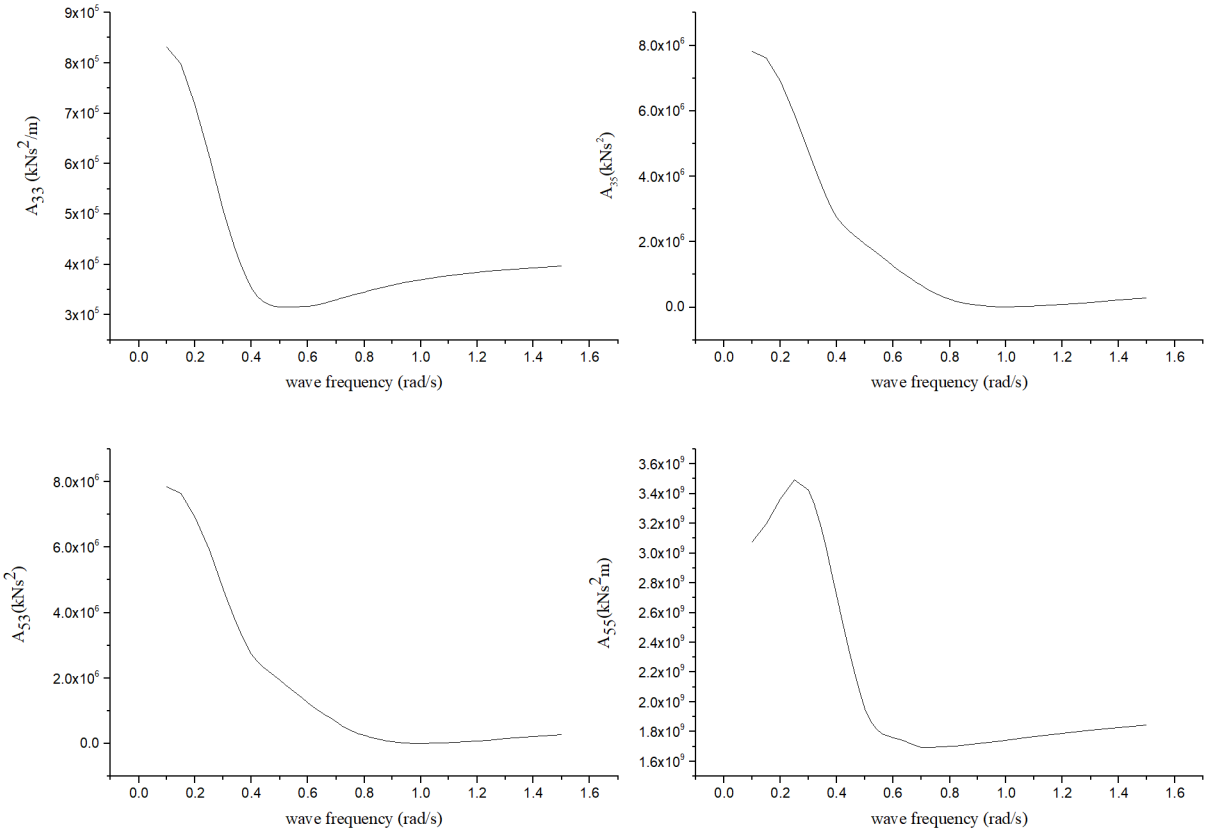

Figure B.2: Frequency dependent added masses at Fn=0.0 (head seas)

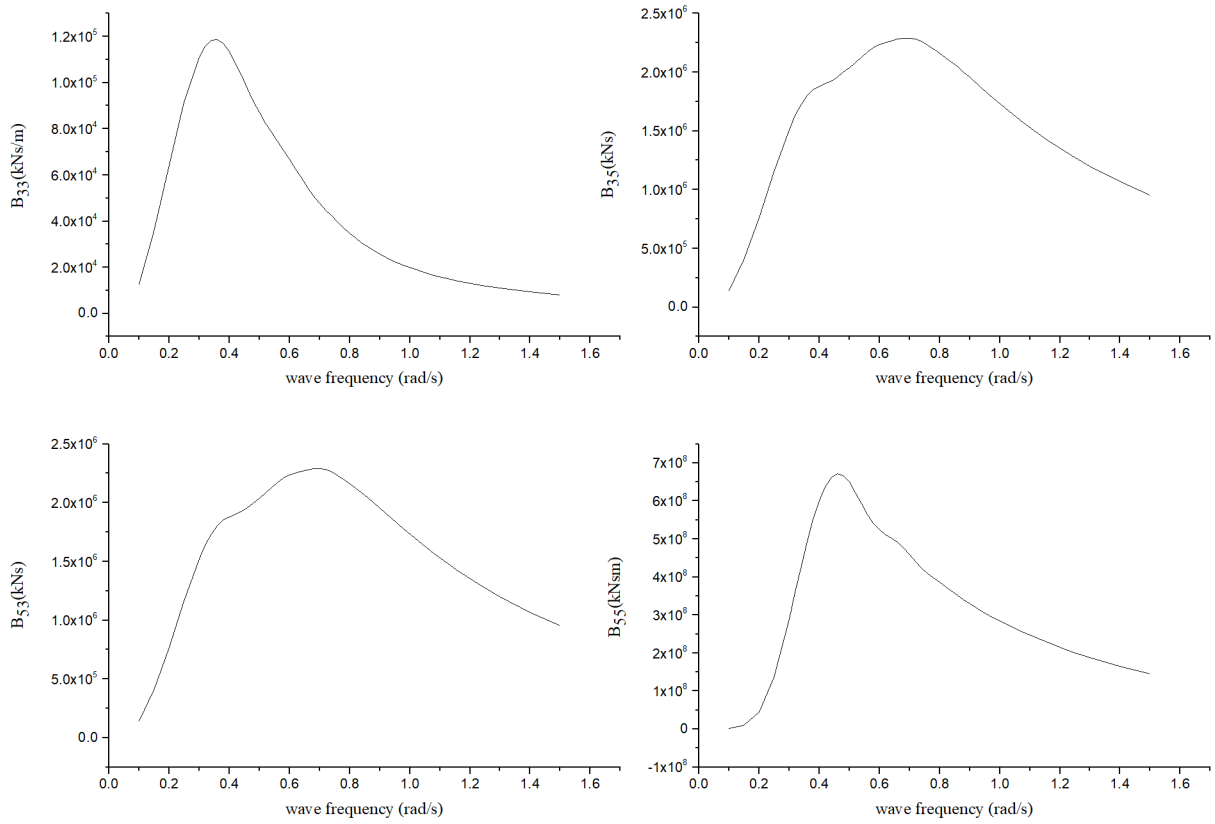

Figure B.3: Frequency dependent damping coefficients at Fn=0.0 (head seas)

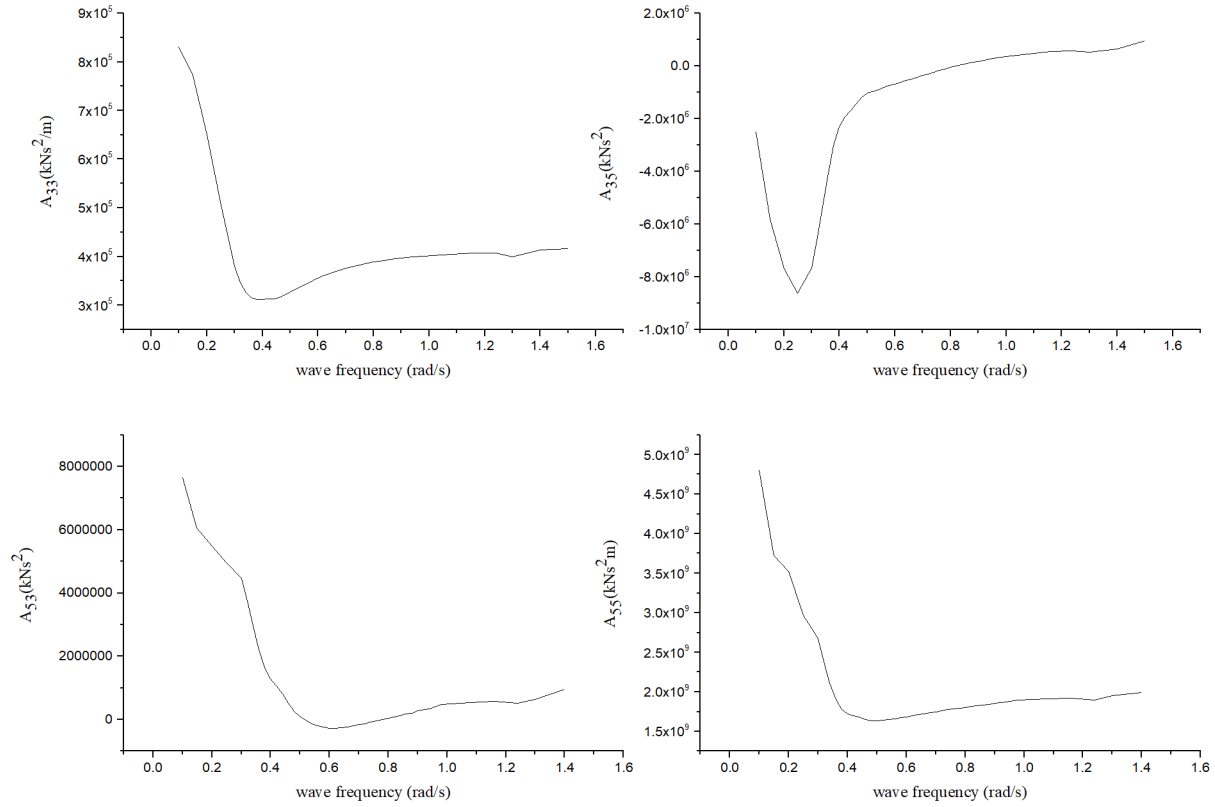

Figure B.4: Frequency dependent added masses at Fn=0.142 (head seas)

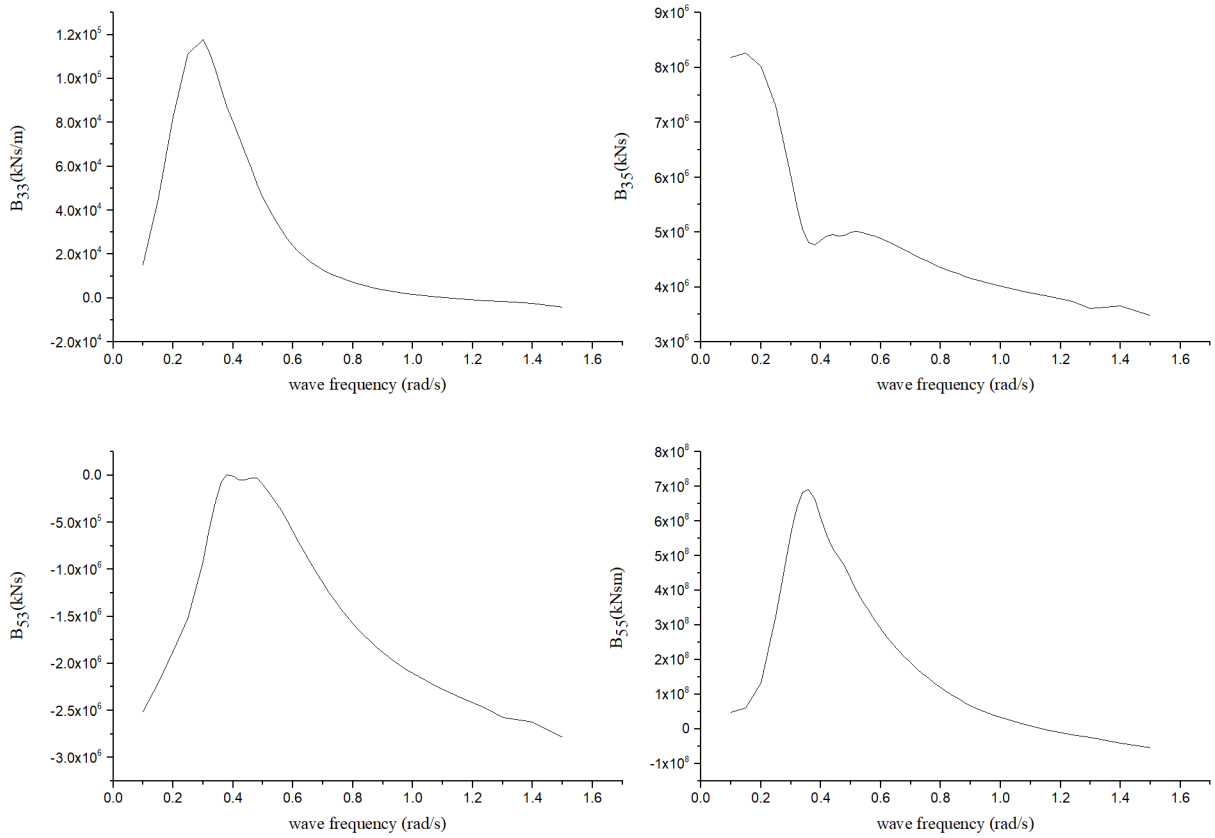

Figure B.5: Frequency dependent damping coefficients at Fn=0.142 (head seas)

Table B.2: Infinite values of added masses of KVLCC2

	A_{33} (kNs^2/m)	A_{35} (kNs^2)	A_{53} (kNs^2)	A_{55} (kNs^2m)
Fn=0	4.193E+05	1.076E+06	1.077E+06	2.013E+09

Infinite added masses are independent of the forward speed value thus, the aforementioned values were used in case of Fn=0.142 as well.

Table B.3: Infinite values of damping coefficients of KVLCC2

	B_{33} (kNs/m)	B_{35} (kNs)	B_{53} (kNs)	B_{55} (kNsm)
Fn=0	0	0	0	0
Fn=0.142	-3.35E+03	3.55E+06	-2.78E+06	-5.81E+07

Since KVLCC2 was used for manoeuvring simulations as well, the presentation of her manoeuvring derivatives, rudder's and propeller's characteristics together with the considered operational parameters is thought as necessary and they are depicted in Tables B.4 and B.5. These data were obtained from Sano and Yasukawa's (2008) publication.

Table B.4: Nondimensional hydrodynamic derivatives and coefficients of KVLCC2

$M' + A'_{11\to0}$	0.3155
$M' + A'_{22\to0}$	0.5161
$I'_{zz} + A'_{66\to0}$	0.0238
X'_0	-0.0217
$X'_{\beta\beta}$	0.0215
$X'_{\beta r} - M' - A'_{22\to0}$	-0.5145
X'_{rr}	0.0198
Y'_{β}	0.3061
$Y'_{r} - M' - A'_{11\to0}$	-0.2357
$Y'_{\beta\beta\beta}$	1.5112
$Y'_{\beta\beta r}$	0.3615
$Y'_{\beta rr}$	0.3979
Y'_{rrr}	0.0094
N'_{β}	0.1382
N'_{r}	-0.0584
$N'_{\beta\beta\beta}$	-0.0043
$N'_{\beta\beta r}$	-0.2925
$N'_{\beta rr}$	-0.056
N'_{rrr}	-0.0129

Table B.5: Rudder, propeller and operational parameters of KVLCC2 at Fn-0.142

$1 - w_{P0}$		0.549
κ		0.6
ε		0.796
$1 - t_P$		0.79
$1 - t_R$		0.837
$\alpha_H = a_1 J^2 + a_2 J + a_3$		
	a_1	-0.502
	a_2	1.022
	a_3	0.183
x'_H		-0.343
γ_R		
	$\beta - l'_R r' > 0$	0.506
	$\beta - l'_R r' < 0$	0.38
l'_R		-0.759

k_T	$-0.139J^2 - 0.275J + 0.293$
RPM	102.3

B2. C11-class Container Ship

This container ship was used in order to verify that ELIGMOS is capable of capturing parametric roll thus, details concerning her seakeeping characteristics, which were derived by use of frequency-domain analysis, are presented herein. The 3D geometry of this ship consists of 2993 quadrilateral panels, which model her half body up to the draft of 14 meters, and is depicted below.

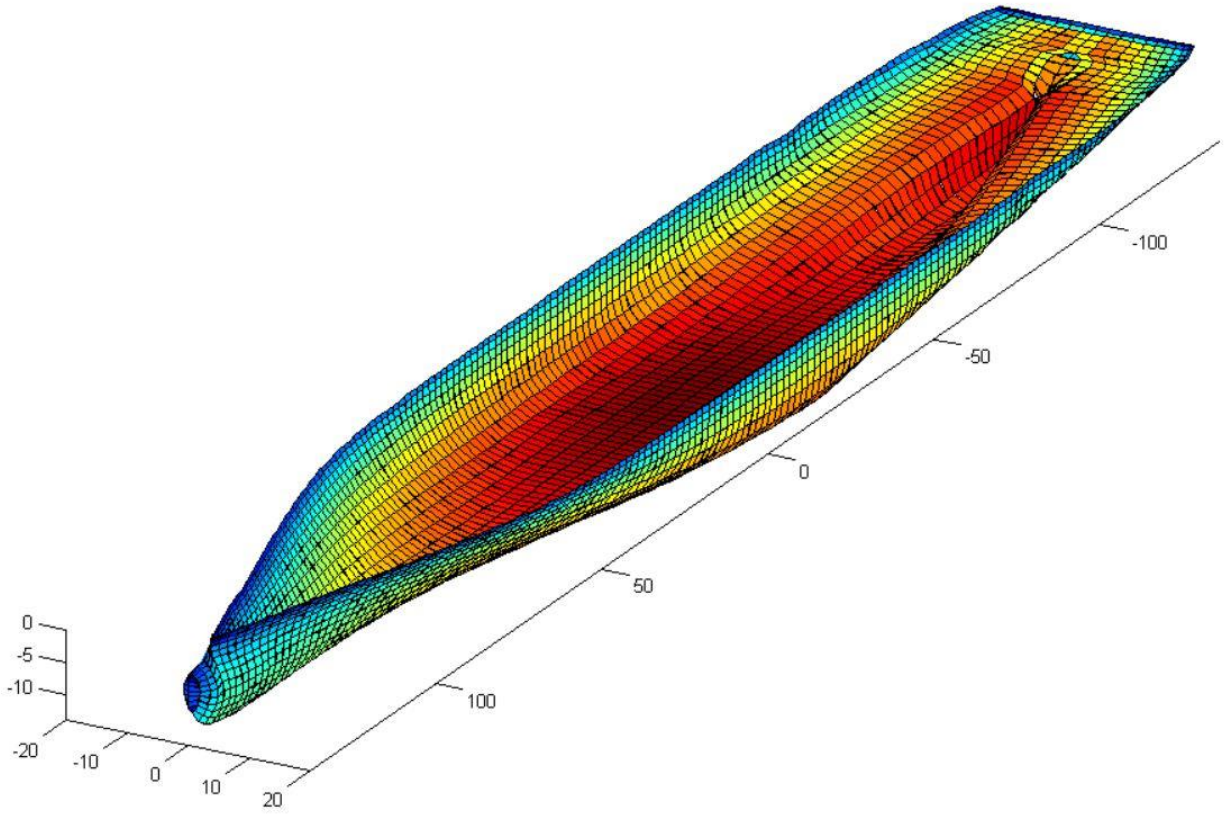

Figure B.6: 3D panel geometry of C11

The principal particulars of the C11-class container ship are summarized in Table B.6.

Table B.6: Principal particulars of C11-class container ship

Ship	C11
L_{pp} (m)	262.0
B (m)	40.0
T (m)	14.0
Δ (tons)	90102.625
C_B	0.60

The vertical position of her center of gravity was properly adjusted (KG=18.306 above the vessel's keel) so that the resulting metacentric height corresponds to the value of GM=1.999 meters.

The curves of the frequency-dependent added masses and damping coefficients for heave, pitch and cross-coupling terms for Fn=0 and Fn=0.1624 in head seas, are illustrated in Figures B.7, B.8, B.9 and B.10.

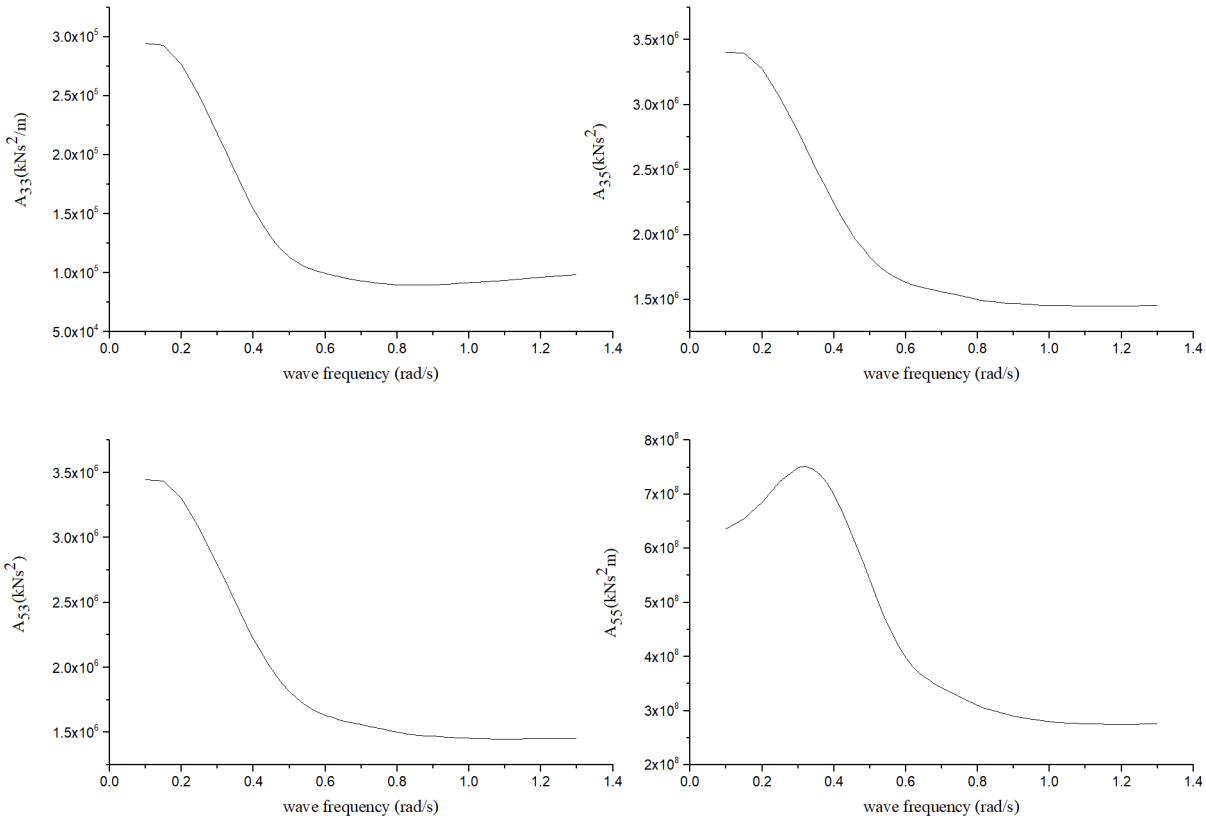

Figure B.7: Frequency dependent added masses at Fn=0.0 (head seas)

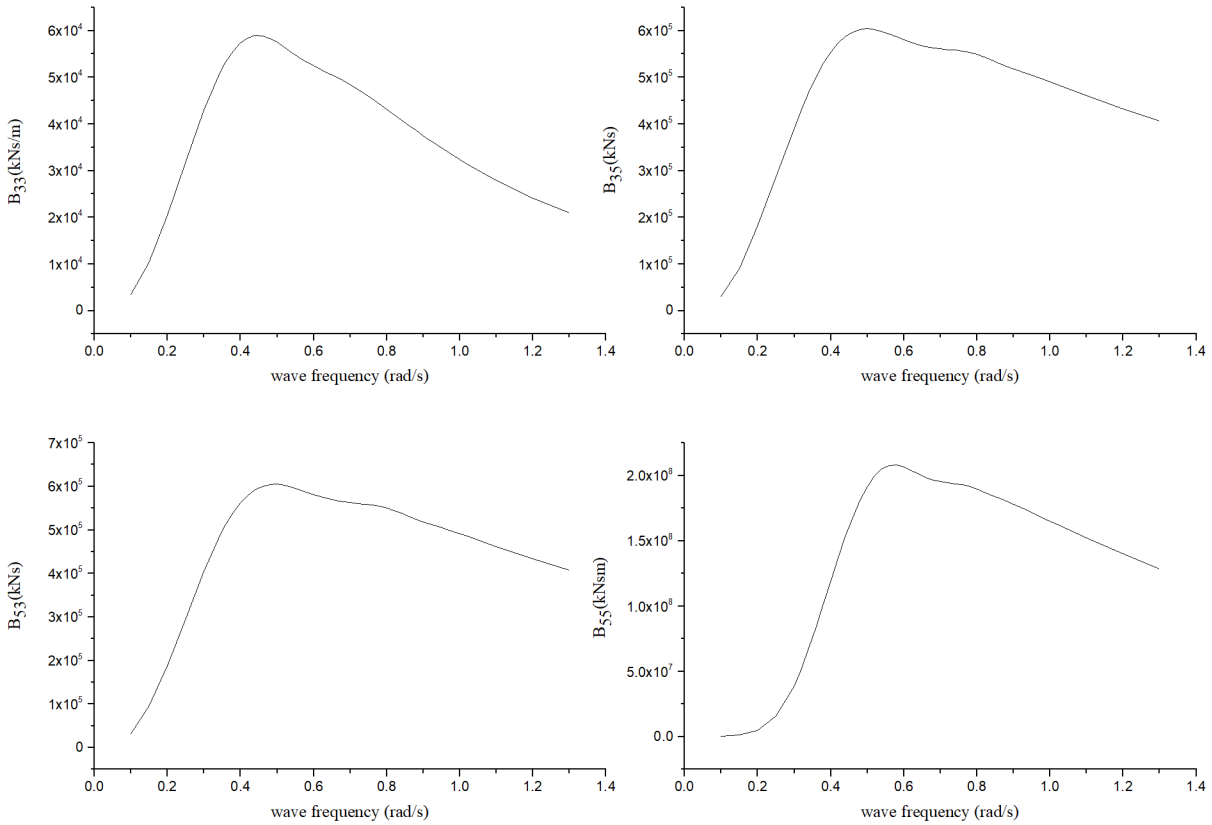

Figure B.8: Frequency dependent damping coefficients at Fn=0.0 (head seas)

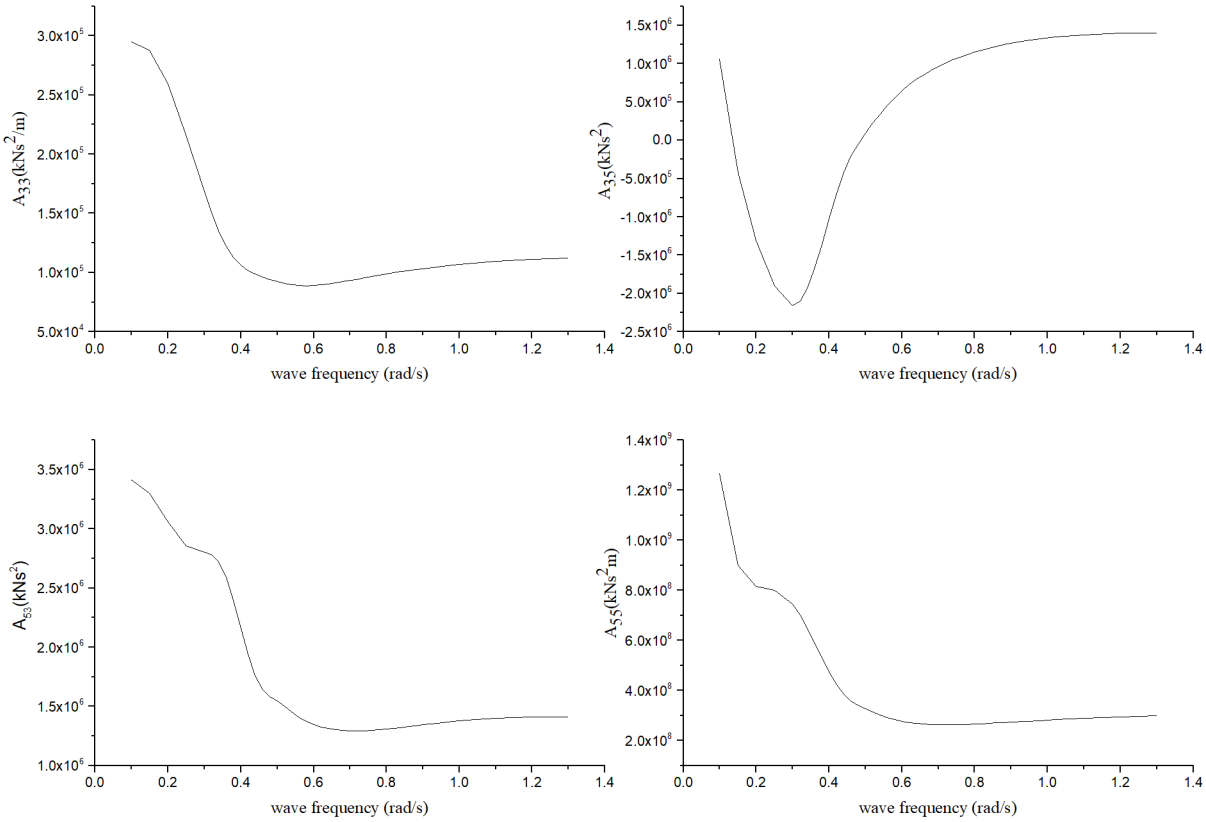

Figure B.9: Frequency dependent added masses at Fn=0.1624 (head seas)

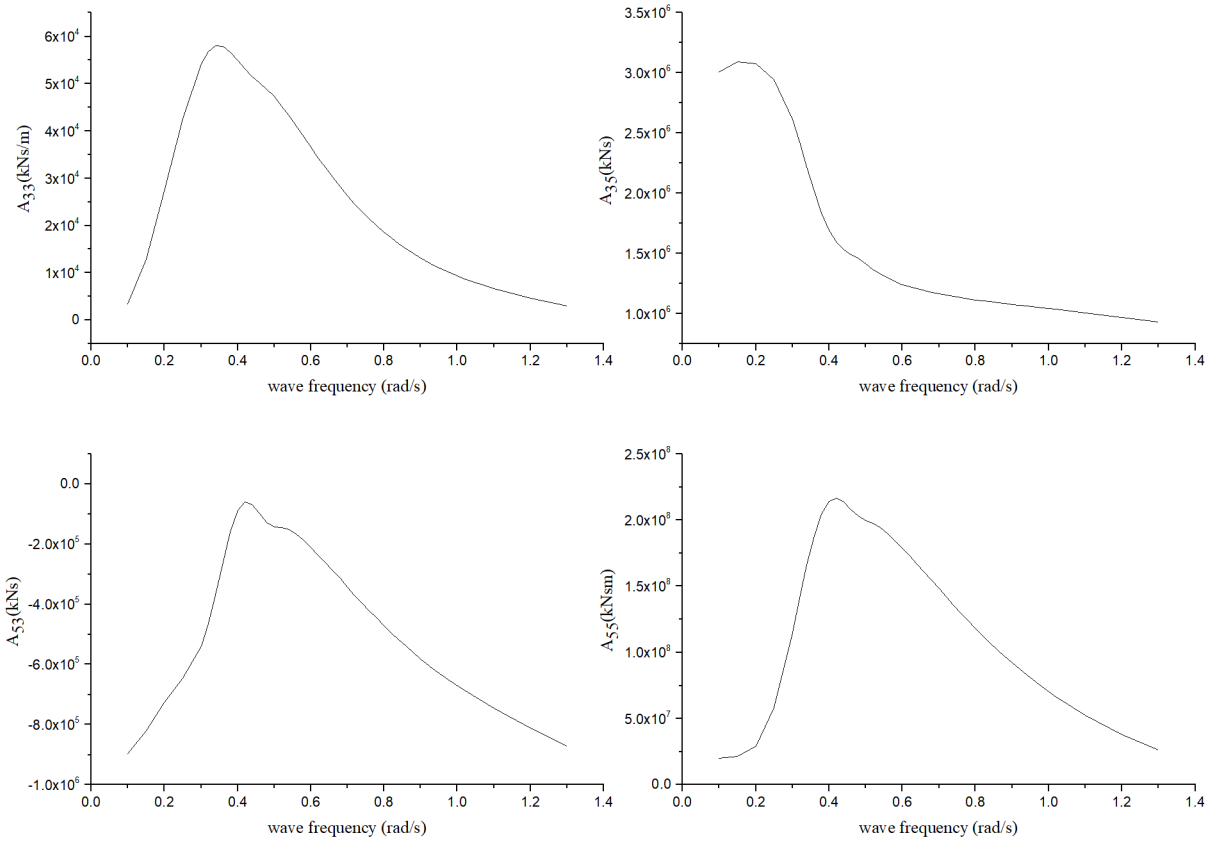

Figure B.10: Frequency dependent damping coefficients at Fn=0.1624 (head seas)

Additionally, the infinite values of the added masses and damping coefficients are illustrated in Tables B.7 and B.8.

Table B.7: Infinite values of added masses of C11

	A_{33} (kNs^2/m)	A_{35} (kNs^2)	A_{53} (kNs^2)	A_{55} (kNs^2m)
Fn=0	1.33E+05	2.01E+06	2.01E+06	4.3E+08

Table B.8: Infinite values of damping coefficients of C11

	B_{33} (kNs/m)	B_{35} (kNs)	B_{53} (kNs)	B_{55} (kNsm)
Fn=0	0	0	0	0
Fn=0.1624	-2.62E+03	9.27E+05	-1.16E+06	-1.83E+07

As it was stated above for KVLCC2, the infinite values of the added masses are the same for any forward speed in case of C11 as well.

B3. S-175 Container Ship

S-175 container ship was used as a reference ship for calm water manoeuvring simulations, as well as, in the context of the present research, it was the only ship whose manoeuvrability was tested in adverse weather conditions in both deep and shallow waters. For this purpose, data were exploited related with both her seakeeping performance and her manoeuvring one. Concerning the former, the second-order wave forces, obtained with NEWDRIFT v.7 numerical code, will be presented in Appendix C. An image of the 3D panel geometry of S-175 at T=9.5m and her principal particulars can be seen below.

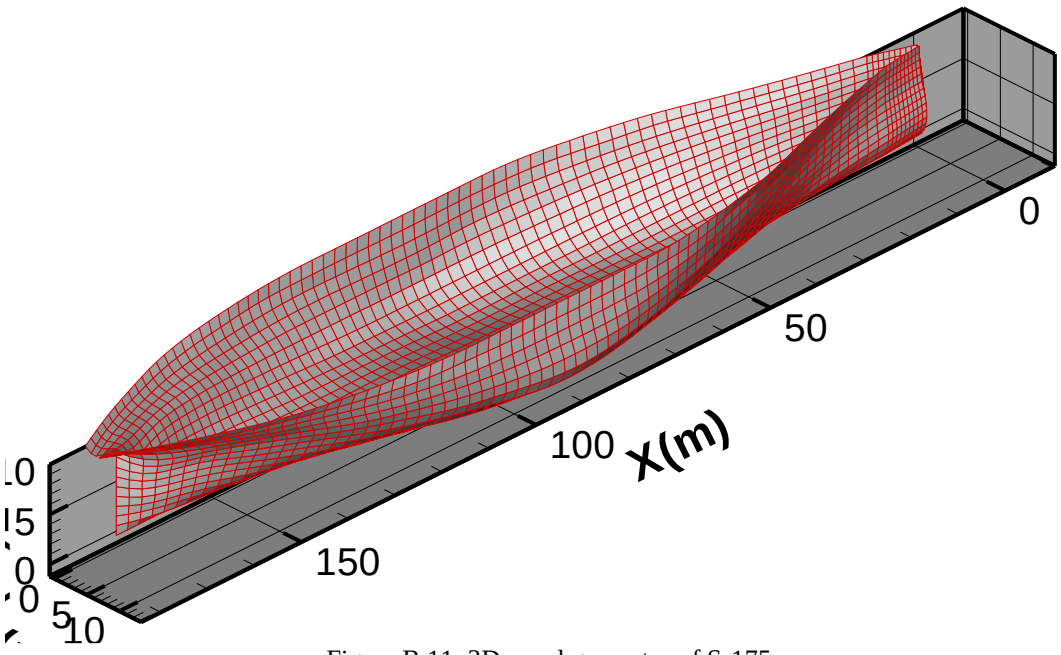

Figure B.11: 3D panel geometry of S-175

Table B.9: Principal particulars of S-175 container ship at full and model scales

Ship	S-175	
Scale	1:1	1:50
L_{pp} (m)	175.0	3.5
B (m)	25.4	0.508
T (m)	9.5	0.19
Δ (tons)	24739.0	0.19357
C_B	0.572	0.572

The manoeuvring-related data of S-175 derived from CMT are summarized in Tables B.10 and B.11. These, concern the calculation of the hydrodynamic forces exerted on the vessel's hull and the forces created from propeller's and rudder's actions.

Table B.10: Nondimensional hydrodynamic derivatives and coefficients of S-175

$A'_{11\to0}$	0.004384
$A'_{22\to0}$	0.12985
$A'_{66\to0}$	0.007718
X'_{0}	0.015632
$X'_{\beta\beta}$	-0.07111
$X'_{\beta r} - A'_{22\to0}$	-0.07256
X'_{rr}	0.003684
Y'_{β}	0.21368
$Y'_{r} - A'_{11\to0}$	-0.10
$Y'_{\beta\beta\beta}$	2.0079
$Y'_{\beta\beta r}$	0.39421
$Y'_{\beta rr}$	0.74605
Y'_{rrr}	0.032605
N'_{β}	0.0710
N'_{r}	-0.0409
$N'_{\beta\beta\beta}$	-0.02748
$N'_{\beta\beta r}$	-0.78105
$N'_{\beta rr}$	-0.02874
N'_{rrr}	-0.04218

Table B.11: Rudder, propeller and operational parameters of S-175 at Fn-0.15

$1 - w_{P0}$	0.8316
κ	0.631
ε	0.921
$1 - t_P$	0.825
$1 - t_R$	0.710
α_H	0.237
x'_H	-0.48
γ_R	
$\beta - l'_R r' > 0$	0.193
$\beta - l'_R r' < 0$	0.088
k_T	$-0.0481J^2 - 0.1971J + 0.2932$
RPM (model scale)	603

APPENDIX C: SECOND-ORDER WAVE FORCES

In the present Appendix, will be depicted figures of the nondimensional second-order forces for the S-175 container ship as obtained from NEWDRIFT v.7 software in deep and shallow water conditions. The dimensional values of second-order forces can be taken by using the quantities $\frac{\rho g \zeta_\alpha^2 B^2}{L}$ (forces) and $\rho g \zeta_\alpha^2 BL$ (moment).

C1. DEEP WATER

The second-order wave forces can be seen below. In each case, the figures refer to Froude numbers 0, 0.05, 0.10 and 0.15. The figures for λ/L=0.5 are omitted since they have been depicted earlier in the text (Figure 4.5).

- λ/L=0.7

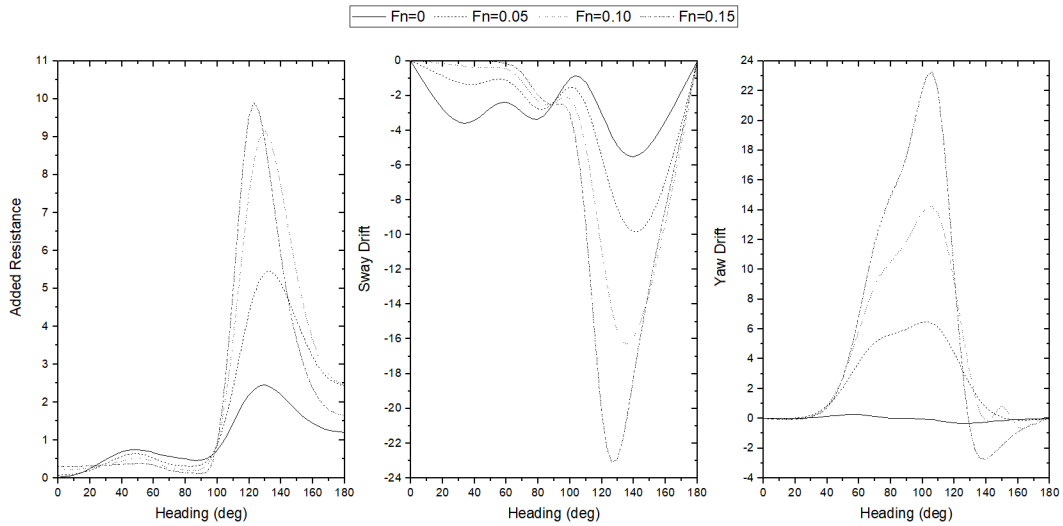

Figure C.1: Nondimensional values of second-order forces at Fn=0, 0.05, 0.10 and 0.15 (λ/L=0.7)

- λ/L=1.0

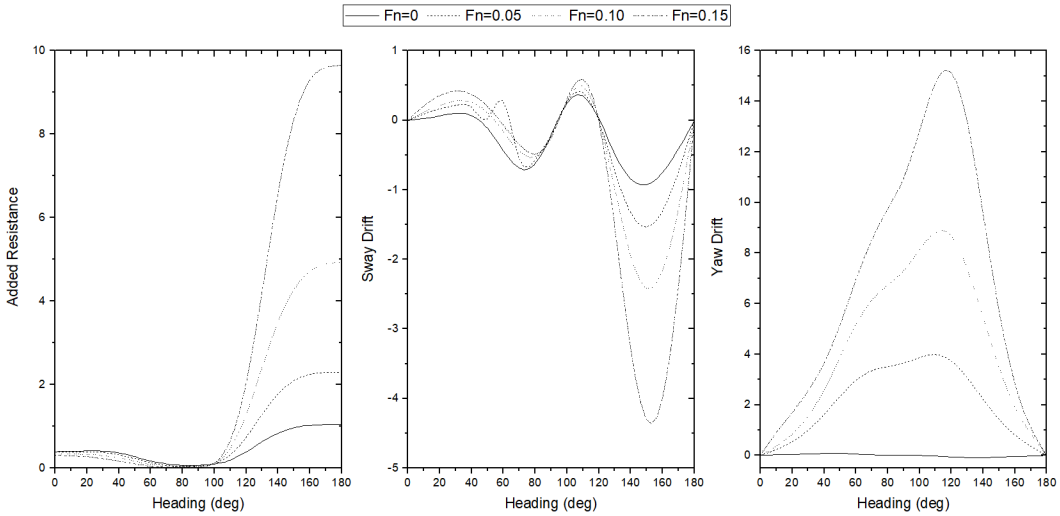

Figure C.2: Nondimensional values of second-order forces at Fn=0, 0.05, 0.10 and 0.15 (λ/L=1.0)

C2. SHALLOW WATER

In case of shallow water simulations, results of second-order wave forces refer to long wave seas (λ/L=1.0, 1.2) and four values of under keel clearance (UKC=3.0, 2.5, 2.0, 1.5).

- λ/L=1.0

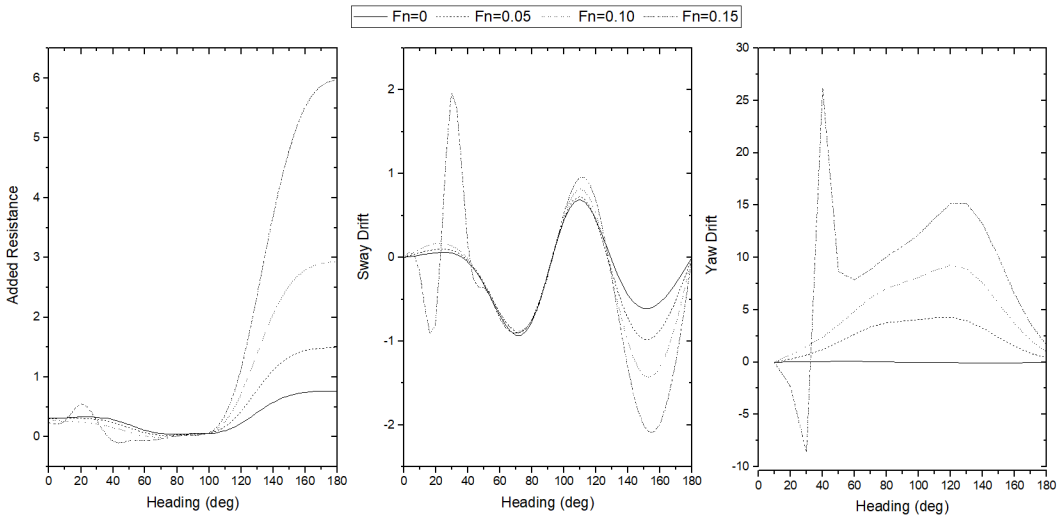

Figure C.3: Nondimensional values of second-order forces at Fn=0, 0.05, 0.10 and 0.15 (λ/L=1.0, UKC=3.0)

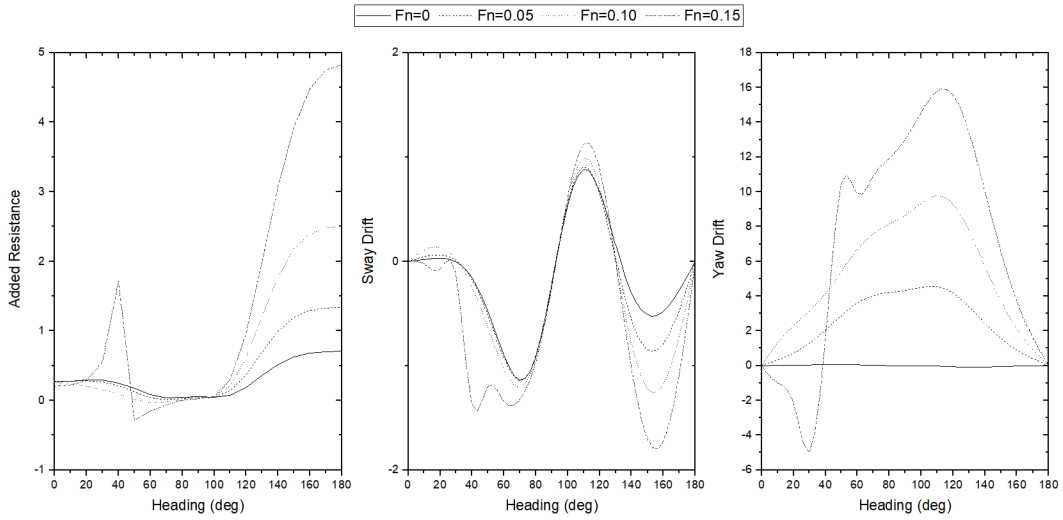

Figure C.4: Nondimensional values of second-order forces at Fn=0, 0.05, 0.10 and 0.15 (λ/L=1.0, UKC=2.5)

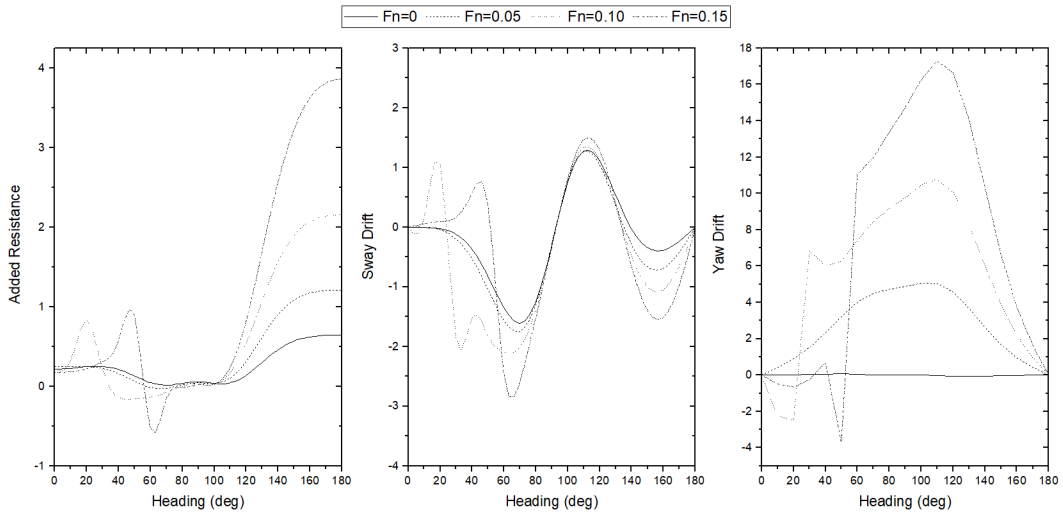

Figure C.5: Nondimensional values of second-order forces at Fn=0, 0.05, 0.10 and 0.15 (λ/L=1.0, UKC=2.0)

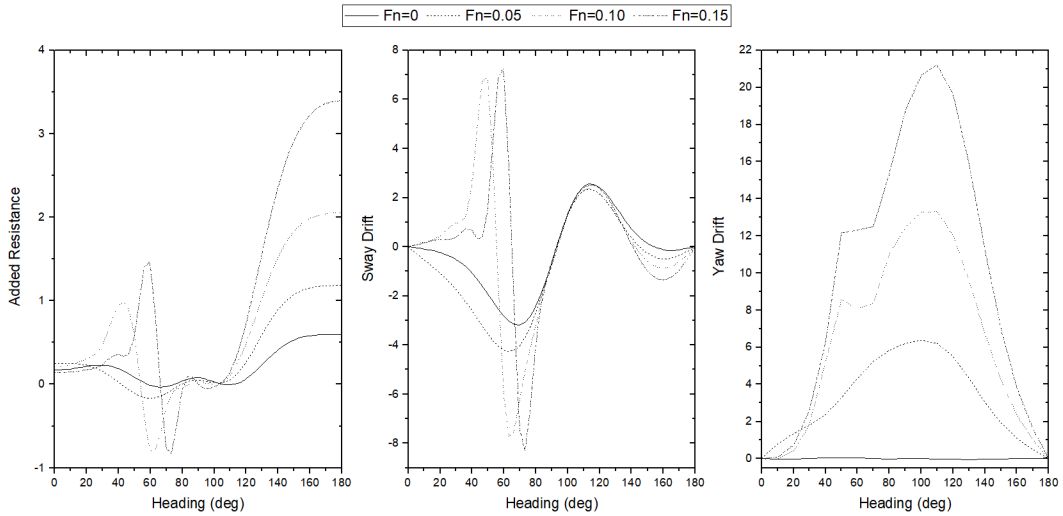

Figure C.6: Nondimensional values of second-order forces at Fn=0, 0.05, 0.10 and 0.15 (λ/L=1.0, UKC=1.5)

- λ/L=1.2

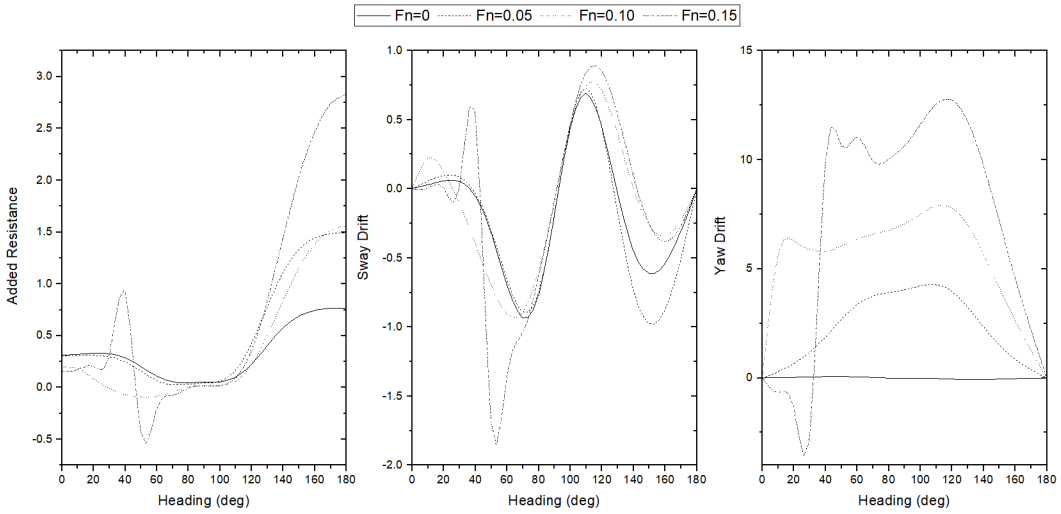

Figure C.7: Nondimensional values of second-order forces at Fn=0, 0.05, 0.10 and 0.15 (λ/L=1.2, UKC=3.0)

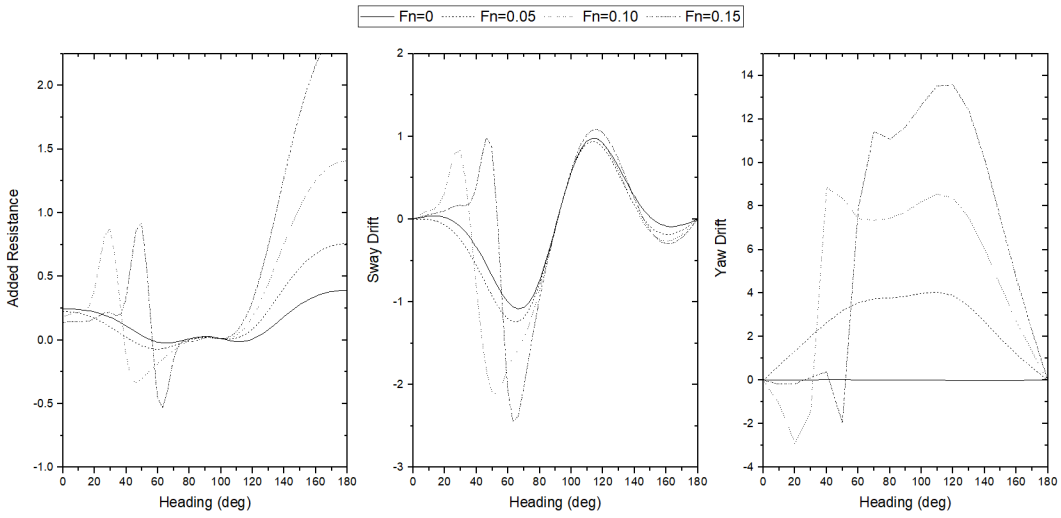

Figure C.8: Nondimensional values of second-order forces at Fn=0, 0.05, 0.10 and 0.15 (λ/L=1.2, UKC=2.5)

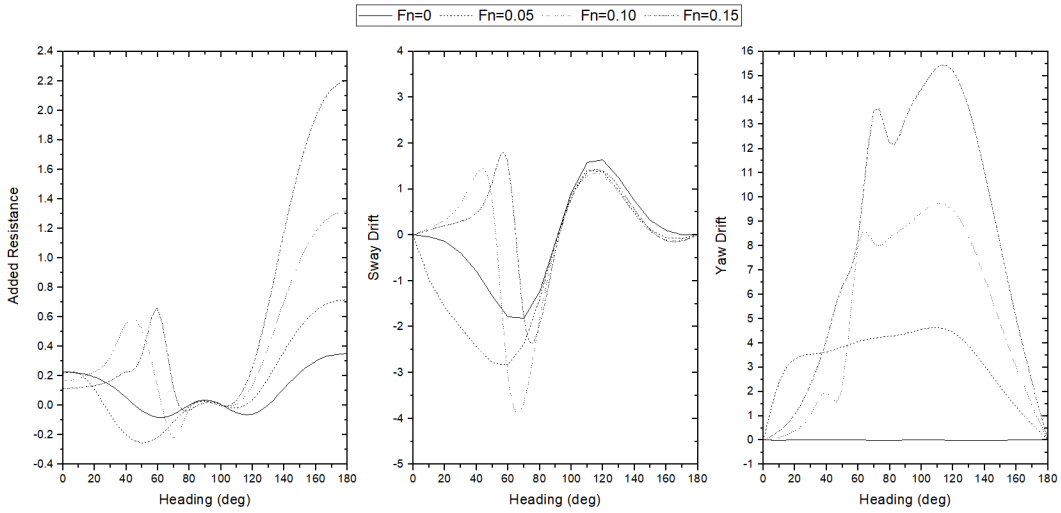

Figure C.9: Nondimensional values of second-order forces at Fn=0, 0.05, 0.10 and 0.15 (λ/L=1.2, UKC=2.0)

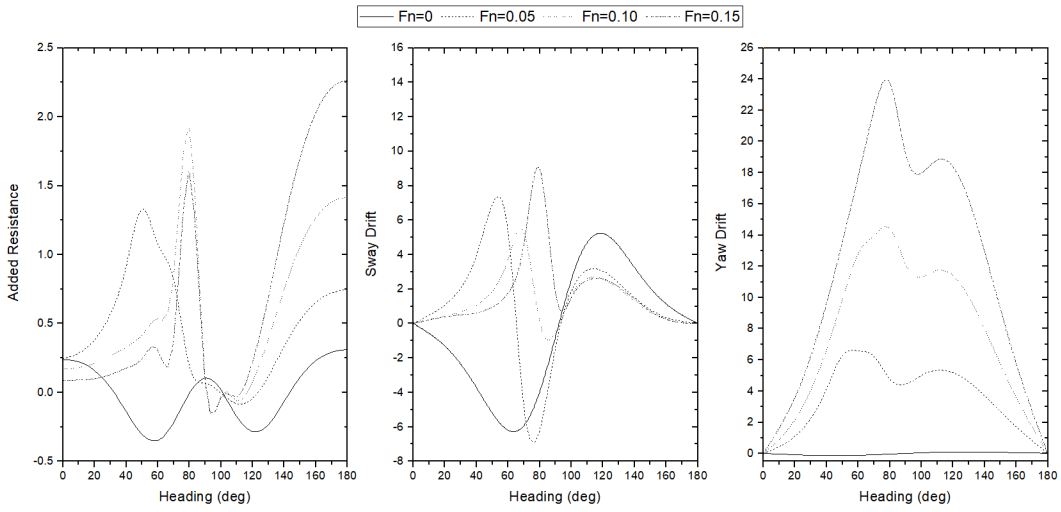

Figure C.10: Nondimensional values of second-order forces at Fn=0, 0.05, 0.10 and 0.15 (λ/L=1.2, UKC=1.5)

Publications During PhD Studies

Conferences:

Pollalis C., Boulougouris E., Turan O., & Incecik A. (2016). ELIGMOS: Time domain simulation of the manoeuvring of ships in deep and shallow waters. *International MSO Conference*, Glasgow, U.K.

Mizythras P., Pollalis C., Boulougouris E., & Theotokatos G. (2017). Simulation of a Ship Propulsion System Performance during Manoeuvring in Shallow Waters. *International Ocean and Polar Engineering Conference (ISOPE)*. San Francisco, California.

Pollalis C., Hizir O., Boulougouris E., & Turan O. (2019). Large Amplitude Time Domain Seakeeping Simulations of KVLCC2 in Head Seas Taking Into Account Forward Speed Effect. *38th International Conference on Ocean, Offshore and Arctic Engineering (OMAE)*. Glasgow, U.K.

Journals:

Mizythras P., Pollalis C., Boulougouris E., & Theotokatos G. A Decision Support System Approach for Collision Avoidance of Ocean-Going Vessels. *Ocean Engineering* (under review)

Mizythras P., Pollalis C., Boulougouris E., & Theotokatos G. Numerical Investigation of Propulsion System Performance in Turning Circle Manoeuvres. (under review)